# Development of a Novel Tissue Expander for Non-Keratinised Epithelial Tissue.

Lucy May Wilson BVMedSci (Hons)

Thesis submitted to the University of Nottingham for the degree of Doctor of Philosophy

June 2022

## Abstract

Cloacal malformations represent one of the most complex forms of paediatric anorectal malformations (ARM). With an incidence of 1 in 50,000 live births, ARMs are rare but have a significant impact on patients' quality of life as they reach puberty and beyond. Surgical intervention is the only treatment option, with the main goals to separate the drainage of faecal and urinary streams, protect renal function, repair the vagina and preserve internal genitalia, allowing patients to become sexually active in the future. The standard practice of surgical intervention can be very invasive for some patients, increasing the morbidity of the procedure. A minimally invasive cloaca repair operation (MICRO) may reduce any additional surgical morbidity. Implanted tissue expanders are preferable to tissue scaffolds or implants as they avoid complications associated with rejection and expansion of native tissue is preferable to implant of tissue from other bodily sites.

Characterisation of the vagina of female pigs (Canberra 12 strain; Landrace/large white/duroc) aged 6 weeks to 6 months has confirmed the suitability of a porcine model for cloacal malformations in paediatric patients. The macroscopic anatomy of female pigs at 8 weeks of age has comparable anatomy to that of children with ARM at an operative age of 6-18 months. Investigations of histology and 3D morphology are also similar, in comparison with human paediatric images. Both species have undifferentiated mesenchyme below the stratified epithelium, with widespread vascular and neural supply to the organ.

An in-house, isotropic self-inflating hydrogel expander has been developed. The hydrogel is comprised of co-polymers; poly (lactic acid), poly (ethyleneglycol 600) diacrylate, acrylic acid, hydroxyethyl acrylate and bis(2,4,6-trimethylbenzoyl)-phenylphosphineoxide, annealed under ultraviolet light for a specified time period. In vitro implantation of the developed hydrogel tissue expanders within porcine vaginal tissue and the conduction of in vitro swelling tests within organ baths has provided vital data for future porcine in vivo expansion trials. The ability for porcine vaginal tissue to withstand the pressure of intraluminal expansion in suboptimal conditions (i.e., within an organ bath) has also been explored. The results suggest that the progression of this work into in vivo implantation trials should produce promising results.

Future in vivo studies would involve the placement of the developed tissue expanders in the vagina of the porcine models and will, ideally, create tissue with the same histological, hormonal, and physiological properties as the native tissue. The newly expanded tissue would then benefit from the resident innervation and blood supply, potentially allowing future patients to experience a better functionality immediately and later in life when reproductive activity commences.

## Publications and Presentations

### Publications

Hendt P Versteegh, David S Gardner, Lucy Scriven, Lisanne Martens, Kirsten Kluivers Geri Hewitt, Ivo de Blaauw, Richard J Wood, Alun Williams, The MICRO group. Reconsidering Diagnosis, Treatment and Post-Operative Care in Children with Cloacal Malformations. Journal of Pediatric and Adolescent Gynecology (2021), DOI: 10.1016/j.jpag.2021.08.009

### Oral Presentations

Lucy Scriven, David S. Gardner, Alun Williams. *Development of a Novel Intraluminal Hydrogel for Epithelial Tissue Expansion*. Nottingham Biotechnology and Biological Sciences Research Council Doctoral Training Partnership Spring School Conference, Nottingham, April 2018

Lucy Scriven, David S. Gardner, Alun Williams. *Minimally Invasive Cloacal Repair Operation: A Porcine Model*. 10th United Kingdom Paediatric Colorectal Group Meeting, Belfast, May 2019.

Lucy Scriven, David S. Gardner, Alun Williams, Jonathan Sutcliffe, Richard J. Wood. *A Porcine Model of Female Cloacal Malformations.* School of Biosciences and School of Veterinary Medicine Postgraduate Symposium, University of Nottingham, June 2019.

Lucy Scriven, David S. Gardner, Alun Williams, Jonathan Sutcliffe, Richard J. Wood. *The Pig as a Model for Urogenital Sinus and Cloacal Malformations*. 66th Annual Congress of the British Association of Paediatric Surgeons, Nottingham, July 2019.

Lucy Scriven, David S. Gardner, Alun Williams. *The Expansion of Vaginal Tissue for Paediatric Surgery*. Nottingham Biotechnology and Biological Sciences Research Council Doctoral Training Partnership Spring School Conference, Nottingham, April 2021.

**Poster Presentations**

Lucy Scriven, David S. Gardner, Alun Williams. *Development of a Novel Intraluminal Hydrogel for Epithelial Tissue Expansion*. School of Biosciences and School of Veterinary Medicine Postgraduate Symposium, University of Nottingham, April 2018.

Lucy Scriven, David S. Gardner, Alun Williams. *Development of a Novel Intraluminal Hydrogel for Epithelial Tissue Expansion*. Nottingham Biotechnology and Biological Sciences Research Council Doctoral Training Partnership Spring School Conference, Nottingham, April 2019.

Lucy Scriven, David S. Gardner, Alun Williams, Jonathan Sutcliffe, Richard J. Wood. *The Pig as a Model for Urogenital Sinus and Cloacal Malformations*. Fertility 2020: Joint Conference of the UK Fertility Societies: The Association of Clinical Embryologists, British Fertility Society and the Society for Reproduction & Fertility. Edinburgh, January 2020.

# Table of Contents

## List of Tables

## List of Figures

## Abbreviations and Acronyms

| | |
|---|---|
| μSLA | Microstereolithography |
| 3D | Three Dimensional |
| Acetyl-CoA | Acetyl Coenzyme A |
| ADP | Adenosine Diphosphate |
| APC | Adenomatous Polyposis Coli (protein) |
| ARM | Anorectal Malformation |
| ATP | Adenosine Triphosphate |
| BMI | Body Mass Index |
| BMP | Bone Morphogenetic Protein |
| CD-1 | Cluster of Differentiation 1 |
| CDH1 | Cadherin 1 |
| Ci | Cubitus Interruptus |
| CK | Cytokeratin |
| CNVs | Copy Number Variations |
| Cos | Costal |
| DBU | 1,8-Diazabicyclo[5.4.0]undec-7-ene |
| DCM | Dichloromethane |
| Dhh | Dessert Hedgehog |
| DKK4 | Dickkopf WNT Signalling Pathway Inhibitor 4 |

| | |
|---|---|
| DMEM | Dulbecco’s Modified Eagle Medium |
| DMPA | 2,2'-dimethoxy-2-phenyl-acetophenone |
| DNA | Deoxyribonucleic Acid |
| ECAD | Epithelial Cadherin |
| ECM | Extracellular Matrix |
| EGDMA | Ethylene Glycol Dimethacrylate |
| EMT | Epithelial-Mesenchymal Transition |
| Eph | Erythropoietin-producing Human Hepatocellular (receptor) |
| FCS | Foetal Calf Serum |
| FDA | Food and Drug Administration (USA) |
| FGF | Fibroblast Growth Factor |
| FGT | Female Genital Tract |
| Gli | Glioma-associated Oncogene Transcription Factors |
| GSK | Glycogen-Synthase-Kinase |
| H & E | Haematoxylin and Eosin |
| HEA | Hydroxyethyl Acrylate |
| HEMA | 2-Hydroxyethyl Methacrylate |
| HPV | Human Papillomavirus |
| IHC | Immunohistochemistry |

| | |
|---|---|
| Ihh | Indian Hedgehog |
| INTU | Inturned Planar Cell Polarity Effector Homolog |
| IPA | Isopropanol (propan-2-ol) |
| IPNs | Interpenetrating Networks |
| LEF | Lymphoid Enhancer Factor (gene) |
| LFB | Luxol Fast Blue (histological stain) |
| MBD | Methyl-CpG Binding Domain |
| MIDAS | Microphthalmia with Linear Skin Defects (syndrome) |
| MICRO | Minimally Invasive Cloacal Repair Operation |
| MURCS | Mullerian, Renal, Cervicothoracic Somite (abnormalities) |
| OEIS | Omphalocele – Exstrophy – Imperforate Anus – Spinal Defects |
| P | Phosphate |
| PμSLA | Projection Microsteroelithography |
| PAA | Poly(Acrylic Acid) |
| PBS | Phosphate Buffer Solution |
| PCL | Poly – Caprolactone |
| PDLA | Poly – D – Lactic Acid |
| PDLLA | Poly – D, L – Lactic Acid |
| PDMS | Polydimethylsiloxane |

| | |
|---|---|
| PEG | Poly(Ethyleneglycol) |
| PEG(600)DA | Poly(Ethyleneglycol 600) Diacrylate |
| PGA | Poly – Glycolic Acid |
| pH | Potential Hydrogen |
| PHEMA | Polymerised 2-Hydroxyethyl Methacrylate |
| PKA | Protein Kinase A |
| PLA | Polylactic Acid |
| PLLA | Poly – L – Lactic Acid |
| PSARVUP | Posterior Sagittal Anorectal Vagino Urethroplasty |
| Ptch 1 | Protein Patched Homolog 1 |
| PVA | Poly(Vinyl Alcohol) |
| R & D | Research and Development |
| ROP | Ring Opening Polymerisation |
| SALL 1 | Sal-like 1 (gene) |
| SEM | Scanning Electron Microscope |
| Shh | Sonic Hedgehog |
| Six | Sine Oculis Homeobox (protein) |
| SLA-DR | Swine Leukocyte Antigen |
| Slimb | Supernumerary Limbs (protein) |
| Smo | Smoothened (protein) |

| | |
|---|---|
| SNPs | Single Nucleotide Polymorphisms |
| TCF | T Cell Factor |
| TE | Tris - Ethylenediaminetetraacetic Acid (buffer) |
| $T_g$ | Glass Transition Temperature |
| $T_m$ | Melting Temperature |
| TUM | Total Urogenital Mobilisation |
| UV | Ultraviolet |
| VACTERL | Vertebral Defects, Anal Atresia, Cardiac Defects, Tracheo – Esophageal Fistula, Renal Abnormalities and Limb Abnormalities |
| WGS | Whole Genomic Sequencing |
| WNT | Wingless – Type Integration Site |
| ZPA | Zone of Proliferation |

## Acknowledgements

This Thesis is a testimony to collaborative research and the value of surgeons working in conjunction with scientists. Over the past few years, numerous people have given their time and expertise and I am grateful to them all.

Firstly, I would like to express my utmost gratitude to my supervisor, Professor David Gardner, for not only making this research project a possibility but also for his unwavering support over the last few years. I am very appreciative for the opportunity to have made my own way through this project and for the acknowledgement of my ideas throughout.

A heartfelt thanks goes to Alun Williams, for his support in my application for this research position as well as his invaluable perspective as a paediatric surgeon. He has been both a constant source of ideas and a pillar of support throughout this venture. Without whom this project would not exist and for that I am eternally grateful.

Next, I would like to thank the MICRO Group, an innovative team of international paediatric surgeons and academics who have warmly welcomed me into their group and continuously supported my endeavours. Thanks goes to Jonathan Sutcliffe, Richard Wood, Ivo de Blaauw, Hendt Versteegh, Kirsten Kluivers and Lisanne Martens. Their input has been invaluable for the progression of this research and has provided an insight into cloacal malformations and repair operations that would otherwise not feature in this Thesis.

A special thanks goes to Richard Wood and Vinay Prasad at Nationwide Children's Hospital, Columbus, Ohio, USA, for the collection and provision of histological images of human paediatric vaginal and common channel tissue. This has been both a rare and vital addition to the project.

I would also like to thank Camilla Easter and Peter Stephenson who, whilst working at Oxtex, supported the development of the initial hydrogel tissue expander and put a lot of time, effort, and resources into its development. Thanks to Florence Hillen for acting as an intermediary between myself and Oxtex during the company's administration and for sourcing the materials for the 'in-house' expander trials.

I am enormously grateful to the Centre of Additive Manufacturing (CfAM), University of Nottingham, particularly members of laboratory A052. Thank you to Professor Ricky Wildman for setting up our collaboration with this department within the Faculty of Engineering. Specifically, I must thank Dr Laura Ruiz Cantu and Dr Yinfeng He, without whom the completion of this project would not have been impossible. Their abundance of knowledge and experience has allowed for this research to continue when its outcome seemed bleak. I would also like to give thanks to Rob Plant for his guidance in the use of desktop stereolithographic 3D printers and to Mark East, CfAM Senior Technician, for accommodating me in his lab and helping me clean up a leaking 3D printer, on multiple occasions!

I would like to give thanks to Dr Llorenc Grau-Roma for his expert histological guidance throughout and for his continuous engagement with the project once leaving the University of Nottingham.

Thanks also extends to additional members of staff of the School of Veterinary Medicine and Science, University of Nottingham. To Dr Adam Blanchard for helping my dip my toes into the world of metagenomics and Professor Nigel Mongan for introducing me to the concept of transcriptomics. Thank you for setting time aside for me and for answering my plethora of questions, repeatedly.

Lastly, I would like to thank my family for their steadfast support over the last five years. To my parents, for always being prepared to listen to me and discuss my ideas, however preposterous they started out. And to my husband Callum, thank you for celebrating the ups and consoling the downs. Though you are still not sure what I have spent the last five years doing, I could never have got this far without you.

xxx

Dedicated to Millie.

(2007 – 2022)

# 1 Introduction

## 1.1 Prologue

One of the most complex forms of paediatric anorectal malformations is the cloacal malformation. Cloacal malformations constitute a group of severe nonhereditary anorectal malformations in neonatal females. The clinical presentation of the condition is a single orifice at the perineum, with the gastrointestinal, urinary and reproductive tracts all draining out of it.

With an incidence of 1 in 50,000 live births having persistent cloaca and around 1 in 20,000 having a persistent urogenital sinus, a tertiary referral centre may encounter only 1 or 2 cases per year. The severe clinical manifestations that arise from the malformations have a significant impact on the patient's quality of life. This being the case, surgical intervention occurs as soon as possible to improve the life the patients will lead. The defects vary in severity from short common channel to long common channel with associated variation in comorbidities, complexity of care and propensity for life long impairment of outcomes.

The main goals of surgical therapy are to separate the drainage of faecal and urinary streams with the protection of renal function, and to repair the vagina and preserve internal genitalia, allowing patients to become sexually active in the future. The denervation and necrosis of the tissue as a result of surgery leads to abnormal function of the tissue i.e., lack of sensation during intercourse and the inability of the vagina it dilate at childbirth. With this being the case, a far less invasive and traumatic technique for repair would be

desirable. Avoidance of multiple reoperations would be better for both patients and resource use.

The research conducted within this Thesis uses the young female pig as a model for human paediatric patients presenting with cloacal malformations. The technique of tissue expansion as a minimally invasive technique for cloacal repairs is investigated. It focuses on the use of a self-inflating tissue expander to produce neovaginal tissue for use in subsequent reconstructive surgeries.

## 1.2 Objectives

The aim of the project is to develop a surgical technique using a self-inflating tissue expander to produce additional in vivo tissue for use in reconstructive procedures. This expander would be placed in the vagina of the patient and will, ideally, create tissue with the same histological, hormonal and physiological properties as the native tissue. The newly expanded tissue would then benefit from the resident innervation and blood supply, potentially allowing the patient to experience a better functionality immediately and later in life when reproductive activity commences.

The specific objectives of this project are:

I. Characterise the anatomy, histology and morphology of the normal, non-expanded porcine vagina, including measurement of the levels of E-Cadherin (a transmembrane protein involved in cellular adhesion commonly used to differentiate invasive tissue), Ki67 (a nuclear protein associated with cellular proliferation) and Vimentin (a stain confirming the mesenchymal origin of a tissue) within the tissues for later comparison to expanded tissue (as outlined in Chapter 3).

II. Develop a novel anisotropic hydrogel expander with an external company (Oxtex Ltd) that is suitable for implantation into the vaginal lumen of young, pre-adolescent pigs (as outlined in Chapter 4).

III. Implant the novel expander into the vaginal lumen of pre-adolescent pigs, allowing for full expansion of the device over a period of time. Remove and characterise the expanded tissue from the animal post-mortem (as outlined in Chapter 5).

## 1.3 Thesis Outline

The literature relating to the work on which this Thesis is based is reviewed in Chapter Two. Anorectal malformations are considered in terms of the methods of classification, techniques of surgical repair and their aetiology. The embryological development of the normal urological and reproductive systems is described. Subsequently, the role of tissue expanders is explored, including balloon and self-inflating expanders. Reference is made to the properties and characteristics of hydrogels, focussing on the components used in the development a tissue expander for this Thesis, incorporating the application of polylactic acid for biomedical devices and tissue engineering. Various models for vaginal epithelial tissue are considered.

The characterisation of the porcine vagina is described in chapter three, referring to the translational anatomy and histological morphology of the juvenile animal and female paediatric patients presenting with cloacal malformation.

Chapter four is devoted to the development of a self-inflating hydrogel tissue expander. This includes contributions and collaborations with an industrial partner and a department within the University of Nottingham. In addition, the modifications made to the design of the hydrogel expander and the requirements of paediatric colorectal surgeons are described.

The penultimate chapter is dedicated to the in vitro trial of the prototype hydrogel tissue expander using the porcine vaginal model. The method of implantation is described along with the methods of histological analysis of the vaginal tissue post-expansion.

Finally, to conclude this Thesis, Chapter 6 reflects on the implications of the loss of the industrial partner and the COVID-19 pandemic on the progression of this project, including the evolution of the hydrogel tissue expander design and the development of collaborations. Areas of future work are also highlighted, including the important considerations when adapting the contents of this Thesis to in vivo employment of the hydrogel tissue expander and prospective analyses.

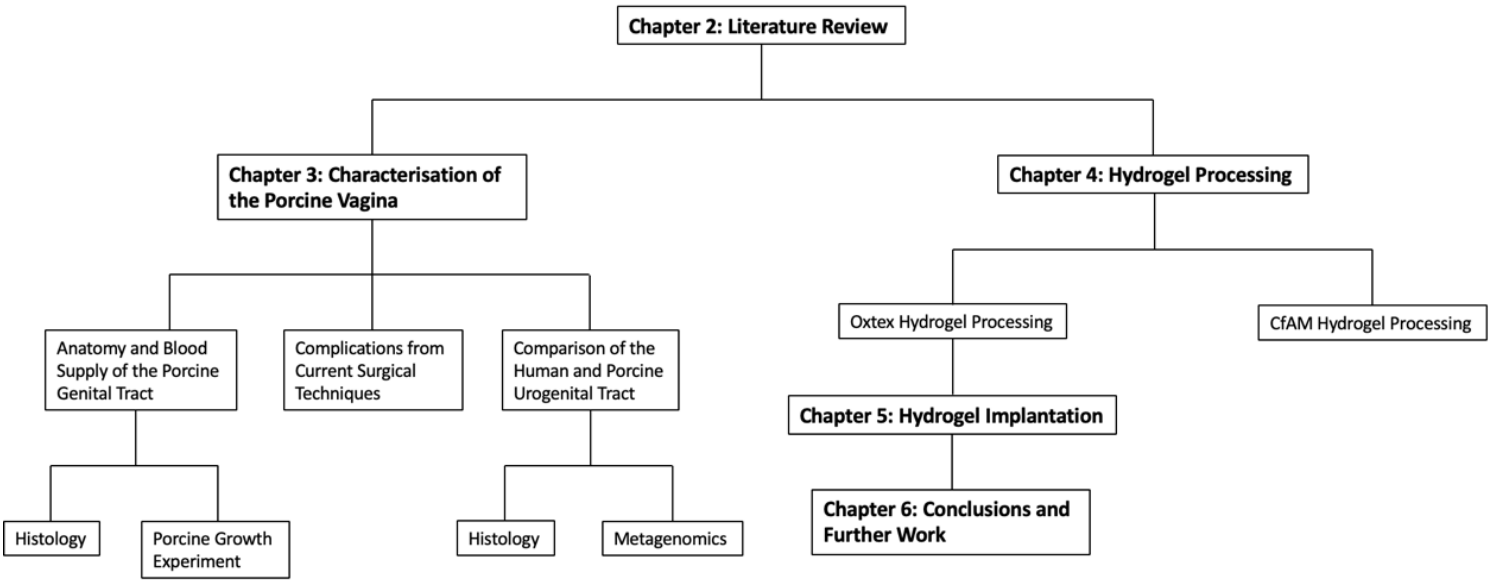


**Figure 1.1: Flow diagram representing the relationship between the chapters within this thesis.**

# 2 Literature Review

## 2.1 Anorectal Malformations

### 2.1.1 Classification of Anorectal Malformations

Cloacal malformations constitute a group of severe nonhereditary anorectal malformations (ARMs) in neonatal females. The term “cloaca” describes not only a transitional organ system in human embryos but also a congenital anomaly and a normal organ in birds. However, each have completely different morphological properties. Anorectal malformations encompass a wide spectrum of diseases, affecting both male and female children, involving the anus and distal rectum primarily, but also the urinary and genital tracts. The defects range from minor complications with simple treatment and a very good functional prognosis, to those that are more complex and challenging to manage. These cases are often associated with multiple abnormalities and have a poor functional prognosis.

Classification of anorectal malformations using surgical reports has resulted in multiple inconsistencies, due to surgeons using different terminologies when referring to types of imperforate anus. From accumulations of surgical reports, Levitt and Peña (Peña, 1990) grouped together the defects that have common diagnostic, therapeutic and prognostic features (Table 2.1). This resulted in a form of classification, but with the spectrum of the defects being so broad, it cannot be deemed completely accurate. Multiple official classification systems have been produced, the first being the Wingspread arrangement, developed at an ARM conference in Wingspread, Wisconsin, USA in 1984. The focus at the time was on the relation of the rectal pouch to the levator muscle complex,

and so the varying anomalies are classified into low, intermediate and high depending on whether the terminal rectal pouch had crossed the levator sling or not (Stephens and Smith, 1986). The more recent form of ARM cataloguing was derived in 2005 at a conference in Krickenbeck, Germany (Table 2.2). The main aim of the conference was to discuss the international classification of ARMs, the criteria for their treatment and development of a scoring system for comparable follow-ups. This system was a derivative from a modified version of Peña's own classification introduced in 1995, as illustrated in Table 2.1.

| NON-SYNDROMIC ARM | With Fistula | | Without Fistula |
|---|---|---|---|
| | Recto-perineal Malformations | Imperforate anus with recto-urethral fistula<br>Recto-urethral bulbar fistula<br>Recto-urethral prostatic fistula<br>Bladder neck fistula | Cloacal malformations with a short common channel (<3cm) |
| | Imperforate anus in Female | Recto-vestibular fistula<br>Recto-vaginal fistula<br>Cloacal malformation | Cloacal malformations with a long common channel (>3cm)<br>H-shaped fistula (recto-vaginal)<br>Rectal duplication |
| **SYNDROMIC ARM** | VACTERL | Pallister-Hall syndrome | Townes-Brock syndrome |
| | MURCS | Lowe syndrome | Ulnar-mammary syndrome |
| | OEIS | Heterotaxia | Okihiro syndrome |
| | Axial mesodermal dysplasia | FG Syndrome | Reiger syndrome |
| | Klipper-Feil Syndrome | X Linked mental retardation | Hirschsprung's disease |
| | Sirenomelia-caudal regression | Ciliopathies | Feingold syndrome |
| | Trisomy 21, 13, 18 | Fraser syndrome | Kabuki syndrome |
| | Pallister-Killian syndrome | MIDAS syndrome | Optitz BBB/G syndrome |
| | Cat-eye syndrome | Christian syndrome | Johanson-Blizzard syndrome |
| | Parental unidisomy 16 | Currarino syndrome | Spondylocostal dysostosis |
| | Deletion 22q11 syndrome (del22q11.2) | Baller-Gerold syndrome | Short rib-polydactyl syndrome |

**Table 2.1: Pena's Classification of ARMs** (Peña, 1990).

The methods of diagnosis of ARMs are predominantly clinical, combined with radiological and potentially endoscopic assessment. Ultrasound maybe performed for urological anomalies. Plain radiographs can show spinal and sacral anomalies as well as determining the internal anatomy of the patient. The main method for determining the precise gastrointestinal, urinary and reproductive anatomy is the use of a high pressure, distal colostography. This is performed after the new-born period and the colostomy has been created in the patient. Hydrosoluble contrast material is injected into the patient's stoma to demonstrate the exact location of the distal rectum and the urinary communication, the contrast material usually fills the bladder and urethra through the fistula. Contrast is instilled until voiding commences and images are obtained to demonstrate the sacrum, height of the rectum, perineum, fistula location, bladder, vesicoureteral reflux, if present, and the urethra (Levitt and Peña, 2007).

One of the most complex forms of ARMs is the cloacal malformation, where the gastrointestinal, urinary and reproductive tract all drain into one common channel. The repair of these deformities is a serious technical challenge for paediatric surgeons, with the prognosis of complete functionality still being quite poor.

## 2.2 Embryological Development of Urological and Reproductive Systems

### 2.2.1 Differentiation of the Female Duct System

The cranial portions of the paramesonephric ducts develop to form the uterine tubes and the caudal portions of the ducts give rise to the horns and body of the uterus. At their cranial aspects, the uterine tubes remain open and communicate with the coelomic cavity. Postnatally, this communication persists from the peritoneal cavity to the exterior. In males, a comparable communication between the peritoneal cavity and the exterior does not exist.

At first, the portions of the ducts which are closed elongate caudally, lateral to the mesonephric ducts. Close to the urogenital sinus, each duct occupies a position ventral to the mesonephric duct and fuses in the midline with the corresponding duct from the opposite side. The closed end of the fused ducts continues to grow caudally to make contact with the urogenital sinus where it induces cellular proliferation of the endoderm of the urogenital sinus and the formation of the vaginal plate (Yerkes and Rink, 2010).

Differences observed in the final anatomical arrangements of the uteri in different species can be attributed to the relative positions of their primordial structures and the extent to which fusion occurs. In rodents, fusion is confined solely to the outer portions of the walls of the ducts while the lumina remains distinct. This results in a separate opening for each uterine lumen into the vagina (uterus duplex). In domestic species, the caudal ends of the ducts fuse. Subsequently, the medial fused walls atrophy resulting in the formation of a single tube, the body of the uterus, which has a single opening into the vagina.

Those portions of ducts cranial to the region of fusion remain distinct and are the primordia of the horns of the uterus and the uterine tubes. Thus, in domestic animals, the uterus which consists of two horns and a body is referred to as a bicornate uterus (Fig. 2.1). In cattle, the primordia of the paramesonephric ducts appear at approximately the 34$^{th}$ day of gestation, and fuse with the urogenital sinus at approximately the 50$^{th}$ day. In primates, including humans, extensive fusion of the paramesonephric ducts occurs with associated atrophy along the medial line of fusion, resulting in the formation of a large uterine body termed uterus simplex (McGeady et al., 2006a).

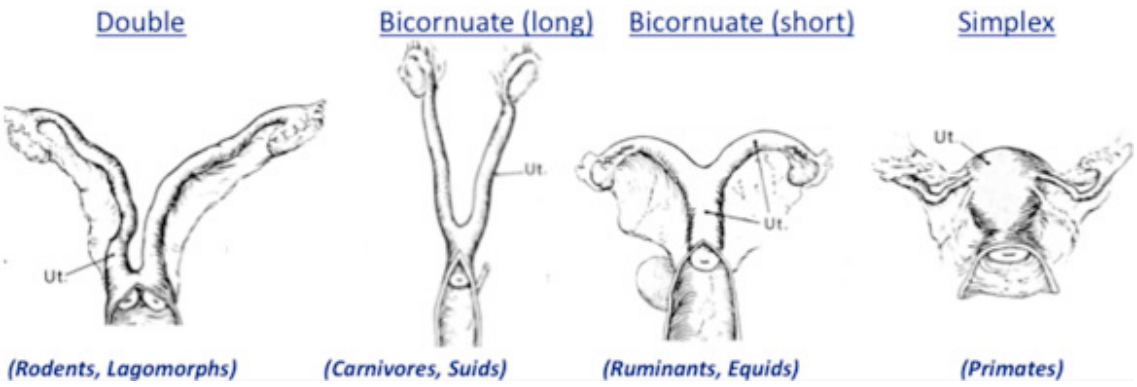


**Figure 2.1: Comparative Anatomy of the Uterus** (Chavatte-Palmer and Tarrade, 2016).

### 2.2.2 Septation of the Cloaca

The cloaca initially develops in the human embryo at 4 weeks post conception, as the part of the hindgut that lies caudal to the allantoic opening. This state is common to that of animals such as avian or reptilian species, acting as a common passage for urinary, reproductive and faecal products, comprising of the urodeum, proctodeum and copradeum respectively (Klasing, 1999). The terminal portion of the hindgut at this stage of development is deemed the cloaca. The cloaca consists of an endoderm lined cavity that is in contact with the ectoderm. The area of contact between the cloacal endoderm and proctodeum ectoderm (anal pit) is the cloacal membrane. The cloaca receives the allantois ventrally and the mesonephric duct laterally and is divided by a coronal sheet of mesenchyme, the urorectal septum, this develops between the allantois and the hindgut. As the septum grows caudally towards the cloacal membrane, it develops extensions that produce in-foldings of the lateral walls of the cloaca. These folds grow towards one another, forming a partition within the cloaca, creating two parts; the rectum and upper anal canal, dorsally, and the urogenital sinus, ventrally.

By the end of 6 weeks gestation, the urorectal septum has fused with the cloacal membrane, dividing it into a dorsal anal membrane and a ventral urogenital membrane. Breakdown of these membranes soon after their formation allows both the alimentary tract and urogenital tract to communicate with the exterior. The urorectal septum fusing with the cloacal membrane forms the central perineal tendon, or the perineal body (Kay and Tank, 1977). The urorectal septum also divides the cloacal sphincter into anterior and posterior parts. The posterior part eventually becomes the external anal

sphincter, and the anterior part develops into the superficial transverse perineum, the bulbospongiosis, the ischiocavernosis and urogenital diaphragm. This explains why one nerve, the pudendal nerve, supplies all the muscles into which the cloacal sphincter divides.

Mesenchymal proliferations around the anal membrane elevate the surface ectoderm, forming a shallow pit known as the proctodeum (anal pit). The anal membrane is now located at the bottom of this pit, or depression. The anal membrane usually ruptures at the end of the 8$^{th}$ week, establishing the anal canal. This also brings the caudal part of the digestive into communication with the amniotic cavity (Moore, 1982).

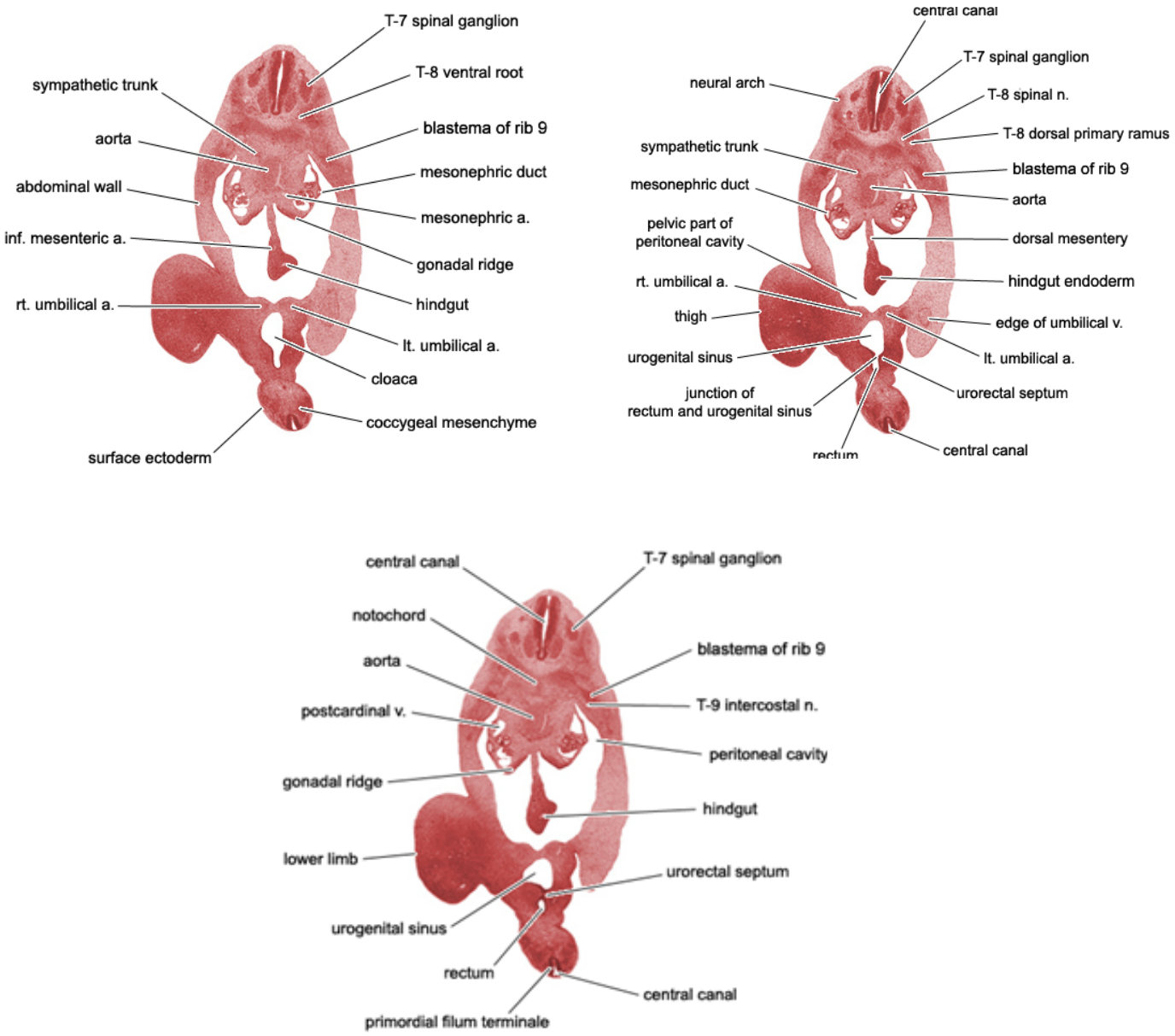


**Figure 2.2: Septation of the Cloaca** (Kruepunga et al., 2018). Histological sections depicting the septation of the cloaca into the urogenital sinus and rectum. The formation of the urorectal septum can be seen.

### 2.2.3 Development of the Bladder and Urethra

The urogenital sinus is made up of three parts, the most cranial being the vesical part, this is the primitive bladder continuous with the allantois, then the middle pelvic part and the caudal phallic part; this is externally closed by the urogenital membrane.

The epithelium of the bladder is derived from the endoderm of the vesicular part of the urogenital sinus. The lamina propia, muscle layers and adventitia develop from the neighbouring splanchnic membrane. Initially the bladder is continuous with the allantois, the lumen of this structure eventually strictures, becoming a thick fibrous cord, the urachus. In infants and children, the urinary bladder is found in the abdomen. It begins to enter the pelvis major at around 6 years of age but is not entirely in the pelvis minor until after puberty. Like the bladder, the entire epithelium of the female urethra is derived from the endoderm of the vesicular part of the urogenital sinus and the connective tissue and muscle layers from the adjacent splanchnic mesenchyme (Moore, 1982).

### 2.2.4 Development of the Uterus and Vagina

In embryos with ovaries, the mesonephric ducts regress and the paramesonephric ducts develop into the female genital tract. The cranial, unfused portions of the paramesonephric ducts develop into the uterine tubes and the caudal, fused, part forms the uterovaginal primordium. This gives rise to the epithelium, glands of the uterus and to the fibromuscular wall of the vagina. The endometrial stroma and myometrium are derived from the adjacent mesenchyme. The uterus is predominantly a pelvic organ in the newborn infant and the cervix is relatively large. During puberty, the uterus grows rapidly. Fusion of the paramesonephric ducts also brings together two peritoneal folds. These form the right and left broad ligaments. Alongside the uterus, between the layers of the broad ligament, the mesenchyme differentiates into layers of loose connective tissue and muscle, known as the parametrium.

The vaginal epithelium derives from the endoderm of the urogenital sinus. The fibromuscular wall of the vagina develops from the uterovaginal primordium. Contact between the urogenital sinus and the uterovaginal primordium induces the formation of paired endodermal sinovaginal bulbs. These bulbs fuse to form the vaginal plate. Later in development, the central cells of the vaginal plate break down, forming a lumen. The remaining peripheral cells become the vagina epithelium. Until late foetal development, the lumen of the vagina is separated from the urogenital sinus by a membrane, the hymen (Fig. 2.3). The hymen usually ruptures during the perinatal period and remains as a thin fold of mucus membrane around the entrance to the vagina. By 12

weeks of embryogenesis, the individual anal canal, vaginal and urethral openings are fully established (Moore, 1982).

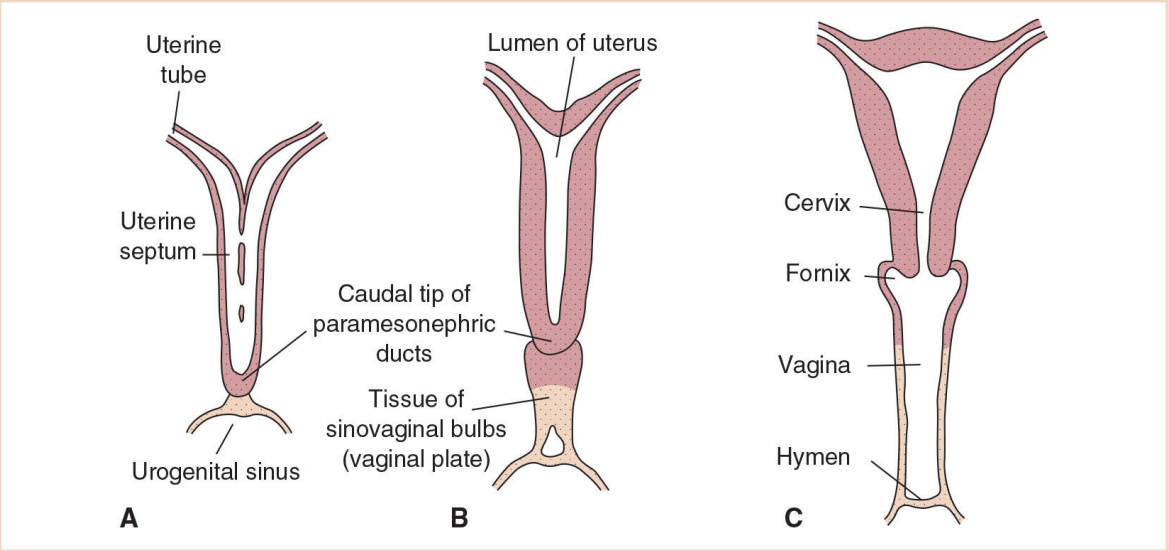


**Figure 2.3: Formation of the Vagina (**Gardner and Shoback, 2017). Contact between the urogenital sinus and the uterovaginal primordium induces the formation of paired endodermal sinovaginal bulbs. These bulbs fuse to form the vaginal plate. Later in development, the central cells of the vaginal plate break down, forming a lumen. The remaining peripheral cells become the vagina epithelium. Until late foetal development, the lumen of the vagina is separated from the urogenital sinus by a membrane, the hymen.

### 2.2.5 Development of External Genitalia

In both sexes, external genital organs are not fully formed until week 12 gestation.

External genitalia undergo an undifferentiated state before distinguishing sexual characteristics appear. In the 4$^{th}$ week, a genital tubercle develops at the cranial end of the cloacal membrane. Then, labioscrotal swellings and urogenital folds form on each side of the cloacal membrane. The genital tubercle soon elongates to form a phallus; this is as large in the female as it is in the male. When the urorectal septum fuses with the cloacal membrane, around week 6, it divides the membrane into the anal and urogenital membranes. These membranes rupture a week or so later, forming the anus and urogenital orifices, respectively. A urethral groove that is continuous with the urogenital orifice forms on the ventral surface of the phallus.

In the absence of androgens, feminisations of external genitalia occur at this stage of development. Initially, the phallus elongates rapidly, but its growth will gradually slow, and the phallus develops into a small clitoris. Unlike the development of the penis, the urogenital folds do not fuse, except at the formation of the frenulum of the labia minora, these unfused folds develop into the labia minora (Fig. 2.4) (Velkey et al., 2015). The labioscrotal folds fuse posteriorly and anteriorly to form the posterior and anterior labial commissures respectively, and the mons pubis. The labioscrotal folds remain largely unfused and develop into the labia majora. The phallic part of the urogenital sinus gives rise to the vestibule of the vagina, in which the urethra, the vagina and the ducts of the greater vestibular glands open (Moore, 1982).

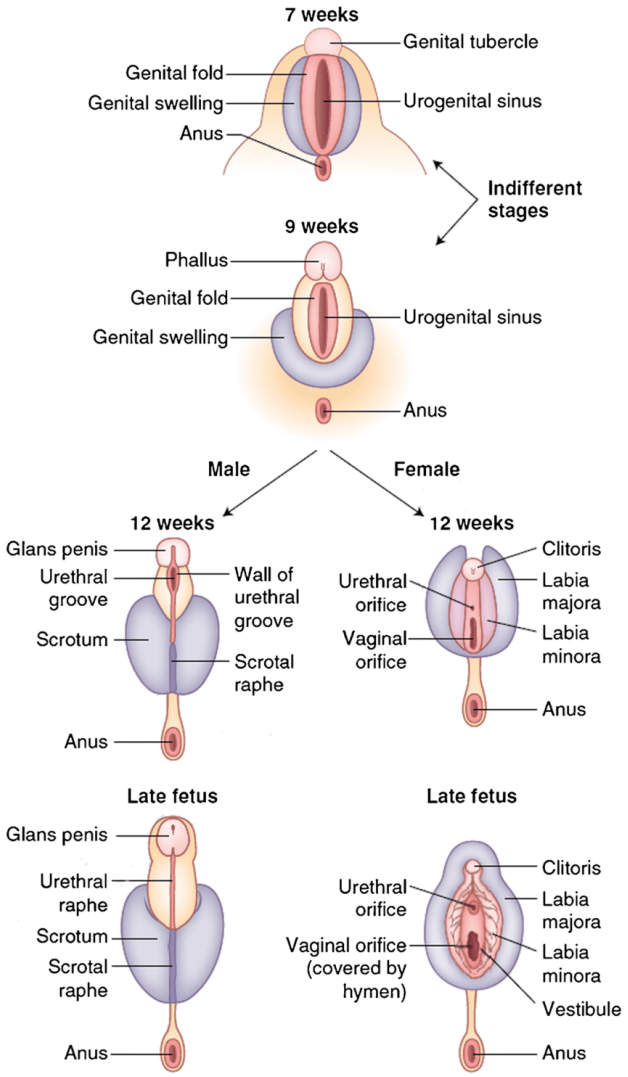


**Figure 2.4: Embryological Development of the Female and Male External Genitalia** (Velkey et al., 2015).

A brief overview of the development of the human urogenital tract, from cloaca to external genitalia for both male and female foetuses is described in figure 2.5 (Barhate, 2020).

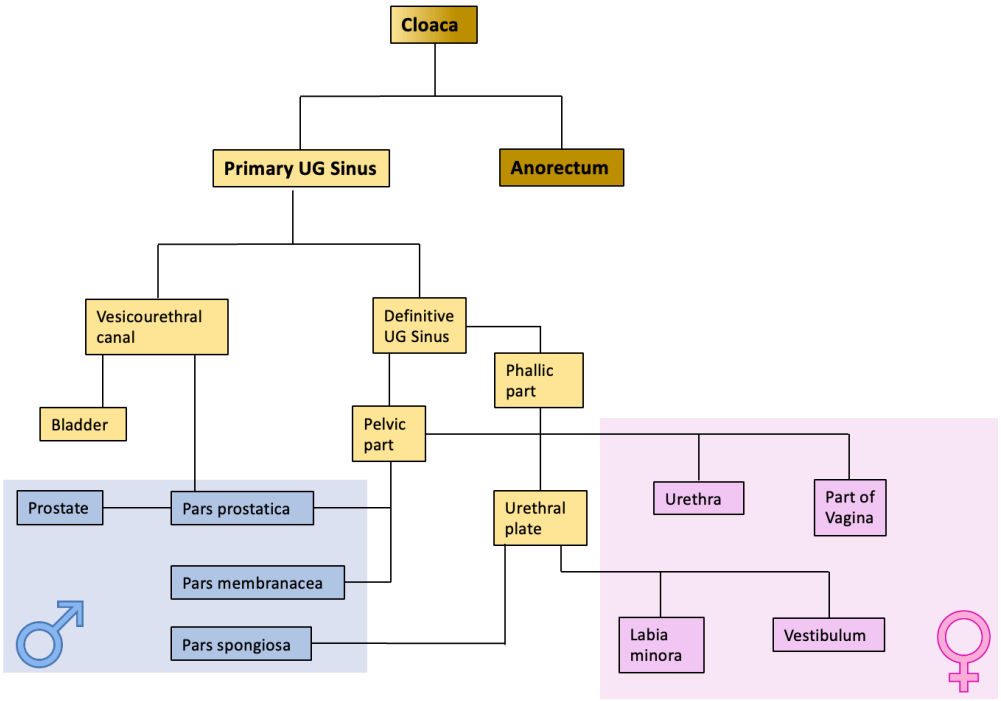


**Figure 2.5: An Overview of Urogenital Development. From cloaca to external genitalia in both male and female foetuses** (Barhate, 2020).

## 2.3 The Congenital Malformations of the Urogenital System

Most anorectal malformations result from the abnormal development of the urorectal septum, resulting in either convergence of the genital, urinary, and intestinal contents into a single common channel (persistent cloaca) or the formation of two channels: a common genitourinary channel (urogenital sinus) separate from the hindgut. The severity of the malformation is dependent on the point of development disrupted and the degree of mutation that has caused the disruption.

Cloacal and urogenital malformations are best understood when considered as a spectrum of anorectal and urogenital malformations. It is common for female patients to present with a single perineal opening, an imperforate anus and small genitalia, though some patients do present with an enlarged clitoris. The persistent cloaca can communicate with the rectum, vagina and urethra at different levels and in some cases, the vagina is septate, or double. This results in patients presenting with variations of rectovaginal and urethrovaginal fistulas, as well as common channels varying in length (Fig. 2.6) (Peña, 1990).

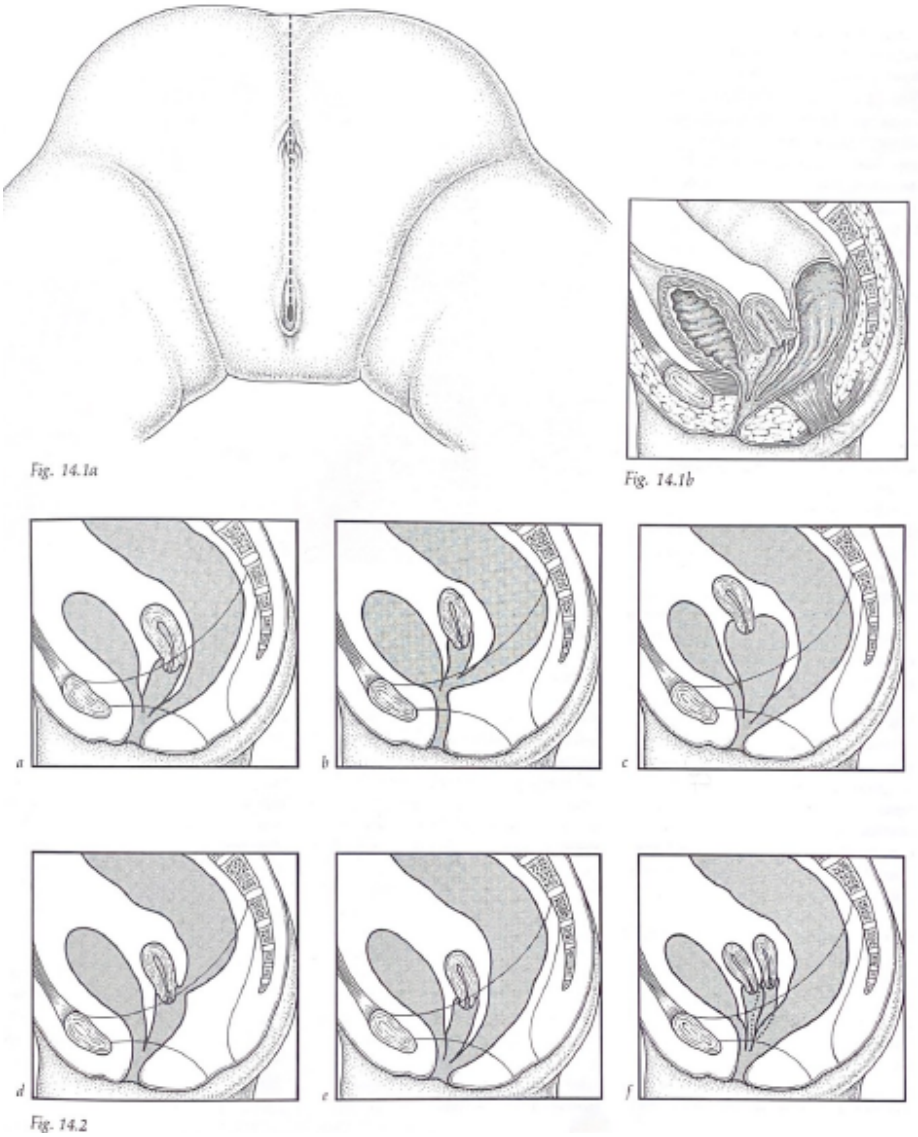


**Figure 2.6: The Spectrum of Cloacal Malformations** (Peña, 1990). It is common for female patients to present with a single perineal opening (14.1a). the persistent cloaca can communicate with the rectum, vagina, and urethra at different levels and in some cases, the vagina is septate or double. (14.2a-4).

Contrast x-ray studies are used to determine the anatomy of patients presenting with cloacal malformations. The combined usage of endoscopy and cloacagrams (injection of contrast material through the single perineal opening) enables the basic characteristics of a patient's anatomy to be determined. Urological investigations for complications such as single ureters, ectopic ureters, ureteroceles and dysplastic kidneys (Hendren, 1988) are vital.

The more severe pathologies like renal agenesis, severe vesicoureteral reflux and pelvic-ureteric obstruction can be life threatening to patients. The clinical symptoms of these problems often present as faecal and urinary incontinence or vesicoureteral reflux, causing perpetual urinary tract infections even with the administration of antibiotic prophylaxis. Patients frequently have hydrocolpos, distended vagina due to urine reflux, again this will causes constant infection without manual drainage of the vagina and surgical intervention (Caldwell and Wilcox, 2016). Rare types of cloacae include complex defects. The rectum may be located behind the urinary tract and open between the urinary tract and the vagina; ureters may open ectopically, often into the vagina. Even more rare presentations of complex persistent cloaca defects result in the patient having a large, wide, cloaca communicating with the intestine and ureters only, with the absence of any recognizable bladder, vagina or rectum. Persistent cloaca is placed under the heading of major clinical groups in the Krickenbeck classification (discussed earlier) of anorectal malformations (Table 2.2) (Gupta, 2005).

| Major Clinical Groups | Rare/Regional Variants |
|---|---|
| **Perineal (cutaneous) fistula** | Pouch colon atresia/stenosis |
| **Rectourethral fistula/atresia/stenosis** | Rectal atresia/stenosis |
| **Bulbar fistula** | Rectovaginal fistula |
| **Prostatic fistula** | H-type fistula |
| **Rectovesical fistula** | Other |
| **Vestibular fistula** | |
| **Cloaca** | |
| **ARMs with no fistula** | |
| **Anal stenosis** | |

**Table 2.2: Krickenbeck Classification of ARMs** (Holschneider et al., 2005).

Important prognostic factors to currently consider with a patient with cloaca are the length of the common channel, the size of the vagina, the condition of the sacrum and the quality of the surrounding muscles. The common channel can vary between 1 and 7 cm in length, generally if the common channel is longer than 3cm there is an increased difficulty in mobilizing the vagina down to reach the external labia. A small vagina is more difficult to dissect and mobilize and is far more likely to become devascularised. A complete sacrum usually indicates than the innervation of the pelvis is normal, indicating a good prognosis in terms of urinary and faecal continence. The quality of the sphincter muscles is determined by examination of the patient's perineum. A marked midline groove and a distinct recognizable anal dimple are usually associated with good external anal sphincter and levator muscles (Bischoff, 2016).

Although rare, with an incidence of 1 in 50,000 live births having persistent cloaca (Warne et al., 2011) and around 1 in 20,000 having a persistent urogenital sinus (Singh et al., 2010), a tertiary referral centre may encounter only 1 or 2 cases per year. However, the severe clinical manifestations that arise from the malformations will have a significant impact on the quality of life of the patients. This being the case, surgical intervention is typically undertaken in the first year of life, although there has been some debate about the timings of each component. The defects can range from minor problems, easily treated with good functional prognosis, to more complex presentations that are very difficult to manage and have very poor prognosis.

Due to the above, neonates born with cloacal abnormalities and other variants of ARMs must undergo numerous surgeries to attempt to repair their anatomy. These procedures often require correcting and may continue up to adolescence as the patient's anatomy and physiology develops.

## 2.4 Surgical Repair of Cloacal Malformations

The main goals of surgical therapy are to separate the drainage of faecal and urinary streams with the protection of renal function, while achieving social continence of both urine and faeces. Another significant goal is the repair of the vagina and the preservation of internal genitalia, to allow patients to become sexually active in the future and if possible, fertile. To achieve this, multiple surgeries are performed on patients from a very young age through to puberty.

### 2.4.1 Posterior Sagittal Anorectal Vagino Urethroplasty

The first specific surgical procedure for repair of cloacal malformations was performed in 1982 (Peña and DeVries). The posterior sagittal anorectal vagino urethroplasty (PSARVUP) repair involves pulling through and reconstructing the urinary, genital and digestive tracts in a one-stage procedure. The technique comprises of a midline incision being made from the sacrum to the perineum, extending through the sphincteric musculature to the terminal bowel and fistula. During this approach, the rectum is separated from the urogenital sinus; this is followed by the separation of the vagina from the urethra to relocate the structures (vagina and urethra) down to the perineum individually. The common channel formed by the malformation is then used to construct a neourethra.

Before this specific technique, the general procedure to cope with cloacal malformations involved an entire hysterectomy to eradicate any reproductive problems the patient may have in the future, practise that would not be ethical now. The technically challenging manoeuvre of separating the vagina from the urinary tract in this procedure has led to a series of complications as a result. These have included the patients developing urethrovaginal fistulas, vaginal strictures and vaginal atresia (Hendren, 1980, Peña, 1989, Peña, 1997).

### 2.4.2 Total Urogenital Mobilisation

The current standard repair, 'total urogenital mobilisation' (TUM), has been in use since 1994 (Peña, 1997). It was developed to avoid the complications described above with the PSARVUP and to improve the outcomes of patients with cloacal malformations receiving surgical treatment. It involves separation of the rectum from the cloaca and mobilising the urethra and vagina together as a single unit down to the perineum, resulting in removal of the urogenital sinus and the creation of three separate openings at the peritoneum. Often this procedure is performed via a posterior sagittal approach, however in patients with a common channel longer that 3 cm it is mandatory to open the abdomen to complete repair, making the procedure far more complex. The bladder must be opened, and catheters introduced into each ureter to reduce damage, the common wall between the bladder and vagina may involve a significant portion of ureter. The vagina must then be separated from the urinary tract, a very delicate and complex procedure.

Of the patients that have undergone PSARVUP surgery, 66.5-76% have voluntary bowel movements by the age of 3, depending on the length of their initial common channel, and 69% of patients with a 'long' common channel (>3cm) require intermittent catheterisation. However, in patients with a shorter channel (<3cm) only 19% required intermittent catheterisation (Hendren, 1980). Considering this, a significant number of patients require bowel management and intermittent catheterisation in order to remain clean to enable social acceptability. The use of the TUM technique is unlikely to improve these functional results because the underlying nerve and muscle function remains the same. The main advantage of the modernised technique is that it provides a smoother urethra and a more visible meatus, enabling easier catheterisation (Peña, 1997, Krstic et al., 2001).

The literature concerning these surgical procedures is very detailed and the authors have published all the outcomes from the surgeries, including those that were unsuccessful. However, published outcomes depend on various biases, including the volume of a centre and the expertise of an individual and the team in which they work. Some pioneers, such as Hendren and Peña, have thought things through from first principles, which confers significant additional insights. Their outcomes may therefore not be representative of most other groups. This limits the comparison of various researchers' techniques and one almost assumes that all surgeons dealing with cloacal malformations perform Peña's technique.

Both the surgical techniques described above (PSVARUP and TUM) can lead to denervation and some necrosis of the urethra, bladder and rectum. Some patients require vaginal replacement, with either rectum, ileum or colon (Hensle et al., 2006). Even after these numerous procedures are performed, many patients are incontinent with both urine (increasing their risk of contracting urinary tract infections) and faeces and once the patients reach puberty, they often have an incapacity to drain menstrual flow, leading to atresia of the uterus, cervix and vagina. The denervation and necrosis of tissue as a result of surgery leads to abnormal function of the tissue i.e., lack of sensation during intercourse and the inability of the vagina to dilate at childbirth.

With this being the case, a far less invasive and traumatic technique for repair must be developed. The possibility of producing more tissue for use in reconstructive surgery may reduce the amount of denervation and necrosis that currently results from surgery. This will involve either the use of some form of tissue graft/implant or a technique that will increase the amount of natural tissue within the patient, such as a tissue expander.

## 2.5 Vaginoplasty Techniques – Tissue Expansion

Various tissue expansion methods for vaginoplasties and the correction of vaginal agenesis have been used over the last 30-40 years. The optimal treatment method is yet to be decided.

### 2.5.1 Non-Surgical Vaginal Tissue Expansion

#### 2.5.1.1 Vaginal Dilator Therapy

The simplest method to achieve vaginal tissue expansion is the use of insertion of dilators directly into the vaginal cavity, with the dimensions of the inserted dilators increasing over time. Vagina dilator therapy as a nonsurgical treatment for congenital agenesis has been in use for many years. When incomplete vaginal development occurs, a soft, pliable span of skin is usually left between the urethral meatus and the anus (Lappöhn, 1995). The ability to develop and expand this tissue with repetitive dilatation was determined after observing that repeated attempts at coitus could eventually lead to successful intercourse (D'Alberton and Santi, 1972). Vaginal formation from progressive dilation was first formally described by Frank (1938), who used handheld Pyrex glass moulds to apply persistent pressure to the perineum. Ingram (1981) later recognised that Frank's method had limiting factors, including fatigue of the patients hands and fingers from holding the dilator in place with constant pressure, the awkward positioning required to place the dilator correctly (squatting etc.) and the inability for the patient to undertake other activities during the hours of pressure application (Lankford and Haefner, 2008). Ingram developed a specially designed stool to use body weight to maintain adequate

dilator pressure, making life much easier for the patient. The method used vaginal dilators mounted on a bicycle seat stool that provides perineal pressure via the narrow and elevated portion of the seat (Lee, 2006). Neovagina depths of up to 10cm within 4 – 6 months were reported with Ingram's technique, but it is uncertain as to how many patients accomplished this. Ingram also implied that his technique was an appropriate secondary approach following neovagina constructive surgery, such as the Abbe-McIndoe technique, a method that will be discussed briefly later in this review. However, some patients that experienced neovagina contracture more than 6 months after their operation complained of mild dyspareunia (painful intercourse) or were still unable to have successful intercourse (Ingram, 1981).

In addition to neovagina formation, vaginal dilators are widely used by physical therapists for the treatment of other pelvic floor disorders, such as levator ani hypertonicity, vaginismus, vulvodynia and dyspareunia (Bergeron et al., 2002, Seo et al., 2005). Vaginal dilators are typically part of a home program to enable patient self-stretching of vaginal tissues and pelvic floor musculature. Dilators are also used as a desensitising technique, utilising graded exposure and increasing size to reduce both the pain and fear associated with dyspareunia (Bergeron et al., 2002, Melnik et al., 2012).

Although dilator therapy is a well-established efficacious, nonsurgical technique for the creation of the neovagina, there are problems with implementing the technique. Lack of motivation, especially in young patients (less than 18 years old), and often a lack of sexual activity, appears to be some of the limiting factors (McVearry and Warner, 2011). The use of graduated vaginal dilators for patients with Mullerian agenesis has been successful in creating a neovagina. A study that followed patients through their dilatation treatment showed that the method produced an effective vaginal canal with respect to its function and anatomy. This was also the case in the event of previous hymenotomy and subsequent scar formation (Roberts et al., 2001). Although the lack of adequate lubrication, pain and difficulty in reaching orgasm is significantly higher in these patients, they experience comparable sexual satisfaction to a normal population (Nadarajah et al., 2005).

The advantages of this non-operative technique include its non-invasive nature, preservation of natural vaginal tissue, low complication rate and lack of hospitalisation. Reasonable results have been achieved, predominantly in older patients, with a longer starting vaginal length. The method has also been successful for postoperative neovagina contracture. With the most effective outcomes occurring when dilators are used within 6 months after surgery. The main disadvantages are the time and persistent discomfort required to create a functional neovagina, often resulting in noncompliance. Though offered as a first approach technique, it may be that the optimal patient for dilatation is an older, more emotionally mature and highly motivated person wishing to avoid surgical intervention (Thomas and Brock, 2007).

### 2.5.2 Surgical Vaginal Tissue Expansion

In patients for whom non-invasive dilatation is unsuccessful or who refuse to attempt the Frank/Ingram technique, surgical creation of a neovagina is the next step. There are multiple surgical techniques available for functional vagina substitute formation, with a variety of tissues used. These include using split thickness (Alessandrescu et al., 1996) and full thickness (Lee et al., 1999) skin grafts, buccal mucosa grafts (Lin et al., 2003), peritoneum (Ismail et al., 2006) and bowel (Hensle et al., 2006) substitution, and tissue expansion vaginoplasty (Chudacoff et al., 1996). A surgical modification of Frank's dilatation method has also been developed – the Vecchietti Method (Vecchietti, 1979). However, this review will concentrate predominantly on methods that involve tissue expansion.

#### 2.5.2.1 Vecchietti Technique

An alternative to Frank and Ingram's manual dilatation techniques, Vecchietti described a modified surgical approach (1979). The principle of the Vecchietti technique is to create a neovagina by gradual stretching of the patient's own vaginal skin. Instead of applying pressure on the perineum from below, it involves placing an olive-like bead onto the vaginal dimple, which is pulled upwards, causing a deep invagination into the vesicorectal space. The bead is held in place by threads that run from the perineum into the pelvis and out through the abdomen where they are attached to the traction device. Subsequently, the tension of the threads is adjusted daily or weekly until an adequate vaginal depth is reached. Following a Pfannenstiel incision, an

incision commonly performed for caesarean section procedures, the peritoneal reflection is incised between the rectum and bladder. An empty ligature carrier is passed transabdominally through the vesicorectal space, piercing the perineal pseudo-hymen. Once the olive bead has been secured, the threads are brought lateral to the rectus and through the skin to be attached to the traction apparatus secured to the skin (Veronikis et al., 1997). A vaginal depth of 10 to 12cm has been reported in 7 to 8 days, expansion of 1-1.5 cm per day. Patients were then encouraged to use vaginal dilators daily to maintain patency until satisfactory and regular sexual activity occurs (Vecchietti, 1979).

A laparoscopic version of Vecchietti's technique was described in 1994 (Fedele et al.) (Fig. 2.7). This method removed the laparotomy aspect of Vecchietti's procedure, resulting in shorter hospitalisation and convalescence. Patients are discharged 48-72 hours postoperatively and progressive traction is performed in outpatient departments every 48hours to adjust the tension of the traction sutures. The dilating olive and Vecchietti threads are removed once a neovagina, at least 7-8cm in length, has formed (Borruto et al., 1999, McQuillan and Grover, 2014). To maintain the neovagina dimensions, patients are instructed to insert a dilator for approximately 8-10 hours per day during the first month. After the first month of dilatation and the start of sexual activity, the period of time for using dilators shortened (Fedele et al., 1994).

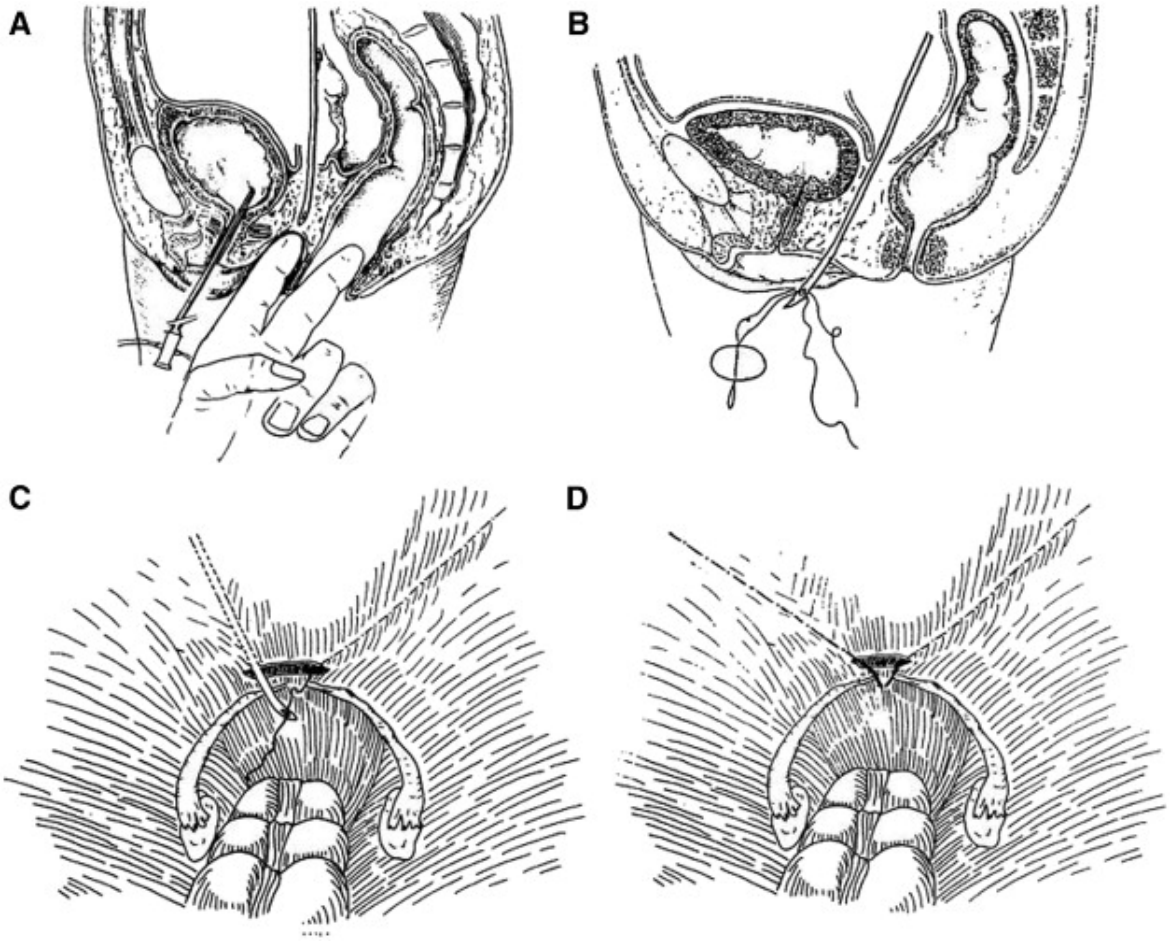


**Figure 2.7: Laparoscopic Vecchietti's Procedure** (Borruto et al., 2007, Fedele et al., 1994). **A**. Under direct vision, the Vecchietti straight thread-bearing cutting needle is introduced and passed subperitoneally until the presumed vesicorectal space is reached, noted by the probe or finger in the rectum and by the index finger to guide the needle between both fingers down through the non-existent vesicorectal space. **B**. The non-absorbable thread, attached to the olive-like bead, is hooked on the needle. **C**. One of the ancillary trocars is removed to allow for the extraction of the thread via the ipsilateral trocar hole. This procedure is repeated on the other side. **D**. Intraoperative view: the threads are tied to the traction device and the strength of tension graduated.

Anatomic success of the Vecchietti technique is defined as a neovagina greater then 6cm in length, allowing easy introduction of two fingers within 6 months after the corrective surgery. Functional success was confirmed if the patient reported satisfactory sexual intercourse, with low use of lubricating gel. At an average of 3 months after surgery, sexual intercourse was reported as

no longer painful or associated with discomfort. After 6 months of regular sexual activity, patients no longer required lubricating gel (Fedele et al., 1994).

Vaginoscopy showed a vaginal-type epithelium coating 80% of the newly formed vagina after 3 months. After 6 months post operation, >90% epithelial growth could be seen on the surface. The external genitalia are essentially normal with a small pouch that is a 1-4cm depth vagina.

Since described in 1994, the technique has been modified into a safer and simpler operation. Specifically, the original Vecchietti suture carrier passes through the vesicourethrorectal space only once, and the traction sutures have a shorter tract intraperitoneally, following a subperitoneal course all the way up to the abdominal wall. The Vecchietti traction device is less likely to cause discomfort, as it does not compress on a healing laparotomy incision. This can allow for increased traction and a quicker formation of the neovagina (Borruto et al., 2007). The adapted technique has reduced the operative time to ~45 minutes (Brucker et al., 2008).

In general, most literature only includes a small number of patients with a relatively short follow up. A study following 20 patients (Brun et al., 2002) showed a mean follow up time of 66 months. The average reported neovagina length was 7.8cm one month post operatively, there was no significant increase in length in patients with a longer follow up. All patients, with 94% stating adequate lubrication and one third complaining of dyspareunia, reported sexual desire and pleasure. The complication rate of the above technique, both laparotomy and laparoscopy, ranged from 5-22%, with satisfying results seen in 83-100% of cases. The most challenging step

appears to be the correct passage of the traction threads in order to avoid rectal and bladder perforation and avoiding the kinking of ureters with traction increase (Fedele et al., 1994).

Comparison of laparotomy and laparoscopy showed no significant difference in vaginal depth, complication rate or sexual satisfaction (Borruto et al., 1999). Patient age is the dominating factor when looking at the suitability of the Vecchietti technique. It is believed that older patients (over 30 years old) and those with perineal scarring may not be suitable due to tissue inelasticity. However, young patients (less than 18 years old) may be too immature and unwilling to persist with postoperative manual dilatation and regular sexual intercourse in order to maintain the neovagina (Brun et al., 2002).

#### 2.5.2.2 Labial Tissue Expansion Technique

Another technique that incorporates the expansion of gynaecological tissue to form a neovagina involves expanding the labia minora into pseudoscrota using injection inflated balloon tissue expanders (Lilford et al., 1989, Johnson et al., 1991). The extra skin is used to line a rectovesicular cavity. The expanders are inserted subcutaneously underneath and slightly medial to each labial minus via tunnelling under the skin, starting from bilateral groin incisions. The expanders are then inflated manually by the patients adding 5ml of saline each day. This continues until each expander contains 80ml, taking 3-5weeks to reach full expansion. During the expanding phase, the labia are checked for chafing, ischemia, and infection, a process that went from being an outpatient procedure to the hospitalisation of patients due to walking becoming difficult.

Once full expansion has been reached, the balloons are removed, under general anaesthesia, and the extra skin created is used to make skin flaps. Where possible, the flaps are created from the non-hair bearing skin on the inside of the labia minora. A rectovesical cavity is created via blunt dissection, lined by the skin flaps, and created into a pouch with a posterior vascular base. Depending on the patient's anatomy, various procedures are used to connect the newly created vagina to their gynaecological anatomy. In patients with haematocolpos, the pouch can remain 'open' at the top and skin flaps are attached to the remaining upper vaginal structure. In women with haematometra and cervical agenesis, the perineal skin flaps are sutured to the inside of the uterus. This procedure creates a long vagina lined with full thickness skin on a vascular pedicle.

The insertion of tissue expanders into the labia minor, an area close to the perineum and a highly contaminated environment, can become infected and then require removal. The hospitalisation required with the described procedure can be up to 2 months, an intrusive period. The patients hospitalised during expansion required counselling and support during their stay. The described surgical procedure had other complications, including damage to the rectum and bladder from the rectovesical space. Discharge from secondary to hair follicles with the vaginal pouch is another disadvantage but could be avoided by using none or lightly hair-bearing skin. This procedure produces a neovagina in the correct axis and of good length. The use if full thickness epithelium as the lining means that it will not contract and does not require dilatation.

#### 2.5.2.3 Abbe-McIndoe Technique

The Abbe-McIndoe technique is described as the use of a split-thickness skin graft and plastic stent placed in the space between the rectum and urethra. Abbe initially reported the use of the skin graft (1898), with McIndoe popularising the method with the introduction of tubularising the graft over a stent (McIndoe and Banister, 1938).

In short, the procedure involves a transverse incision in the perineum and the formation of a 10-12cm dissection into the vesicorectal space. A split thickness skin graft is then harvested from various sites, including the lower abdomen, thigh or buttocks, and placed around a mould. The graft and mould are then inserted into the created space. Patients are instructed to wear the mould continuously for 3-6 months and then maintain neovagina patency with the use of vaginal dilators and regular sexual intercourse (Seccia et al., 2002, Klingele et al., 2003).

A modification of the Abbe-McIndoe technique for the treatment of congenital absence of the vagina, used a cylindrical tissue expander wrapped in a mesh split-thickness skin graft, instead of a rigid silicone mould (Serra et al., 1993). The expander was kept in place for a period of two to six months, with the expander valve placed within the inner thigh. The six patients treated reported a functional result of 100%. The age range of the patients was 18 to 27 years, and the result was good or very good in five of the six women. Only one patient complained of occasional dyspareunia. This technique does not require any abdominal incision in order to produce a neovagina of adequate depth and diameter, providing the postoperative regime is followed (Seccia et al., 2002).

This method also removes the pain of progressive passive dilatation associated with the Vecchietti and non-operative technique.

However, the Abbe-McIndoe technique has the potential to undergo numerous complications. Some of these are characteristic of all vaginal surgeries, such as, vesicovaginal fistulas, rectal and/or bladder perforation, vaginal prolapse and haematoma formation. Inadequate lubrication leading to dyspareunia is another problem that can arise, as well as complications with the graft site, such as, infection and/or keloid scar formation. It has also been reported that some patients found the graft harvest site to be disfiguring. A high frequency of graft stenosis, requiring frequent and potentially lifelong dilatation, is the most overwhelming postoperative complication. The likelihood of this occurring is increased if the mould/expander is removed prematurely. When looking at the complications that arise from the described vaginoplasty techniques, they can be grouped into three forms of arising complications: intraoperative, immediate and long-term postoperative complications.

Naturally, there are no cases of intraoperative complications with the vaginal dilatation techniques. Urological injuries, including damage to the bladder and/or uterus and postoperative urinary retention, occurred most commonly with the Vecchietti method (Fedele et al., 2010). Postoperative bleeding is generally associated with procedures that involved the use of parts of the bowel to form a neovagina, with the requirement of blood transfusions, higher estimated blood loss and haematomas being reported (Cai et al., 2007, Khen-Dunlop et al., 2007).

Postoperative period complications occur with a variety of the vaginoplasty techniques. The success of the Abbe-McIndoe technique relies heavily on the integration of the graft tissue within the newly created vaginal canal and therefore risk of infection will affect the likelihood of a successful surgery (3-5% incidence of graft infection) (Alessandrescu et al., 1996). Unsuccessful attempts at this procedure have resulted in the need for scar revisions (from the graft harvest site), graft failure and dehiscence, requiring additional surgery to repair the initial graft or the implantation of newly harvested graft (Elkafrawi and Abdelal, 2013). Other complications have included vaginal hair growth, vaginal prolapse and even vaginal carcinomas, both squamous cell and adenocarcinoma (Steiner et al., 2002, Fedele et al., 2011). The growth of vaginal hair only occurred with the techniques that involved mobilisation of vulvar hair bearing areas within the vagina, such as the labia minor expansion techniques previously described. Neo-vaginal prolapse has been reported most frequently in sigmoidal vaginoplasties, but can also present in passive dilations, Frank and Ingram methods, and the techniques described above (Fedele et al., 2011). The possible vaginal carcinomas that arise with vaginoplasty surgery are method specific, with adenocarcinomas only occurring when parts of the bowel are used to form a neovagina (Kokcu et al., 2011). Squamous cell carcinomas have occurred most frequently in Abbe-McIndoe graft and tissue expansion technique (Hopkins and Morley, 1987). The fact that this technique has the longest patient follow up reported (up to 50 years) may be a contributing factor to this frequency. There have also been reports of human papilloma virus (HPV) lesions found in patients that

underwent Vecchietti vaginoplasty, in both the vulva and neovagina itself (Frega et al., 2011).

## 2.6 Aetiology of Anorectal Malformations

In normal embryological development of the human foetus, the anorectal and urogenital systems arise from the common cloaca, defined as a small cavity at the posterior end of the endoderm lined gut tube, surrounded by mesenchyme derived from splanchnopleuric mesoderm. Complete development results in septation of the cloaca and development of the multiple compartments; anal canal, rectum, vagina, urinary bladder and urethra. ARMs are one of the most common abnormalities of the digestive system; they occur due to disrupted embryonic development in the hindgut at 4-8 weeks gestation. The precise embryology of the irregular anorectal development is still unclear (Kluth, 2010).

### 2.6.1 Genetic Risk Factors of Anorectal Malformations

In around 10% of patients, ARM develops due to a chromosomal disorder or a single mutation causing syndrome (Cuschieri, 2002). Evaluation of several chromosomal abnormalities described in patients with ARMs included 13q depletion, cat eye syndrome and trisomy 13, 18 and 21, Patau syndrome, Edwards syndrome and Down syndrome respectively (Kohlhase et al., 1998, Ross et al., 1998, Marcelis et al., 2011). These loci predispose for ARM, but it is unclear whether the genes in these regions cause syndromic or nonsyndromic ARM. Syndromic ARM is most frequently connected with Currarino syndrome (HLBX9 mutation causing anal/rectal atresia and other related abnormalities), Pallister-Hall syndrome (Gli3 mutation causing polydactyl, cutaneous syndactyly and malformations of the airways) and

Townes-Brocks syndrome (SALL1 mutation causing abnormalities of the external ear, renal system and heart). All these syndromes are inherited in an autosomal dominant pattern.

Aetiology of nonsyndromic ARM in not entirely known, but is believed to be multifactorial, concerning both genetic and non-genetic risk factors. Only 2-8% of patients with ARM have an affected first- or second-degree relative (Stephens and Smith, 1986, Forrester and Merz, 2002, Falcone et al., 2007, Stoll et al., 2007, Van Rooij et al., 2009, Wijers et al., 2010). However, it seems that ARM occurs more often among family members than expected, should the malformations arise by chance (Lie et al., 2001, Øyen et al., 2009, Van Rooij et al., 2009, Wijers et al., 2010). Genetic studies on the aetiology of nonsyndromic ARM are few and far between, with most studies focusing on the screening for specific genes in ARM cases, looking for casual mutation or genetic polymorphisms.

The wide spectrum of anomalies, as described in the Krickenbeck classification (Holschneider et al., 2005), are most likely consequences from the timing of embryological development disruption. ARM is generally accompanied by one or more other congenital malformations in up to 70% of patients (Hassink et al., 1996). Most of these malformations are characterized under the VACTERL (Vertebral, Anal, Cardiac, Tracheo-Esophageal, Renal and limb defects) abbreviation. The precise aetiology of the development arrest is not entirely known, but studies have indicated that the pathogenesis results from complications in signalling pathways such as; sonic hedgehog (Shh), wingless-type integration site (WNT), fibroblast growth factor (FGF) and bone morphogenetic protein (BMP) (Wijers, 2016) as opposed to teratogenic

or hereditary causes. These mediators of embryonic development are initiated via paracrine signalling. This is a short-range form of signalling that does not require cell-to-cell contact. The secreted messenger molecules reach local targets via diffusion; they bind rapidly to cells in proximity. These molecules can be immobilised by extracellular matrixes, ensuring that their effects are restricted (Gilbert, 2010).

**Induction Cell Signalling**

Induction cell signalling describes a process by which transmitted signals can impact the developmental fate of other cell types. There are two types of induction: instructive and permissive. Instructive induction refers to cells following a particular developmental pathway in response to given signals, however the cells will embark on a different developmental pathway in the absence of these signals. Permissive induction occurs when the responding cell is already committed to a specific developmental pathway, but requires additional signalling to continue along or complete that pathway (Holtzer, 1968).

During induction, the signals that a cell receives are dependent on its microenvironment during embryonic development, this is in addition to the cells 'competence' to receive, interpret and respond to appropriate signals. A cells competence is defined by the cells ability to respond to certain inductive signals. In terms of paracrine signalling, a competent cell must have the capacity to respond to the original signal in the suitable manner. The competent cell must have receptors capable of binding to signalling molecules, this is in addition to intra-cellular transduction apparatus proficiency in forming

a link with the final intra-cellular target. For example, the activation of individual genes or sets of genes by transcription factors. Cells induced by neighbouring cells, via cell-to-cell signalling, may become incompetent by breaking contact with the inducing cell, a consequence of cellular migration (McGeady et al., 2006c).

#### 2.6.1.1 Sonic Hedgehog

The hedgehog (Hh) family consists of an array of secreted proteins, all of which play an essential role in metazoan development. Hedgehog signals can function differently in different contexts. They can regulate cell fate specification, cell proliferation and cell survival. Their signalling can be short or long range, direct or indirect, as well as concentration dependent. Defects in any of the Hh signalling pathways can lead to congenital abnormalities, like holoprosencephaly (abnormal forebrain development) and certain forms of cancer. The significance of Hh throughout embryogenesis was first discovered in 1980 by Nüsslein-Volhard and Wieschaus (Nusslein-Volhard and Wieschaus, 1980), during a genetic screening for mutations that disrupt larval patterns in Drosophila melanogaster.

Drosophila only contain a single Hh gene, whereas the mammalian genome encodes for three Hh ligands; dessert hedgehog (Dhh), Indian Hedgehog (Ihh) and sonic hedgehog (Shh), all of which stimulate the vertebrate Hh pathway in a similar fashion. Shh is the most widely expressed of the signalling pathways and much of what is known about Hh signalling is derived from Shh studies. The cellular response to hedgehog protein is controlled by two

transmembrane proteins: Smoothened (Smo) and Patched (Ptch1, an inhibitor of Smo). When hedgehog protein binds to a Ptch1 receptor, a conformational change is induced in the receptor, preventing the inhibition of the Smo transmembrane protein. Subsequently, the Smo protein releases Cubitus interruptus (Ci) protein from microtubules, the addition of phosphate groups to Costal (Cos) and fused proteins breaks the complex binding Ci protein to the microtubules. The Smo protein also inactivates Slimb and PKA proteins, both of which cleave Ci protein, changing it into a transcriptional repressor. In the absence of Slimb and PKA, the Ci protein remains intact and acts as a transcriptional activator for hedgehog responsive genes (Fig. 2.8).

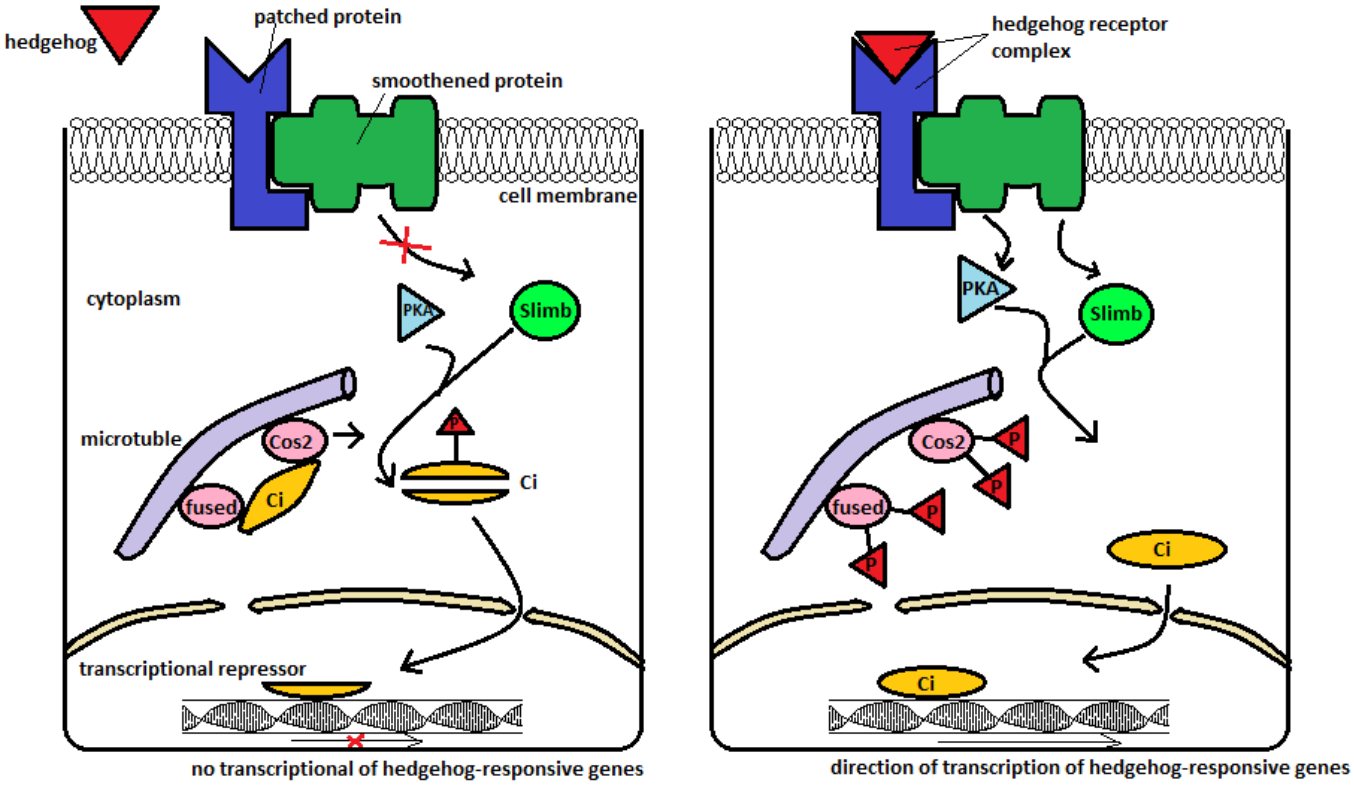


**Figure 2.8: The Cellular Response to Hedgehog Protein** (McGeady et al., 2006b).

Shh functions as a morphogen (governing the pattern of tissue development and establishing positions of various specialised cell types), mitogen (triggering signal transduction pathways involving mitogen-activated protein kinase, leading to mitosis) and survival factor to regulate the development and patterning of many tissues in the vertebrate embryo.

Expression of Shh has been detected in the primitive notochord and throughout the notochord, in the floor plate of the neutral tube, early gut endoderm and in the limb buds. Shh has a range of roles throughout embryological development and continuing after birth (Ahlgren and Bronner-Fraser, 1999, Locker et al., 2006). In the embryonic neural tube, floor plate derived Shh promotes the proliferation, survival, and specification of neural progenitors (Rowitch et al., 1999). Shh arising from the zone of proliferation (ZPA) of the limb bud regulates digit formation and specification in the embryonic limb and in the developing foregut, endoderm derived Shh provides instructional prompts to surrounding mesoderm, resulting in correct development of the gastrointestinal tract and lungs. Post-partum, Purkinje cell derived Shh is vital for granule cell precursor proliferation in the developing cerebellum. Even in the adult, Shh is required to maintain stem cell populations in the brain and epithelium (Varjosalo and Taipale, 2008). Shh is expressed in the cloacal endoderm and has functions in both early and late embryogenesis, these influence development of anorectal and urogenital development (Seifert et al., 2009). Defects in Shh signal pathway have been associated with numerous congenital abnormalities, including tracheal-oesophageal fistula, polydactyl and evidently anorectal malformations. This shows the importance of the Shh signalling in normal embryological development.

While loss of Shh signalling leads to the complications described, increased pathway activation has been associated with some forms of cancer. Somatic mutations in the Shh receptor, Ptch1, and a potent inhibitor of the pathway are observed in almost all cases of basal cell carcinoma, a common skin cancer. Likewise, inactivating mutations in Ptch1 or activation of smoothened (SMO), a downstream protein in the pathway, is observed in a subset of medulloblastomas, a malignant tumour of the cerebellum, the most common paediatric brain tumour. Some cancers, such as pancreatic ductal adenocarcinoma, display paracrine Shh signalling, whereby the tumour cells secrete Shh into the surrounding stroma and influence the tumour microenvironment (Boylston and Brenner, 2012).

To determine the role of Shh in foetal hindgut development, Mo et al. (2001) used mutant mice with varying defects in the Shh signalling pathway to mimic the anorectal malformations found in humans. This study is one of the first to determine one of the specific genetic pathways capable of producing the broad spectrum of anorectal malformations that are found in humans. The foetal mice underwent SEM, light microscopy and histological analysis. Shh null mice showed a persistent cloaca, with the lower urinary tract and anorectum sharing a common outlet. Mice that lacked Gli2 or Gli3, zinc related transcription factors involved in Shh signalling, exhibited imperforate anuses, recto-urethral fistulas and anal stenosis. The results produced by the study showed that Shh signalling is essential for the development of the distal hindgut and that mutations in Shh and its downstream mediators, Gil2 and Gil3, results in a wide range of anorectal malformations (Fig. 2.9). The study also showed that varying gene doses of Gil2 and Gil3 controlled the severity of malformations

seen in the mice, meaning that a very precise level of Shh signalling is required during embryogenesis for normal development of the rectum and anus.

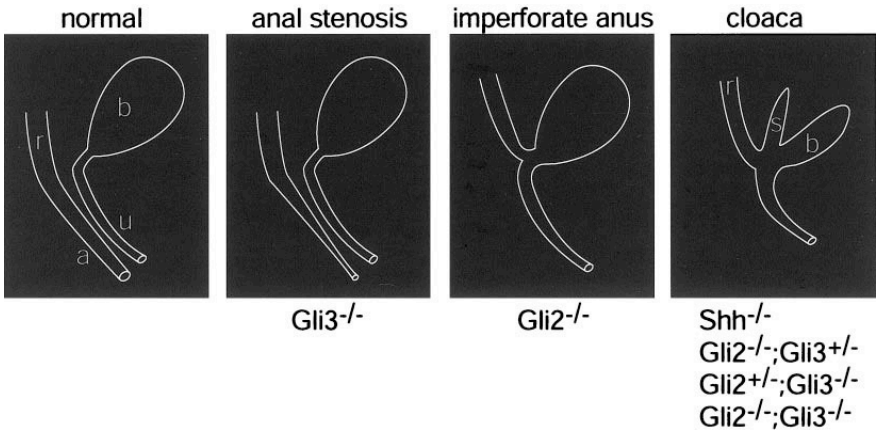


**Figure 2.9: The role of Shh in foetal hindgut development,** (Mo et al., 2001). The results produced by the study showed that Shh signalling is essential for the development of the distal hindgut and that mutations in Shh and its downstream mediators, Gil2 and Gil3, results in a wide range of anorectal malformations.

Other studies that have involved Shh mutant mice have shown that the animals in the study showed malformation from all aspects of the spectrum seen in human patients (Kim et al., 2001, Mo et al., 2001, Haraguchi et al., 2007, Lin et al., 2009, Seifert et al., 2009). However, there have been studies that have shown significantly lower Shh, Gil2 and BMP4 expression in the posterior wall of the terminal rectum in patients with ARM when compared with controls (Zhang et al., 2009), but two studies with 15 and 88 patients, showed no relevant functional mutations in Shh and Gil3 (Seri et al., 1999, Garcia-Barceló et al., 2008). Single-nucleotide polymorphisms (SNPs) at predicted regulatory sites in the Shh pathway, including Gil2 and BMP4 were suggested to be associated with isolated ARM (Carter et al., 2013). These associations were no longer present after adjusting for multiple testing. The lack of replicated findings could be explained by small sample sizes, inclusion of

different phenotypes of ARM, or possible mutations in surrounding regulatory DNA elements or in upstream components of the same pathway.

#### 2.6.1.2 Fibroblast Growth Factor

The fibroblast growth factor (FGF) family consists of more than 20 structurally related proteins. These proteins are multifunctional and are alternatively referred to as ‘pluripotent’ and/or ‘promiscuous’ growth factors due to the variety of actions on multiple cell types (Green et al., 1996). Members of the FGF family can activate the fibroblast growth factor receptors of the tyrosine kinase class. Receptor tyrosine kinases are proteins that protrude through the cell membrane.

The ligand binding aspect of the protein is on the extracellular side of the cell membrane, with the dormant tyrosine kinase on the intracellular side. Tyrosine kinase is an enzyme with the ability to phosphorylate target proteins. When FGF binds to the extracellular receptor, the dormant tyrosine kinase is activated and in turn, phosphorylates internal proteins (Fig. 2.10). This leads to the activation of target proteins, allowing them to perform new functions within the cell (McGeady et al., 2006b).

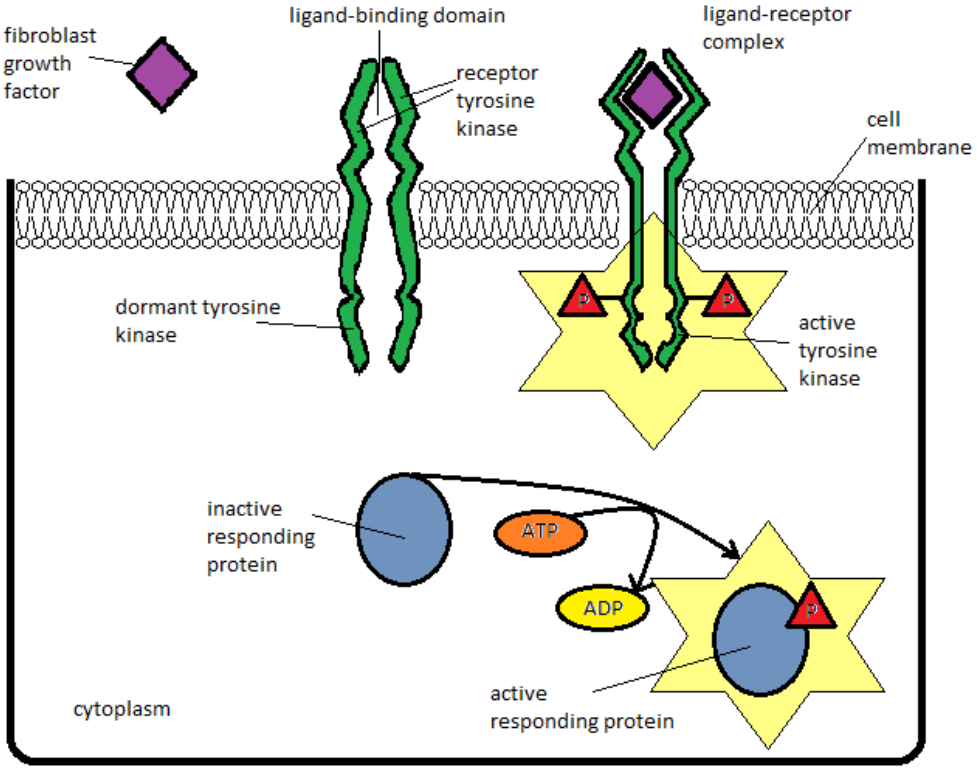


**Figure 2.10: The Cellular Response to Fibroblast Growth Factor** (McGeady et al., 2006b).

The function of FGF is dependent on the signal pathway between the FGF family and their receptors. Many studies have reported that FGFs have functions such as cell proliferation, migration, differentiation and even angiogenesis in some cells and tissues.

| Function | Subfamily related to function | Target Cell |
|---|---|---|
| **Cell Proliferation** | FGF1, FGF2 | Preadipocyte Endothelial cell, epithelial cell, fibroblast cell, neural stem cell |
| | FGF4 | Trophoblast stem cell |
| | FGF7, FGF10 | Epithelial cell |
| | FGF18 | Osteoblast, chondrocytes, osteoclast |
| **Cell Migration** | FGF2 | Astrocyte, myogenic cells |
| | FGF4 | Myogenic cell |
| | FGF7 | Epithelial cell, keratinocyte |
| | FGF8 | Neural crest cell |
| **Cell Differentiation** | FGF1, FGF2 | Neuroepithelial |
| | FGF7 | Keratinocyte |
| | FGF20 | Monkey stem cell |
| **Angiogenesis** | FGF1, FGF2 | Endothelial cell |

**Table 2.3: Fibroblast Growth Factors: Biology, Function and Application for tissue Regeneration** (Yun et al., 2010).

Cell proliferation by FGFs has been reported in many cell types, including endothelial cells, epithelial cells, and stem cells (both neural and trophoblast). FGF1 is a proliferative factor for human preadipocytes that contribute to the regulation of human adipogenesis (Widberg et al., 2009). However FGFs are also involved in pathogenic mechanisms, FGF10 plays a role in the pathogenesis of prostate cancer by facilitating epithelial proliferation (Thomson and Cunha, 1999). Fibroblast growth factors have to ability to stimulate both normal cell and cancer cell proliferation.

Cell migration is an essential process in the development and maintenance of multicellular organisms. Embryonic development relies on the coordinated movement of cells in particular direction to specific locations. Cell migration of FGFs varies within the subfamilies. FGF2 and FGF4 stimulate cell migration of mouse embryonic limb myogenic cells (Webb et al., 1997) and FGF8 is a potent chemoattractant in the migration of mesencephalic neural crest cells (Kubota and Ito, 2000). Cellular differentiation occurs numerous times during the development of multicellular organisms as they progress from a single zygote to a complex of various tissues and cell types. As with cell migration, cell differentiation varies within FGF subfamilies. FGF2 stimulates the differentiation of neuroepithelial cells into mature neurons and glia (Murphy et al., 1990).

Angiogenesis is the process by which new blood vessels are formed from pre-existing blood vessels, a process that plays a key role in both physiological and pathological conditions including, embryonic development, inflammation and tumour growth (Carmeliet and Jain, 2000). Angiogenesis is a multistage process that begins with the degradation of the basement membrane by activated endothelial cells that migrate and proliferate, this leads to the formation of solid endothelial sprouts into the stromal space. Then, vascular loops are formed and capillary tubes develop with the formation of tight junctions and deposition of new basement membrane (Carmeliet, 2000). FGF1 and FGF2 induce the promotion of endothelial cell proliferation and the physical organisation of endothelial cells into tube-like structures, promoting angiogenesis (Javerzat et al., 2002).

#### 2.6.1.3 Wingless Family

The Wingless (Wnt) gene family consists of structurally related genes encoding cysteine-rich secreted glycoproteins, which act as extra-cellular signalling factors. Wnt genes are involved in a wide variety of biological processes, including cell fate determination. Like Shh, these genes can influence the body plan early in embryological development as well as postnatal cell growth and differentiation.

Members of the Wnt family paracrinally react with transmembrane receptors that are members of the frizzled proteins family. In most cases, binding of a Wnt signalling factor to a frizzled protein results in the activation of dishevelled protein. Activated dishevelled protein inhibits glycogen-synthase-kinase-3 enzyme (GSK-3) activity. Functional GSK-3 inhibits the dissociation of β-catenin from adenomatous polyposis coli protein (APC). Inhibited GSK-3 allows β-catenin to dissociate from APC and enter the nucleus of the cell. Once in the cell, β-catenin can form complexes with DNA-binding proteins LEF or TCF. Following binding, these complexes become active transcription factors, capable of activating Wnt-responsive genes (Fig. 2.11) (McGeady et al., 2006b).

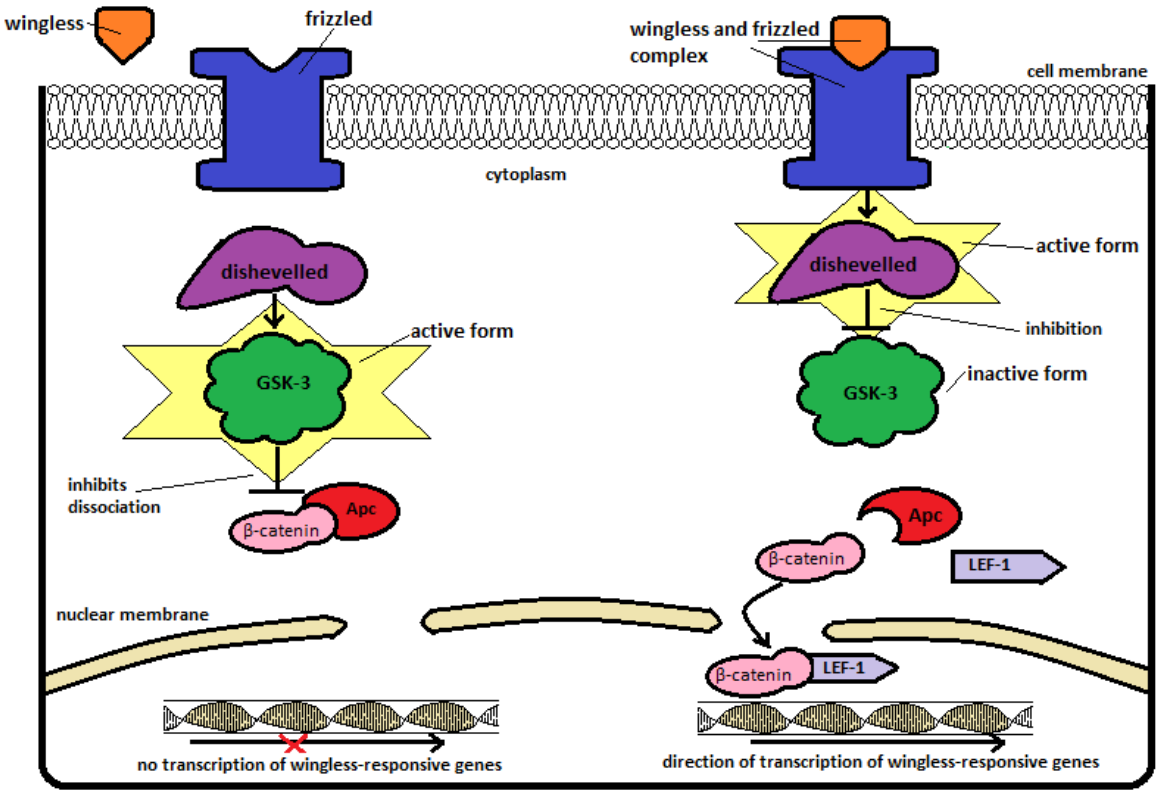


**Figure 2.11: The Cellular Response to Wingless Signalling Proteins** (McGeady et al., 2006b).

Wnt signalling was first identified for its role in carcinogenesis, then for its function in embryonic development. The embryonic processes it controls include body axis patterning, cell fate specification, cell proliferation and migration. This was discovered when genetic mutations in Wnt pathways produced abnormal fruit fly embryos. The signals also control tissue regeneration in adult bone marrow, skin and intestine (Goessling et al., 2009).

Wnt signalling is involved in the axis formation of specific body parts and organ systems later in development. In vertebrates, both sonic hedgehog and wingless morphogenetic signalling gradients establish the dorso-ventral axis

of the central nervous system during neutral tube axis patterning. High Wnt signalling establishes the dorsal region and high Shh signalling indicates the ventral region (Ulloa and Martí, 2010).

#### 2.6.1.4 Cell Signalling

There are multiple methods of cell signalling that impact on the embryological development of the cloaca into the individual anorectal and urogenital systems. Paracrine factors that mediate cross communication between the mesenchyme and epithelium are vital for normal development. An example of this is the asymmetrical expression of transcription factors Six1 and Six2 in the mesenchyme that surrounds the embryonic cloaca. These transcription factors are required for normal urogenital tract formation, mainly the septation of the cloaca (Wang et al., 2011). The asymmetrical expression creates unbalanced growth of the mesenchyme, aiding in the formation of the septum of the cloaca (Wang et al., 2013). The morphogenetic movement described here is also seen in the formation of the urorectal septum, where BMP7 promotes cell proliferation and survival of embryological cloacal endoderm (Wu et al., 2009).

Cell-cell adhesion is another form of cell signalling that is important during the migration of cells, promoting cloacal septation. The Eph family of receptor tyrosine kinase and their corresponding ligands are essential in cell adhesion. One study has shown that mice with mutations for these signalling genes develop hypospadias and incomplete cloacal septation (Dravis et al., 2004). This shows that the bidirectional signalling that these proteins mediate has a very important role in the normal formation of the anorectal and urogenital

organs. Another aspect of cell signalling that influences the septation of the embryonic cloaca is asymmetric cell division, a process by which the mitotic spindle of the cell nucleus orientates perpendicularly to the basement membrane (Roegiers and Jan, 2004). In some epithelia, for example the skin, asymmetric cell division is needed to ensure proper columnar stratification, differentiation, and tissue organisation (Lechler and Fuchs, 2005). A de novo duplication of a WNT signalling pathway inhibitor (DKK4) was identified in an ARM patient and a deletion in the inturned planar cell polarity effector homolog (INTU) gene in two ARM patients (Cherny et al., 2012). It is uncertain whether the deletion in the INTU gene was inherited from unaffected parents or a de novo mutation.

### 2.6.2 Nongenetic Risk Factors of Anorectal Malformations

The other aetiological aspect of ARM to consider is the potential non-genetic risk factors, such as environmental factors, fertility treatments and lifestyle factors.

#### 2.6.2.1 Facilitated Reproduction

One of the main nongenetic risk factors is assisted reproduction. Several studies have shown a highly increased risk estimates that range from 2.3 to 13.3 (Robert and Francannet, 1996, Källén et al., 2005, Midrio et al., 2006, Reefhuis et al., 2009, Zwink et al., 2012), with the highest risks being observed in studies that compared parent personal interviews with register-based control data (Midrio et al., 2006, Zwink et al., 2012). The effect of facilitated reproduction appeared far less in multiple births than in singletons (Reefhuis et al., 2009, Zwink et al., 2012), this appeared to be similar for various manifestations of ARM, including isolated incidences of ARM and ARM associated with other VACTERL malformations (Zwink et al., 2012).

Other studies have shown minimal or no correlation between ARM and assisted reproduction (Källén et al., 2005, Van Rooij et al., 2009, Reefhuis et al., 2011, Wijers et al., 2013). The study by Källén et al. (2005), combined several aspects of previous studies using datasets from previous time periods, hypothesizing that the risk associated with facilitated reproduction may have been randomly low or have reduced over time. The second study suffered from a specific exposure assessment (Van Rooij et al., 2009) and the third

concentrated specifically on the effect of clomiphene citrate (Reefhuis et al., 2011); a common hormonal treatment for ovulation induction. Other studies have shown a connection between ARM and ovulation induction (Robert and Francannet, 1996, Wijers et al., 2013). One study looked into parental subfertility, but only showed an association between paternal subfertility and ARM, not maternal (Van Rooij et al., 2009). This association was mainly found in fathers of ARM-VACTERL patients, whom a five-fold increased risk of ARM had been shown. The same study showed a prolonged time-to-pregnancy for parents of patients with ARM, compared to controls. There have been studies looking into the associations between ARM and common methods of contraception, including male condoms, spermicides, oral contraceptives and intrauterine devices (Stoll et al., 1997, Gallaway et al., 2009, Waller et al., 2010). However, no correlation was found.

#### 2.6.2.2 Parental Characteristics

Parental characteristics, such as maternal and paternal age, may contribute to the occurrence congenital malformations. This can be due to a biological factor, such as ovarian age or mutations in sperm, or a non-biological factor, such as a lifestyle change. Yet, most studies have shown that a higher parental age at time of conception does not increase the risk of ARM (Harris et al., 1995, Stoll et al., 1997, Forrester and Merz, 2002, Kazaura et al., 2004, Yang et al., 2007, Materna-Kiryluk et al., 2009, Van Rooij et al., 2009, Gill et al., 2012, Carter et al., 2013). Two studies that showed a correlation between ARM and higher paternal ages (Hay and Barbano, 1972, Myers et al., 2001).

There is a mix of studies looking at the relationship between maternal parity (number of pregnancies carried to full term) and risk of ARM. Some have shown that there is an increased risk of a child from a first pregnancy having ARM (Harris et al., 1995, Van Rooij et al., 2009, Duong et al., 2012, Carter et al., 2013, Wijers et al., 2013), with an equal number of studies showing no associations (Hay and Barbano, 1972, Stoll et al., 1997, Forrester and Merz, 2002, Miller et al., 2009).

Apart from three studies (Harris et al., 1995, Duong et al., 2012, Wijers et al., 2013), ARM was consistently found to occur more frequently in multiple compared to singletons (Forrester and Merz, 2002, Miller et al., 2009, Zhang et al., 2011, Zwink et al., 2012, Källén, 2014). These results were not adjusted for confounders, such as use of assisted reproduction, in any of the studies referenced.

Associations have been made between ARM and low birth weights and preterm delivery, with relatively consistent reports (Mili et al., 1991, Stoll et al., 1997, Rasmussen et al., 2001, Forrester and Merz, 2002, Miller et al., 2009, Van Rooij et al., 2009). It is very likely that these factors share a common pathway with congenital ARM but unlikely that they are causal of the abnormalities. A select few maternal health issues that complicate pregnancies in relation to risks of ARM have been explored, with maternal obesity being the main factor. A collation of papers showed that mothers that are overweight (25<body mass index [BMI]>30kg/$m^2$) or obese (BMI≥30kg/$m^2$) before pregnancy, had an increased risk of ARM offspring (Waller et al., 2007, Miller et al., 2009, Van Rooij et al., 2009, Blomberg and Källén, 2010), with one study showing an elevated risk of isolated ARM separately among obese

mothers (Waller et al., 2007). There have been no reports observing an associated between ARM and underweight mothers.

Researchers found there to be an increased risk of ARM in mothers with pre-existing diabetes mellitus (Stoll et al., 1997, Correa et al., 2003, Frías et al., 2007, Correa et al., 2008, Correa et al., 2012). Some studies do not confirm these results (Martínez-Frías, 1994, Bánhidy et al., 2010a, Garne et al., 2012, Wijers et al., 2013), but this may be due to a lack of power or the use of children with other congenital abnormalities as controls. It is known that pre-existing diabetes is a strong risk factor for many congenital abnormalities and so the use of these controls may have led to an underestimation of the effect of diabetes.

Most studies were unable to show an obvious association between ARM and gestational diabetes (Martínez-Frías, 1994, Frías et al., 2007, Bánhidy et al., 2010a, Carter et al., 2013), apart from (Correa et al., 2008). However, this was only the case when isolated ARM was looked at. Gestational diabetes usually develops after the critical period for ARM development and so any positive correlations may be due to undiagnosed pre-existing diabetes in the mother. It has been hypothesised that overweight/obesity and diabetes mellitus may be factors in the same causal pathway for ARM, in that alternations between glycaemic control and hyperglycaemia my increase the risk of ARM (Waller et al., 2007). Correlations between ARM and high dietary glycaemic intake among non-diabetic mothers strengthens this indication (Yazdy et al., 2011, Parker et al., 2012). Studies on pre-pregnancy BMI excluded mothers with pre-existing diabetes and still resulted in an association between ARM and overweight and/or obesity (Waller et al., 2007, Blomberg and Källén, 2010).

However, mothers with undetected or subclinical diabetes were included in the study, this may have influenced the outcome.

It is reported that the risk of ARM increases significantly (95%) when mothers with diabetes mellitus did not take multivitamins containing folic acid during the critical period of ARM development (Correa et al., 2012). In this study, the critical period or ARM development consists of the month before conception and the first three months of pregnancy. Other possible pregnancy complications and their associations with ARM have not been studied as extensively. Studies showed that chronic hypertension during pregnancy and the drugs taken to manage it has little impact on the risk of ARM (Stoll et al., 2007, Miller et al., 2009, Banhidy et al., 2011). Preeclampsia is shown to have no association with ARM (Bánhidy et al., 2012, Wijers et al., 2013), but has been reported to be related to other congenital abnormalities (Wijers et al., 2013). Common colds, maternal influenza and acute respiratory infections during the second and third month of pregnancy did not appear to increase the risk of ARM, but these results are from individual studies (Stoll et al., 1997, Ács et al., 2005, Ács et al., 2006a, Ács et al., 2006b). Stoll's study found no association between ARM and maternal fever during the critical period of development, but other studies showed an increase in risk of ARM for mothers who contracted a fever in the first trimester of pregnancy (Van Rooij et al., 2009, Wijers et al., 2010, Wijers et al., 2013), mainly with ARM and other congenital abnormalities.

#### 2.6.2.3 Maternal Medication

The use of various therapeutic drugs during pregnancy and their association with the risk of ARM were investigated in many studies. Drugs such as antimicrobials or antibiotics (Czeizel et al., 2001b, Czeizel et al., 2001c, Crider et al., 2009), antipyretics and analgesics (Czeizel et al., 2000, Feldkamp et al., 2010, Broussard et al., 2011, van Gelder et al., 2011), antihistamines (Gilboa et al., 2009), antidepressants (Alwan et al., 2007, Källén and Olausson, 2007, Reis and Källén, 2010), hypotension medication (Bánhidy et al., 2010b), decongestants (Yau et al., 2013) and barbiturates (Browne et al., 2014) did not seem to have an association with an increased risk in ARM, it is important to bear in mind that separate medical drugs were mostly only evaluated in one study. It appears that the maternal use of opioid analgesics during the early stages of pregnancy increased the risk of ARMS, mainly for isolated cases (Broussard et al., 2011). There were inconsistent results for the use of antifungals, antimicrobials, and the increased risk of ARM, with miconazole and metronidazole showing a positive association (Czeizel and Rockenbauer, 1998, Kazy et al., 2005), but other antifungal drugs did not (Czeizel et al., 1999, Carter et al., 2008).

The most investigated therapeutic drugs were benzodiazepines and other similar psychotic drugs. This is especially the case for the Hungarian Case-Control Surveillance of Congenital Anomalies (Czeizel et al., 2001a). Increased risk of ARM was observed with the maternal use of various or combinations of benzodiazepines during the critical period of foetal development in three studies (Bonnot et al., 2001, Eros et al., 2002, Czeizel et al., 2003), but some studies contradicted this finding (Czeizel et al., 2004,

Kjær et al., 2007). However, it should be noted that one of the studies, (Kjær et al., 2007), combined benzodiazepines and other psychotic drugs in one exposure group, it is possible that drug-drug interactions altered the effect of the benzodiazepines on the foetal development. The findings in the studies cannot be deemed completely reliable as the information obtained was mainly from hospital records or retrospective collection through interviews or questionnaires, a method that is prone to recall problems and underreporting. It is difficult to determine whether the therapeutic medication or the underlying disease it was prescribed for are involved in the aetiology of ARM.

#### 2.6.2.4 Parental Lifestyle

The final branch of nongenetic risk factors of ARM are the occupational and lifestyle factors of parents. Although parental occupational exposures have not been studied at great length, it is reported that mothers prenatally exposed to industrial cleaning agents and solvents whilst working as cleaners etc. appeared to have an increased risk in giving birth to a child with ARM or other congenital malformations (Van Rooij et al., 2009, Herdt-Losavio et al., 2010, Wijers et al., 2010, Lin et al., 2013). One of the studies also showed an increase in risk of ARM offspring for mothers employed as scientists during pregnancy (Herdt-Losavio et al., 2010). Other maternal occupational exposures did not appear to be associated with ARM.

Paternal occupations that involved exposure to exhaust fumes showed indications of an elevated risk in ARM (Schnitzer et al., 1995, Van Rooij et al., 2009), but a replication study did not agree with these results (Wijers et al.,

2010). Single studies showed possible increases in risk of ARM in fathers working as artists, guards, printers, policemen and vehicle manufacturers (Schnitzer et al., 1995, Desrosiers et al., 2012), but the statistical significance could be questioned. For many other exposures and jobs among fathers no obvious correlations were seen (Schnitzer et al., 1995, Van Rooij et al., 2009, Desrosiers et al., 2012). Maternal smoking was not associated with ARM in most studies (Shiono et al., 1986, Eeden et al., 1990, Yuan et al., 1995, Stoll et al., 1997, Honein et al., 2001, Van Rooij et al., 2009) and only three showed a slight correlation (Källén, 2000, Miller et al., 2009, Carter et al., 2013). Paternal smoking and/or exposure to environmental tobacco smoke at embryogenesis was seen to be associated with ARM in two studies (Miller et al., 2009, Van Rooij et al., 2009), however two other studies counteracted the research (Yuan et al., 1995, Wijers et al., 2010). Neither parental alcohol consumption nor maternal illegal drug use, such as cannabis, cocaine or other similar stimulants, used during pregnancy were found to be associated with the aetiology of ARM (Yuan et al., 1995, Stoll et al., 1997, Miller et al., 2009, van Gelder et al., 2009, Van Rooij et al., 2009). However, maternal caffeine intake, of over 300mg/day, has been associated with an increased risk of ARM (Miller et al., 2009).

Three out of five studies investigating the effect of folic acid use on ARM aetiology showed a reduced risk, though the results were only marginally statistically significant (Czeizel et al., 1996, Myers et al., 2001, Källén, 2007, Van Rooij et al., 2009, Correa et al., 2012). The results of maternal multivitamin use during the critical period of embryogenesis showed to have no effect (Correa et al., 2003) or even an adverse effect in increasing ARM

risk (Van Rooij et al., 2009). Living in rural or suburban areas appears to have no effect on the risk of ARM (Stoll et al., 2007), although one study in South America showed an increased prevalence in ARM births at high altitudes (Castilla et al., 1999).

In summary, the results from the above studies are generally inconsistent when focusing on the aetiology of ARM. Many of the studies were singular, with no repeated studies to support the reports and were limited by the sample size, due to the rather rare occurrence or ARM.

### 2.6.3 Nature or Nurture?

The precise aetiology of nonsyndromic ARM in still not completely known, but the above literature shows that both genetic and nongenetic factors are involved. ARM includes both monogenic and multifactorial forms, the proportion of each form can only be speculated due to the lack of genetic research on ARM specifically. With most genetic studies being based on a candidate gene approach and multiple studies contradicting one another, the exact genetic aetiology is not yet determined. Potential copy number variations (CNVs), the number of copies of a particular gene that varies from one individual to the next, have aided in determining the aetiology of heritable ARM, but information on de novo occurrences is lacking.

Multiple nongenetic factors have been studied, but only a few appear to have a significance to ARM; assisted reproduction, multiple pregnancy, maternal obesity and pre-existing diabetes. However, the true causal factors behind these are unknown.

The studies on these factors showed that they are not exclusive to ARM and have been associated with other congenital malformations, such as neural tube defects, hypospadias and cardiac defects. This suggests an element of nonspecificity of the discussed nongenetic factors, as the timing of exposure during embryogenesis is not necessarily relevant, particularly with assisted reproduction.

## 2.7 Tissue Expanders

The concept of tissue expansion for surgical reconstruction was first reported in 1957 (Neumann), but the technique did not gain popular acceptance until the 1980s when it was used predominantly in delayed breast reconstruction (Radovan, 1982, Bostwick, 1988, Lejour, 1989). Tissue expansion is a common surgical procedure used to grow extra skin through controlled mechanical overstretch. It creates skin that matches the colour, texture, and thickness of the surrounding tissue and allows for the retention of specialised structures such as sweat glands or hair follicles (Argenta, 1984, Sasaki, 1988, Zöllner et al., 2012). Skin stretched beyond its physiological limit, activates mechanotransduction pathways. This leads to cell growth as well as to the formation of new cells (Neumann, 1957).

Although the origin of the additional skin produced during expansion is ambiguous, it arises from four certain factors, (Austad et al., 1986, Austad, 1987, van Rappard et al., 1988):

- the recruitment of adjacent tissue which is then drawn centrally with expander inflation
- acute and chronic stretching of the overlying skin and tissues with accompanying stress relaxation or ‘mechanical creep’ (Hirshowitz et al., 1986, Shuter et al., 1994)
- redistribution of locally expanded skin and cell division
- the de novo formation of new skin/ ‘biological creep’ (Austad et al., 1982, Johnson et al., 1988, Pasyk et al., 1988, Shuter et al., 1994)

The use of tissue expanders in surgery reduces the risk of rejection of tissue implants, such as the use of skin grafts in reconstructive surgery. The technique allows for a more 'natural' development of tissue. Surgeries involving expanders are less dramatic and invasive as often the number of surgeries required for the repair are reduced. The surgery is deemed as less traumatic due to a decrease in blood loss and in the length of hospital stay required by the patients. With this being the case, the recovery of patients is often much faster that those who have undergone a more invasive surgery.

### 2.7.1 Balloon Tissue Expanders

Traditional tissue expansion utilises an implantable subcutaneous silicone balloon that is gradually inflated by injecting saline solution through a buried filling port. Inflation continues until the desired degree of soft tissue expansion is obtained (Lapin et al., 1985). Although widely used in a range of reconstructive applications, they have several inherent limitations. In the past, complication rates of the use of these balloon expanders has reached 50% (Austad, 1988), with problems including scar widening and leakage at filling point to infection, haematoma formation and bone resorption (Malata et al., 1995). They are generally large and unwieldly and therefore of limited use for intricate anatomical locations such as the urogenital and anogenital tracts. This is particularly the case in paediatric surgery; percutaneous inflation is often uncomfortable and poorly tolerated by children. Furthermore, the balloon expands isotropically (equally in all directions), this could be detrimental when working in the urogenital tract. Expansion in multiple directions could lead to

neotissue invading intricate structures and causing further complications i.e., ureter or urethra obstruction.

### 2.7.2 Self-Inflating Tissue Expanders

Self-inflating expanders in their simplest form consist of a silicone semi permeable membrane shell containing a substance, such as sodium chloride, in substantial amounts to create an osmotic gradient across the wall of the implant. The hypertonic interior of the implant causes a net influx of water, leading to expansion of the device in a non-invasive manner (Austad, 1991, Wiese et al., 1999). This method of inflation is a potentially preferable approach to surgery in urogenital area of young children. The lack of inflation port allows a much smaller device to be used and makes the likelihood for them to be tolerated much higher.

### 2.7.3 Hydrogel Self-Inflating Tissue Expanders

The requirement of a tissue expander for an area of anatomy as delicate as malformed urogenital tracts is very specific. The recent development of an anisotropic self-inflating hydrogel expander (Wiese et al., 2001) may provide an ideal implant for use in these surgeries. In comparison to currently available self-inflating tissue expanders, hydrogels provide a higher degree of expansion and a much slower expansion rate of around 4 – 8 weeks as opposed to the few days of non-hydrogels (Swan et al., 2011, Swan et al., 2012). The proposed self-inflating hydrogel expander to be used in this project displays a triphasic swelling profile in vivo (Figure 2.12). The first phase

represents the biodegradable ‘time switch’ which delays the onset of expansion following implantation for the period dictated by the clinician, typically 2 weeks, this delay allows for the implantation wound to heal somewhat before expansion commences. In phase two, the rate of osmotic expansion is carefully controlled by an integral polymer scaffold or an external semipermeable membrane. This prevents the undesirable effects of excessive expansion, such as pain and/or necrosis. The third and final phase; is when the final degree of swelling achieved, up to 1500%, is controlled and is determined by the hydrogel formulation used (Fig. 2.12). The device is entirely inert and remains quiescent during this phase until surgically removed in order to perform the desired reconstruction (Oxtex, 2015).

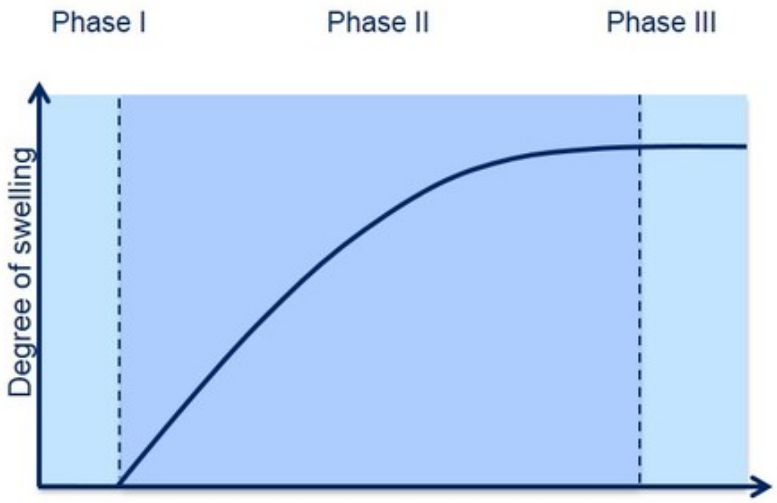


**Figure 2.12: A Graphical Representation of the Triphasic Swelling of the Oxtex Self-Inflating Hydrogel Expander** (Oxtex, 2015). Phase I represents the delay in swelling after implantation. Phase II shows the controlled expansion of the hydrogel and phase III represents complete expansion**.**

The increased expansion volume would reduce the number of surgical procedures required and therefore the risk of surgery. The slower rate can avoid tissue necrosis and even promote the growth of neotissue during the expansion process. The anisotropic property of the hydrogel expanders will potentially remove the chances of creating further complications such as obstructions and will allow surgeons to implant them at a specific orientation to obtain maximum expansion.

### 2.7.4 Current Use of Hydrogel Self-Inflating Tissue Expanders

There have been multiple successful procedures in veterinary medicine involving the use of hydrogel expanders (Expaniderm, 2014, 2015, 2016). The most relevant being the repair of the vaginal/rectal wall of a mare that had a 3rd degree perineal laceration from foaling (Fig. 2.13) (Expaniderm, 2014). Three expansion devices were implanted within the submucosa of the defected border between the rectum and vagina on the right-hand side of the laceration (Fig. 2.13 (B)). The horse was hospitalised for the duration of the expansion phase, 14 days. During the expansion process, the two most caudal devices fell out early due to wound dehiscence. This problem was due to the use of absorbable suture material. The cranial device remained in place for the full 14 days expansion (Fig. 2.13 (D)). It was then removed, and the first stage of reconstruction was carried out (Fig. 2.13 (E)). The hydrogel implant provided sufficient extra tissue to reduce the tension in the reconstruction site resulting in a successful reconstruction of the vaginal wall and a successful foaling the following season.

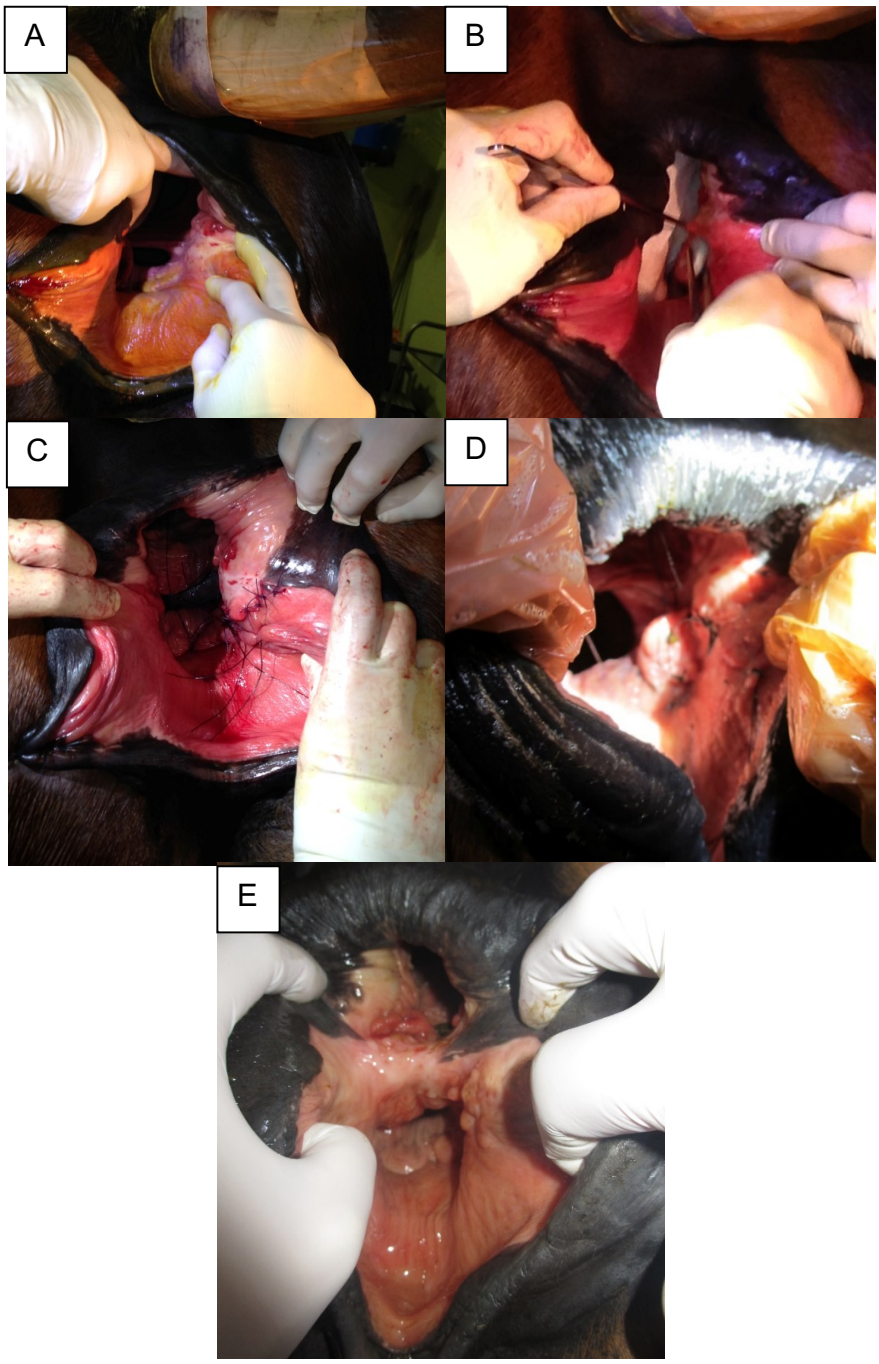


**Figure 2.13: Equine 3rd degree perineal laceration in May 2014 and subsequent successful reconstruction** (Expaniderm, 2014). **A**. Image of the perineal laceration. **B**. Image of the insertion of expansion devices into the submucosa of the defected area of the rectal/vaginal wall (right hand side). **C**. Image of the laceration post operation. The devices have been enclosed in the mucosa using vicryl suture material. **D.** Image of the implanted device, 14 days post-implantation. An expanded area of mucosa can be seen. **E**. Image of stage one reconstruction. The extra tissue provided by the tissue expander provided less tension within the reconstruction site, resulting in very successful results.

### 2.7.5 The Properties and Characteristics of Hydrogels

Hydrogels are three-dimensional, hydrophilic, polymeric networks capable of imbibing large amounts of water or biological fluids (Peppas and Mikos, 1986, Brannon-Peppas, 1990). The networks are composed of homopolymers or copolymers, and are insoluble due to the presence of chemical crosslinks (tie-points, junctions), or physical crosslinks, such as entanglements or crystallites (Peppas and Merrill, 1976a, Peppas and Merrill, 1976b, Peppas, 1986, Stauffer and Peppas, 1992, Hickey and Peppas, 1995, Peppas and Mongia, 1997). The latter provide the network structure and physical integrity. These hydrogels exhibit a thermodynamic compatibility with water, which allows them to swell in aqueous media (Flory and Rehner Jr, 1943, Flory, 1953, Brannon-Peppas, 1990, Stauffer and Peppas, 1992).

There are various applications of these hydrogels, in particular in the medical and pharmaceutical sectors (Peppas and Langer, 1994, Peppas, 2019, Hoffman, 2012). Hydrogels resemble natural living tissue more than any other class of synthetic biomaterials. This is due to their high water contents and soft consistency, which is similar to natural tissue (Hoffman, 2012). Furthermore, the high-water content of the materials contributes to their biocompatibility. Thus, hydrogels can be used as contact lenses, membranes for biosensors, linings for artificial hearts, materials for artificial skin, and drug delivery devices (Peppas and Langer, 1994, Peppas, 1997, Hoffman, 2012, Peppas, 2019).

There are numerous ways that hydrogels can be classified; as neutral or ionic, based on the nature of the side groups. According to their mechanical and structural characteristics, they can be classified as affine or phantom networks. Additionally, they can be homopolymer or copolymer networks, based on the

method of preparation. Finally, they can be classified based on the physical structure of the networks as amorphous, semicrystalline, hydrogen-bonded structures, supramolecular structures and hydrocolloidal aggregates. (Peppas and Merrill, 1976a, Peppas and Merrill, 1976b, Peppas, 1986, Peppas and Mikos, 1986, Brannon-Peppas, 1990, Stauffer and Peppas, 1992, Hickey and Peppas, 1995, Peppas and Mongia, 1997, Peppas et al., 2000).

Hydrogels may also show a swelling behaviour dependent on the external environment. These polymers are physiologically responsive hydrogels, where polymer complexes can be broken, or the network can be swollen as a result of the changing external environment. These systems tend to show drastic changes in their swelling ratio as a result. Some of the factors affecting the swelling of physiologically-responsive hydrogels include pH, ionic strength, temperature and electromagnetic radiation (Peppas, 1991). Hydrogel gels are made via free radical polymerisation mechanism, where monomer units are connected into long chains through double bonds. The crosslinking agent, a monomer with two or more double bonds, provides the polymer network structure by connecting the long, linear chains in these polymerisations. The main disadvantage of hydrogels is their relatively low mechanical strength, but this can be overcome by either cross-linking, the formation of interpenetrating networks (IPNs) or crystallisation (Aharoni, 1992, Sperling and Mishra, 1996).

#### 2.7.5.1 Factors Affecting Swelling of Hydrogels

The crosslinking ratio is one of the most important factors that affects the swelling of hydrogels. It is defined as the ratio of moles of crosslinking agent to the moles of polymer repeating units. The higher the crosslinking ratio, the more crosslinking agent is incorporated in the hydrogel structure. Highly cross-linked hydrogels have a tighter structure and will swell less compared to the same hydrogels with lower crosslinking ratios. Crosslinking hinders the mobility of the polymer chain, hence lowering the swelling ratio. The chemical structure of the polymer may also affect the swelling ratio of the hydrogels. Hydrogels containing hydrophilic groups swell to a higher degree compared to those containing hydrophobic groups. Hydrophobic groups collapse in the presence of water, thus minimizing their exposure to the water molecule. As a result, the hydrogels will swell much less compared to hydrogels containing hydrophilic groups.

Swelling of environmentally sensitive hydrogels can be affected by specific stimuli. Swelling of temperature-sensitive hydrogels can be affected by changes in the temperature of the swelling media. Ionic strength and pH affect the swelling of ionic strength- and pH-sensitive hydrogels, respectively. There are many other specific stimuli that can affect the swelling of other environmentally responsive hydrogels. Mechanical properties of hydrogels are very important for pharmaceutical applications. For example, the integrity of the drug delivery device during the lifetime of the application is very important to obtain FDA approval, unless the device is designed as a biodegradable system. A drug delivery system designed to protect a sensitive therapeutic

agent, such as protein, must maintain its integrity to be able to protect the protein until it is released out of the system.

Changing the degree of crosslinking has been utilised to achieve the desired mechanical property of the hydrogel. Increasing the degree of crosslinking of the system will result in a stronger gel. However, a higher degree of crosslinking creates a more brittle structure. Hence, there is an optimum level of crosslinking to achieve a relatively strong and yet elastic hydrogel. Copolymerisation has also been utilised to achieve the desired mechanical properties of hydrogels. Incorporating a co-monomer that will contribute to H-bonding can increase the strength of the hydrogel. Cell culture methods, also known as cytotoxicity tests, can be used to evaluate the toxicity of hydrogels. Three common assays to evaluate the toxicity of hydrogels include extract dilution, direct contact and agar diffusion. Most of the problems with toxicity associated with hydrogel carriers are the unreacted monomers, oligomers and initiators that leach out during application. Therefore, an understanding the toxicity of the various monomers used as the building blocks of the hydrogels is very important.

The relationship between chemical structures and the cytotoxicity of acrylate and methacrylate monomers has been studied extensively (Yoshii, 1997). Several measures have been taken to solve this problem, including modifying the kinetics of polymerisation to achieve a higher conversion, and extensive washing of the resulting hydrogel. The formation of hydrogels without any initiators has been explored to eliminate the problem of the residual initiator. The most commonly used technique has been gamma irradiation (Nedkov and Tsvetkova, 1994). Hydrogels of PVA have been also made without the

presence of initiators by using thermal cycle to induce crystallisation (Hickey and Peppas, 1995). The crystals formed act as physical crosslinks. These crystals will be able to absorb the load applied to the hydrogels.

Development of polymeric materials requires understanding of how the polymerisation reaction conditions affect the final polymer structure and the resulting material properties. The degree of crosslinking in a polymer network dictates the mechanical strength, swelling ratio, and many other properties of the polymer gel by influencing the molecular weight between crosslinks ($M_c$). The degree of crosslinking of a polymer is controlled by the fraction of crosslinking agent present in the copolymerisation and the double bond conversion. Smaller amounts of crosslinking agent and diminished final conversion both lead to a less densely cross-linked material. Additionally, not all the crosslinking double bonds react to form crosslinks. Potential crosslinking is also lost due to intramolecular cyclisation reactions, where both ends of the crosslinking agent react into the same growing polymer chain, forming a loop structure (Fig. 2.14). Although the equivalent amount of crosslinking agent may be present and incorporated into the network, when cyclisation occurs, the polymer produced is less cross-linked and does not exhibit the expected mechanical properties, equilibrium swelling and diffusional properties (Elliott et al., 2004).

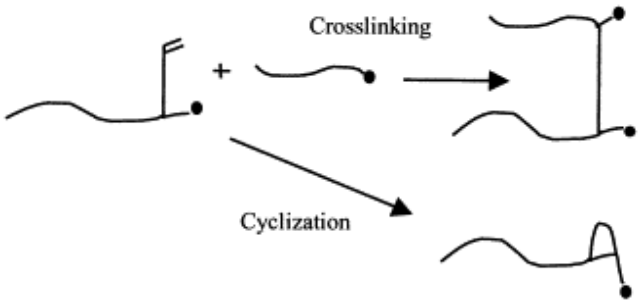


**Figure 2.14: Crosslinking and cyclization of a polymer that can occur during double bond conversion** (Elliott et al., 2004). Not all the crosslinking double bonds react to form crosslinks. Potential crosslinking can be lost due to intramolecular cyclisation reactions, where both ends of the crosslinking agent react into the same growing polymer chain, forming a loop structure.

### 2.7.6 The Application of Polylactic Acid for Biomedical Devices and Tissue Engineering

The development of biomaterials with required characteristics to aid in the recovery of tissues damaged by accident or disease has been undergoing for some time now. The use of biopolymers as an alternative to traditional biocompatible materials, such as ceramics and metals, and non-biodegradable polymers has multiple applications (Peter et al., 1998, Temenoff and Mikos, 2000, Chen et al., 2002, Nair and Laurencin, 2007).

One of the first studies that involved the implantation of pure poly-lactic acid (PLA) was in 1966 (Kulkarni et al.). This study involved the implantation of PLA implants into the subcutaneous ventral wall of guinea pigs. The implants remained in the animals for varying amounts of time, up to 6 weeks, to monitor the immunological reaction the tissue had to the poly-lactic acid. Within the first week, there was only a very mild response with a very thin reactive zone consisting of a thin layer of polyphonuclear leukocytes and a few lymphocytes and eosinophils. An initial formation of oedema was seen in the tissue during this period. After two weeks, fibroblastic activity was seen in the histological study and after four weeks, there was a formation of a sheet of connective tissue around the implant, similar to that seen with a surgical scar. Kulkarni stated '*Strikingly, there were no indications of inflammatory reaction from the implants made, thus giving evidence of inertness and tissue receptivity*.'

Synthetic biodegradable poly-lactones such as poly-lactic acid (PLA), poly-glycolic acid (PGA) and poly-caprolactone (PCL) as well as their co-polymers are now commonly used in biomedical devices (Cheng et al., 2009), due to

their exceptional biocompatibility. These polymers are degraded by hydrolysis of the ester bonds, a reaction that does not require the presence of enzymes and therefore does not elicit an immune response. The products from this degradation process are then converted into non-toxic sub-products and then eliminated through normal cellular activity and urine.

Synthetic degradable polyesters have been used in surgery as bone fixation devices and suture materials for the last forty years. Lactic acid and glycolic acid were proposed as degradable matrixes for the sustained delivery of bioactive substances back in 1973 (Auras et al., 2004). PLA has been demonstrated to be a suitable bioabsorbable polymer for use in fixation devices such as resorbable plates and screws. These devices have been used extensively as dissolvable suture meshes and by orthopaedic surgeons (Waris et al., 2004, Lovald et al., 2009).

Absorbable systems are highly advantageous when compared with metallic implants, as they do not erode bone when placed in the human body (Lindqvist et al., 1992, Dearnaley et al., 2007). Furthermore, bioabsorbable devices do not require a second surgery to remove the implant and allow for the gradual recovery of tissue function, as the device is degraded. Synthetic bioabsorbable polymers have the ability to stimulate isolated cells to regenerate tissues and can release drugs such as painkillers, anti-inflammatories and antibiotics (Wood, 1980, Laitinen et al., 1992).

Polylactic acid has proved effective in implants and supports within the human body. The characteristics of the material means that it can take from 10 months to up to 4 years to degrade, depending on the microstructural factors, such as

chemical composition, porosity and crystallinity. These may influence the tensile strength of the material. PLA, alone or in combination with other biodegradable polymers, has proven to provide good support for cell growth when used as a scaffold in tissue engineering. The purpose of the scaffold is to act as an extracellular matrix (ECM) onto which cells can adhere and grow into fully functional tissues. This reflects the importance of mechanical strength in the initial stages and therefore biological performance is significant too. Polymeric biodegradable scaffolds combine the advantages of both synthetic and natural materials. The physical properties of the synthetic polymers can be easily adjusted and controlled. PLA as a scaffold has significant advantages over polymer films, as a high level of porosity is needed to accommodate large number of cells. This is where the pore diameter (interstitial space) becomes important for cell growth, vascularization, and the diffusion of nutrients. Three-dimensional porous scaffolds formed for culturing different cell types, such as cardiovascular, muscle, bone and cartilage have been produced from polylactic acid (Coutu et al., 2009). PLA can be designed and produced into various shapes, as is required of the organ construction.

PLA has an extensive mechanical property profile and is thermoplastic with high biocompatibility and biodegradable properties (Auras et al., 2004, Gupta et al., 2007). It is obtained from lactic acid and hydrolytically degradation converts it back to its acid of origin. Lactic acid is a naturally occurring organic acid that can be produced by fermentation of sugars. When obtained from a renewable source such as sugarcane. PLA has the potential to be produced and in used in an environmentally friendly cycle (Auras et al., 2004).

The fabrication of PLA is neither easy of simple to execute. It's synthesis requires rigorous control of conditions (temperature, pressure and pH), the use of catalysts and long polymerisation times, implying high energy consumption (Lasprilla et al., 2012). Current studies are directed towards the development of materials by blending PLA with other biodegradable polymers, such as polycaprolactane, chitosan and polyethylene oxide. The idea being that a matrix is developed with the degradation behaviour, morphology and biological performance that is appropriate for specific medical applications, such as implants, prosthetic devices, catheters, vascular grafts, sutures and ligament repair materials (Gupta et al., 2007).

### 2.7.7 Lactic Acid

Lactic acid (2-hydroxypropionic acid) is a chiral molecule that exists as two enantiomers, L- and D-lactic acid (Fig. 2.15), which differ in their effect on polarized light. The L isomer rotates the plane of polarised light clockwise, the D isomer, anticlockwise. The optically inactive D, L or meso form is an equimolar (racemic) mixture of D(−) and L(+) isomers. Lactic acid is produced naturally in mammalian muscle cells during glycogenolysis and is involved in the Krebs cycle via pyruvic acid and acetyl-CoA. It is considered the most potential monomer for chemical conversions because it contains a carboxylic and a hydroxyl group (Varadarajan and Miller, 1999).

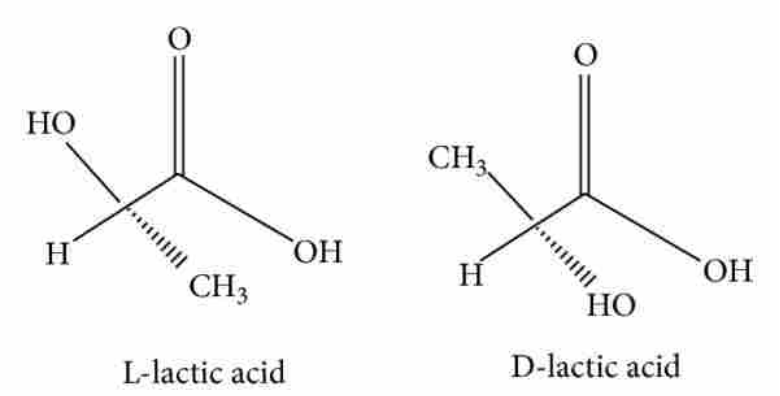


**Figure 2.15: Lactic Acid, a chiral molecule** (Hernández et al., 2014). The L isomer rotates the plane of polarised light clockwise (laevorotatory lactic acid), the D isomer, anticlockwise (dextrorotatory lactic acid).

Lactic acid production has a great worldwide demand due to its versatile applications in pharmaceutical, food, leather, textile, and chemical industries (John et al., 2009) and as monomer in the production of biodegradable polymers (Adsul et al., 2007). Lactic acid can influence the metabolic function of cells in a variety of ways, as it can serve as an energy substrate and given

its uncharged character and small size, it can permeate through the lipid membrane (Philp et al., 2005). In addition to its role as an energy substrate for cells, lactic acid has been shown to have antioxidant properties that may serve to protect cells from damage due to free radicals that are naturally produced throughout the cell life cycle (Lampe et al., 2009).

Lactic acid is produced by fermentation of carbohydrates or chemical synthesis of acetaldehydes. The chemical synthesis is mainly based on the hydrolysis of lactonitrile by a strong acid, where a racemic mixture of the two forms (D(−) and L(+)) lactic acid is produced. The biotechnological production of lactic acid has received significant interest. Fermentation is an attractive process in terms of its environmental impact and its combination of low production cost from sugarcane fermentation, decreased fossil-based feedstock dependency, reduced $CO_2$ emission, biocatalyst use, and high product specificity (Lunelli et al., 2010) and the option to produce optically pure L- or D-lactic acid, depending on the strain selected (Adsul et al., 2007). Approximately 90% of the total lactic acid produced worldwide is made by bacterial fermentation and the remaining portion is synthetically synthesised by reacting acetaldehyde with hydrogen cyanide and hydrolysing the resultant lactonitrile (Adsul et al., 2007, Gupta et al., 2007).

Lactic acid producing bacteria can be divided into two classes: homofermentative bacteria like *Lactobacillus casei* and *Lactococcus lactis*, producing two moles of lactate from one mole of glucose, and heterofermentative species producing equally one mole of lactate, acetic acid, ethanol and carbon dioxide from one mole of glucose (König et al., 2009). Like all biological lactic acid, the lactic acid produced with this method is exclusively (>99.5%) L-lactic acid (Lunt, 1998, Lunt and Shafer, 2000).

### 2.7.8 Polylactic Acid (PLA)

PLA is an adaptable biodegradable polymer, which can be customised into different resin grades for processing into a wide spectrum of products. As lactic acid is a chiral molecule, the term “poly-lactic acid” actually refers to a family of polymers: pure poly-L-lactic acid (PLLA), pure poly-D-lactic acid (PDLA), and poly-D,L-lactic acid (PDLLA) (Fig. 2.16) (Griffith, 2000, Chan et al., 2017). Depending on the composition of the optically active L- and D, L-enantiomers, PLA can crystallize in three forms (α, β, and γ). The α structure is more stable and has a melting temperature, $T_m$, of 185°C compared to the β structure, with a $T_m$ of 175°C (Auras et al., 2004, Lim et al., 2008).

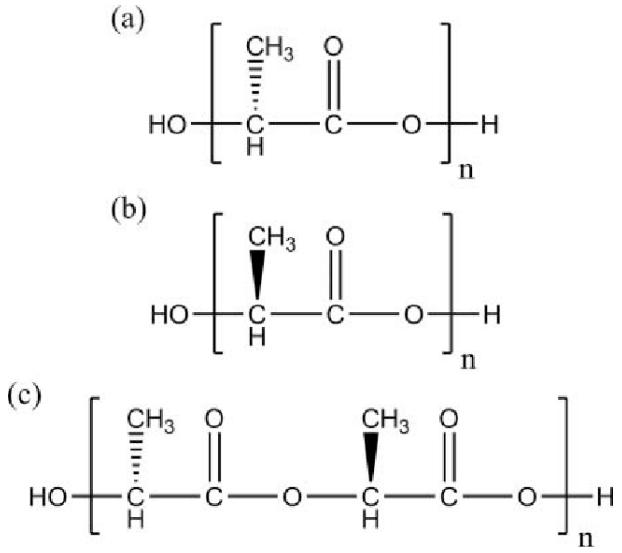


**Figure 2.16: Chemical structures of polylactic acids** (Chan et al., 2017). (**a**) poly(L-lactide) (PLLA); (**b**) poly(D-lactide) (PDLA); (**c**) poly(D, L-lactide) (PDLLA).

Lactic acid-based polymers were first successfully used commercially as fibre materials for resorbable sutures. Since then, a variety of prosthetic devices have been developed (Auras et al., 2004). These days, PLA resins are

approved by the US Food and Drug Administration (FDA) and European regulatory authorities for all food applications and some chirurgical applications such as drug releasing systems (Lampe et al., 2009).

Pure poly-L-lactic acid (PLLA) has acquired attention due to its outstanding biocompatibility and mechanical properties, including its high mechanical strength. However, the high crystallinity of it fragments together with its long degradation times can cause inflammatory reactions in the body. In order to overcome this, PLLA can be used as a material combination of L -lactic and D, L-lactic acid monomers, as the D, L-lactic acid monomers are degraded without formation of crystalline fragments during the process (Fukushima and Kimura, 2008).

PLA chemistry involves the processing and polymerisation of lactic acid monomers. PLA is a chiral polymer containing asymmetric carbon atoms with a helical conformation. It has stereocenters in its repeating units (Lim et al., 2008). A stereocenter is an atom that has four molecular attachments that are different from one another, this means that that the altered position of any of the attachments would cause the formation of a new, different molecule (Fig. 2.17). The stereocenter repeating unit can exhibit two structures of order, isotactic and syndiotactic. In isotactic polymers all the substituents are located on the same side of the macromolecular backbone. In the case of PLA, this is a carbon atom. The substituents of syndiotactic polymers have alternating positions along the carbon chain. Atactic polymers substituents are placed randomly along the macromolecule chain.

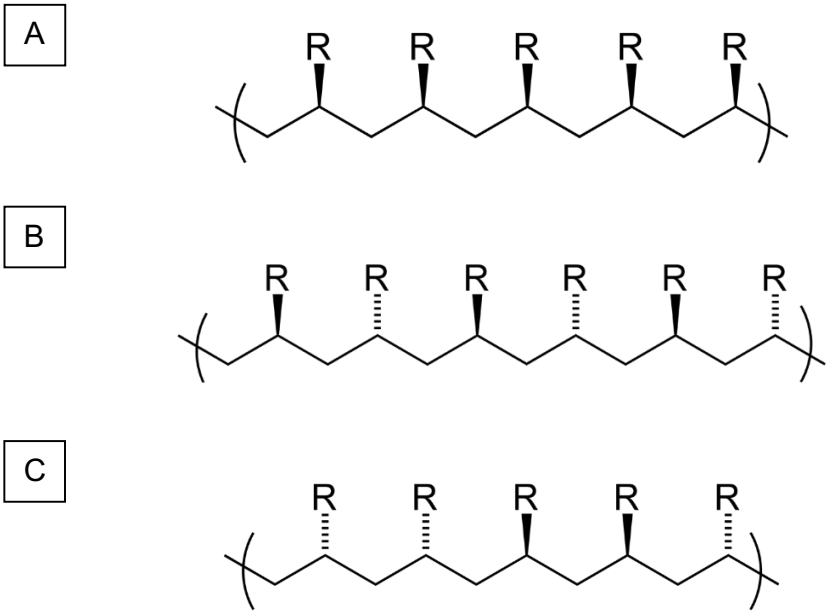


**Figure 2.17: PLA is a chiral polymer with stereocenters in its repeating units** (Stevens, 1990). **A**. In isotactic polymers all the substituents are located on the same side of the macromolecular backbone. In the case of PLA, this is a carbon atom. **B**. The substituents of syndiotactic polymers have alternating positions along the carbon chain. **C**. Atactic polymers substituents are placed randomly along the macromolecule chain.

Isotactic and optically active PLLA and PDLA are crystalline, whereas PDLLA is relatively atactic and optically inactive and therefore amorphous (non-crystalline) (Bouapao et al., 2009).

### 2.7.9 Polylactic Acid Synthesis

PLA can be prepared from lactic acid by various polymerisation processes including: polycondensation, ring opening polymerisation and direct methods like azeotopic dehydration and enzymatic polymerisation (Fig. 2.18) (Lim et al., 2008). Currently, direct polymerisation and ring opening polymerisation are the most used production techniques. Polycondensation is the least expensive method for obtaining PLA. However, it is very difficult to produce a solvent-free high molecular weight PLA with this method (Auras et al., 2004). In polycondensation, solvents and/or catalysts are used under high vacuum and temperatures for the removal of water produced in the condensation. The resultant polymer is a low molecular weight material, which can be used as is, or can be coupled with isocyantes, epoxides or peroxide to produce a range of molecular weights (Lunt, 1998, Lunt and Shafer, 2000).

Polycondensation is carried out in three stages; removal of free water, oligomer polymerisation and melt condensation of high molecular weight PLA. In the first and final stage, the removal of water is the rate-determining step. In the second stage, the chemical reaction is the rate-determining step and so is dependent on the catalyst used (Lasprilla et al., 2012). Chain coupling agents are an effective way to achieve high molecular weight lactic acid-based polymers by polycondensation. In this method, the intermediate low molecular weight is to treat polymers with chain extenders, which link the low molecular weight prepolymer into a polymer of high molecular weight. This method produces oligomers with average molecular weights of several tens of thousands and additional offside reactions can occur, such as transesterification, resulting in the formation of ring structures as lactide.

These side reactions have a negative influence on properties of the final polymer. This subproduct production cannot be excluded, but can be controlled by the use of different catalysts and functionalization agents, as well as by varying the polymerisation conditions (Gu et al., 2008).

Ring opening polymerisation (ROP) is the most common route to produce PLA polymers with high molecular weight. This process consists of three steps: polycondensation, depolymerisation and the ring opening polymerisation. In this solvent-free process, a cyclic intermediate dimer, commonly referred to as lactide, is produced and purified by distillation. Catalytic ring-opening polymerisation of the lactide intermediate results in PLA with controlled molecular weight. By controlling residence time and temperatures in combination with catalyst type and concentration, it is possible to control the ratio and sequence of D- and L-lactic acid units in the final polymer (Gupta et al., 2007). ROP can be carried out in melt, bulk or in solution, and by cationic, anionic and coordination-insertion mechanisms, depending on the catalyst.

Azeotropic dehydration is a direct method for producing high molecular weight PLA. With this method, the removal of water formed from the reaction medium becomes relatively easier and a higher molecular weight PLA is achievable. Enzymatic polymerisation has emerged as one of the most viable alternatives and is an environmentally friendly method that can be undergone in mild conditions (Fig. 2.19). The methodology provides adequate control of the polymerisation process (Cheng et al., 2009).

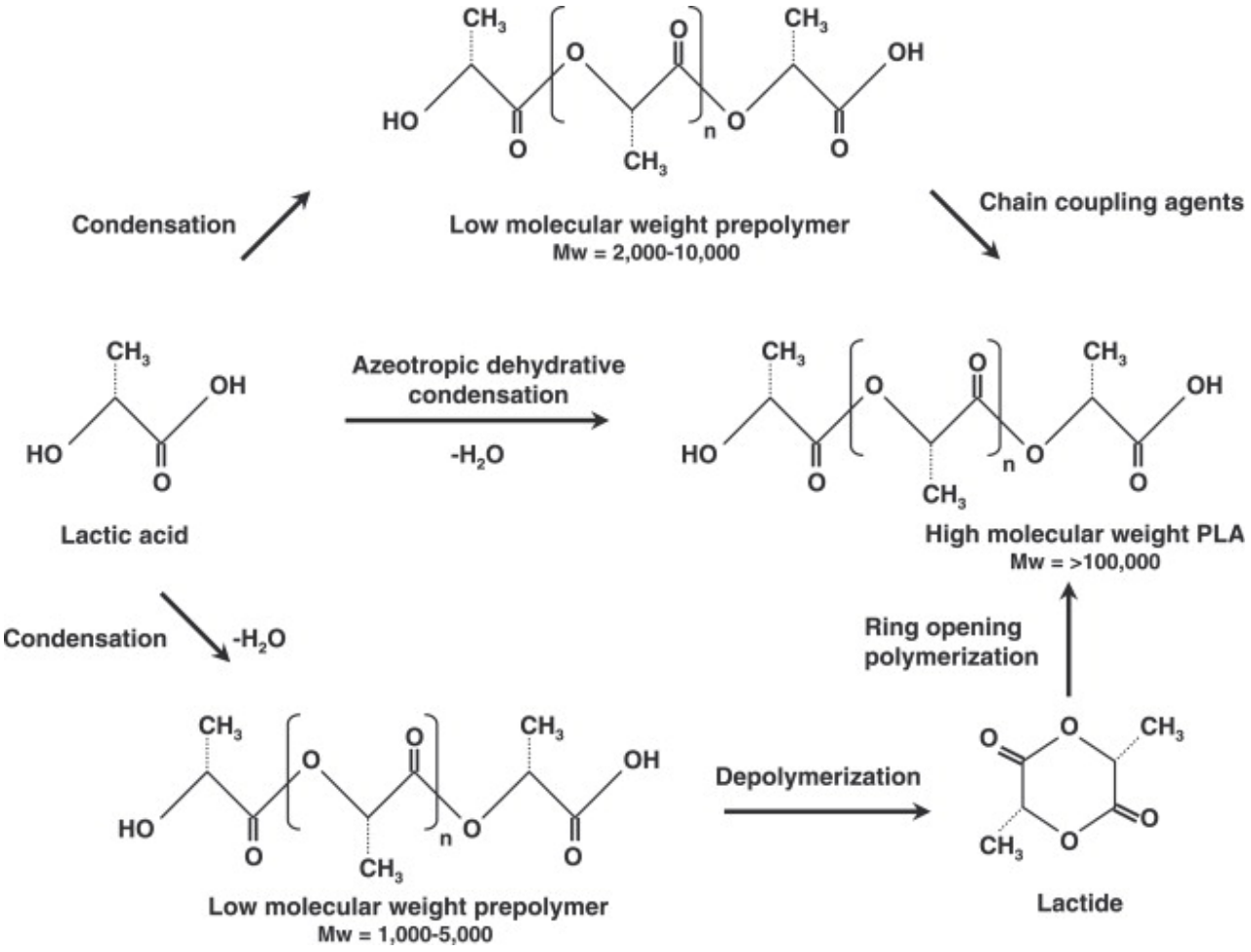


**Figure 2.18: Polylactic Acid Synthesis techniques** (Gupta et al., 2007). PLA can be prepared from lactic acid by various polymerisation processes including polycondensation, ring opening polymerisation and direct methods like azeotopic dehydration and enzymatic polymerisation. Currently, direct polymerisation and ring opening polymerisation are the most used production techniques.

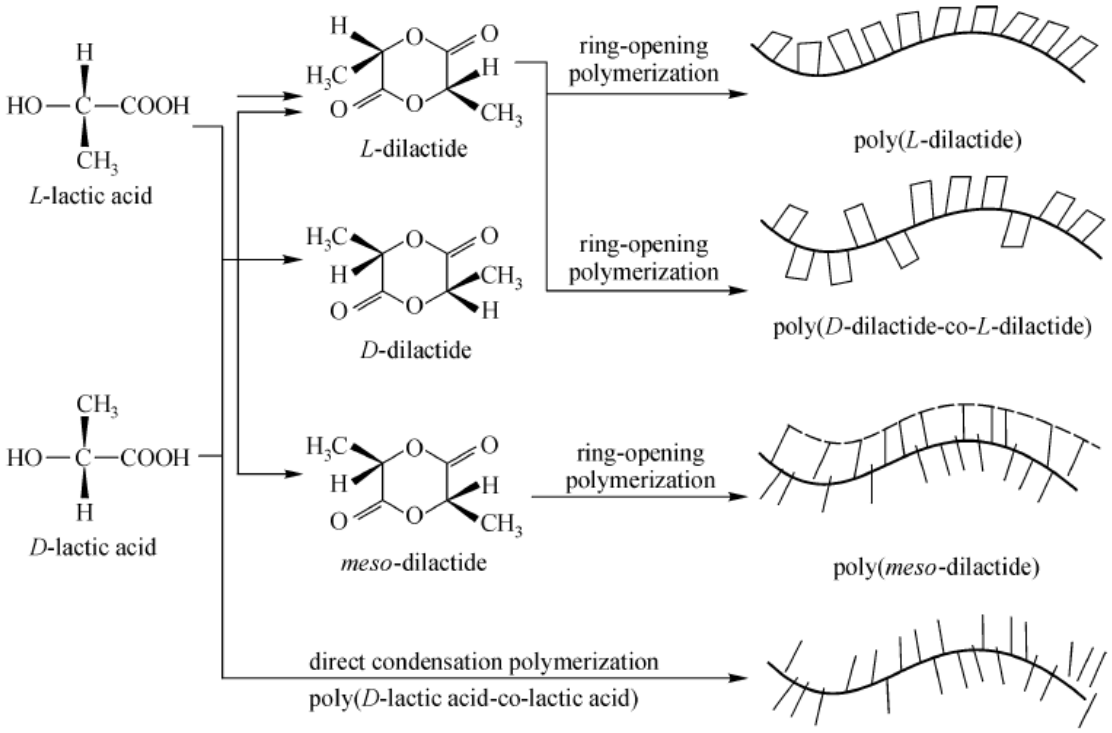


**Figure 2.19: Products of Polylactic acid synthesis** (Cheng et al., 2009). Polymerisation of L-lactic acid, D-lactic acid and a mixture of the two isomers results in various polymers. These include poly(L-dilactide), poly(D-dilactide-co-L-dilactide) and poly(meso-dilactide).

### 2.7.10 Polylactic Acid Properties

The stereochemistry and thermal history have direct influence on PLA crystallinity, and therefore, on its properties in general. PLAs with a PLLA content above 90% tend to be crystalline, whereas less optically pure polymers are amorphous. The melting temperature, $T_m$, and the glass transition temperature, the temperature at which 30-50 carbon chains start to move, $T_g$, of PLA decrease with decreasing amounts of PLLA (Lasprilla et al., 2012). Physical characteristics such as density, heat capacity, and mechanical and rheological properties of PLA are dependent on its transition temperatures. For amorphous PLA, $T_g$ is one the most imperative parameters as substantial changes in polymer chain mobility occur at and above $T_g$. For semi-crystalline PLA, both $T_g$ and $T_m$ are important physical parameter for predicting PLA behaviour (Auras et al., 2004, Bouapao et al., 2009).

| Lactic Acid Polymers | Glass Transition Temperature, $T_g$ (°C) | Melting Temperature, $T_m$ (°C) | Density (g/cm$^3$) | Good Solubility in Solvents |
|---|---|---|---|---|
| PLLA | 55 - 80 | 173 – 178 | 1.290 | Chloroform, Furan, Dioxane and Dioxolane |
| PDLLA | 43 – 53 | 120 – 170 | 1.250 | PLLA solvents and Acetone, Ethyl lactate, Tetrehydrofuran and Ethyl acetate |
| PDLA | 40 - 50 | 120 - 150 | 1.248 | Dimethylsulfoxide, N, N xylene and Dimethylformamide |

**Table 2.4: Properties of the various Lactic Acid Polymers** (Madhavan Nampoothiri et al., 2010).

The properties of PLAs can by controlled by using catalysts with isotactic (a polymer in which all of the pendant groups are located on the same side of the hydrocarbon backbone chain) and syndiotactic (a polymer in which the pendant groups have a regular, alternating pattern along the hydrocarbon backbone chain) contents differing in enantiomeric (isomers that are non-superimposable images of one another) units, i.e. different levels of purity (Gupta et al., 2007). PLA formulations can also be personalised by integrating the co-polymerisation of the lactide with either; other lactone-type monomers, a hydrophilic macro-monomers, such as polyethylene glycol (PEG), or monomers with functional groups, like amino and carboxylic groups, and blending PLA with other materials (Cheng et al., 2009). Blending can drastically alter the resultant properties, which depend on the mechanical properties of the components as well as the blend microstructure and the interface between the phases (Auras et al., 2004).

The degradation of PLA primarily occurs via hydrolysis after several months of moisture exposure. The degradation happens in two stages. Initially, random non-enzymatic chain scission of the ester groups within the polymer leads to a reduction in the molecular weight. The molecular weight is then reduced until the lactic acid and low molecular weight oligomers, fragments of the polymer, are naturally metabolised to yield carbon dioxide and water (Auras et al., 2004). The rate of degradation is largely determined by polymer reactivity with water and catalysts. Factors that affect the reactivity and the accessibility, such as temperature, particle size and shape, crystallinity, moisture, % isomer, residual lactic acid concentration, water diffusion, molecular weight and metal impurities from the catalyst, will all affect the

polymer degradation rate (Cha and Pitt, 1990, Drumright et al., 2000, Tsuji and Ishida, 2003, Auras et al., 2004). In vivo and in vitro degradation has been evaluated for PLA surgical implants. In vitro studies showed that the pH of the solution does contribute to the in vitro degradation, and in vivo studies can be used to determine the in vivo degradation of PLA (Auras et al., 2004).

In conclusion, PLA has multiple advantages; it is biocompatible and biodegradable and can readily be broken down by thermal hydrolysis. It is available via renewable agricultural resources, and there is a reduction in carbon dioxide emissions when compared to the conventional petroleum-based commodity plastics. The most important property of polylactic acid is the ability to be able to tailor its physical properties by material modifications.

### 2.7.11 2-Hydroxyethyl Methacrylate

Copolymerisation of 2-hydroxyethyl Methacrylate (HEMA) is a widely used process for the development of hydrogels. Hydrogels are three-dimensional networks of hydrophilic polymers that can absorb substantial amounts of water. Hydrogel materials possess a good biocompatibility; this is due to multiple factors. Firstly, the hydrophilic surface of a hydrogel has a low interfacial free energy in contact with body fluids. This means that there is a very low tendency for proteins and cells to adhere to the surface. Second, the polymer chains at the surface of hydrogels are very mobile, this contributes to the prevention of proteins adsorption and cell adhesion. Finally, the soft and rubber like nature of hydrogels minimises the irritation caused to surrounding tissues (Park and Park, 1996, Cadée et al., 2000).

The use of hydrogels for contact lenses have been studied extensively due to their superior wearer comfort and oxygen permeability. The HEMA hydrogel is widely used and can have a water content of 38 to 85% (Grobe III et al., 1996). The copolymerisation of monomers allows chemical and physical properties, such as water content, oxygen permeability, refraction index and hardness to be controlled. The first synthesis and polymerisation of 2-hydroxyethyl methacrylate was described in 1936 (Nemours), with the first applications of the polymers as hydrogels being reviewed in 1960 (Wichterle and Lim). The synthesis of HEMA from methyl methacrylate can be done via two methods, in a single step. The first requiring transesterification reaction with ethylene glycol and the second being the reaction of ethylene oxide and methacrylic acid.

The resultant HEMA contains varying percentages of impurities, methacrylic acid from the hydrolysis reaction and EGDMA (ethylene glycol dimethacrylate) from the esterification of methacrylic acid and ethylene glycol or HEMA and ethylene glycol, and so there are multiple purification methods for obtaining a clean product. The main procedures utilise the solubility of HEMA in water or diethyl ether and its insolubility in hexane. The EGDMA impurity is soluble in hexane. Therefore, HEMA can be dissolved in water and then the EGDMA extracted with hexane. Then the aqueous solution of HEMA is salted to complex methacrylic acid and extracted with diethyl ether. The solution is then dried, and the HEMA distilled under vacuum (Meier, 1969, Rego and Huglin, 1991). Another method of methacrylic acid impurity extraction is carried out by soaking technical HEMA with anhydrous sodium carbonate and extracting

EGDMA with hexane and then HEMA with diethyl ether, and distillation under vacuum (Pinchuk et al., 1984).

The use of ion-exchange resins is a simple method of methacrylic acid elimination, but they have a relatively poor yield (Tippett and O'brien, 1975). N,N'-Dicyclohexylcarbodiimide has also been used, but variations in the quality of the reagent can outweigh the value of the method (Montheard et al., 1992). Lastly, EGDMA can be extracted with hexane followed by the washing of a dilute solution of HEMA in water with sodium hydroxide or sodium bicarbonate. The extraction of HEMA with chloroform gives a product of high purity, after the drying and evaporation of chloroform (Montheard et al., 1992). As with the majority of methacrylic derivatives, HEMA can be polymerised by radical initiators or by various other methods, including, UV and plasma. When the monomer is purified, a soluble polymer can be synthesised, but, if the monomer contains even a small percentage of EGDMA, the prepared copolymers produce swollen gels (Wichterle and Lim, 1960).

Polymerised HEMA (PHEMA) has numerous applications in biomedical fields. The low toxicity of HEMA is widely accepted and its resistance to degradation make it a prime applicant for implantation. By using various additives, the mechanical properties of PHEMA hydrogels can be adjusted to many biomedical applications (Migliaresi et al., 1981). HEMA/methacrylic acid copolymers are more biocompatible than PHEMA alone, due to the giant cell inflammatory response that PHEMA induces when implanted (Smetana Jr et al., 1990). Composites with low collagen contents were found to be better preserved in long-term implantations. Implants with higher collagen contents exhibited calcification the early stages and this was followed by full

biodegradation. Calcification of synthetic biomaterials implies poor biocompatibility (Cífková et al., 1987).

### 2.7.12 Poly(ethyl glycol) Diacrylate

Polyethylglycol (PEG) hydrogels are cross-linked, fluid-filled, three-dimensional networks. They comprise of covalently bonded PEG chains and can be formed from multifunctional PEG precursors. PEG hydrogels can be produced by photopolymerisation of PEG precursors, modified with either acrylate or methacrylate, in the presence of photoinitiators (Pathak et al., 1992). On exposure to UV light, photoinitiators fragment into free radicals. These radicals attack carbon–carbon double bonds present in the acrylate groups, initiating polymerisation and thus forming a hydrogel network. When exposed to aqueous solvents, the cross-linked network swells until the retractive (elastic) forces of the polymer chain are balanced by swelling forces of the network (Flory and Rehner Jr, 1943). A more tightly cross-linked hydrogel will have larger retractive forces, resulting in less water being imbibed within the network (Peppas et al., 2000).

The structure and swelling properties of PEG hydrogels is affected by molecular weight and concentration of the precursors. Mesh size ($\xi$), the average distance between adjacent crosslinks, is a measure of the space available between PEG chains. Mesh size increases with molecular weight but decreases as PEG concentration increases. PEG molecular weight and concentration have similar effects on the average molecular weight between crosslinks ($M_c$), a measure of the degree of crosslinking of PEG hydrogels. In

parallel, the volumetric swelling ratio, the volume of hydrogel relative to the volume of polymer, increases with PEG molecular weight and decreases with PEG concentration (Lunt, 1998, Griffith, 2000, Lunt and Shafer, 2000, Lim et al., 2008, König et al., 2009).

### 2.7.13 Poly(Acrylic Acid)

Hydrogels formed with poly(acrylic acid) (PAA) can absorb many times their own weight in water. They are the basis of a class of materials called Super Absorbents. These polymers are used in multiple applications such as nappies, personal hygiene products, controlled release devices, membranes for dialysis and ultrafiltration and ion exchange resins (Huglin, 1989, Gudeman and Peppas, 1995, Ende and Peppas, 1996, Buchholz and Graham, 1998).

The ability for PAA to swell so extensively is facilitated by the carboxylic acid groups within the polymer chain, which strongly associate with water molecules (Fig. 2.20). The carboxylic acid groups are easily ionisable and sensitive to the effects of pH and ionic strengths and so the rate of swelling can be affected by the pH and ionic strength of the solution that they are swelling in (Shefer et al., 1993, Scott and Peppas, 1999).

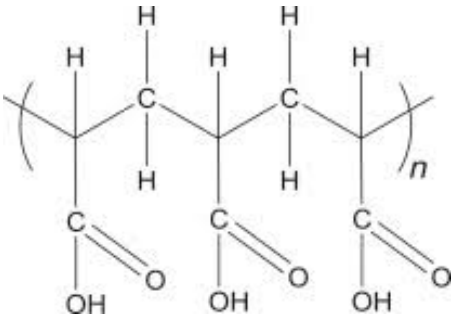


**Figure 2.20: The Structure of Poly (Acrylic Acid)** (Brady et al., 2017). It contains an ionisable carboxylic acid group in each repeating unit.

An experimental study was conducted to explore the network structure of loosely cross-linked PAA hydrogels formed by copolymerisation with poly (ethyleneglycol 600) diacrylate (PEG(600)DA) (Elliott et al., 2004). Experiments were designed to examine the effects of monomer concentration, pH and ionic strength during polymerisation on the cross-linking density and subsequent equilibrium swelling. Copolymers of 1mol% PEG(600)DA and 99mol% acrylic acid were made at various pH and ionic strengths and swollen in buffers at several pH. The results of the swelling experiments showed that the concentration of monomer during polymerisation significantly affects the succeeding equilibrium swelling. It was also seen that the amount of water present during the polymerisation increases primary cyclisation rates, and this change affects the subsequent swelling behaviour of the acrylic acid hydrogel. The effects of ionic strength and pH on the network structure are interconnected. An increase in the pH lead to a decrease the degree of primary cyclization while an increase in the ionic strength increased cyclisation.

## 2.8 Models for Vaginal Epithelial Tissue

### 2.8.1 The Use of Animal Models in Research

Animal models are an essential tool for gaining insight into disease and development mechanisms of the human urogenital system (Lantier, 2014). Predominantly rodents are used as models in preclinical trails, having a clear advantage regarding practicality; they are small and relatively easy to handle, and economically; being relatively affordable and efficient to keep (De Clercq et al., 2013, O'Meara et al., 2014). Rodents also provide a unique opportunity; genetically modified knockout strains can be developed, to study the role of specific signalling mediators in embryogenesis and gestational development (Tai et al., 2009, Wu et al., 2009).

When evaluating various animal models, different parameters must be considered, depending on the purpose of the model. These include, face validity, predictive validity and target validity (Denayer et al., 2014). Face validity is the similarity in biology and symptoms between the animal model and the human disease; often hampered by the lack of understanding of the biology of the underlying disease. Predictive validity is the demonstration that clinically effective interventions demonstrate a similar effect in the model, this is often difficult to achieve given incomplete correlations between animal and human disease mechanisms. Finally, target validity is how similar a role the target of interest plays in the model compared to humans, i.e. the beta-3-adrenergic receptor plays an important role in energy metabolism in rodents but not in humans (Weyer et al., 1999).

The pig has become an increasingly popular model, especially within the fields of diabetes and atherosclerosis research, due to its physiological and anatomical similarities to humans (Turk et al., 2005, Squier et al., 2008, Bode et al., 2010). Pigs of reduced size, such as Göttingen Minipigs, are popular with their reduced size at sexual maturity and lower growth rate than conventional pigs (Ellengaard). However, there are no studies reporting any physiological differences between minipigs and conventional pigs. Meaning either are suitable models for humans.

### 2.8.2 Cell, Tissue, and Organ Culture Models

One of the main ways to avoid the many ethical and regulatory issues that are involved when working with animals and humans is the use of cell, tissue or organ culture as in vitro culture models for the human organ or body system that is being studied.

Studies of the way the vaginal mucosa reacts to microbicides and spermicides have used human vaginal cells that have been grown in culture as primary cell lines (Krebs et al., 2000) transformed to produce immortalized cell lines (Fichorova et al., 2001, Peterson et al., 2005) or passaged and expanded to provide confluence cultures (Fichorova et al., 1997, Ayehunie et al., 2006). The main problem with the use of in vitro cell lines as a model is the inadequate information provided that is relative to the in vivo state. There is a lack of a functional permeability barrier and other cellular components such lymphocytes, macrophages or dendritic cells, cells that are derived from

underlying connective tissue, that are required for normal physiology to commence.

In theory, a way of overcoming some of the disadvantages of a cell monolayer culture is the growth of stratifies, differentiated human vaginal epithelium as a form of organotypic culture (Sobel et al., 1979). Though when put into practice, the growth of an organ culture with barrier function as operational as the vaginal mucosa has demonstrated to be difficult, with the organoculture producing a barrier with permeability 10 – 6 times greater than that determined for equivalent normal tissue (van Eyk and van der Bijl, 1998, Bijl and van Eyk, 2004). Following on from this, a human organotypic vaginal-ectocervical model has been established for examining the effects of potentially irritant topical agents (Ayehunie et al., 2006). The epithelial response to the irritants appears to be representative to that of the in vitro equivalent, however, the lack of normal connective tissue reduces the inflammatory response that would normally occur with irritant application. Should a study wish to examine the response to a physical or mechanical stress on the tissue, the lack of supportive connective tissue and normal blood and nerve supply will render this method unusable.

### 2.8.3 Human Ex Vivo Tissue Model

The use of surgical specimens or human tissue biopsies provides a means for avoiding some of the drawbacks that were discussed in the use of culture models as well as still avoiding the ethical and regulatory issues that come with live animal and human models. There have been a series of studies (van der Bijl et al., 1997, van Eyk and van der Bijl, 2004) that have characterised the barrier properties of the human vaginal mucosa, generally in comparison to the human buccal mucosa, describing the permeability of an in vitro model to a variety of compounds. The predominant human vaginal tissue samples were specimens of postmenopausal women undergoing hysterectomy, an abundant source of human vaginal tissue. Studies of vaginal tissue from postmenopausal women may limit the representation of the population overall. Postmenopausal women have a thinner vaginal epithelium and a reduced blood supply to the vagina compared to that of premenopausal women. The age of the women providing sample must be considered when interpreting the data provided from these studies (Sassi et al., 2004).

### 2.8.4 Invertebrate Model

There have been some attempts of non-vertebrate models for vaginal mucosa, these involve the use of Arion lusitancius (Belgian and Swiss slugs) for mucosal irritation tests (Adriaens and Remon, 2002, Dhondt et al., 2004, Dhondt et al., 2006). The body wall of the slugs consists of a single cell epithelium, with mucosal glands covering connective tissue. When the animals are exposed to an irritating agent, mucus is produced to defend the body wall. Irritation is determined by measuring the amount of mucous produced by the slugs during a repeated contact time (Dhondt et al., 2004). Irritation of the slug body wall can lead to membrane break down, this is detected by the release of proteins and enzymes from the body wall (Adriaens et al., 2005). This model may not be appropriate for human vaginal tissue responses as human vaginal mucosal tissue does not contain mucous-secreting glands and the structure and permeability of the ventral surface of the slug is not reported, limiting the comparability between the slug and human tissues.

### 2.8.5 Live Animal Models

The anatomy of the avian cloaca consists of a single tract divided into the coprodeum (where the colon enters), urodeum (where the ureter and oviduct enter) and proctodeum (the segment that opens onto the external surface of the bird) by complete annular folds (Klasing, 1999). Although the terminology is similar, there is no resemblance between the cloacal malformations of female infants and the anatomy of the hindgut of the chicken, and so the bird is not a suitable model for the project.

There have been several studies using laboratory rats and mice for the study of genital irritation. But the thick keratinised stratified squamous epithelium of rodents significantly limits the ability to apply the results from the model to human vaginal tissue (Davis et al., 2001). A study has shown that the keratinised epithelium of the rodent experienced no histological disruption when exposed to spermicide N-9 (Catalone et al., 2004), a spermicide that has been reported to cause cervical and vaginal bleeding and erythema in women, a clear sign of histological disruption of the vagina (Niruthisard et al., 1991).

As it stands, the rabbit has been the most frequently used animal model for vaginal irritation studies, mainly contraceptives (Castle et al., 1998). The FDA claim that ‘Vaginal irritation tests should be carried out in rabbits with daily applications for ten days. If rabbits are adequately tested by the vaginal route for adverse effects in toxicology studies, no separate vaginal irritation study is required.’ (Administration, 2015). Clearly stating that the use of rabbits for a model of the human vaginal epithelium is adequate for preclinical safety evaluations. However, only a small proportion, (approximately one-third) of the rabbit’s vagina is lined with stratified squamous epithelium, the same type of

epithelium that is found in the human vagina (Barberini et al., 1992). The remainder of the organ, the proximal two-thirds which in the rabbit it comparatively long to the human, around 13-14cm, is lined with a single cell epithelial layer of columnar ciliated and microvillus cells (Barberini et al., 1991). The single columnar epithelium tends to be more permeable and therefore more resistant the damage that the stratified squamous epithelium of the human vaginal epithelium.

Of the possible larger animal models, the pig is extraordinarily similar to the human in terms of anatomy, physiology and pathology (Swindle, 2007). The use of conventional pig is popular in studies that will require frequent repeated blood sampling, multiple blood samples can be taken from the animals without causing dramatic change to the animal physiological condition. Over the past few years, the pig has become a well-established large animal model for studies of skin epithelium and inflammatory processes (Biggar et al., 1985). Pigs are suitably large that conventional clinical devices used for monitoring physiological parameters in humans, can monitor the animals' cardiac and respiratory functions (Miwa et al., 2006). Squire *et al.* (2008) have undergone numerous studies, relating to both morphology and functionality of species tissue (Thompson et al., 2001), that have displayed the similarities in the histology, barrier composition and permeability between porcine and human vaginal mucosa (Table 2.5).

Moreover, the pig is well suited for colposcopic observations and obtaining multiple biopsies for evaluating the cervicovaginal gene expression profile of inflammatory mediators to specific topical agents (D'cruz et al., 2005). Additionally, studies of the physiological factors influencing ovulation,

fertilization and establishment of pregnancy in pigs have been well documented (Hunter, 1975, Hunter, 1977). When compared to humans, the pig shows similarities in acidic vaginal pH (during oestrus) and barrier permeability's.

| Compound | Human Vaginal Mucosa | Porcine Vaginal Mucosa |
|---|---|---|
| **Water** | 3600 | 3500 |
| **Vasopressin** | 96 | 110 |
| **Oxytocin** | 300 | 500 |
| **17 β-estradiol** | 301 | 350 |
| **r-Arecoline** | 700 | 620 |

**Table 2.5: Comparison of Human and Porcine Vaginal Barrier Permeability** (Squier et al., 2008).

## 2.9 Comparison of the Human and Porcine Female Genital Tract

### 2.9.1 General Anatomy of the Urogenital Tract

#### 2.9.1.1 Vagina

The distal aspect of the female porcine urogenital tract, often denoted as the 'vagina', consists of two parts. The cranial part, technically deemed as the vagina, is a reproductive only passage that extends from the cervix to the point of urethra entrance. The caudal part, the vestibule, runs from the point of urethral entrance to the external vulva, it combines both the reproductive and urinary systems. A combination of the vagina and vestibule make up the female copulatory organ and the birth canal (Singh, 2018). This anatomical arrangement is consistent for many mammals, including humans, with the main anatomical difference occurring between the lengths of the vagina and vestibule of the animal.

In veterinary anatomy, the female copulatory organ is a relatively long, thin-walled channel that is distensible in both length and width. It occupies a median position within the pelvic cavity and lies between the ventral aspect of the rectum and the dorsal aspect of the urethra and bladder. It is mostly retroperitoneal, although some of the cranial features of the organ are covered with peritoneum.

The muscles of the vagina have a similar disposition to that of the uterus, although slightly weaker. The mucosa of the vagina is lined with stratified squamous epithelium, which reacts to varying hormone levels throughout the oestrus cycle of the animal; the magnitude of reaction varies between species.

Generally, glands are limited to the cranial portion of the vagina, but the moisture produced may diffuse more widely throughout the organ. The surface is smooth, with longitudinal and circular folds in the wall extending into the lumen of the inactive organ. In some animals the cervix protrudes into the lumen of the vagina, forming a ring-like structure often referred to as the fornix. A transverse fold of mucosal tissue, known as the hymen, sometimes marks the junction between the vagina and the vestibule. It may be present in virgin animals but is seldom prominent; the hymen is most established in porcine and equine species (König et al., 2007).

In the human, the vagina is around 10cm long (adult) and extends from the cervix to the outside of the body. As described above, the mucous membrane of the human vagina is lined with a stratified squamous epithelium, this surrounded by a smooth muscle layer that allows the vagina to increase in size during coitus and parturition. There are longitudinal ridges, columns, which extend the length of the vagina's posterior and anterior walls, with transverse ridges, rugae, extending between columns. Like some animals, the human vagina has a proximal fornix and attaches to the sides of the cervix in such a way that the cervix protrudes into the vagina (Seeley et al., 1995). The hymen in normal human infants appears as a membranous mucosal partition, varying in shape and size, surrounding the vaginal orifice. It takes a variety of forms, but is typically circular or crescentic due to its perforation by one or several holes (Seeley et al., 1995, Hobday et al.).

#### 2.9.1.2 Vestibule and Vulva

The vestibule is much shorter than the vagina; it mainly lies caudal to the ischial arch in domestic mammals. The walls of the vestibule come together to decreasing the lumen to a vertical cleft when at rest and are less elastic than those of the vagina. The urethra opens onto the ventral aspect of the vestibule, directly caudal to any hymenal indication that may be present. In some animals a suburethral diverticulum can be found in close proximity to the urethral opening into the vestibule. Caudal to the urethral opening, ducts from the vestibular glands mark the walls of the vestibule. The glands can appear in a major or minor formation, which the major vestibular glands being more common in larger domestic mammals such as bovine and equine species. The major vestibular glands consist of a large glandular mass with a single duct draining into the vestibule. The minor vestibular glands are generally present in small species, such as canine and feline species, these are much more numerous, smaller glands with multiple duct orifices that form a linear series when entering the vestibule. The glands produce a mucous secretion for lubrication of the passage during coitus and parturition. The wall of the vestibule is well vascularised, with a concentration of veins forming a patch of erectile tissue on the lateral aspect of the wall. This area is regarded as the female equivalent to the bulb of the penis (König et al., 2007).

The vestibule opens to the exterior at the vulva. The vertical vulvar opening is surrounded by labia that meet at dorsal and ventral commissures. In most domestic species, the dorsal commissure is rounded and the ventral one pointed. These labia correspond to the labia minora of human anatomy; the labia majora are suppressed in domestic species. The clitoris, the female

homologue of the penis, is found just within the ventral commissure. It is formed of two crura and a glans, similar to that of the male penis. The labia majora in the woman are two very prominent, rounded folds consisting of mainly subcutaneous fat. Most of the time, the labia majora are in contact with one another, concealing the deeper structures within the vestibule. Their medial surfaces are covered with numerous sebaceous and sweat glands.

In the human, the vagina opens directly to the outside body. Therefore, the vestibule is almost non-existent. The vestibule is dramatically shorter in the human female, but remnants of it are present as part of external genitalia. Like the pig, on either side of the vestibule is the opening for the duct of the greater vestibular gland, with the lesser vestibular glands having multiple duct openings located closer to the clitoris and urethral opening.

In the adult porcine species, the vagina is around 7 to 12cm in length. It is relatively unremarkable, and the vestibule is comparatively long. The porcine vestibule contains minor vestibular glands, with multiple openings into the lumen, and solitary lymph nodes. The ventral commissure of the vulva faces obliquely upwards, gilts (young female pigs) with an infantile vulva are common, it is often a result of poor development of the reproductive organs and is associated with poor fertility.

### 2.9.1.3 Blood Supply of the Female Reproductive System

The uterine artery derived from the internal iliac artery, indirectly, runs within the broad ligament that surrounds the reproductive tract. It releases a series of anastomosing branches over the body and horn of the uterus. The cranial anastomoses extend to the ovarian artery and the most caudal running down to the vaginal artery (Figs. 2.21 and 2.22). An arterial complex runs the length of the reproductive tract, supplying the tract with blood from all angles.

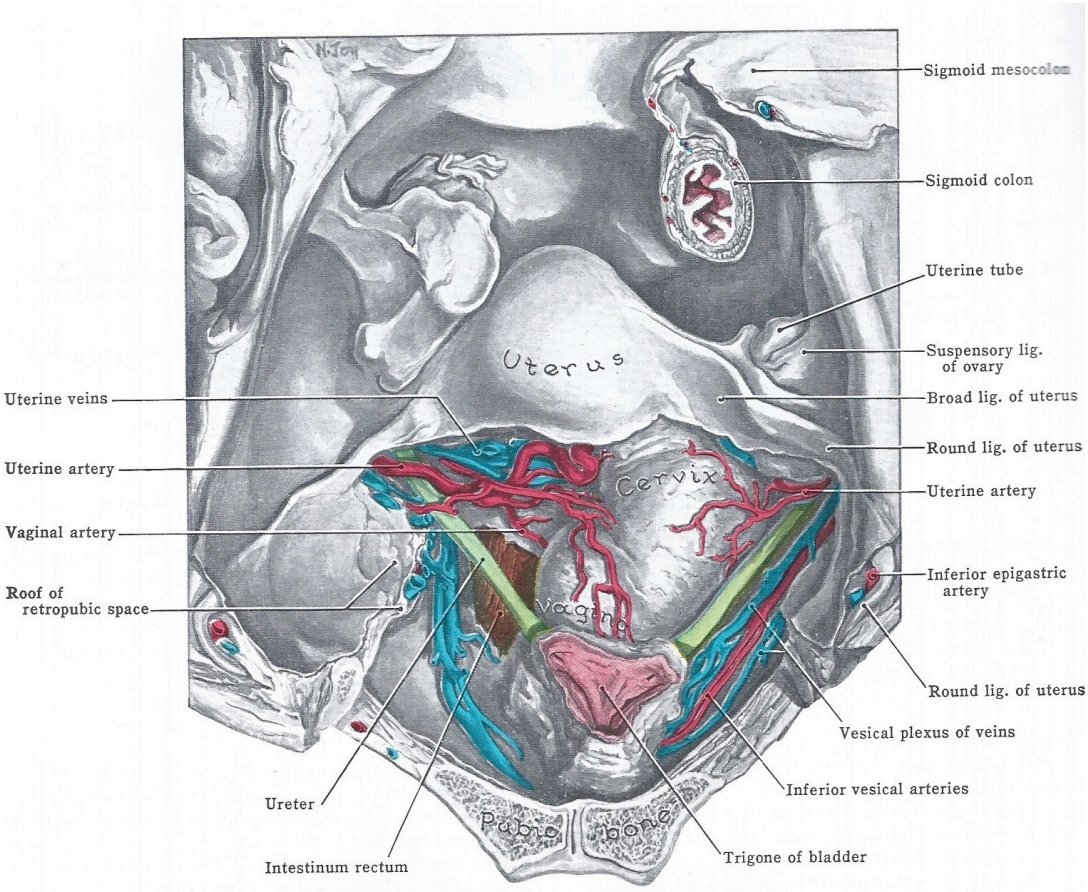


**Figure 2.21: The blood supply of the female human genital organs** (Anderson, 1978). The arteries are red, the veins blue and the structures in green are the ureters of the female.

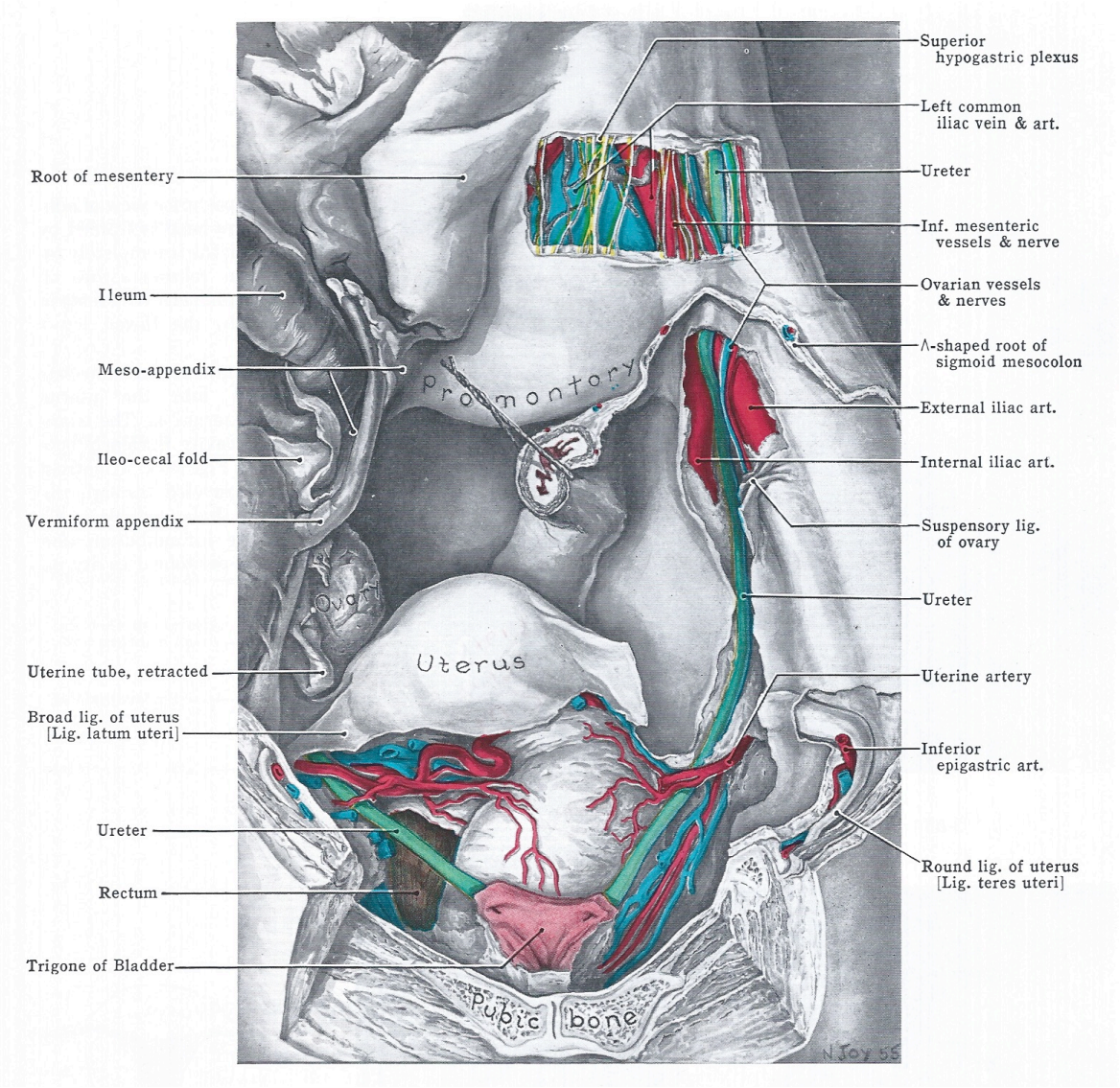


**Figure 2.22: The blood supply and innervation of the female human genital organs** (Anderson, 1978). The arteries are in red, the veins blue and the nerves in the superior hypogastric plexus are yellow.

#### 2.9.1.4 Innervation of the Female Reproductive System

Both sympathetic and parasympathetic fibres provide innervation of the female reproductive organs. The fibres to the uterine tube, uterus and vagina mainly follow the corresponding arteries to form plexuses within the broad ligaments and genital organs themselves. In the caudal part of the broad ligament, sympathetic fibres that travel by way of the plexus are in the retroperitoneal pelvic tissue. The parasympathetic fibres branch from the pelvic nerves and reach the genital organs via the pelvic plexus. A large proportion goes to erectile tissue.

### 2.9.2 Hormonal Cycles of Human and Porcine Females

Comparison between the human and porcine female genital tract (FGT) has shown obvious similarities between the species (Table 2.6). The anatomical and morphological construction and proportion of layers with cyclic alterations is very similar in humans and pigs. The hormonal cycles are closely related, only differing slightly in cycle duration and origin of luteolysing hormone. In women, the menstrual cycle is described according to gonadal activity and/or endometrial changes (Seeley et al., 1995). In pigs, the oestrous cycle is classified by sexual behaviours; oestrus, when the animal is sexually receptive and non-oestrus (Senger, 2012). Both cycles can be described with two phases, the luteal and follicular, separated by ovulation (Fig. 2.23) (Lorenzen et al., 2015).

| | **Women (menstrual)** | **Non-human primates (menstrual)** | **Minipigs (oestrous)** | **Mice (oestrous)** |
|---|---|---|---|---|
| **Cyclicity** | Continuous cycling | Seasonal Poly-oestral | Continuous cycling | Continuous cycling |
| **Age of Sexual Maturity** | 12.9 years | 3 years | 4-6 months | 6-8 weeks |
| **Length of Cycle** | 28 days | 28-33 days | 19-21 days | 3-5 days |
| **Follicular/Luteal Phase** | 10-14 days/12-15 days | 8 days/ 9 days | 5-6 days/ 15-17 days | 2 days/ 2-3 days |
| **Endometrial Sloughing/Menstruation** | Yes | Yes | No | No |

**Table 2.6: Comparison of the hormonal cycles of the woman, non-human primates, pigs and mice** (Lorenzen et al., 2015). There are multiple similarities between humans and pigs, highlighted in bold. The predominant differences being the sloughing of endometrium that occurs in the woman and the age of sexual maturity.

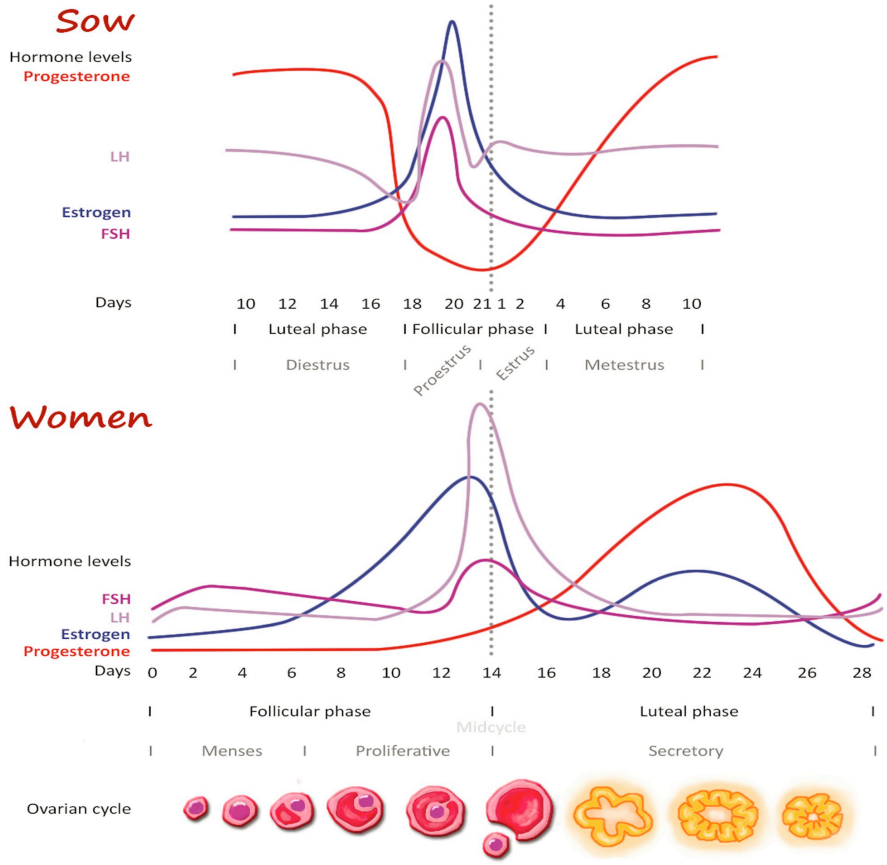


**Figure 2.23: Comparison of the hormonal reproductive cycles in women and pigs** (Lorenzen et al., 2015). In the pig, the significant follicular growth occurs during the luteal phase this results in a cycle shorter than the woman, 19-21 days compared to 28 days, Both women and pigs are spontaneous ovulators and cycle continuously. Both the hormonal cycles are under control of the hypothalamic-pituitary-ovarian axis.

The predominant difference between the species is the pigs bicornate uterus with a urogenital sinus and cervical pulvini (a number of interdigitating prominent solid mucosal folds and protrusions throughout the length of the porcine cervix) (Eurell JA, 2006). However the normal urogenital sinus of the pig is an ideal model for the patients born with malformations causing cloaca or urogenital sinus formation (Gruber et al., 2011).

## 2.10 Summary

In summary, cloacal malformation represents one of the most complex forms of paediatric anorectal malformations. It is rare (incidence of 1 in 50,000 live births, 1 in 20,000 having a persistent urogenital sinus), but has a significant impact on the patient's quality of life as they reach puberty and beyond. Surgical intervention is the current standard treatment option, with the main goal to separate the drainage of faecal and urinary streams, protect renal function, and to repair the vagina and preserve internal genitalia, allowing patients to become sexually active in the future. Minimally invasive cloaca repair operation (MICRO) is preferred. Here, this thesis explores the possibility of developing a MICRO technique using the young, female pig as an animal model.

The overarching aim of the project is to develop a MICRO technique using a self-inflating tissue expander to enable additional native vaginal tissue to be used in reconstructive procedures. This expander would be placed in the vagina of the patient and will, ideally, create tissue with the same histological, hormonal and physiological properties as the native tissue. The newly expanded tissue would then benefit from the resident innervation and blood supply, potentially allowing the patient to experience a better functionality immediately and later in life when reproductive activity commences.

The objectives of this project are to:

I. Characterise the anatomy, histology and morphology of the normal, non-expanded porcine vagina, including measurement of the levels of E-Cadherin (a transmembrane protein involved in cellular adhesion commonly used to differentiate invasive tissue), Ki67 (a nuclear protein associated with cellular proliferation) and Vimentin (a stain confirming the mesenchymal origin of a tissue) within the tissues for later comparison to expanded tissue (as outlined in Chapter 3).

II. Develop a novel anisotropic hydrogel expander with an external company (Oxtex Ltd) that is suitable for implantation into the vaginal lumen of young, pre-adolescent pigs (as outlined in Chapter 4).

III. Implant the novel expander into the vaginal lumen of pre-adolescent pigs, allowing for full expansion of the device over a period of time. Remove and characterise the expanded tissue from the animal post-mortem (as outlined in Chapter 5).

# 3 Characterisation of the Porcine Vagina

## 3.1 Introduction

This chapter addresses the first objective of the project. It describes the characterisation of the anatomy and morphology of the normal, non-expanded porcine vagina (Canberra 12 strain: Landrace/large white/duroc). The macroscopic anatomy of the porcine vagina has been characterised via the method of resin corrosion casting. The vasculature of the urogenital tract was also assessed in this manner.

The metagenomic profile of the adult and prepubescent porcine vagina is also characterised. Extraction and quantification of microbiota present within the lumen of the vagina was undergone and the whole genomic sequencing results are presented in order of abundance. This report provides a baseline report of the porcine vaginal microbiome and will allow for any changes resulting from expansion of the tissue to be identified. It is essential to detect any changes in the metagenomic profile as it may be an indicator of the expanding devices predisposing the animals to urogenital bacterial infections, a serious complication that will hinder the tissue expanders standing in surgical implants.

Tissue samples were collected for histological analysis. The microscopic anatomy was characterised by use of Haematoxylin & Eosin, Picrosirius red and Luxol fast blue stains. Immunohistochemistry was performed on the tissue, resulting in slides of Ki67, Vimentin, E-Cadherin and S-100. The majority of IHC markers used in this study were chosen for their reputation as cancer markers. Ki67 is commonly used as a marker for tumour proliferation.

Vimentin is an indicator of cells undergoing epithelial – mesenchymal transition. E-cadherin is associated with epithelial differentiation, a decrease in E-cadherin levels in expanded tissue could indicate cancer progression or metastasis. S-100 was used as a marker for neural tissue within the slides.

One of the main factors to consider when using commercial pigs as a model for paediatric patients, is the animals' growth rate. The genetic selection that occurs within breeding animals for human consumption results in a much faster rate of growth, especially when compared to humans. One of the main complications that could arise with the commercial porcine growth rate is the inability for the hydrogel device, in the vagina lumen, to increase to a size large enough to cause tissue expansion.

To address this, we conducted a study to measure the animals' vaginal dimensions over a two-week period, as well as their increasing weight. This study has been deemed the 'Porcine Growth Experiment' within the chapter.

## 3.2 Methodology

### 3.2.1 Animal studies and experimental design

All procedures involving animals conducted in this thesis complied with UK Animals (Scientific Procedures) Act, 1986 and European Directive (2010/63/EU) and individual studies were pre-approved by the local ethical review and animal welfare board (AWERB, University of Nottingham). Whilst no in-vivo work was conducted and all pig work was conducted after schedule 1 cull (thus no procedures conducted on any animal), a project licence was nevertheless approved by the UK Home Office (PPL: P36AB74D4) in anticipation of conducted in vivo work. Pre-study protocols were submitted and approved by the Biomedical Services Unit, University of Nottingham.

Any study-specific details about female pigs (Canberra 12: Duroc/large-white/landrace; 55-65 kg; 10-12 weeks of age, in good health and sourced from an accredited supplier) were acclimatised for 7 days before *a priori* assignment

### 3.2.2 Resin Corrosion Casting

Batson's No.17 Plastic Replica and Corrosion Kit was used to determine the size and anatomy of the urogenital sinus of the pigs (Canberra 12 strain; Landrace/large white/duroc), both young (6-week-old, 10kg) and adult, kill weight (6-months-old, 70kg), and to observe the blood supply to the organ.

#### 3.2.2.1 Adult Urogenital Tract Corrosion Cast

Urogenital tracts of adult pigs (6-month-old, 70kg) were obtained from the abattoir. To make the corrosion cast of the urogenital sinus of the adult pigs, 12ml of catalyst was added to 40ml of base solution A. Red dye was added and the mixture was allowed to stand at room temperature whilst the tissue specimen was prepared.

Any tissue that was not of interest, such as the anus and rectum, was removed from the specimen. A three-way cannula was inserted into the vulva of the porcine urogenital tract and was tied in with string, using the labia minor to create a seal. 2ml of promoter C was added to the base solution A and catalyst mixture. The resulting mixture was injected into the urogenital sinus of the specimen via the cannula; the cannula tap was turned off once maximum resin had been injected. Two 20ml syringes were used to inject the mixture.

Throughout this methodology, the term ‘urogenital sinus’ is used to describe the area of urogenital tract between the vulva and the urethral opening.

On observation, the cervix of the sample formed a complete seal, no liquid resin was present in the uterus, and so the remaining reproductive tract proximal to the cervix was removed. The specimen was kept on ice for 3 hours to allow the resin to set and to prevent expansion or distortion of the specimen from the exothermic polymerisation reaction occurring.

Standard procedure requires the use of a maceration solution to remove the tissue from the resin cast once polymerisation has occurred. However, in this case the simple shape of the mould and the nature of the tissue surrounding it allowed the tissue to be removed via blunt dissection. The vagina and

vestibule were cut away and the cervical section of mould 'unscrewed' from the tissue cervix. The cast was cleaned and dried to render it suitable for examination

#### 3.2.2.2 Prepubescent Porcine Urogenital Tract Corrosion Cast

The resin cast of the young (6-week-old, 10kg) pigs was performed in a similar process. The resin solution was made up identically as above. The urogenital tract remained in situ whist resin was being injected. Again, using a three-way cannula, the resin was injected into the urogenital sinus of the animal slowly, with the vulva skin used to create a seal. In the younger pigs, the cervix did not form a complete seal as in the adult, and so the resin progressed up the genital tract and filled both horns of the uterus. The bladder was tied off just above the neck so as not to waste resin; the bladder was seen to be starting to fill instead of the rest of the urogenital tract. Once the substantial filling had occurred, the entire tract was removed from the animal and kept on ice for at least 3 hours, until the resin had set.

The resin mould for the young (6-week-old, 10kg) pigs was more fragile than that of the larger animals and so the maceration protocol was used. Once the resin had set, the urogenital tract was immersed in a solution of 20% potassium hydroxide (KOH), enough to cover the entire tract, and left at room temperature overnight (12-18hrs). After this time, the majority of the tissue

surrounding the mould had disintegrated and any remaining tissue came away when the mould was washed with disinfectant and water.

#### 3.2.2.3 Weaner Prepubescent Porcine Vascular Corrosion Cast

This resin cast was performed in the same manner as described above, but the quantities required were greater, and so were scaled up to produce enough resin to fill the vasculature of the animal. To fill the vasculature, a long-needled catheter was inserted into the descending aorta at the level of the renal kidneys. The red liquid resin was slowly injected into the aorta until the blood supply was perceived as full; no more resin could be injected into the vessel with reflux from the hole in the aorta (120-160ml).

A contrasting blue resin was injected into the urogenital tract of the animal, to allow the organs to be identified once the tissue was removed. The method used was identical to that described above for the prepubescent urogenital tract corrosion cast.

The carcass was kept on ice in a walk-in fridge for 2-3 hours until the resin had set. Following that, the tissue from the point on the aorta of catheter insertion and above and the legs from the point of the patella were removed. The remaining pelvic region was submerged in 5L of 20% KOH and kept at 50°C for 3 days. Once most of the tissue had been digested, the remaining cast was washed with disinfectant and water.

### 3.2.3 Urogenital Dissection and Histology

Cadaveric urogenital tracts obtained from pigs culled at different ages; one and a half months (6 weeks), 7 months and 30 months (2.5 years) were used for gross anatomy and histological study. Dissection and histological sampling of the tissue was performed within an hour to preserve the integrity of the tissues.

#### 3.2.3.1 Preparation of Tissue Samples

The tissue specimens for histological analysis were preserved in 10% buffered formaldehyde solution prior to processing. The tissue dissected from the various aged animals was sectioned into both transverse and longitudinal strips of tissue, approximately 5mm thick. The tissue was obtained from different areas of the porcine urogenital sinus; the cervical region (known to be vaginal tissue), the vulva region (known to be vestibule tissue) and the region of entrance of the urethra into the urogenital sinus. The samples were placed in embedding cassettes and kept in 70% ethanol prior to paraffin wax perfusion. The samples were infiltrated with paraffin via a mechanical processor overnight. The samples were manually embedded. Once processed, the cassettes were placed in a 58°C paraffin bath to melt the wax formed in the mechanical processor. The samples were placed in a paraffin mould, appropriate size allowed for at least 2mm of wax the tissue and embedded in paraffin wax.

Five micrometre microtome sections of the samples were cut and air dried on individual glass slides at 60°C for 5 hours. The slides were manually stained

with Haematoxylin & Eosin (H&E) and Picro-Sirius Red, later some were stained with Luxol Fast Blue. H&E is a routinely used stain for biological specimens. The basic haematoxylin dye stains basophilic structures, such as nuclei, blue-purple and the acidic alcohol-based eosin stains eosinophilic structures, such as cytoplasm, pink.

Picro-Sirius red is an azo dye, primarily used for staining collagen. The collagen fibres appear a vibrant red and are rendered birefringent; the tissue has a refractive index that depends on the polarisation of light, a property that allows for slides to be viewed under polarised light. For some of the analysis of tissue samples, the wax blocks were sent to Bridge Pathology Ltd to obtain successful immunohistochemistry (IHC). The IHC was Ki67, Vimentin, E-Cadherin and S-100. The first three are predominantly used to detect possible cancerous tissue and identify malignant tissue. Ki67 is a cellular marker for proliferation, it is present during all active phases of the mitotic cell cycle and is absent during cellular quiescence. Nuclei that are undergoing mitosis stain a dark brown colour, whilst the remaining cellular components remain blue from the haematoxylin counter stain. Vimentin is a type III intermediate filament protein expressed in mesenchymal cells; it is the major cytoskeleton component of these cells. Stained vimentin is used as a marker for mesenchymal-derived cells or cells that are undergoing epithelial to mesenchymal transition. This can occur during both normal development and metastatic progression. The cells that are positive for vimentin stain brown and the remaining tissue appears blue due to the haematoxylin counterstain.

E-cadherin (epithelial cadherin) is a protein that at encoded for by the CDH1 gene, this is a tumour suppressor gene. E-cadherin is a calcium-dependent

cell-cell adhesion glycoprotein; loss of function of this gene contributes to the progression of cancer by increasing proliferation, invasion and/or metastasis. Downregulation of E-cadherin decreases the strength of cellular adhesion within a tissue, resulting in cellular motility. This allows cancer cells to cross the basement membrane and invade surrounding tissue. Like vimentin, cells that are positive for E-cadherin stain brown, and negative E-cadherin cells appear blue due to the haematoxylin counterstain.

S-100 proteins are normally present in cells derived from the neural crest, such as Schwann cells, melanocytes and dendritic cells. This makes them excellent markers for neural tissue within a histological slide. The proteins have been associated with a variety of intra- and extracellular functions. This includes the regulation of protein phosphorylation, transcription factors, enzyme activities and cell growth. In the case of this study, the S-100 IHC was used to identify the nervous supply of the porcine vagina.

### 3.2.4 Metagenomic Characterisation of the Porcine Urogenital Sinus

A metagenomic study of the microbiome of the urogenital sinus of various aged pigs, 6-weeks-old and 6-months-old, was performed. The swab samples were taken immediately after euthanasia of the animals. The vulvar area of the pig was cleaned to avoid contamination of the swab as it was inserted into the urogenital sinus. Once the swab samples were taken, they were processed within an hour, maintaining the integrity of the sample contents. The swabs were vortexed within their amies transport solution at 700 – 800 rpm for 5 minutes. The supernatant was transferred into a fresh, sterile 1.5ml Eppendorf and centrifuged at 13,000g. The supernatant from this was pipetted off, carefully to not displace the pellet, and discarded. The remaining pellets were stored at -80°C until DNA extraction was performed.

#### 3.2.4.1 DNA Extraction

DNA was extracted from the samples using the QIAmp cador Pathogen Mini Kit. 20µl of proteinase K and the samples were pipetted into a 2ml micro centrifuge tube. PBS was added to make up the sample and proteinase K solution to 200µl. 100µl of Buffer VXL was added and the mixture was vortexed briefly and left to incubate at 20-25°C for 15 minutes. Then 350µl of Buffer ACB was added and ensuring there were no droplets trapped in the lid of the tube, the mixture was vortexed. The contents of the tube (around 500µl) were transferred to a QIAmp Mini Column with a 2ml collection tube. This was then centrifuged at 8000rpm, for 1 minute. The mini column was then transferred to

a clean collection tube and the supernatant discarded. 600µl of Buffer AW1 was added to the mini column and centrifuged at 8000rpm for 1 minute. The mini tube was then transferred to a clean collection tube and again, the filtrate was discarded. The 600µl of Buffer AW2 was added and again, the mixture was centrifuged at 8000rpm for 1 minute, the mini tube moved to a clean collection tube and the filtrate discarded. Then centrifugation of the mini column at 14,000g for 2 minutes was performed and the mini column was transferred to a low-binding 1.5ml micro tube and the collection tube, containing filtrate, was discarded. 35µl of Buffer AVE was added and the mixture was left to incubate at room temperature for 1 minute. Finally, the tube was centrifuged at 14,000rpm for 1 minute.

#### 3.2.4.2 Quantification of Extracted DNA

The QUBIT 3.0 Fluorometer was used to quantify the DNA that had been extracted from the samples via the process described above. The Fluorometer was programmed with to the settings, double stranded DNA and high sensitivity. The QUBIT working solution was made up by combining 1µl of DsNA HS reagent with 199µl, this amount is for the use with one sample only. 2µl of DNA extracted sample was combined with 198µl of the QUBIT working solution. The mixture was left to incubate at room temperature for 2 minutes and then placed in the Fluorometer to be read and results were recorded.

### 3.2.4.3 Microbe DNA Enrichment

The NEBNext Microbiome DNA Enrichment Kit was used to enrich the microbial content of the DNA samples that had previously been extracted and quantified. To use the kit, calculation was required to determine the amount of MBD2-Fc-bound magnetic beads needed for each sample. For each 6.25ng of in Put DNA, 1µl of beads was needed, therefore:

***Y = amount of MBD2-Fc-bound magnetic beads (µl) = input DNA (ng) / 6.25 ng/µl***

### 3.2.4.4 Pre-binding of MBD2-Fc Protein to Magnetic Beads

The NEBNext Protein A magnetic beads were re-suspended by gently pipetting the 'slurry' up and down until the suspension became homogenous. The beads should not be vortexed. The 1x bind/wash buffer was prepared by diluting 1-part NEBNext bind/wash buffer (5x) with 4 parts DNAse-free water (one individual reaction requires 4mls of 1x bind/wash buffer). In a low binding microtube, 0.1 (Y) of MBD2-Fc protein and (Y)µl of magnetic beads, the two were mixed by pipetting the solution up and down multiple times. The bead-protein mixture was then left to incubate at room temperature, on a rotator for 10 minutes. The microtube was then placed on a magnetic rack for 2-5 minutes, until the beads had completely collected on the wall of the tube and the solution is clear. The supernatant was then carefully removed with a pipette, so as not to disturb the beads, and discarded. Then 1ml of the 1x bind/wash buffer was added to the tube to wash the beads, again the mixture

was mixed by pipetting up and down. The beads were then mixed on the rotator for 3 minutes at room temperature. Following this, the tube of beads was placed on the magnetic rack for 2-5 minutes until the beads had collected and the solution was clear. The supernatant was then removed as before and discarded. The process of washing, rotating and separating of the beads was repeated once more and the supernatant was discarded. The tube was removed from the magnetic rack and Y amount of 1x bind/wash buffer was added to re-suspend the beads. This bead mixture remains stable for seven days when kept at 4°C.

#### 3.2.4.5 Capture of Methylated Host DNA

DNA methylation is a biological process by which methyl groups (CH3) are added to a DNA molecule. Y amount of MBD2-Fc-bound magnetic beads was added to 15µl of DNA sample. The bind/wash buffer (5x) was added to DNA input sample to create a final concentration of 1x (15µl of DNA input sample + 3.75µl of bind/wash buffer (5x). The reaction was left to incubate for 15 minutes at room temperature, with rotation and resulted in the methylated host DNA being collected by the magnetic beads and the target microbial DNA being present in the remainder of the sample.

#### 3.2.4.6 Collection of Enriched Microbial DNA

After incubation, the tube was placed on the magnetic rack for 5 minutes, until the beads collected, and the solution appeared clear. The supernatant, containing the target DNA, was carefully removed and placed into a low-binding, DNAse free eppendorf. The sample could be stored at -20°C until further processing.

#### 3.2.4.7 Clean-Up of Microbial DNA Samples using Agencourt AMPure XP Beads

Once the beads had reached room temperature, they were thoroughly mixed. Then 1.8x the volumes of beads were added to the sample eppendorfs and mixed by gentle pipetting. The mixture was then left to incubate at room temperature for 5 minutes. The eppendorfs were then pulse-span in the mini centrifuge and places on the magnet rack for at least 5 minutes, the supernatant was carefully removed and discarded. Keeping the eppendorf of the rack, 400µl of freshly prepared 80% ethanol was added, left for 30 seconds and then removed and discarded. This process was then repeated so that the beads had been washed with 80% ethanol twice. The eppendorf was then pulse-span, returned to the magnetic rack and residual ethanol was gently removed. With the eppendorf remaining on the rack, the cap was opened, and the beads were left to air dry for 5 minutes at room temperature. The beads were then re-suspended in 50µl of 1x TE buffer. Finally, the beads were pulse-span, returned to the magnetic rack and the supernatant was collected and stored at -20°C.

### 3.2.5 Randomised Histological Slide Imaging

The random sampling strategy was obtained from the Open University. The microscope objective was placed over the centre of the area of interest. Images were taken at 100x magnification. The field of view was then altered by moving the slide approximately 0.3mm to the left (by turning the microscope control a quarter turn to the left) and then approximately 0.3mm up (by turning the microscope control a quarter turn down). This technique produces a sampling pattern slide like the one displayed in figure 3.1.

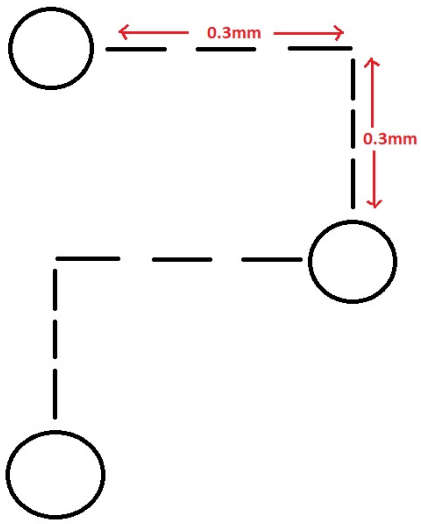


**Figure 3.1: Schematic diagram of the sampling pattern across a slide when taking images at random.**

### 3.2.6 Quantification of Random Sample Images

Image J software was used to quantify the intensity of staining in the sample images. The images were converted to black and white 16-bit images before they could before analysis could occur (image → type → 8-bit → 16-bit). Using the adjustment features within the software, the threshold of the image was altered to the point that only the positive stained structures within the image were seen (image → adjust → threshold). This formed a binary image. The particles within the image were then analysed (analyse → analyse particles → select the following boxes [display results, summarise, exclude on edges, include holes and show nothing]). The results obtained show the count of the number of particles as well as the percentage area and average size of particle.

### 3.2.7 Threshold values for altering images in Image J

- Ki67: 0 – 125 pixel intensity
- ECAD epithelium: 0 – 100 pixel intensity
- ECAD mucosa: 0 – 130 pixel intensity
- Vimentin epithelium: 0 – 100 pixel intensity
- Vimentin mucosa: 0 – 130 pixel intensity

### 3.2.8 Animal Housing for the Porcine Growth Experiment

The work conducted in this experiment was authorised within the Home Office License PPL: P36AB74D4.

Nine juvenile pigs, with an averaging weight of 15kg, were weighed and kept in the biosecurity unit of the Sutton Bonington Campus of the University of Nottingham. The animals were weighed on arrival. All the weights recorded were live animal weights. The animals were euthanised, via schedule 1 methods, in groups of 3 at weekly increments. Their weights were recorded each week and on the day of euthanisation.

The pigs were housed as a complete group of nine and were fed an ad libitum diet, to allow the animals to grow at a natural rate, instead of weight gain for human consumption.

### 3.2.9 Vaginal Corrosion Casts for the Porcine Growth Experiment

Once euthanised the urogenital tracts of the animals were removed, and resin casts were taken using Batson's No. 17 kit. Using a three-way cannula, the resin was injected into the urogenital sinus of the animals slowly, with the vulva skin used to create a seal. The bladder was tied off just above the neck so as not to waste resin. Once filled, the tracts were kept in formaldehyde solution in a laboratory fridge, to preserve the tissue and render it viable for histological analysis.

The resin casts were removed from the urogenital tracts, the following dimensions were measured with callipers: vagina length, maximum vagina diameter and minimum vagina diameter.

### 3.2.10 Tissue Preservation for the Porcine Growth Experiment

The removed tissue was sectioned into transverse sections, approximately 5mm thick. The samples were placed in embedding cassettes and kept in 70% ethanol prior to paraffin wax perfusion. The samples were infiltrated with paraffin via a mechanical processor overnight. The samples were manually embedded. Once processed, the cassettes were placed in a 58°C paraffin bath to melt the wax formed in the mechanical processor. The samples were placed in a paraffin mould, appropriate size allowed for at least 2mm of wax around the tissue and embedded in paraffin wax. 5µm microtome sections of the samples were cut and air dried on individual glass slides at 60°C for 5 hours. The slides were manually stained with Haematoxylin & Eosin (H&E).

## 3.3 Results

### 3.3.1 Resin Corrosion Casts

#### 3.3.1.1 Prepubescent Porcine Urogenital Corrosion Cast

The image below shows the prepubescent porcine urogenital tract resin corrosion cast (Fig. 3.2). The resin was inserted into the vulva of the cadaver via a catheter, which was tied into place and remains as part of the cast. The urogenital sinus extends from the string seen in the image to the point of confluence between the urethra and vagina. There was a form of stricture observed between the urogenital sinus and the vagina. As discussed earlier, the pig is one of the mammals with an obvious hymen, as well as the human, a possible reasoning for the stricture.

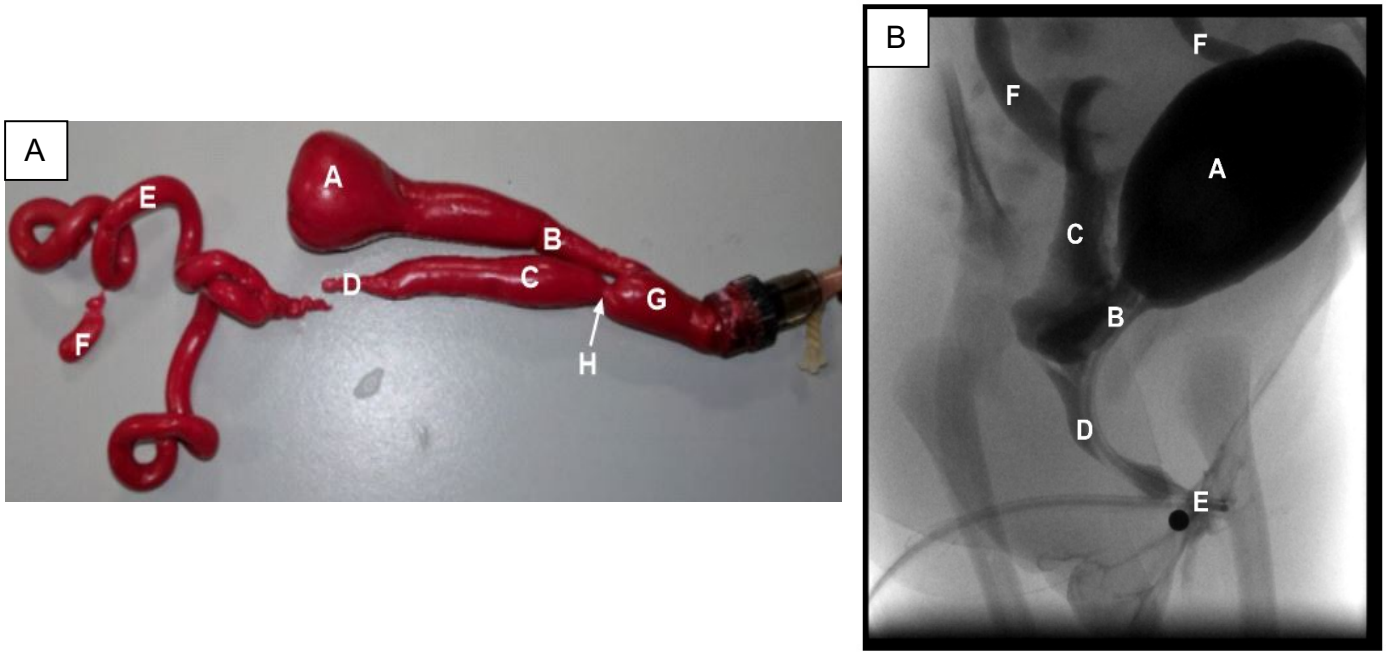


**Figure 3.2: Urogenital anatomy of prepubescent pig and paediatric patient.**
**A**. Image of the prepubescent (6-week-old) female porcine urogenital tract corrosion cast. **A** = bladder. **B** = urethra. **C** = vagina. **D** = cervix. **E** = uterine horn. **F** = ovary. **G** = urogenital sinus. **H** = stricture between the urogenital sinus and the vagina, possible hymen.
**B**. Micturating cystogram of 1 week old female patient. **A** = bladder. **B** = urethra. **C** = vagina/uterus. **D** = long common channel/urogenital sinus. **E** = single opening on perineum. F = bilateral ureteric reflux, dilated ureters

Images of a patients micturating cystogram were donated to this project by Queen's Medical Centre, Nottingham, UK. The results of a micturating cystogram in a 1-week-old female patient shows similar anatomy. A clear common channel is seen in the radiograph, with the bladder and vagina draining into it, and a single opening on the perineum is present (Fig. 3.2 (B)).

One of the prepubescent porcine corrosion casts presented with duplex vagina (Fig. 3.3 (A)). The same female patient represented in figure 3.2, also presented with a uterus didelphys and a vaginal septum. The patient had a duplicate vagina, both draining into a common channel (Fig. 3.3 (B)).

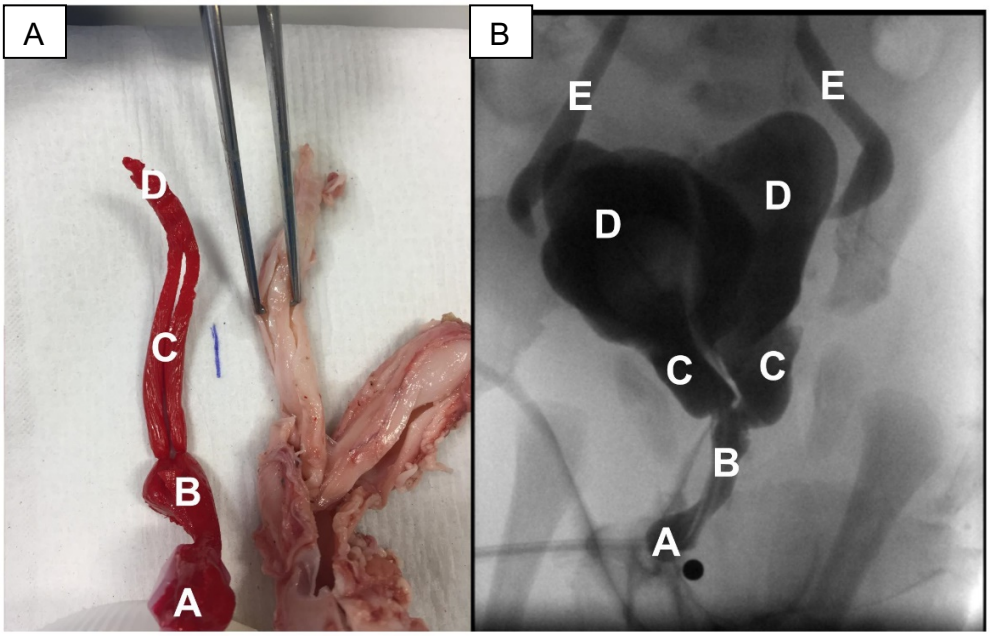


**Figure 3.3: Vaginal septation in porcine and human reproductive tracts. A**. Image of the reproductive tract, including cast, of a prepubescent (6-weeks-old, 10kg) porcine reproductive tract, with a duplex vagina. **A** = perineal opening of urogenital sinus. **B** = point of confluence of the vagina and urethra. **C** = duplex vagina. **D** = single cervix. **B**. Micturating cystogram of 1 week old female patient, with a uterus didelphys with vaginal septum. **A** = Perineal opening of the common channel. **B** = point of confluence of the vagina and urethra. **C** = duplex vagina. **D** = uterus didelphys. **E** = dilated ureters.

### 3.3.1.2 Adult Porcine Genital Tract Corrosion Cast

A resin corrosion cast of the adult female porcine genital tract was performed with the same technique as for the prepubescent cast. The resulting cast predominantly filled the vagina and urogenital sinus sections of the tract (Fig. 3.4).

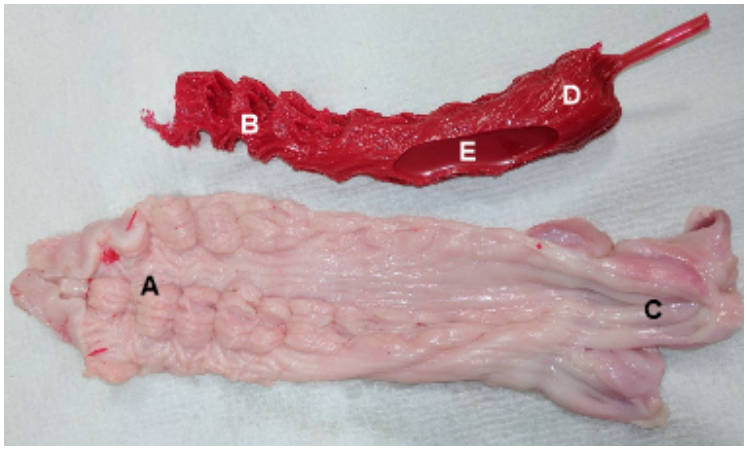


**Figure 3.4: Resin corrosion cast of the adult (70kg) female porcine genital tract and the opened fresh specimen that the cast was taken from. A** = cervical region of vagina within the tissue specimen. **B** = cervical region of vagina in the cast, the beginning of the 'corkscrew' structure of the cervix can be seen. **C** = the urogenital sinus of the tissue specimen. **D** = the urogenital sinus of the cast. **E** = the point of confluence between the vagina and urethra, it is possible that air trapped in the bladder prevented the resin from entering the urethra.

#### 3.3.1.3 Prepubescent Porcine Vascular Corrosion Cast

The labelled images displayed below show the blood supply of the young porcine reproductive tract at various planes, starting with external arterioles supplying the surrounding tissue and then dissecting down to the more internal organs, such as the uterus and vagina. The red resin was injected into the blood supply of the animal and the blue into the vestibule of the animal, allowing for clear identification of the urogenital tract. Initially the descending aorta, external iliac arteries and femoral arteries can be seen clearly with obvious tracking from the abdomen, through the pelvis to the beginning of the hind legs. The urethra and bladder or the most ventral structures of the corrosion cast, with the uterine horns lying dorso/-cranially to them (Fig. 3.5).

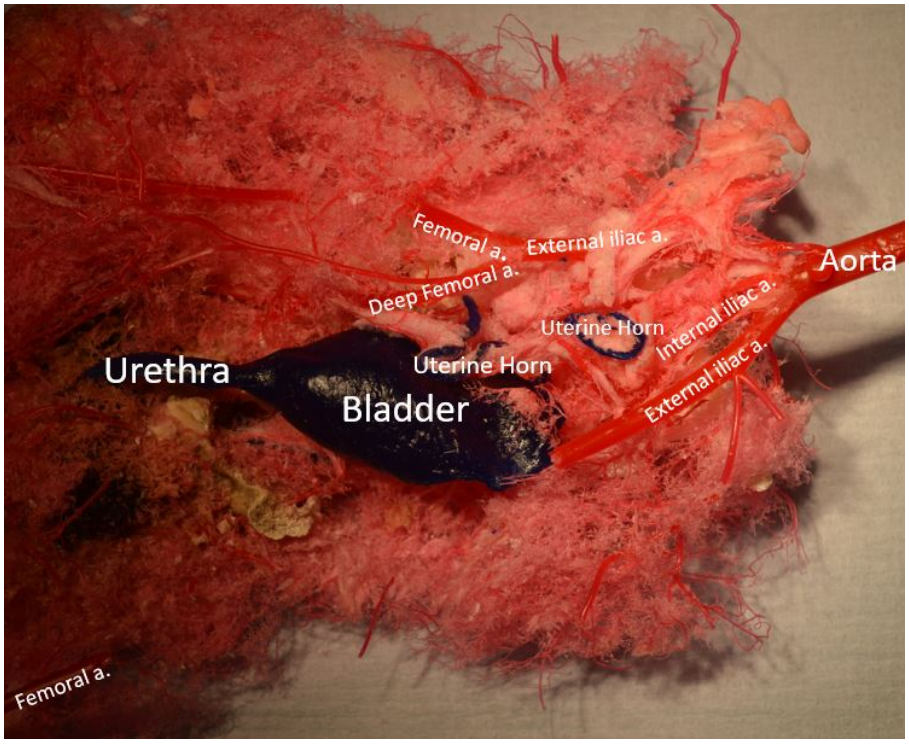


**Figure 3.5: Vascular corrosion cast of the pelvic region of a 6-week-old (10kg) female pig, bladder in situ.** The red resin represents the blood vessels supplying the urogenital organs of the animal. The blue resin represents the urogenital organs, starting with the urogenital sinus, the most caudal structure, and more cranially, the bladder and the horns of the uterus.

Once the bladder and urethra were removed, the underlying blood supply to the reproductive system could be seen more clearly. With the vagina and cervix seen lying cranial to the pelvic symphysis, the multiple plexuses and anastomoses of blood vessels supplying the organ are difficult to distinguish. The main arteries than can be identified near the vagina are the internal iliac, internal pudendal and uterine artery (Fig. 3.6).

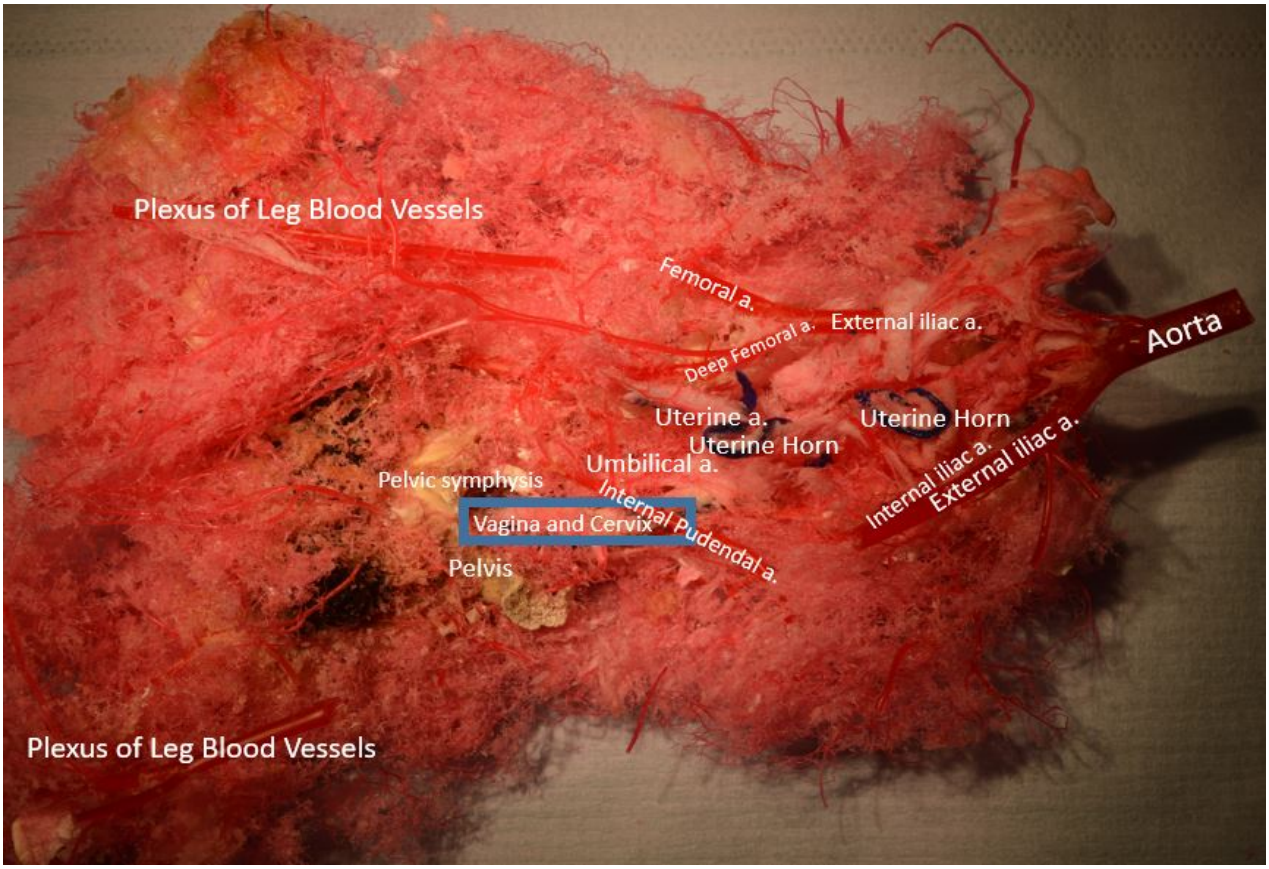


**Figure 3.6: Vascular corrosion cast of pelvic the region of a 6-week-old (10kg) female pig; bladder removed.** The blue resin structure that filled the bladder has been removed, revealing the arteries supplying the vagina and cervix; the internal iliac, internal pudendal and uterine arteries.

Removal of the uterine horns from the cast and rotation of the vagina and cervix away from the spine allow for clear viewing of the tracts taken by the blood vessels from the aorta towards the urogenital tract. The general direction of the vessels is caudal, with the vast number of branches heading in a similar direction (Fig. 3.7). The careful dissection of the vagina and cervix from the corrosion cast show the smaller blood vessels wrap around the organ, supplying as much of the surface of the organ as possible. The larger blood vessels seen within the plexus are the various branches from the uterine and vaginal arteries (Fig. 3.8).

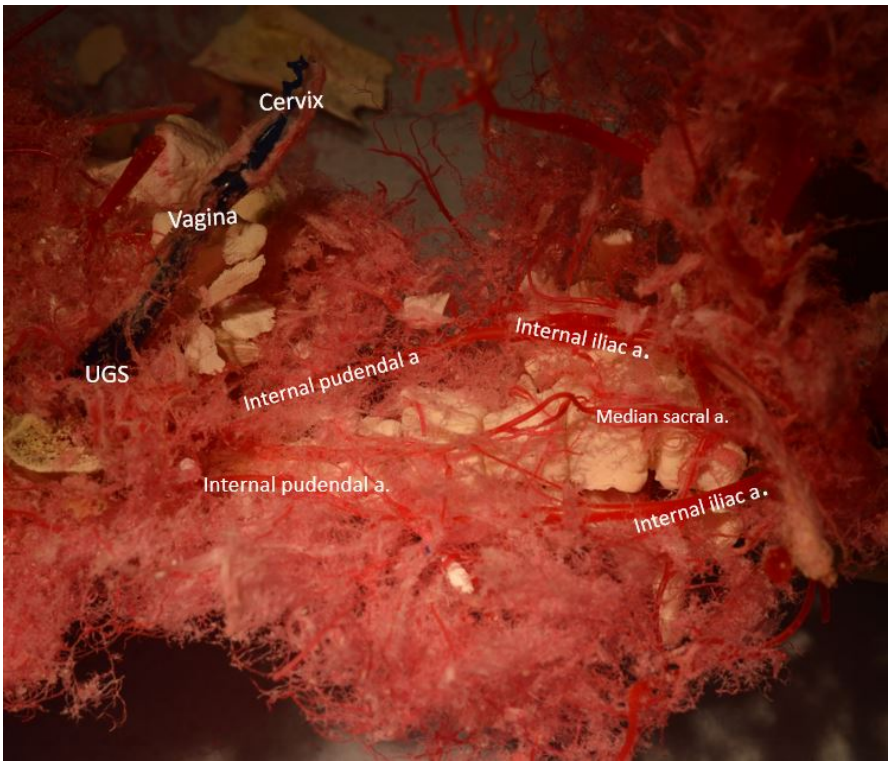


**Figure 3.7: Vascular corrosion cast of pelvic the region of a 6-week-old (10kg) female pig, bladder and uterine horns removed.** The urogenital sinus, vagina and cervix remain in situ. Remnants of the sacrum and pelvic symphysis is seen.

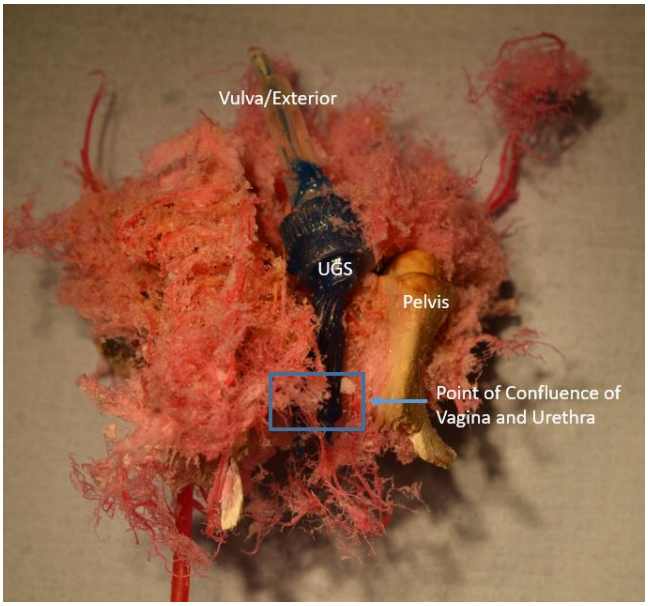


**Figure 3.9: Vascular corrosion cast of the pelvic region of a 6-week-old (10kg) female pig.** The bladder, uterine horns, sacrum, cranial blood supply and the blood supply to the legs removed. The urogenital sinus and the catheter used to fill the urogenital organs can be seen in situ.

The vestibule of the pig remained in situ when the vagina was removed, due to the catheter used to insert the resin disrupting its normal anatomical shape and preventing it from being removed (Fig. 3.9).

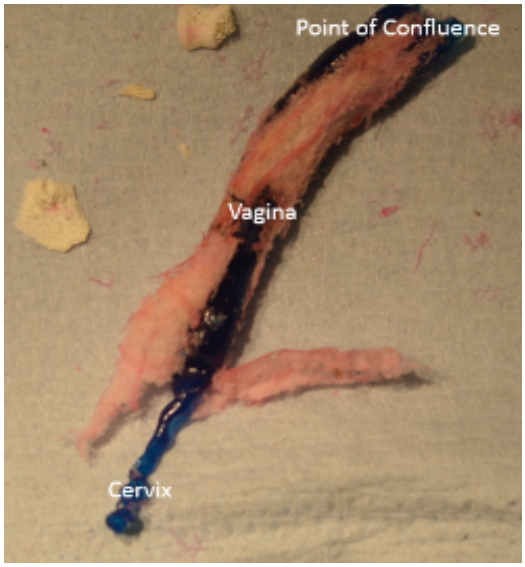


**Figure 3.8: Vascular corrosion cast of the vagina and cervix of a 6-week-old (10kg) female pig.** The blue resin shows the true morphology of the labelled structures; the 'corkscrew' shape of the cervix is clearly seen. The resin surrounding the vagina represents the vascular meshwork that surrounds the structure.

Once the urogenital sinus cast had been removed, a clear channel formed by the blood vessels surrounding it was seen. The larger branches from the uterine and vaginal artery can be seen running longitudinal along the channel, with multiple anastomoses forming between them (Fig. 3.10).

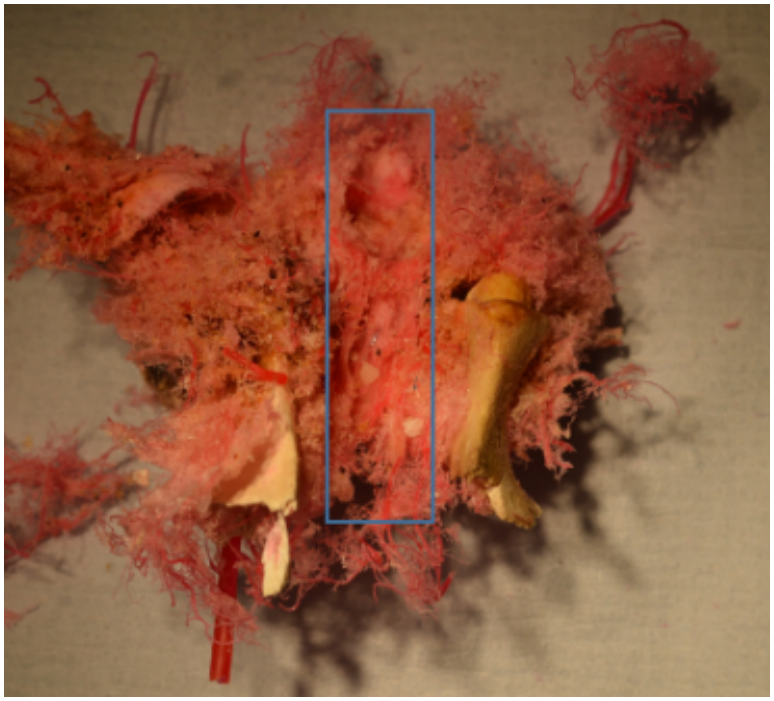

**Figure 3.10: Vascular corrosion cast of the pelvic region of a 6-week-old (10kg) female pig.** The image shows the same structures as in figure 9, but the blue resin cast of the urogenital sinus has been removed. The blue box highlights the channel formed by the vascular system surrounding the urogenital structure. Some larger blood vessels can be seen in the channel, but most of the blood supply arises from the vast network of fine branches and anastomoses.

## 3.3.2 Histology

### 3.3.2.1 Haematoxylin and Eosin Stain

The histological layers of porcine vaginal tissue present as the following: the most superficial layer is the mucosa; this comprises of the epithelium and the lamina propia. The surrounding layers comprise of the smooth muscle and adventitia layers. As was described earlier, the epithelium of the porcine vagina is non-keratinised stratified squamous epithelium (Fig. 3.11 (A)). This morphological presentation can also be seen in adult vaginal tissue the sample image in figure 3.11 (B) was obtained from an online histology and morphology learning resource (Michigan, 2018). The individual layers described above can be seen clearly in both adult porcine and human tissue samples (Fig. 3.11 and 3.12).

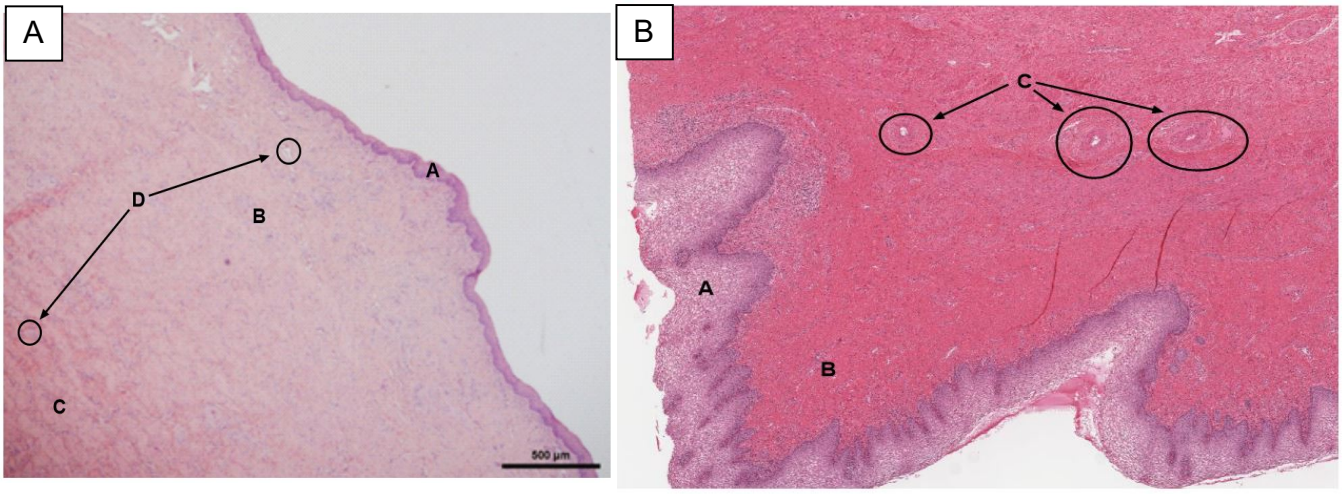


**Figure 3.11: Vaginal tissue of adult female pig and adult human. (A)** Vaginal tissue of an adult (70kg) female pig. H&E stain, 40x magnification. **A** = non-keratinised stratified squamous epithelium. **B** = lamina propia. **C** = smooth muscle tissue. **D** = blood vessel present in both the lamina propia layer and within smooth muscle tissue. **(B)** Vaginal tissue of an adult human. H & E stain, 2x magnification (Michigan, 2018). **A** = non-keratinised stratified, squamous epithelium. **B** = lamina propia. **C** = blood vessels present within smooth muscle tissue.

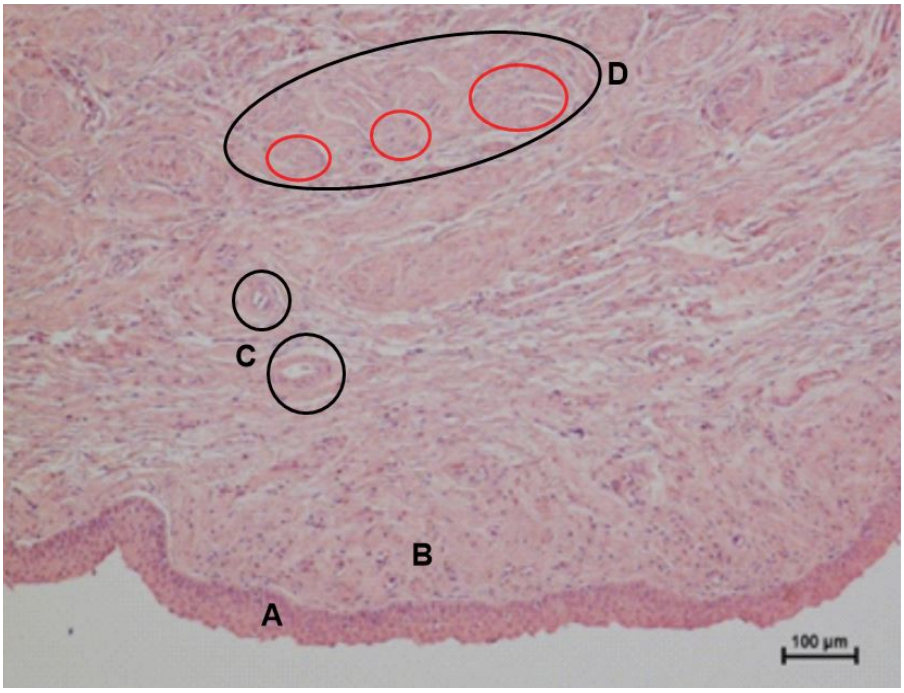


**Figure 3.12: Vaginal tissue of adult (70kg) female pig. H&E stain, 100x magnification. A** = non-keratinised stratified squamous epithelium. **B** = lamina propia. **C** = blood vessels, most likely arterioles present within the lamina propia and the smooth muscle tissue. **D** = a single smooth muscle fascicle surrounded by the endomysium, within which multiple bundles of myofibrils (examples circled in red) are present.

However, when observing tissue samples from the youngest aged pigs (6-weeks-old) the ability to distinguish between the layers described above was far more difficult. The tissue underlying the epithelium had a homogenous appearance, with the cells presenting with a morphology generally associated with mesenchymal cells. The muscle layer is scarcely identifiable, with the main structures that are recognisable consisting of blood vessels and nerves (Figs. 3.13 and 3.14).

The epithelium of the young porcine tissue did not have the same expected structure as the adult tissue. At varying magnifications, the epithelium presented as single cell columnar. In some of the images of the tissue, the epithelium appeared to be ciliated (Fig. 3.15).

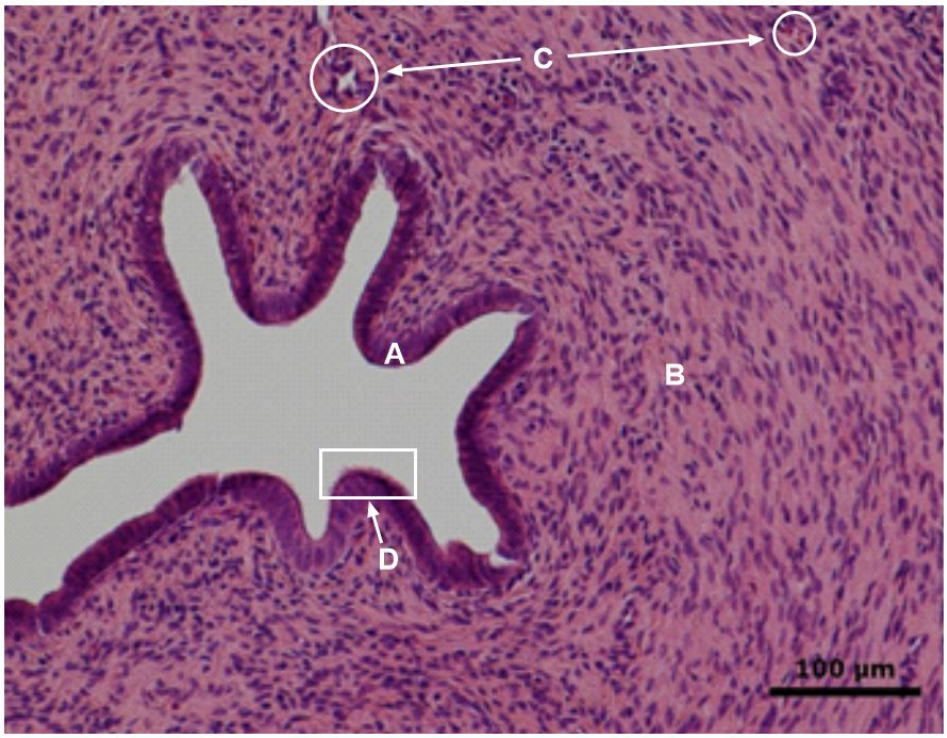


**Figure 3.14: Lumen of the vagina of a 6-week-old (10kg) female pig. H & E stain, 200x magnification. A** = single cell columnar epithelium. **B** = homogenous mesenchymal tissue underling the epithelium. **C** = lumen of blood vessels and red blood cells within the mesenchymal tissue. **D** = possible ciliated epithelium.

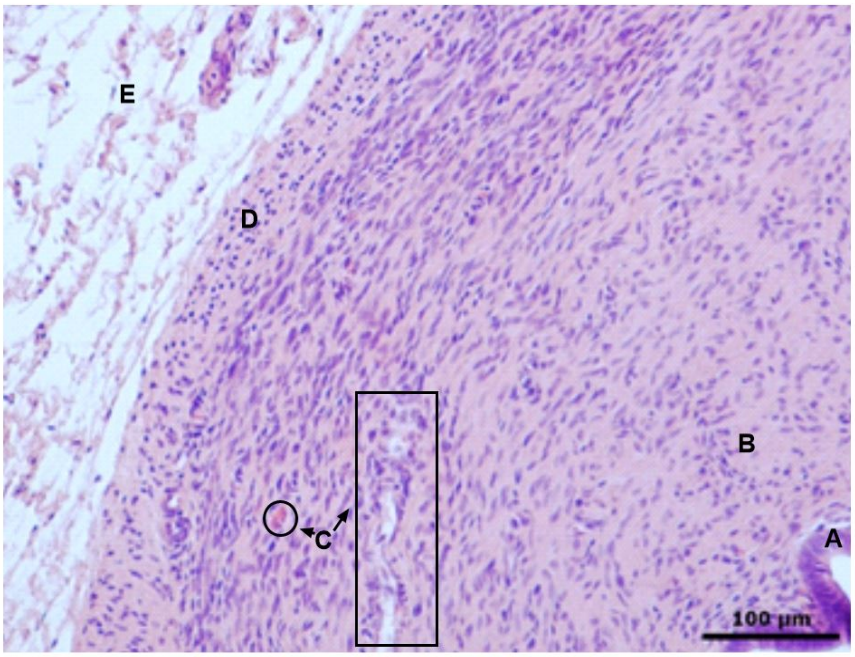


**Figure 3.13: Vagina of a 6-week-old (10kg) female pig. H & E stain, 200x magnification. A** = single cell columnar epithelium. **B** = homogenous mesenchymal tissue underling the epithelium. **C** = lumen of blood vessels and red blood cells within the mesenchymal tissue. **D** = possible differentiation of tissue into muscle tissue. **E** = lateral loose connective tissue.

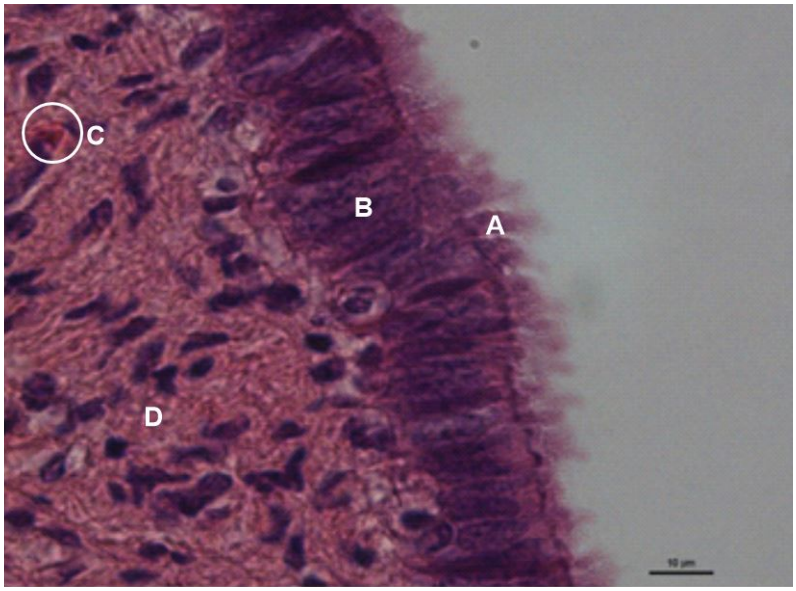


**Figure 3.15: Epithelium of the vagina of a 6-week-old (10kg) female pig. H & E stain, 1000x magnification. A** = possible cilia on the lumen side of the epithelium. **B** = single cell columnar epithelium. **C** = red blood cells within the tissue underlying the epithelium. **D** = undifferentiated, mesenchymal tissue underlying the epithelium.

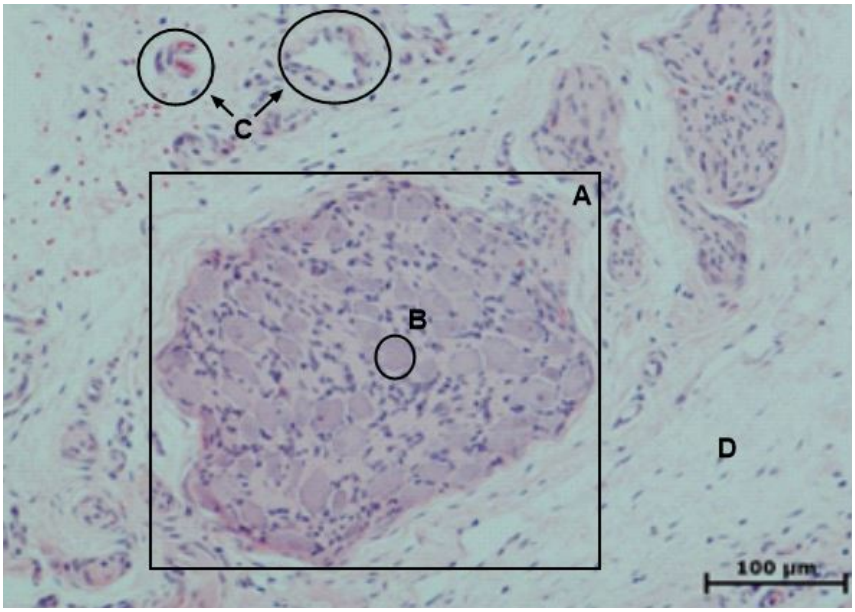


**Figure 3.16: Nerve plexus within the adventitia of the vagina of a 6-week-old (10kg) female pig. H&E stain, 200x magnification. A** = the whole nerve plexus. **B** = an individual nerve cell surrounded by endoneurial tissue within the plexus. **C** = blood vessels surrounding the nerve plexus. **D** = adventitial loose connective tissue.

Figure 3.16 shows the normal presentation of nerve plexuses stain with H&E at a high magnification (20x). The myelin sheath of individual axons is surrounded by endoneurial connective tissue; this brings the axons together to form a fascicle. The fascicle is surrounded by perineurial connective tissue and multiple fascicles are arranged in bundle like formations by loose epineurial tissue. This tissue contains large blood vessels in addition to the capillaries that are present in the perineurium and endoneurium.

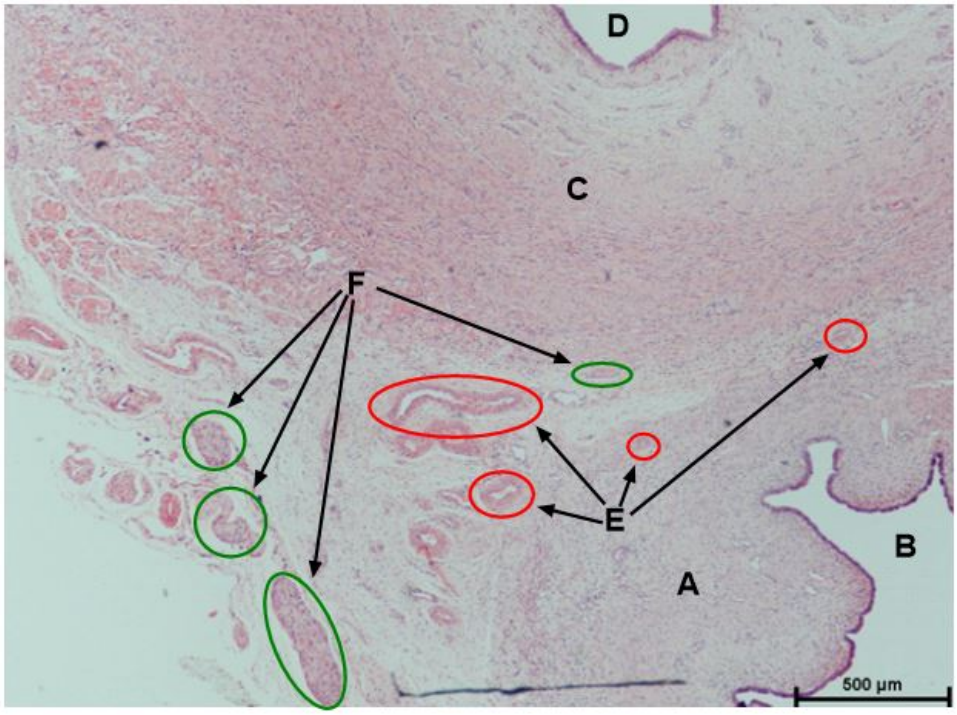


**Figure 3.17: Loose connective tissue between the vagina and urethra of a 6-week-old (10kg) female pig. H & E stain, 40x magnification. A** = undifferentiated mesenchymal tissue underlying vaginal epithelium. **B** = lumen of the vagina. **C** = lamina propia of the urethra. **D** = lumen of urethra. **E** = blood vessels within the connective tissue and between the vagina and urethra. **F** = nerve bundles within the connective tissue and between the vagina and urethra.

Figure 3.17 shows the configuration of blood vessels and nerves in the connective tissue joining the vagina and urethra. Both the blood vessels and nerve bundles run within the tight junction of the two structures, supplying them simultaneously.

### 3.3.2.2 Comparison of Neonatal Human and Porcine Histology

Histological images of vaginal tissue from patients with cloaca were donated to this project by Nationwide Children's Hospital, Columbus, USA. Figure 3.18 shows images of this tissue (Fig. 3.18 (A)) alongside one of our own porcine samples (Fig. 3.18 (B)). The human tissue samples were instantly fixed live samples and so the blood vessels within them are easily identifiable. The represent the density of the blood vessels within the porcine tissue, they have been highlighted with red rings.

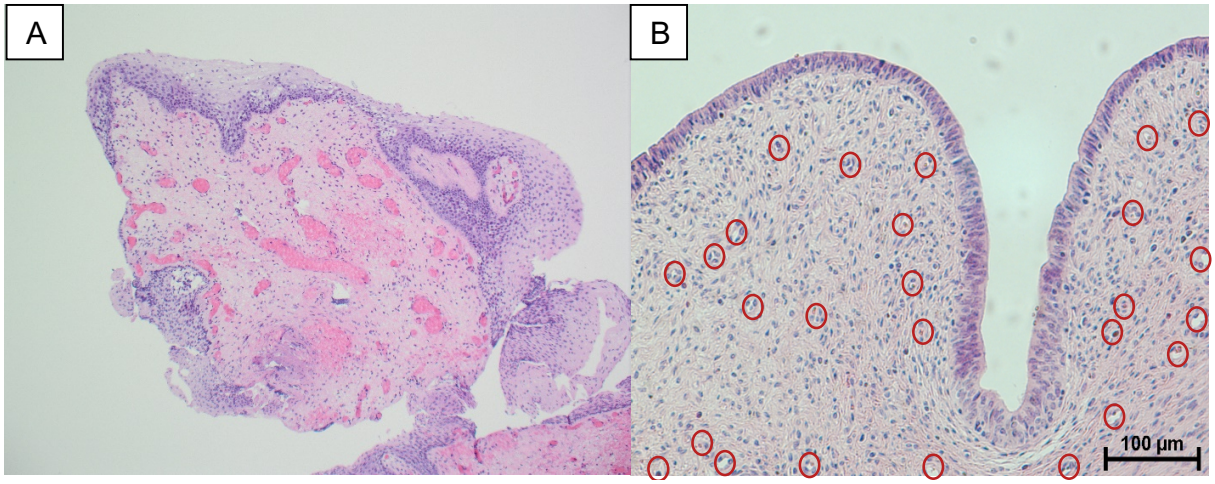


**Figure 3.18: Neonatal human (12 months) and pre-pubescent (8 weeks) porcine vaginal tissue. H&E stained**. **A** shows neonatal human vaginal tissue at 100x magnification. This was a live sample and so the blood vessels are easily identified. **B** shows prepubescent porcine vaginal tissue at 200x magnification. This was a post-mortem sample, the blood vessels within the tissue have been highlighted for comparison with the human sample.

#### 3.3.2.3 Picrosirius Red Stain

Picrosirius red histological stain assisted in visualising the collagen distribution within the porcine tissue samples. When comparing adult vaginal tissue with that of the younger animal under polarised light, there is a clear difference in the appearance of the tissue.

The adult tissue showed prominent strands of thick collagen, these appeared yellow under polarised light (Fig. 3.19). Smaller strands of collagen should appear green under polarised light, these strands cannot be seen in either tissue samples.

The picrosirius red stain also allows for the distinguishing if the differentiated histological layers on slides. Both normal lighting and polarised lighting of the slides clearly showed the muscle layer in the adult tissue and the lamina propia between the muscle and the epithelium. Again, in the younger animal, these structures are not identifiable under either lighting, maintaining the homogenous, mesenchymal appearance. The single cell epithelial structure of the young pigs can be seen unmistakably in the picrosirius red stained samples (Fig. 3.20).

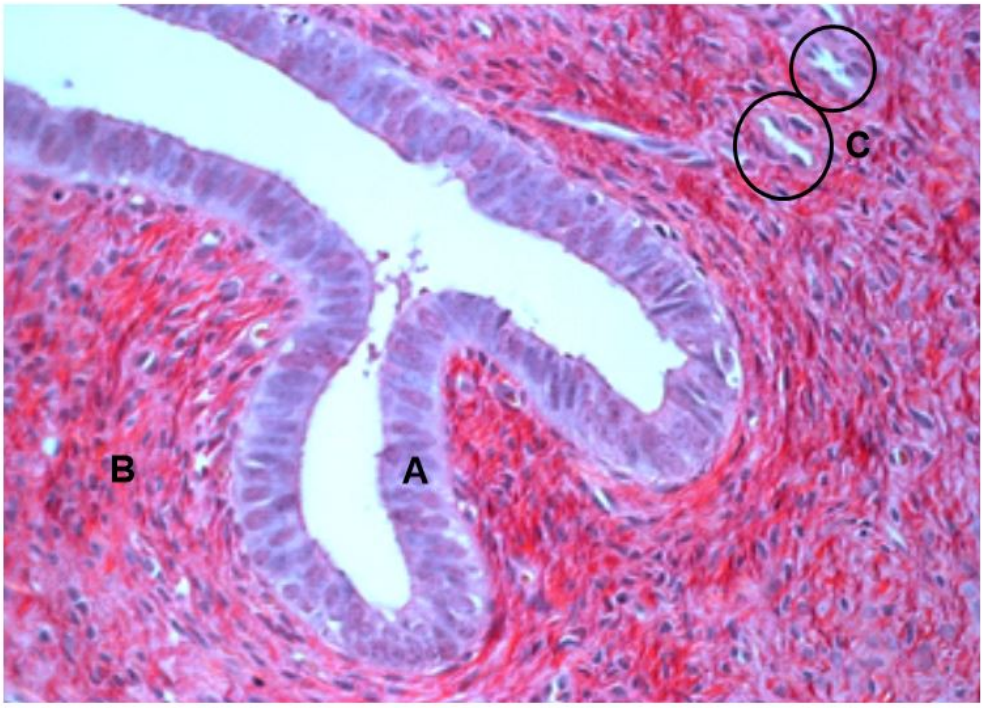


**Figure 3.19: Lumen of the vagina of a 6-week-old (10kg) female pig. Picrosirius red stain, under polarised light at 200x magnification. A** = single celled columnar epithelium. **B** = underlying mesenchymal tissue. **C** = lumens of blood vessels running throughout the tissue.

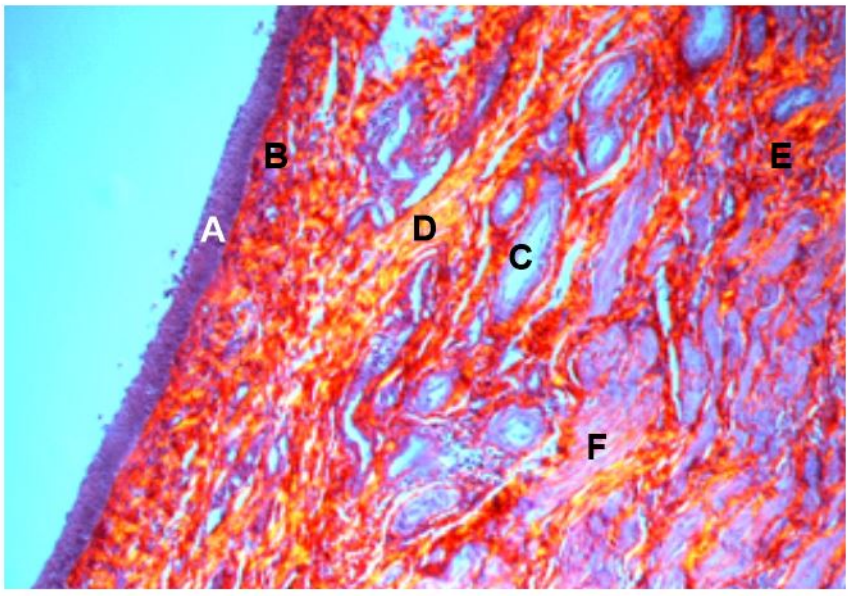


**Figure 3.20: Vaginal tissue of an adult (70kg) female pig. Picrosirius red stain, under polarised light, 100x magnification. A** = non-keratinized stratified squamous epithelium. **B** = lamina propia. **C** = lumen of blood vessels. **D** = connective tissue rich in collagen. **E** = loose connective tissue poor in collagen. **F** = muscle tissue.

### 3.3.2.4 Luxol Fast Blue Stain

Figures 3.21 and 3.22 show the normal presentation of nerve plexuses stain with Luxol Fast Blue at varying magnifications. The individual nerve cells do appear with the stain, they present with a light blue cytoplasm and a darker blue exterior, but they are not clearly marked.

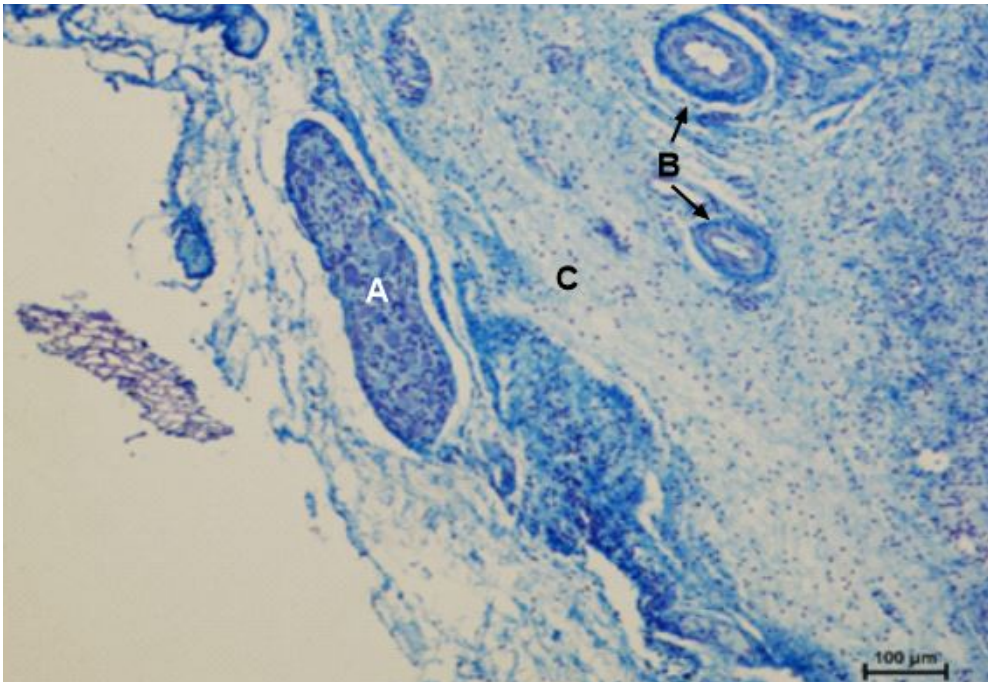


**Figure 3.21: Nerve plexus within the adventitia of the vagina of a 6-week-old (10kg) female pig. Luxol Fast Blue stain, 100x magnification. A** = the whole nerve plexus. **B** = blood vessels within the lose connective tissue; the tunica adventitia of the vessels has also stained a darker blue. **C** = adventitial loose connective tissue.

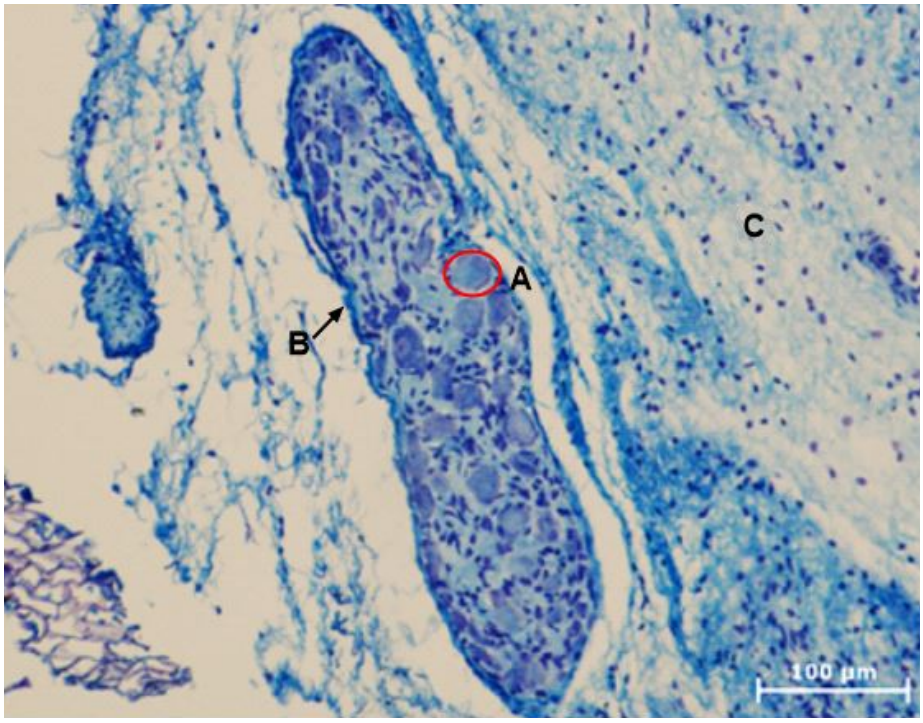


**Figure 3.22: Nerve plexus within the adventitia of the vagina of a 6-week-old (10kg) female pig. Luxol Fast Blue stain, 200x magnification. A** = individual nerve cell, these appear purple when stained with LFB. **B** = endoneurial tissue surrounding the nerve plexus, the myelin present stains blue with LFB. **C** = adventitial loose connective tissue**.**

### 3.3.2.5 S-100 Immunohistochemistry

A specific nerve immunohistochemistry for S-100 proteins was a performed. This provided excellent results, see images below, the nerve cells can be clearly seen, and the nuclei of the cells are well presented (Figs. 3.23 and 3.24).

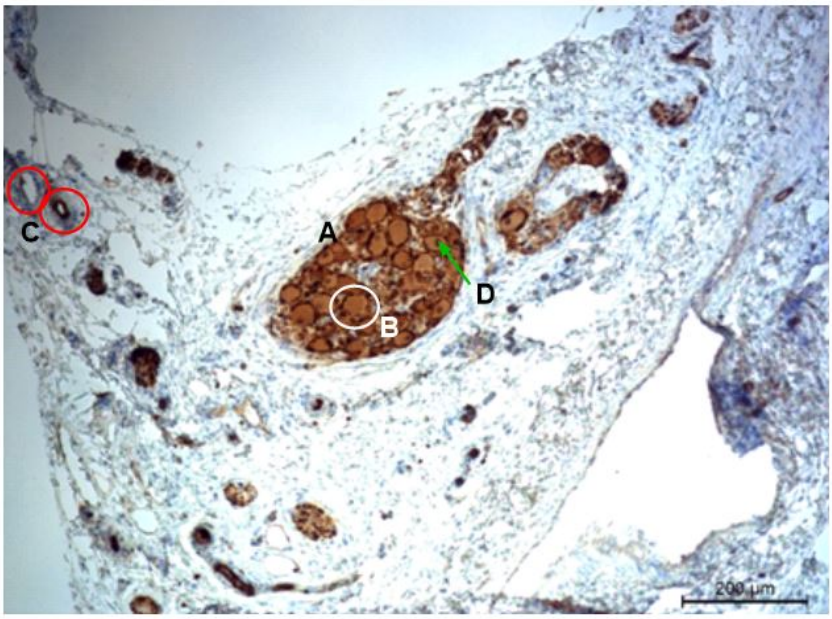


**Figure 3.23: Nerve plexus within the adventitia of the vagina of a 6-week-old (10kg) female pig. S-100 IHC, 100x magnification. A** = whole nerve plexus. **B** = individual nerve cell. **C** = blood vessels within the loose connective tissue, the endothelium of the artery has stained positive for S-100 proteins. **D** = nucleus of a nerve cell.

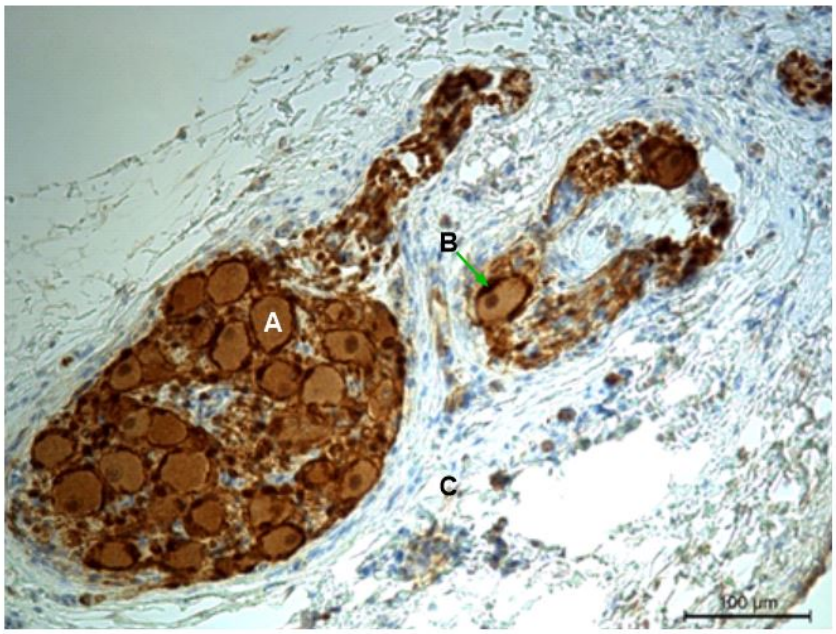


**Figure 3.24: Nerve plexus within the adventitia of the vagina of a 6-week-old (10kg) female pig. S-100 IHC, 200x magnification. A** = individual nerve cell. **B** = strong positive staining of the cell membrane of a nerve cell. **C** = adventitial loose connective tissue.

The images of the vagina of the young pig (6-weeks-old), showed that the majority of nerve bundles supplying the organ are present in the loose connective tissue around the vagina. From the images presented, the nerves appear to have an even distribution within the connective tissue (Figs. 3.25 and 3.26). There was some staining of the epithelium of the vagina and the endothelium of some of the arteries supplying blood to the organ.

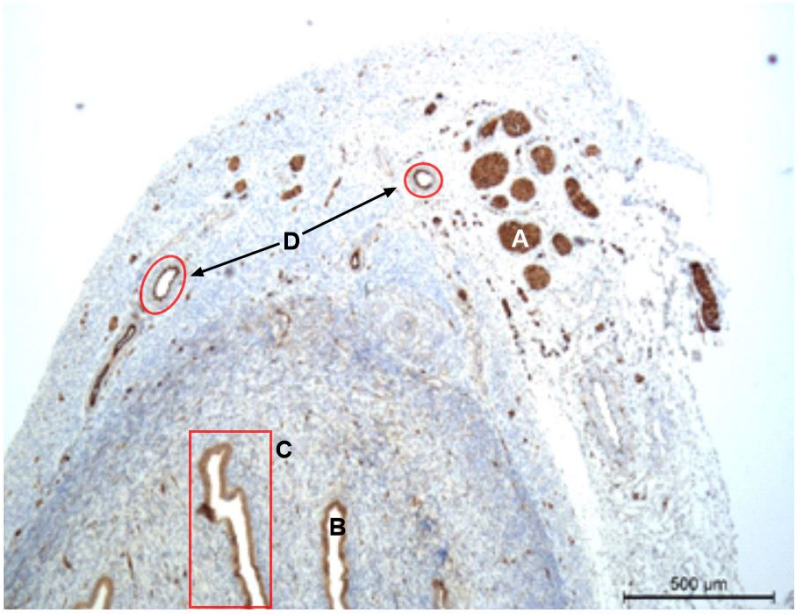


**Figure 3.25: Vagina of a 6-week-old (10kg) female pig. S-100 IHC, 40x magnification. A** = specific staining of S-100 proteins expressed in never cells. **B** = lumen of the vagina. **C** = staining of the single celled columnar epithelium. **D** = staining of the endothelium of large blood vessels**.**

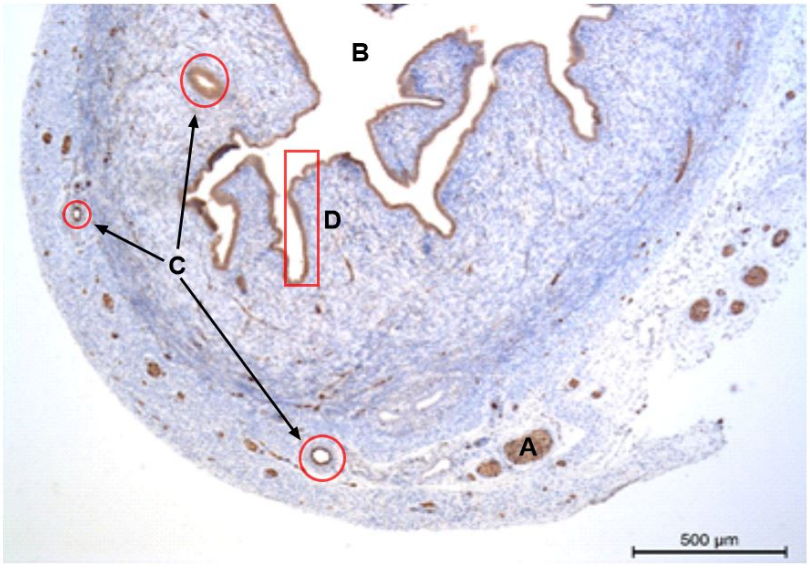


**Figure 3.26: Vagina of a 6-week-old (10kg) female pig. S-100 IHC, 40x magnification. A** = specific staining of S-100 proteins expressed in never cells. **B** = lumen of the vagina. **C** = staining of the endothelium of large blood vessels. **D** = staining of the single celled columnar epithelium.

S-100 IHC of the tissue between the urethra and vagina, septum, of the young (6-week-old) pig showed obvious blood vessels and tracts of concentrated S-100 stain (Fig. 3.27). It is possible that the areas stained positively with S-100 are tracts of nerve within the septum. The blood vessels and nerves that are present supply both the urethra and vagina via the septum.

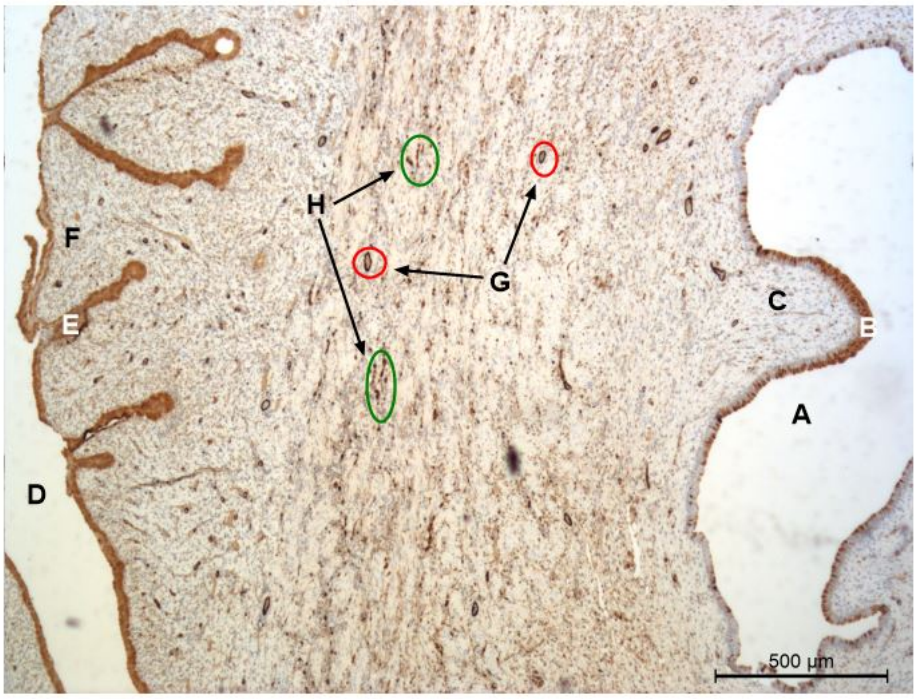


**Figure 3.27: Septum between the urethra and vagina of a 6-week-old (10kg) female pig. S-100 IHC, 100x magnification**. **A** = lumen of the vagina. **B** = epithelium of the vagina. **C** = undifferentiated mesenchymal tissue of the vagina. **D** = lumen of urethra. **E** = epithelium of urethra. **F** = lamina propia of urethra. **G** = small blood vessels running within the septum. **H** = concentrations of S-100 stain, possibly nerve tracts, within the septum.

### 3.3.2.6 Ki67 Immunohistochemistry

Ki67 IHC staining is used as a cellular marker for proliferation, it is present during all active phases of the mitotic cell cycle and is absent during cellular quiescence. Staining and quantification of the amount of staining in various samples of porcine vaginal tissue. Animals of several different ages (6 weeks, 7 months and 2.5 years) were analysed for the levels of Ki67 staining. The results obtained from the quantification of these samples will be used as a control level to compare Ki67 levels of expanded tissue. This is an important factor, especially when considering neoplastic properties.

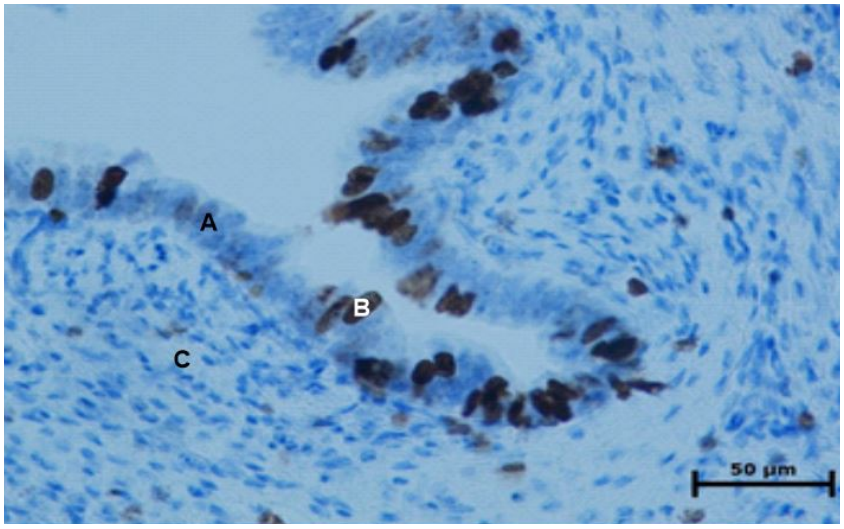


**Figure 3.28: Epithelium of the vagina of a 6-week-old (10kg) female pig. Ki67 IHC, 400x magnification. A** = single columnar cell within the epithelium, the nucleus is negatively stained for Ki67. **B** = single columnar cell within the epithelium, the nucleus is positively stained for Ki-67. **C** = underlying undifferentiated mesenchymal tissue.

Figures 3.28 and 3.29 show the specificity of the staining, individual nuclei within the epithelial cells can be seen.

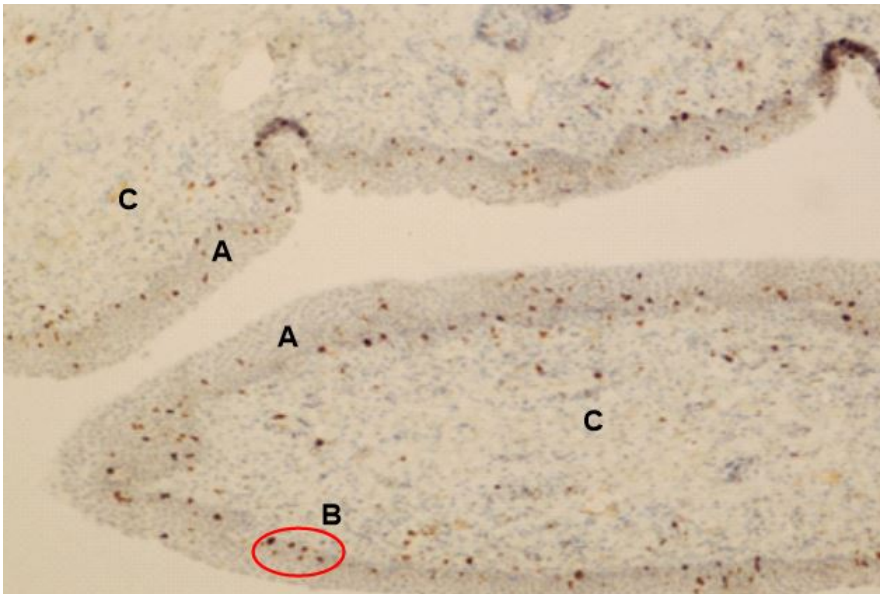


**Figure 3.29: Epithelium of the vagina of an adult (70kg) female pig. Ki67 IHC, 100x magnification. A** = non-keratinised stratified squamous epithelium. **B** = a cluster of nuclei positively stained for Ki67 within the epithelium. **C** = lamina propia.

The results shown in the graph figure 3.30 show that there is a significant difference between the levels of Ki67 staining within the epithelium of the samples and the underlying tissue (labelled Mucosa in the graph) in animals aged 1.5 and 6 months. The younger animals had a higher proportion of positive Ki67 cells within their epithelium. There was less of a significant difference between the epithelium and underlying tissue of the oldest animals. This in indicated by the overlap of the uncertainty bars for epithelial and mucosal tissue of animals aged 30 months. The general trend in the epithelial staining showed a decrease in the percentage total of the slide image as the age of the animal increased. There was little difference in the staining levels of the mucosa between all ages of pigs.

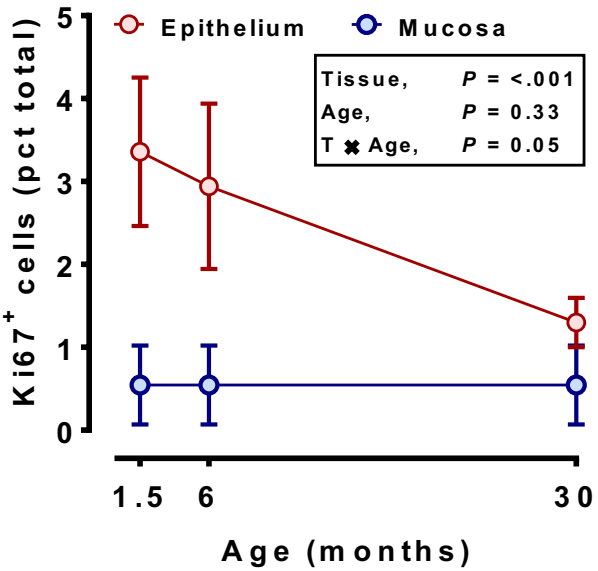


**Figure 3.30: Graph to represent the levels of positive Ki67 staining in the various ages of porcine samples.**

### 3.3.2.7 Vimentin Immunohistochemistry

As well as using Ki67 as a marker for possible increases in cellular proliferation, IHC stains for vimentin and E-cadherin were used on tissue samples similar to those stained for Ki67 (Figs. 3.31 and 3.32). Stained vimentin is used as a marker for mesenchymal-derived cells or cells that are undergoing epithelial to mesenchymal transition.

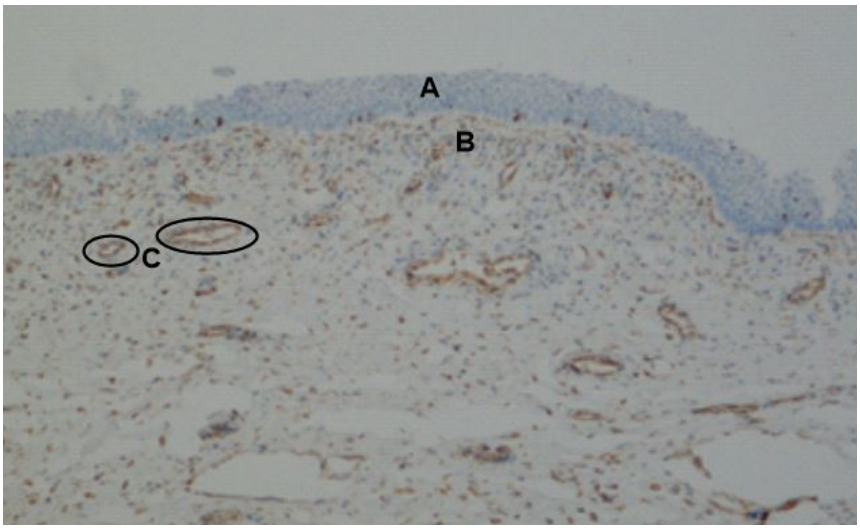


**Figure 3.31: Epithelium and lamina propia of the vagina of an adult (70kg) female pig. Vimentin IHC, 100x magnification. A** = non-keratinised stratified, squamous epithelium. **B** = lamina propia. **C** = blood vessels within the lamina propia.

As with the Ki67 quantification results, there was a significant difference in the levels of vimentin staining between the epithelium and the underlying tissue (labelled mucosa on the graph) in all ages of pigs. There was only a slight increase in staining in the epithelium as the age of animal increased and a significant increase in staining of the mucosa as the age of the animal increased (Fig. 3.33).

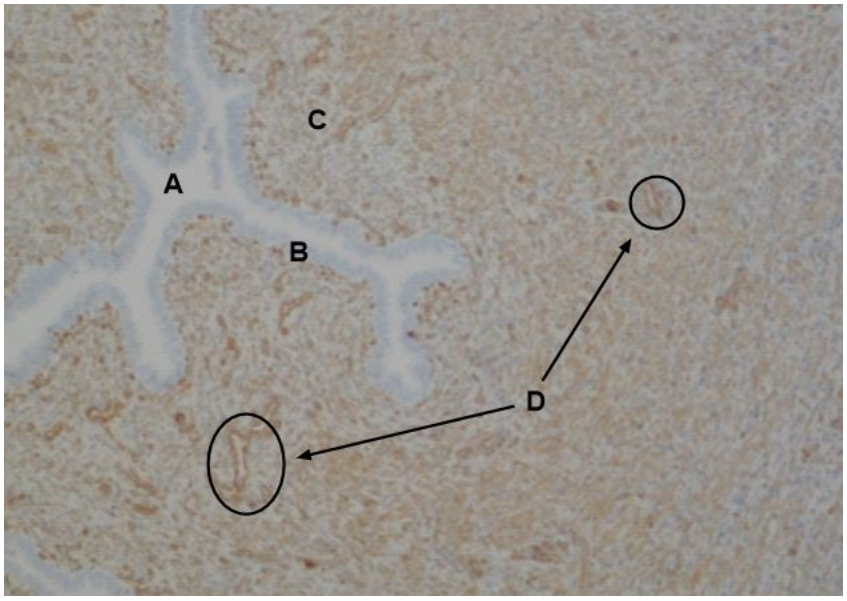


**Figure 3.32: Epithelium of the vagina of a 6-week-old (10kg) female pig. Vimentin IHC, 10x magnification. A** = lumen of the vagina. **B** = single cell columnar epithelium. **C** = underlying undifferentiated mesenchymal tissue. **D** = blood vessels within the underlying tissue.

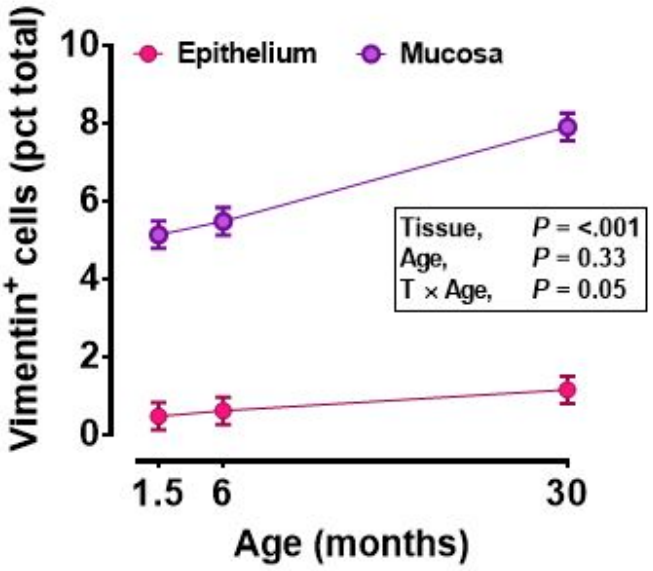


**Figure 3.33: Graph to represent the levels of positive vimentin staining in the various ages of porcine samples.** There is a general trend of an increase in levels as the age of the animal increases.

### 3.3.2.8 E-Cadherin Immunohistochemistry

E-cadherin is a calcium-dependent cell-cell adhesion glycoprotein, loss of function of this gene is believed to contribute to the progression of cancer by increasing proliferation, invasion and/or metastasis. Images of the stained histological slides were taken using the same method as described for Ki67 stained slides and the quantification method was identical (Figs. 3.34 and 3.35).

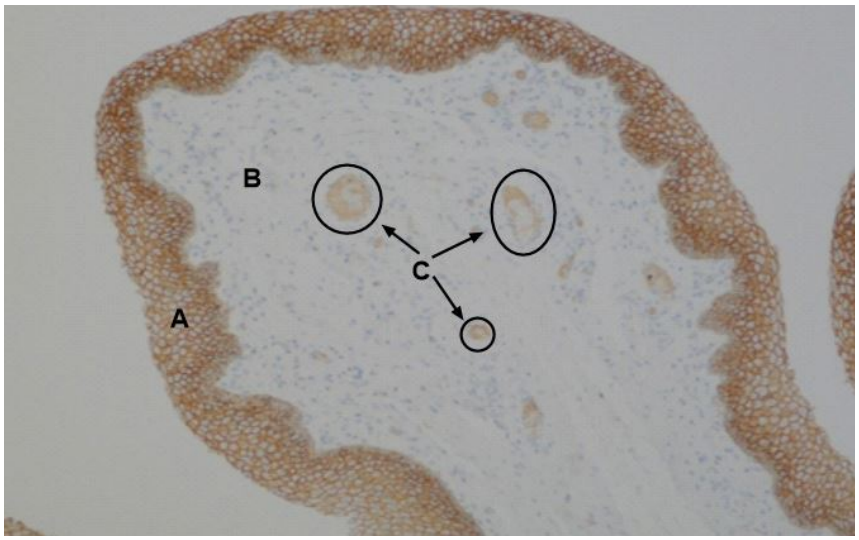


**Figure 3.34: Epithelium and lamina propia of the vagina of an adult (70kg) female pig. E-Cadherin IHC, 100x magnification. A** = non-keratinised stratified, squamous epithelium. **B** = lamina propia. **C** = blood vessels within the lamina propia.

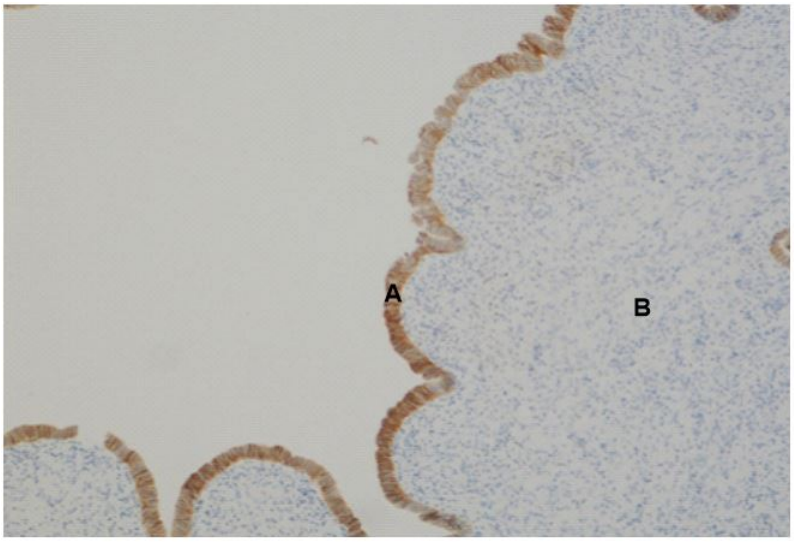


**Figure 3.35: Epithelium of the vagina of a 6-week-old (10kg) female pig. E-Cadherin IHC, 100x magnification. A** = single cell columnar epithelium. **B** = underlying undifferentiated mesenchymal tissue.

Staining for E-Cadherin proteins and quantification of the images produced the following results (Fig. 3.36). There was a significant difference in the amounts of E-cadherin staining in the epithelium and the mucosa of vaginal tissue in all ages of pig. The trend in the staining of mucosa tissue is a slight decrease as the age of the animal increases.

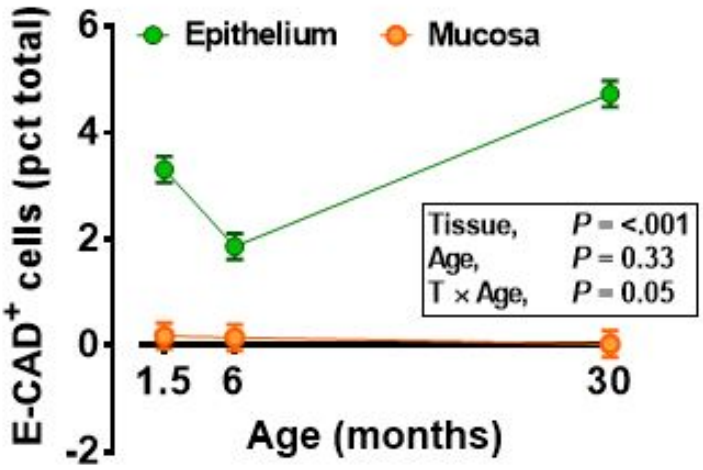


**Figure 3.36: Graph to represent the levels of positive E-Cadherin staining in the various ages of porcine samples.**

### 3.3.3 Metagenomics

The WGS (Whole Genomic Sequencing) results of the porcine vagina samples were arranged in order of abundance, for each sample. All results that were present within the samples at an abundance of ≥1%, were considered relevant to the sample. The results of the samples were classified at various levels of taxonomic levels, Species, Genus, Family and Order.

#### 3.3.3.1 Species Level Classification

The majority of the samples have a few dominating species of bacteria at a higher abundance, with the remaining species existing at a significantly lower level. Only two of the samples had the same bacteria species, Bacteroides fragilis, being the most abundant. None of the collected samples had more than one species of bacteria in common within their most abundant species. Samples 2, 3 and 8 all contained *Bacteroides* fragilis within their most abundant species samples 3, 7 and 14 all contained *Lactobacillus* amylovorus within their most abundant species and samples 2 and 6 both contained *Riemerella* anatipestifer within their most abundant species of bacteria.

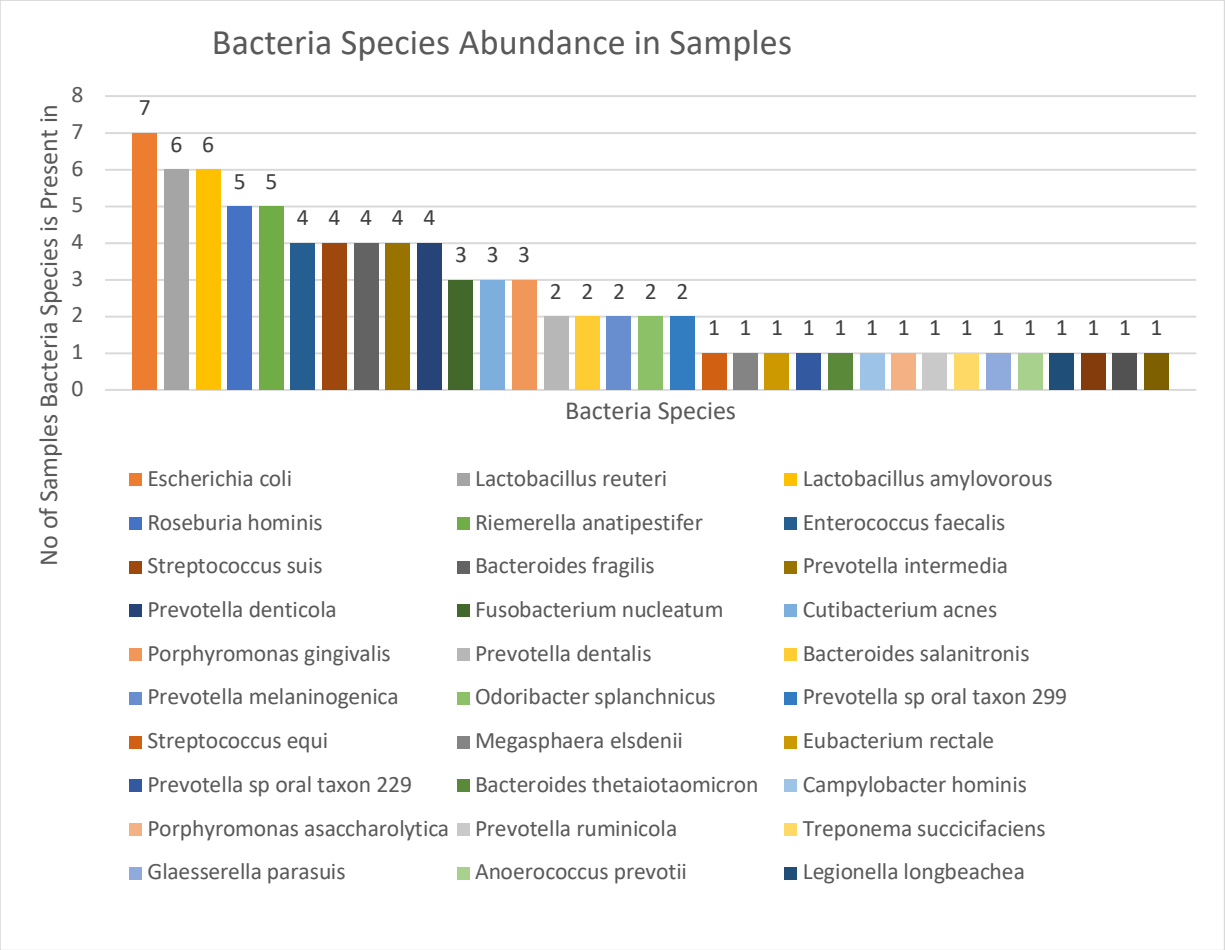


**Figure 3.37: Abundance of individual bacteria on a species level in all samples.**

Figure 3.37 represents the number of samples each of the individual bacteria species were found in. There were 30 bacteria species, with an abundance of ≥1%, detected in total. The only species that was present in all samples, be that at varying levels of abundance, was *Escherichia* coli. *Lactobacillus* reuteri and *Lactobacillus* amylovorous were present in six out of the seven sample taken. The bacteria species that were found in multiple samples were often not the most abundant species within those samples.

### 3.3.3.2 Genus Level Classification

The genomic sequences of bacteria genera within the samples were analysed with the same method as species level analysis. The majority of the samples had one dominating genera of bacteria at a higher abundance, with the remaining genera present at a lower quantity. Three out of the seven samples (samples 2, 3 and 6) had the same bacteria genus, *Prevotella*, being the most abundant. None of the samples had more than one genus of bacteria in common within their most abundant genera. Samples 6 and 8 both contained *Bacteroides* within their most abundant genera and samples 7 and 14 both contained *Lactobacillus* in their most abundant genera. The most abundant genus in sample 5 was *Campylobacter*, this result was unique to this sample.

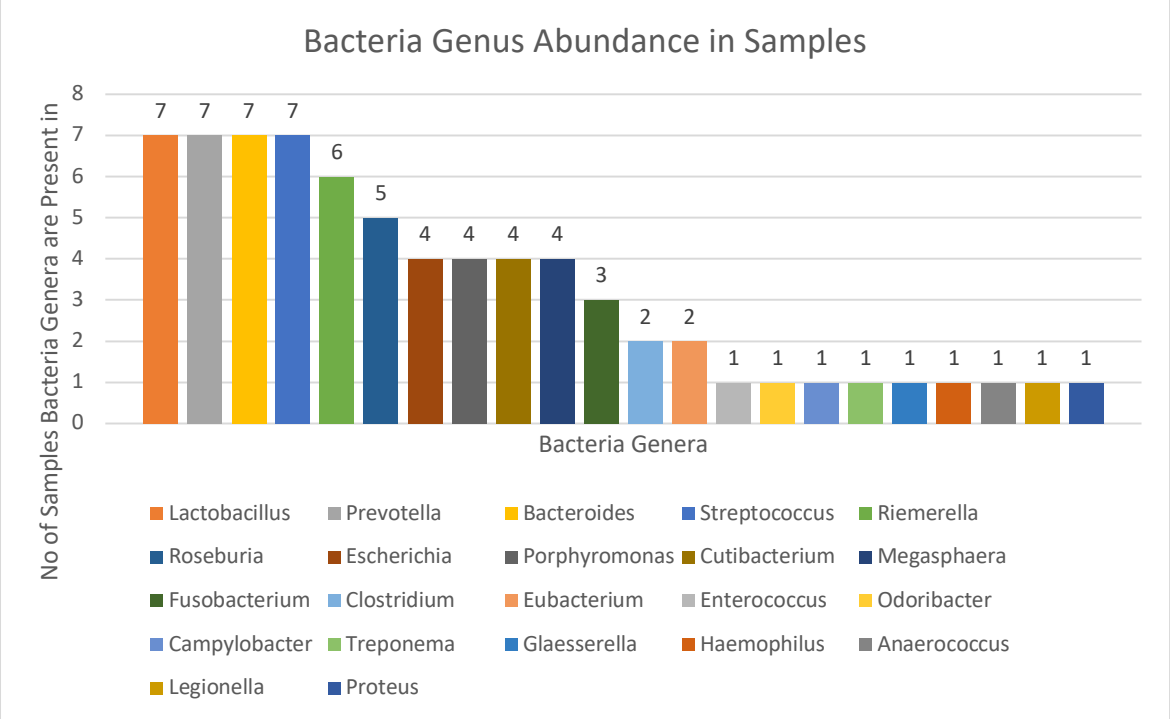


**Figure 3.38: Abundance of individual bacteria on a genus level in all samples.**

Figure 3.38 denotes the number of samples each of the individual genera were found in. There were 22 bacteria genera, with an abundance of ≥1%, detected in total. There were four genera that were present in all seven samples: *Lactobacillus*, *Prevotella*, *Bacteroides* and *Streptococcus*. Apart from sample 5, these genera were the most abundance in all the sample collected. Campylobacter was the most abundant genus in sample 5 and was present in this sample only.

#### 3.3.3.3 Family Level Classification

The majority of the samples had one dominating family of bacteria at a higher abundance, with the remaining families present at a lower level. As with the genus level characterisation, three of the samples had the same bacteria family, Prevotellaceae, being the most abundant. None of the samples had more than one family of bacteria in common within their most abundant families. Samples 6 and 8 both contain Bacteroidaceae within their most abundant genera and Lactobacillaceae was present in sample 7 and 14. The most abundant family in sample 5, was Campylobacteraceae, this result is unique to this individual sample.

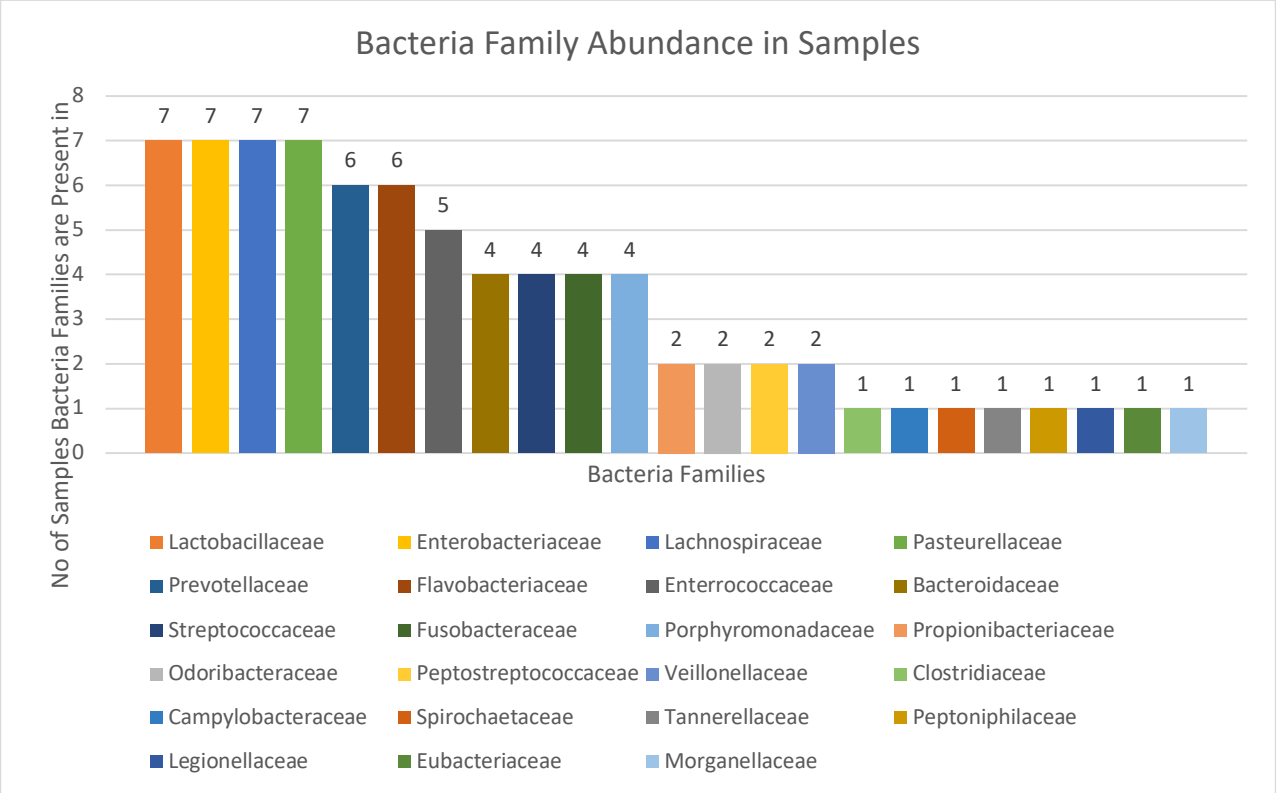


**Figure 3.39: Abundance of individual bacteria on a family level in all samples.**

Figure 3.39 denotes the number of samples containing each of the individual families. There were 23 bacteria families, with an abundance of ≥1%, distinguished in total. Four families were present in all seven samples: Lactobacillaceae, Enterobacteriaceae, Lachnospiraceae and Pasteurellaceae. Interestingly, they were only the most abundant families in three of the samples. Although Prevotella appeared as the most abundant family in the most samples, it was only detected in four samples in total and Lachnospiraceae did not appear as the most abundant in any of the samples but is present in all seven samples collected.

### 3.3.3.4 Order level Classification

The majority of the samples had one dominating order of bacteria at a higher abundance, with the remaining orders present at a lower level. As with the previous taxonomic levels of characterisation, most of the samples had the same bacteria order, Bacteroidales, being the most abundant. None of the samples had more than one family of bacteria in common within their most abundant orders. Samples 7 and 14 both contain Lactobacillales within their most abundant order and Enterobacterialles was present in sample 14, a result that was unique to this sample.

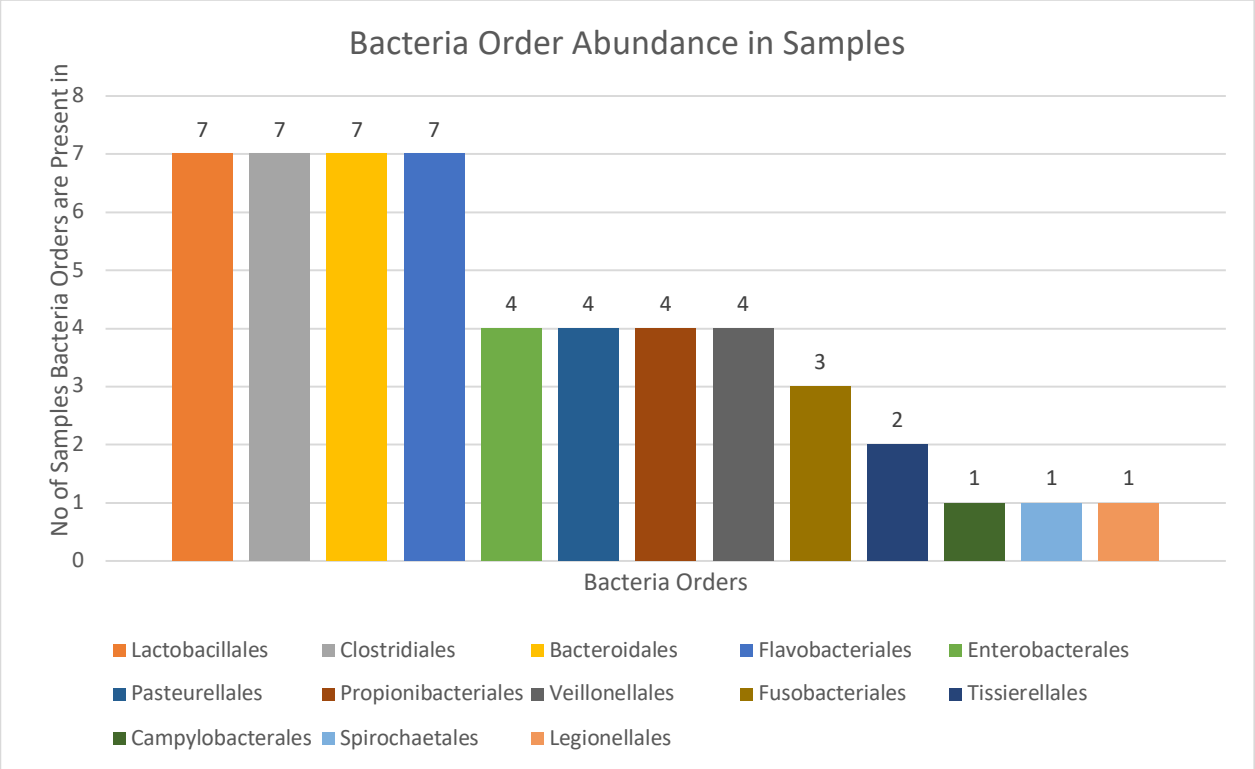


**Figure 3.40: Abundance of individual bacteria on an order level in all samples.**

Figure 3.38 denotes the number of samples containing each of the individual orders. There were 13 orders of bacteria, with an abundance of ≥1%, identified in total. Four orders were present in all seven samples: Lactobacillales, Clostridiales, Bacteroidales and Flavobacteriales. These orders of bacteria were the most abundant in all the samples. Although Clostridiales appears in all the samples, it does not appear as the most abundant order in any of the samples collected.

### 3.3.3.5 Average Abundance of Bacteria at Genera and Bacteria Level Classification

Initial comparisons of the results discussed in the introduction (Lorenzen, 2015) with those produced in this study involved investigation of the ten most abundant bacteria within each taxonomic category. Similar bacteria families and genera were present in both sets of results, figures 3.40 and 3.41. Lactobacillaceae and Enterobacteriaceae families were present in both sets of results, as were the genera Proteus and Lactobacillus.

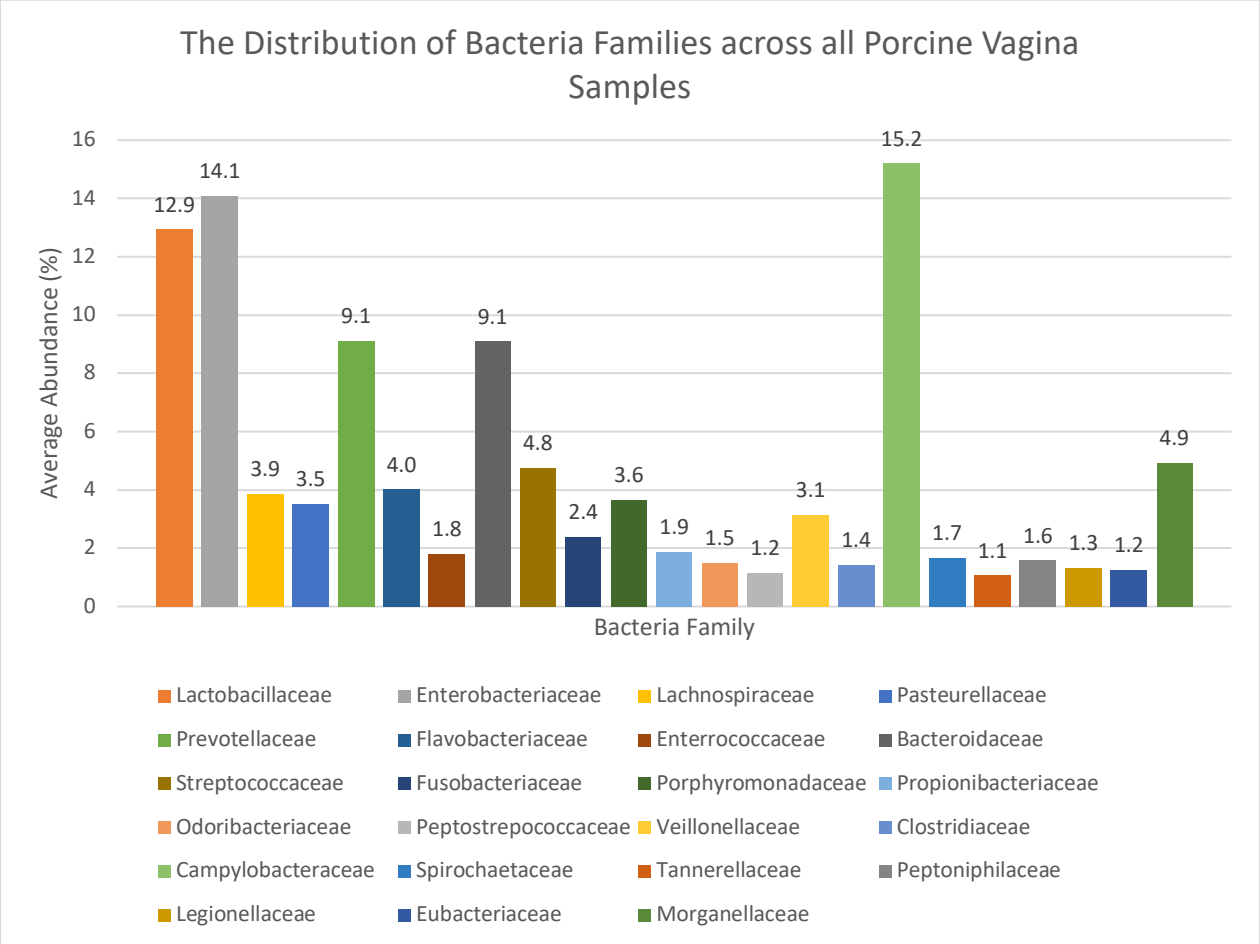


**Figure 3.41: Graph to represent the average abundance of bacteria families within the samples collected for this study and data collected in previous porcine metagenomic studies.**

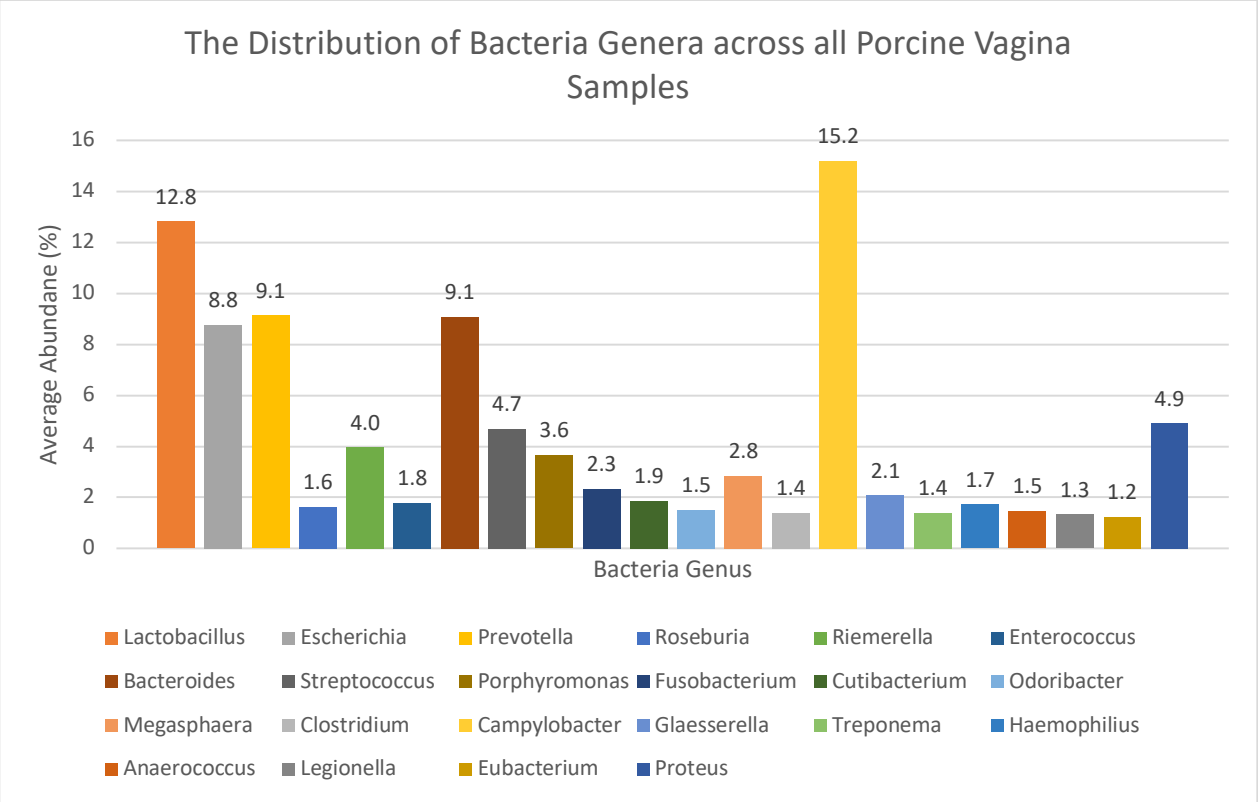


**Figure 3.42: Graph to represent the average abundance of bacteria genera within the samples collected for this study and data collected in previous porcine metagenomic studies.**

### 3.3.4 Porcine Growth Experiment

The live weights of the pigs throughout the experiment were recorded. The initial weight of the animals was between 14.6-16.6kg, with only one animal outlying these values. The animals selected for the experiment were chosen according to their age, believed to be between 8 to 9 weeks. The possible variation in age accounts for the initial outlier. At this point, three of the animals were euthanised. The remaining six pigs all gained a similar amount of weight in the 7 days that followed. A comparable result was seen with the final three animals at the end of the growth study.

The vagina dimensions were recorded by measuring the resin casts with callipers. Over the two weeks the changes in vagina length varied between ages, with the 8-week-old pigs having the smallest lengths, as expected. The 9-week-old animals appeared to have the longest vaginas, with the oldest animals measuring shorter in length. There was a range of vagina diameters across the ages. The maximum vagina diameters did not vary much between the different aged pigs. A similar result was seen with the minimum vagina diameter measurements. In fact, the majority of the youngest pigs had the largest vagina diameters.

One of the factors impacting the results from this growth experiment was the order that the pigs were euthanised. The animals were selected at random and had varying weights. If smaller animals were euthanised at 9 weeks old, with smaller vaginal dimensions, this may give the impression that the vagina dimensions are decreasing. Like the results portrayed in figure 3.43, particularly vaginal length.

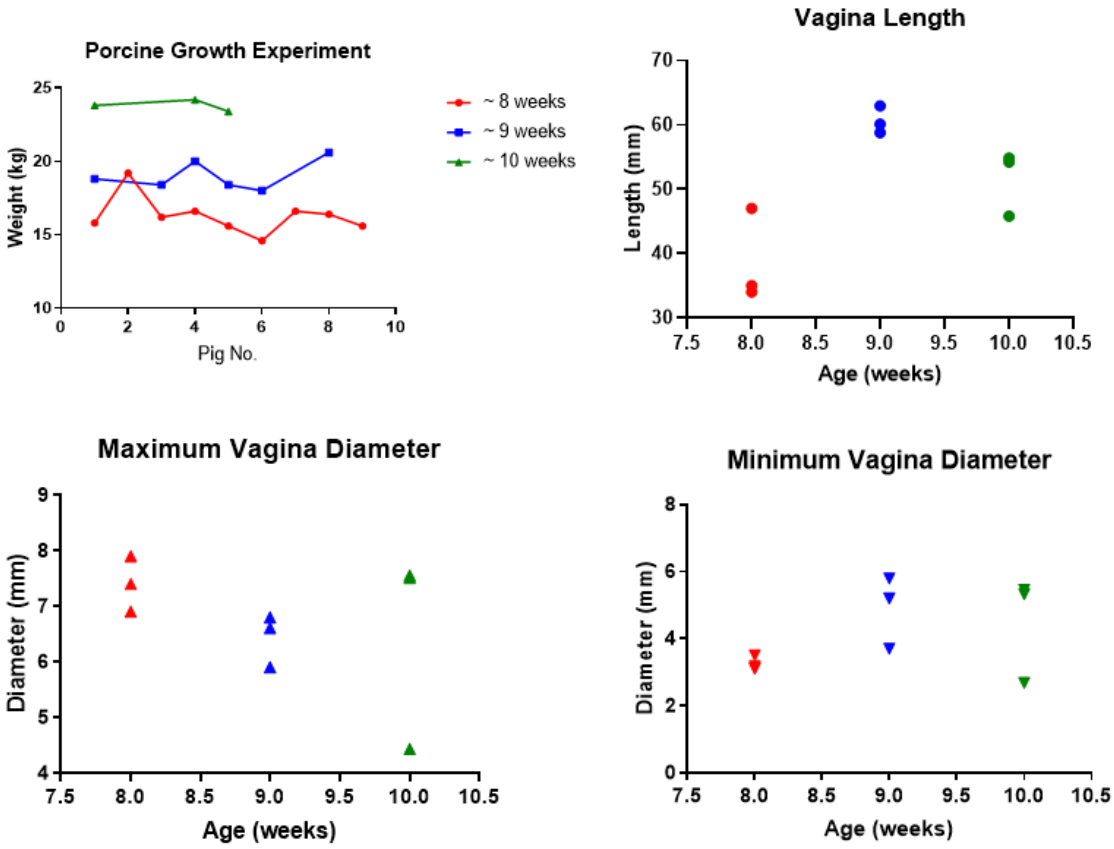


**Figure 3.43: Graphs representing the variations in measured parameters throughout the porcine growth experiment.** Data presented in red, green and blue represents animals aged 8, 9 and 10 weeks respectively. **A**. Graph to show the live weights of the pigs at weekly intervals. The number of pigs measured each week reduces as the animals are euthanised to produce vaginal corrosion casts. **B**. Graph to show the vagina length measurements obtained from the vascular corrosion casts. **C**. Graph to represent the maximum vagina measurements of the porcine resin casts. **D**. Graph to represent the minimum vagina measurements of the resin casts.

## 3.4 Discussions

### 3.4.1 Gross Anatomy of the Porcine Urogenital Tract

In this study, the gross anatomy of the urogenital tract of the pig at varying ages as well as the vasculature and innervation of the animals, via the use of resin corrosion casting and histological investigation.

The results obtained so far have comprised of data to characterise the normal porcine vagina. The various corrosion casts have shown the anatomy of the porcine urogenital system, mainly the relationship between the vagina and the urogenital sinus. The anatomy of the urogenital tract of the adult observed with the cast was as expected. The dimensions of the cast were within the normal ranges described in various veterinary anatomy textbooks (König HE, 2009, Singh, 2018).

Previous research has investigated the structure of the vagina and urogenital sinus of young sows. Baxter (1934), studied the vagina in a sow aged 6-weeks-old, the same age as some of the animals used in this study. He focused on the possibility of the animal having a hymenal structure between the vagina and urogenital sinus. Baxter worked with a fresh tissue sample of porcine genital tract and when laying out the sample from the ventral aspect, he stated '*There is clearly seen to be a circular fold of mucous membrane constricting the vagina and separating off an upper part from the remainder. This upper portion shows numerous delicate longitudinal ridges and furrows, and quite definitely corresponds with the upper tubular part of the vaginal anlage of early stages. A short distance below the circular fold there is seen on each side the opening of Gartner's duct, and below this level is the opening*

*of the urethra into the urogenital sinus.*' This statement corresponds identically with the structure produced by the corrosion cast of the 6-week-old female pig. There was an obvious stricture present between the vagina and the urogenital sinus; this could arguably be a hymenal structure.

The resin casts of the prepubescent urogenital tracts showed a clear urogenital sinus extending from the external vulva to the point of confluence between the urethra and vagina. There was a form of stricture, possibly the hymen, observed between the urogenital sinus and the vagina

The results of a micturating cystogram in a 1-week-old female patient shows similar anatomy. A clear common channel is seen in the radiograph, with the bladder and vagina draining into it, and a single opening on the perineum is present (Fig. 3.2(B))

The same female patient presented with a uterus didelphys and a vaginal septum. Uterus didelphys is the complete non-fusion of 2 uteri and 2 cervices, separated by normal myometrium. The patient also has a duplicate vagina, that both drain into the common channel (Fig. 3.3(B).). Duplicate vaginas are present in 75% didelphys uteri (Fajardo, 2011). One of the prepubescent porcine corrosion casts presented with duplex vagina. Both vaginas had individual orifices at the urogenital sinus, with a lack of septum at the proximal end of the vagina's leading to the single corkscrew cervix (Fig. 3.3(A))

### 3.4.2 Blood supply of the Porcine Urogenital Tract

Upon dissection of the pelvic region of the 6-week-old pig cadaver (section 3.3.1.3.), it appeared that the urogenital tract had very little attachment within the pelvis. One of the reasons for this is due to the orientation of the animal, with a stance on all four limbs, the need for the pigs' pelvic floor muscles to retain abdominal contents as securely as in humans is less, and so they are less developed. With the ease of the removal of the urogenital tract, the integrity of the vascular supply to the organs was questioned.

Although the blood supply of the urogenital tract of the pig appears to consist of mainly small and fragile vessels, the sheer extent of branching and anastomosing between them allows for a rich supply of blood. With the age of the animal considered, the genital tract receives a generous blood supply, even in undeveloped prepubescent animals. This is an essential factor to consider with the proposition of implantation of an expanding device in the lumen of the vagina. In skin expansion, compromise of the vascularity or any ischaemia in the expanded skin flaps is generally due to the pressure from the underlying inflating expander. This is often caused by creating a skin flap that is too thin, but it can also be due to the use of poor quality skin (Wagh and Dixit, 2013). This complication could be applied to the expansion of the vagina, in that substandard perfusion of the organ could make the organ be perceived as poor quality. However, with the result obtained in this study, the perfusion quality of the vagina appears to be more than adequate to endure expansion.

### 3.4.3 Complications from Current Surgical Techniques

The results obtained from the various histological studies revealed the exact positioning of blood vessels and nerves with respect to the tissue shared between the vagina and urethra just cranial to the point of confluence. This was the reasoning behind the use of S-100 IHC. S100 proteins are low-molecular-weight proteins characterized by two calcium-binding sites that have helix-loop-helix conformation. In the case of this study, the nerve plexuses present in the sample tissues specifically stained positively for S-100. This revealed their precise location in the tissue, providing information about some of the problems caused by the surgery performed on paediatric patients.

The use of the PSVARUP technique in reconstructive surgery of patients with cloacal malformations, involves complete separation of the vagina and urethra. In the histological slides of the area of the point of confluence of these two structures, nerve cells and blood vessels are clearly observed throughout the conjoining tissue (Figs. 3.17 and 3.27). Any dissection of this tissue will cause severe disruption of the vasculature and innervation of the two structures and is most likely the reason that various segments of the resulting reconstruction undergo varying amount of necrosis. With the disruption of the innervation of the urethra and vagina together disrupted so severely, it is not surprising that the resultant surgery does not provide functional anatomy for the patients and that many of the surgeries performed require correcting as the patient ages.

### 3.4.4 Comparison of the Human and Porcine Urogenital Tract

Basic analysis of porcine and human vaginal mucosa revealed similarities in the morphology between species. Predominantly that fact that both possess a non-keratinized, stratified, squamous surface epithelium. Figure 3.11 shows the morphological similarities between the two species. Figure 3.11 (A) shows the porcine vagina, presented in the results chapter earlier, and figure 3.11 (B) shows the human vagina, the sample image was obtained from an online histology and microscopy learning resource (Michigan, 2018). Apart from the discrepancy in staining, there is a clear resemblance between the two samples.

Comparative studies of human and porcine vaginal mucosa have been undertaken previously. As well as the histological morphology, a study into the intra-epithelial dendritic cell system showed that porcine vagina contains CD-1 and SLA-DR positive cells (Squier et al., 2008), parallel to that described for human vagina (Patton et al., 2000). Squier et al. (2008) also performed permeability studies in the porcine vagina, investigating the functionality of the barrier lipids. The results obtained showed that the permeability of the porcine vagina at 37°C was 3999±238 s.e.m. When compared to the value for human vagina, 4155±70 (van der Bijl et al., 1998), there is a clear overlap of the two values. Multiple studies, including the one performed by myself, have shown that the similarities between the porcine and human vaginal mucosa deem the pig as a suitable model for the human.

Baxter (1934) first describes the epithelial layer of the vagina as a single layer of columnar cells in a developing foetal pig (at the 12.4cm stage). At this stage in development the Mullerian ducts are fused but the Wolffian ducts have not yet regressed. The vaginal plate has not yet cannulised, meaning the utero-vaginal canal is separate from the urogenital sinus. The same epithelium is described at a later stage of development (18.2 cm stage) and at the point that Baxter investigated the urogenital tract of a 6-week-old sow. This result is identical to the epithelial morphology found in this study, when looking at the 6-week-old pig.

However, there is no description, in Baxter's paper or others, of the morphology of the tissue underlying the epithelium in an animal of this age. Therefore, the aspect of this study that researched the histological morphology of the tissue underlying the epithelium in the young (6-week-old, 10kg) porcine vagina is novel work. The tissue underlying the epithelium in the young pig has an undifferentiated, homogenous mesenchymal appearance (Fig. 3.14).

Rare histological samples of human cloaca vaginal tissue were obtained from Nationwide Children's Hospital, Columbus, USA. Figure 3.47 shows an image of this tissue alongside our own porcine vagina sample. The human tissue sample was an instantly fixed live sample and so the blood vessels within the sample are easily identifiable, as they still contain blood. To compare the density of blood vessels within the tissue, they have been highlighted (red rings) in the porcine sample.

The samples have a similar density of blood vessels within them, the porcine vessels appear smaller due to post-mortem collapsing. This is an important observation when considering tissue expansion. With both species' vaginal tissue receiving a comparable blood supply, it is possible that the human tissue will react in a similar manner to the porcine tissue when under expansion. For example, if ischaemia or necrosis of porcine tissue is seen in future tissue expansion trials, it is most likely that this has occurred due to lack of blood supply and so a similar result can be expected in the human neonate.

Another observation of note is that both species have a stratified squamous epithelium lining the lumen of the vagina. The epithelium of the human neonate appears to be more developed, with multiple layers of cells seen. This will be an advantage when the expansion trials eventually progress to human trials. Conducting experiments in animals of varying ages allows for investigation into the robustness of the tissues, and their potential suitability for use in reconstructive surgery.

Finally, comparison of the two species shows that at the age of surgery in humans (~12 months) and the chosen age of animals used for our cloaca model (8 weeks), both present with undifferentiated mesenchymal cells within the submucosa (Fig. 3.18). The differentiation of this tissue could potentially be influenced by the inflation of a tissue expander within the lumen.

### 3.4.5 Immunohistochemistry Staining

The origin of the tissue underlying the epithelium of the vagina in the young (6-weeks-old) pig became apparent with the use of vimentin IHC. As described earlier, vimentin IHC is used to identify mesenchymal-derived cells. When comparing the young porcine samples with the adult samples (6-months-old), the difference in distribution of cells positively staining for vimentin became apparent.

Vimentin staining in the adult porcine vagina (Fig. 3.31) is generally concentrated in the endothelium of the blood vessels within the tissue, with a slightly increased density of staining seen in the lamina propia of the tissue. However, in the young porcine vagina (Fig. 3.32) the vimentin staining distributed evenly throughout the tissue underlying the epithelium. There is no positive staining in the single cell columnar epithelium of the young porcine vagina. A slight increase in density of staining around the blood vessels is seen, but the majority of cells appear to have the same level of vimentin staining, confirming their lack of differentiation and mesenchymal origin. Due to ethical laws, there is a lack of human tissue samples from children of the same age or stage in development as our pig model making comparison difficult. Explorations for any possible tissue samples are ongoing, including searching the UKCRC Tissue Directory and Coordination Centre.

Confirmation of the origin of the cells underlying the epithelium in the young porcine vagina was one of the reasons for choosing to use vimentin IHC stain. The use of this IHC also allowed for a baseline or control measurement of vimentin staining in non-expanded tissue to be obtained.

The presence of vimentin in cells is an indicator that the cells are undergoing epithelial – mesenchymal transition (EMT). EMT is a process that permits a polarized epithelial cell to undergo numerous biochemical changes enabling it to undertake a mesenchymal cell phenotype. This provides the cell with the following properties: invasiveness, greater migratory capacity and an increased resistance to apoptosis (Kalluri and Neilson, 2003). Accomplishment of EMT is indicated by the degradation of the underlying basement membrane and the formation of a mesenchymal cell that can migrate from the epithelial layer that it once originated (Kalluri and Weinberg, 2009). An alternative IHC process to vimentin is specific cytokeratin staining. Particular keratin types detected in given neoplasms follow known patterns of gene expression, allowing precise identification of the cells containing them. For example, soft tissue or bone tumours that are cytokeratin-reactive, like epithelioid sarcomas and chordoma express CK8, CK18 and CK 19 only (Dabbs, 2018). The specificity of this IHC may lead to it being used in this project in the future.

Once the hydrogel expanders have been implanted into our test pigs and full expansion has occurred, the expanded tissue will be removed, and histological immunohistochemistry can be performed on the tissue. Identical IHC staining of vimentin will be performed and analysed, considering any changes seen in the levels of staining. A significant increase in the levels of positive vimentin staining may be an indicator of the formation of neoplastic cells that have undergone genetic and epigenetic changes. These changes affect oncogenes and tumour suppressor genes that can result in carcinoma cells that can invade and metastasize, leading to cancer progression (Thiery, 2002).

The majority of the IHC markers used in this study were chosen for their reputation as cancer markers. E-cadherin is a calcium-dependant transmembranous intracellular adhesion molecule, associated with epithelial differentiation. This marker is commonly used on epithelial neoplasms and mesenchymal tumours (Sato et al., 1999, Laskin and Miettinen, 2002). With the origin of the cells in the vagina of the young pig taken into consideration, it is appropriate to use this marker to measure changes in the epithelium. If a decrease in E-cadherin levels is observed in the expanded tissue, this is an indicator for cancer progression and metastasis.

Ki67, another marker of tumour proliferation, is one of the most widely practised IHC measurement for various cancers (Johnson and Atkinson, 2009, Snoj et al., 2009, Catapano and Lanzino, 2010, Vasudev and Banks, 2011, Lu and Madu, 2014, Saad, 2015). The monoclonal antibody Ki67 detects a nuclear antigen that is only present in proliferating cells. Ki67 is present in phases S, G, M of the cell cycle, but not in $G_0$ (Gerdes et al., 1984). The protein is predominantly found in the nucleolar cortex and dense fibrillary components of the nucleus during interphase; during mitosis, it becomes associated with the periphery of condensed chromosomes (Verheijen et al., 1989, Isola et al., 1990).

The results obtained from this study showed that the levels of Ki67 positively stained nuclei in the epithelium were much higher in the young porcine (6-weeks-old, 10kg) tissue samples than in the oldest (30-months-old) pigs (Fig. 3.28). This was not a surprising result as younger animals have a higher rate of cellular proliferation whilst they grow. This result can be interpreted in different ways; the increased proliferation in the younger animal means that

expansion of the vagina will be tolerated more and the likelihood of neotissue being formed is greater. Alternatively, the already high proliferation rate may be increased even more with expansion of the vagina leading to mutations within the cells and increased probability of uncontrolled cell proliferation occurring, a feature of cancers. Once expansion of the vagina has occurred, Ki67 IHC will be performed on the tissue and the levels will be compared with that of the normal, non-expanded tissue to look for these properties.

### 3.4.6 Submucosal Expansion vs. Intraluminal Expansion

The initial idea for this project was to implant the hydrogel expanders into the submucosa of the vagina, as was done in the successful procedure performed on the horse described in the introduction (Expaniderm, 2014). The notion being that an additional tissue flap would be grown in situ of the animal model and then used in reconstructive surgery to separate the urogenital sinus into two lumens: the urethra and vagina. Discussions with product designers at Oxtex concluded that the probability of the expanded tissue flap having an adequate blood supply and not become necrotic was unlikely. The pressure exerted on the tissue, be that closer to the epithelium or the adventitia, would be too great for successful expansion. The results from the various histological and resin corrosion cast investigations showed that there is a very intricate blood supply in the vagina and so disruption of this via implantation of an expanding device between the tissue layers could cause more damage that benefit, a similar circumstance to the PSARVUP surgical technique.

### 3.4.7 Metagenomics

Initial comparisons of the results discussed in the introduction (Lorenzen, 2015) with those produced in this study involved investigation of the ten most abundant bacteria within each taxonomic category.

Similar bacteria families and genera were present in both sets of results, section 3.3.3.5. Lactobacillaceae and Enterobacteriaceae families were present in both sets of results, as were the genera Proteus and Lactobacillus.

The similarities seen between the published data (Lorenzen, 2015) and the metagenomic sequencing undertaken in the study allows us to use our data as a baseline measurement of the pig vaginal microbiome.

Though the microbiome of the 'normal' pig is important, we will be focussing on any differences that occur when analysing the microbiome of the pigs that have undergone vaginal tissue expansion. As described earlier, it is the changes in a women's microbiome that predispose them to cervicovaginal infections and alterations in their genital immune system. It is essential for us to detect any changes in our pigs' metagenomic profile as they may be indicators of the expanding devices predisposing the animals to urogenital bacterial infections, a serious complication that will hinder the tissue expanders standing in surgical implants.

### 3.4.8 Porcine Growth Experiment

The results obtained show that the porcine vagina has the potential to increase in length by almost 30mm (34mm to 62.94mm length increase). Comparisons of the vaginal diameters show that there is very little difference between the various aged animals, with the occasional outlier, meaning that the diameter will remain constant throughout our vaginal expansion trials.

It is vital for us to know the natural growth that will occur within the pigs during the ages of interest of this project. For the hydrogel expander to exert pressure on the vaginal tissue and active the biomechanical transduction pathways of the tissue, the device must remain to be slightly larger than the vagina lumen.

With the results obtained from this growth experiment, we can now determine the starting dimensions of the hydrogel expander and adjust the composition of the expander to ensure that it reaches optimum expansion and produces substantial, functioning tissue whilst expanding.

From the collated data of this study, we have concluded that the ideal starting dimensions for our hydrogel expander is 40mm in length and 7mm in diameter. We are hoping to adapt the conformation of the silicone coating to allow the devices to expand to at least 70mm.

# 4 Hydrogel Processing

## 4.1 Introduction

This chapter describes the multiple methods endeavoured to produce a self-expanding hydrogel for eventual use in minimally invasive cloacal repair surgery. This is the second objective initially outlined in the introduction of this Thesis.

The first hydrogel processing work was undertaken with the project's industrial partner, Oxtex. To establish the performance of the porcine vaginal expander, we developed a prototype and tested its expansion properties in the laboratory of Oxtex. The dimensions used for this experiment were estimated based on our want to develop a pencil shaped device.

The next stage in the project was to develop the true sized hydrogel expanders with the industrial partners. However, in January 2019, Oxtex appointed a new Chief Executive Officer. Since this development in the company, the production department has grown vastly, with the majority of resources contributing to the production of their commercial products.

In September 2019 we were informed that Oxtex were no longer in a position to support development of tissue expander devices and shortly after the company went into administration and withdrew from being industrial partners in this project. This impacted the progression of the project and lead to the investigation of alternative methods for developing a self-expanding hydrogel for vaginal tissue expansion. With the Oxtex tissue expander devices having approval of use in surgery, we wanted to try to utilise as much of the resources that the company had provided us when falling into administration.

From the initial development experiments undertaken at Oxtex and the porcine growth experiment it was clear that the initial design of expander was too small and the devices would expand to a size half of what would be required to initiate neotissue growth in the pigs. With this in mind, we attempted to use the products provided to us to create our own expansion device that would reach the required dimensions to instigate tissue expansion. We were provided with non-expanded hydrogel rods and pre-fabricated silicon sleeves, used to control the rate of expansion. The trial in-house expander processing was not fruitful and so use of the resources from Oxtex ceased.

After searching for alternative suppliers of hydrogels, including those used for many tissue reconstruction operations we were unable to find a suitable product. A new collaboration with the Centre of Additive Manufacturing department, part of the Faculty of Engineering at the University of Nottingham, was developed. Initial meetings included encouraging discussions of the use of 3D printers to produce hydrogel structures. Their expertise in materials development for additive manufacturing as well as inkjet and 3D printing of additive materials allowed the project to continue. This collaboration has resulted in the successful in-house development of a self-expanding hydrogel that increases in size at a rate that is competitive with the growth rate of the animal model.

## 4.2 Methodology

### 4.2.1 Oxtex Hydrogel Development

#### 4.2.1.1 Hydrogel Dimensions

The hydrogel rods used for the initial devices were supplied by Contamac in a cured (removal of residual mechanical stress), homogeneous, isotropic state. The xerogel transparent rods were provided in dimensions of 13.00 x 7.00mm, ensuring that no additional trimming would be required post-manufacturing (Fig. 4.1).

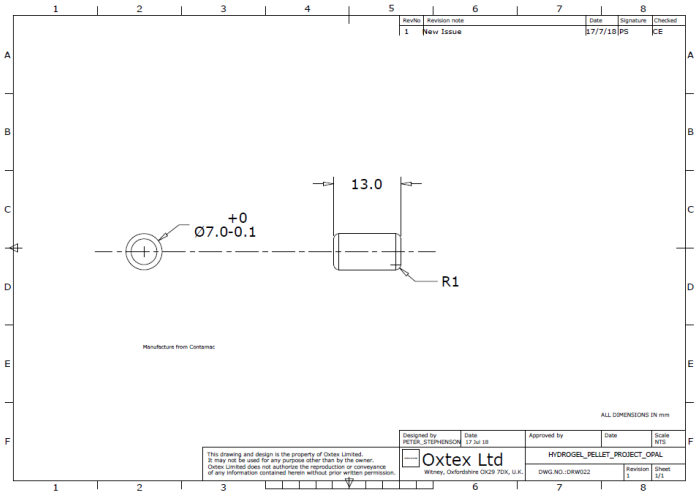


**Figure 4.1: Oxtex hydrogel rod prototype dimensions, pre-expansion.**

#### 4.2.1.2 Hydrogel Hydration

Prior to construction of the proposed expander, the unreacted monomeric and/or oligomeric elements of the xerogel rods were extracted by immersing the co-polymer in a bath of sterile distilled water, supplied by Baxter Healthcare, for a minimum of 3 days and a maximum of 5 days. In this time the hydrogel pellets expand fully to their maximum dimension.

#### 4.2.1.3 Hydrogel Drying

The hydrated pellets were then air dried for a minimum of 3 days. The pellets undergo further drying, at 70°C, for 12 – 24 hours. Preceding hot moulding of the hydrogel, that pellets are oven dried for a second time at 70°C for 12 – 24 hours.

#### 4.2.1.4 Hot Moulding

The R&D hot moulding set OX-MOL-XX is cleaned and made free from hydrogel residue with acetone and brush. Ensuring the mould is well is positioned on the flat base, the hydrogel pellet is then placed inside the hot mould central hole so that it is sandwiched between the top and bottom inserts (Fig. 4.2).

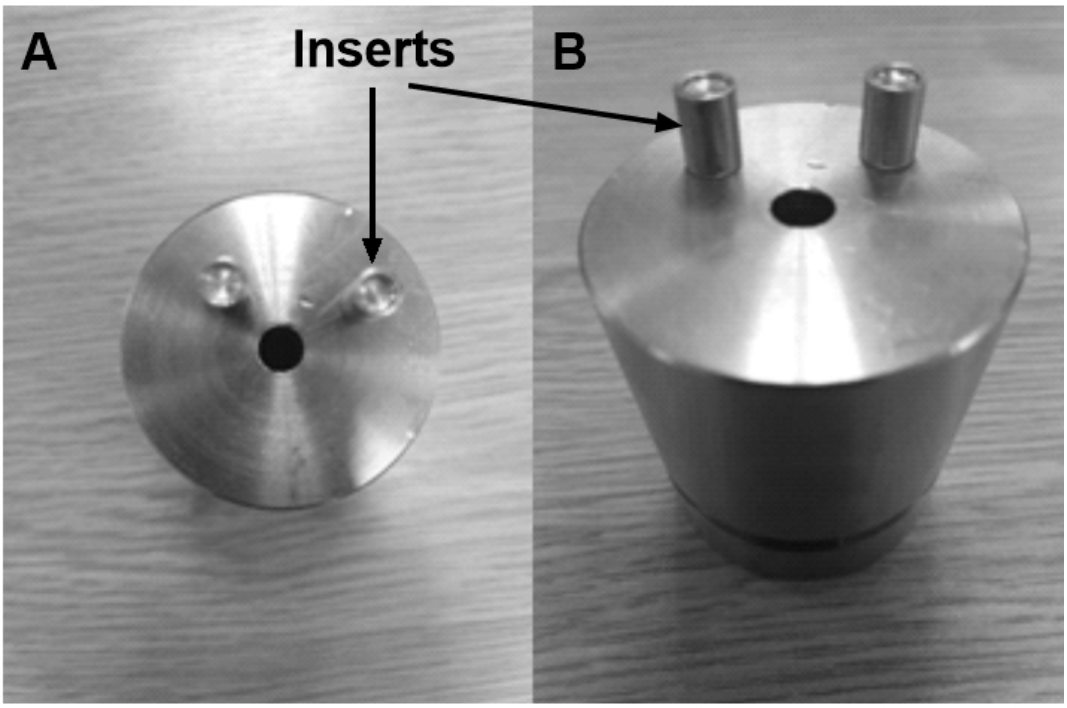


**Figure 4.2: Hydrogel mould, bottom insert. A**. Top view of the mould. **B**. Side view of the mould.

Using a mould holder, the mould is put inside the oven at 170-180°C and heated for 40-60 minutes. Then 1T pressure is applied until the moulding set has cooled off, when the pressure is applied, the hydrogel is crushed axially. Using an extraction well and rod, the hydrogel from inside the mould is pushed out of the mould well. Hot moulded hydrogel appears cylindrical in shape as shown in figure 4.3.

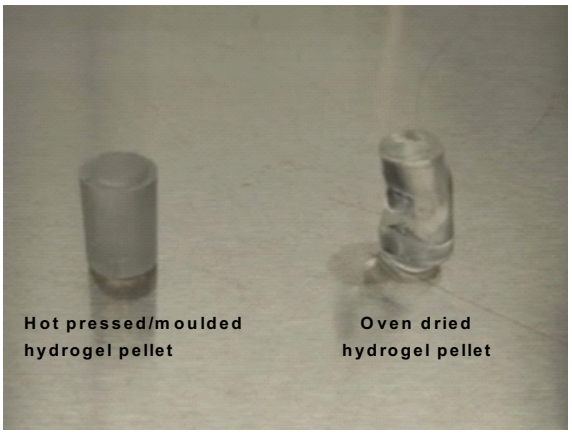


**Figure 4.3: Hydrogel rod in moulded and oven dried state.** The moulded hydrogel pellet maintains a uniform cylindrical shape. The oven dried pellet has an irregular form.

#### 4.2.1.5 Silicone Coating

The MED4211 silicone parts A and B are mixed in a ratio of 10:1 into a cartridge. The two components were mixed gently using a pair of spatulas, producing as little gas bubbles as possible. The mixed silicone is then degassed in a vacuum chamber to remove air bubbles formed during mixing.

Once degassing is complete, the cartridge is attached onto its silicone dispenser and manually dispense the mixed silicone into the mould well, OX-SILWELL-XX (Fig. 4.4). The well is filled all the way to the top, the top insert for the mould is put in place and then the whole mould is put on a vibrator plate for 5-10 minutes. The silicone coat mould is then placed in an oven at 170-180°C for 10-15 min. Once the mould is removed from the oven, cooled and safe to touch, the silicone can be removed from the well.

The moulded hydrogel pellet is then inserted inside the silicone jacket and a few drops of medical grade MED 4211 impermeable silicone are dispensed on the top to cap the open end. The thickness of the silicone on the end cap region should be 1.00mm. The silicone encapsulated hydrogel is then placed in the oven at 40°C for a minimum of 4 hours and a maximum of 24 hours to cure the freshly added silicone.

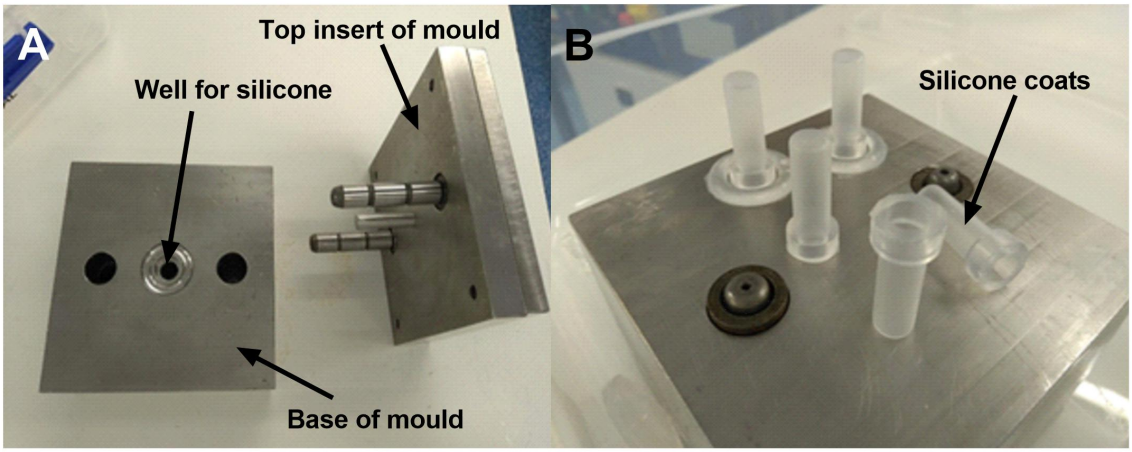


**Figure 4.4**: **Silicone coat mould and products. A.** Complete components of the silicone coat mould. Silicone is injected into the well and insertion of the top insert causes the silicone to spread around the central rod and from a hollow cylinder. **B.** Products of silicone coat moulding. Hollow cylinders are formed and then trimmed once hydrogel pellets have been inserted.

#### 4.2.1.6 Final Product Quality Control Check

Check the product has no damages or cuts in the silicone coat. A second checker will also carry inspection of these devices. Only products that have passed this final product QCC can be sent for sterilization or put in water bath for testing expansion of the devices.

#### 4.2.1.7 Water Bath Testing

All three expander devices were placed in 200ml lidded vessels, the vessels were filled with Hartmann's solution and securely sealed. Hartmann's solution, or compound sodium lactate, is a clear colourless solution considered to be more 'physiological' than normal saline as it contains additional electrolytes in concentrations similar to plasma. The vessels were placed in a water bath set to 37°C. The hydrogel expander dimensions, length and width, were measured

daily along with the temperature and pH of the Hartmann's solution within the vessels. The Hartmann's solution was changed on day 10 of the experiment.

### 4.2.2 Centre of Additive Manufacturing Hydrogel Development

#### 4.2.2.1 Synthesis of Polylactic acid with 2-hydroxyethyl methacrylate (PLA HEMA)

20ml glass vials were used for this synthesis, the vials were placed in an incubator/oven at 50°C overnight before use. Initially, 1g of PLA HEMA was produced. In one vial, 1g of lactate monomer, 26mg of hydroxyethyl acrylate (HEMA) and 5ml of dichloromethane (DCM) and a magnet were placed and sealed. The vial was then put on a heated mixing plate at 30°C. In a separate vial, 30mg of 1,8-diazabicyclo[5.4.0]undec-7-ene and 1ml of DCM were mixed. The two vials were then combined, and the mixture was placed on a heated magnetic plate at 30°C for 1 hour. Before use, 40ml of hexane was placed in a falcon tube and cooled in a -80°C freezer for 10 minutes. The vial containing lactate, HEMA, DCM and DBU was then added to the hexane via pipette, slowly, drop by drop, allowing polylactic acid to precipitate.

The falcon tube was then centrifuged at 4900 rpm, 3°C for 5 minutes. Once centrifuged, the hexane supernatant was discarded. 40ml of diethyl ether was then added to the remaining precipitate, the solution was shaken to allow for any remaining monomer to be washed away from the produced polymer. Again, the solution was centrifuged at 4900 rpm, 3°C for 5 minutes and the diethyl ether supernatant was discarded.

The falcon tube containing polylactic acid was placed in a zero-pressure chamber, with no lid, and tissue paper was placed over the opening of the tube

and secured with an elastic band. This was left overnight, as the polymer dries, it forms a foam like structure.

To produce larger quantities of PLA HEMA, the above method can be scaled up to the desired quantity. It is recommended to make up an extra 1 or 2ml of DBU+DCM solution as this has a fast evaporation rate and so some of the solution will be lost when pipetting.

### 4.2.2.2 Production of Hydrogel Formulations

#### 4.2.2.2.1 First Trial Formulations

Using a total volume of 500µl, six formulations with varying concentrations of Polylactic acid (PLA), poly(ethylene glycol)diacrylate (Mn 700) PEGDA) and 2-hydroxyethyl methacrylate (HEMA).

The following concentrations were used:

| Vial | PLA %(w/w) | PEGDA %(w/w) | HEMA %(w/w) | DMPA %(w/w) |
|---|---|---|---|---|
| A | 10% | 10% | 80% | 1% |
| | 50mg | 50µl | 400µl | 5mg |
| B | 5% | 15% | 80% | 1% |
| | 25mg | 75µl | 400µl | 5mg |
| C | 15% | 5% | 80% | 1% |
| | 75mg | 25µl | 400µl | 5mg |
| D | 5% | 5% | 90% | 1% |
| | 25mg | 25µl | 450µl | 5mg |
| E | 2.5% | 7.5% | 90% | 1% |
| | 12.5mg | 37.5µl | 450µl | 5mg |
| F | 7.5% | 2.5% | 90% | 1% |
| | 37.5mg | 12.5µl | 450µl | 5mg |

**Table 4.1: Concentrations of PLA, PEGDA, HEMA and DMPA used in the first trial formulations of hydrogels.**

The PEGDA solidifies when kept in the fridge and so must be melted on a 60°C hot plate. The various components were combined in a 5ml vial in the following order:

1. **PLA, via spatula and balance**
2. **HEMA, via pipette**
3. **PEGDA, via pipette**
4. **DMPA, via spatula and balance**

Any work done involving DMPA was performed in a fume hood. Once DMPA was added to the vials, they were covered with foil to protect the contents from reacting with light. The foil-covered vials were kept on a 60°C hot plate until ready for casting. Plastic tubing with an inner diameter of ~2mm and 10mm in length was used as a cast for the trial hydrogels.

50µl of the hydrogel solution was pipetted into the cast and then placed, individually, under a UV lamp, wavelength 380-420nm) for 60 seconds. This initiated the formation of cross-linkages, converting the hydrogel from liquid to solid. A total of 30 trials hydrogels were made, 5 casts for the contents of each vial.

The removal of the hydrogels from their casting required heating on a hotplate of 50°C and gentle rolling of the cast to break the seal within the tubing. The hydrogels could then be pushed out of the casts with tweezers or any other suitably small implement.

#### 4.2.2.2.2 First Trial Formulations Swelling Tests

Following removal from castings, the weight, length and diameter of the hydrogels was measured. They hydrogels were then individually placed in 20ml glass vials with 5ml of phosphate-buffered solution (PBS) and kept at in an incubator at 37°C. The weight, length and diameter were measured daily for the next 8 days.

#### 4.2.2.2.3 Second Trial Formulations

Using a total volume of 500µl, six formulations with varying concentrations of Polylactic acid (PLA), poly(ethylene glycol)diacrylate (Mn 700) PEGDA) and 2-hydroxyethyl methacrylate (HEMA).

The following concentrations were used:

| Vial | PLA %(w/w) | PEGDA %(w/w) | HEMA %(w/w) | DMPA %(w/w) |
|---|---|---|---|---|
| G | 17.5% | 2.5% | 80% | 1% |
| | 87.5mg | 12.5µl | 400µl | 5mg |
| H | 9% | 1% | 90% | 1% |
| | 45mg | 5µl | 450µl | 5mg |
| I | 3.2% | 1.8% | 95% | 1% |
| | 16mg | 9µl | 475µl | 5mg |
| J | 1.7% | 0.8% | 97.5% | 1% |
| | 8.5mg | 4µl | 487.5µl | 5mg |
| K | 0.65% | 0.35% | 99% | 1% |
| | 3.25mg | 1.75µl | 495µl | 5mg |

**Table 4.2: Concentrations of PLA, PEGDA, HEMA and DMPA used in the second trial formulations of hydrogels.**

The method conducted in part 4.2.2.2.1 was repeated.

A total of 21 trial hydrogels were made, 5 casts for the G formulation of hydrogel and 4 casts for the contents of the other vials.

The altered formulations of the hydrogel expanders made their composition much more brittle and so it was more difficult to remove them from their casts.

Many of the expanders lost fragments of material when being removed from the casts and the K formulation casted the hydrogels to shatter on removal. It is for this reason that the starting lengths of the expanders are much more varied than the Formulation 1 test and the K formulations are much smaller than the other expanders are.

#### 4.2.2.2.4 Second Trial Formulations Swelling Tests

Following removal from castings, the weight, length and diameter of the hydrogels was measured. They hydrogels were then individually placed in 20ml glass vials with 5ml of phosphate-buffered solution (PBS) and kept at in an incubator at 37°C. The weight, length and diameter were measured daily for the next 10 days.

#### 4.2.2.2.5 Third Trial Formulations

Using a total volume of 500µl, four formulations with varying concentrations of Polylactic acid (PLA), poly(ethylene glycol)diacrylate (Mn 700) (PEGDA) and acrylic acid.

The following concentrations were used:

| Vial | PLA %(w/w) | PEGDA %(w/w) | Acrylic Acid %(w/w) | DMPA %(w/w) |
|---|---|---|---|---|
| L | 1% | 0% | 99% | 1% |
| | 5mg | 0µl | 495µl | 5mg |
| M | 0.5% | 0.5% | 99% | 1% |
| | 2.5mg | 2.5µl | 495µl | 5mg |
| N | 0% | 1% | 99% | 1% |
| | 0mg | 5µl | 495µl | 5mg |
| O | 0% | 10% | 90% * | 1% |
| | 0mg | 50µl | 450µl | 5mg |

**Table 4.3: Concentrations of PLA, PEGDA, Acrylic Acid and DMPA used in the third trial formulations of hydrogels.**

*The acrylic acid component of formulation O consisted of a mixture of acrylic acid and hyaluronic acid in a ratio of 10:1. This mixture that previously produced positive results when used in past hydrogel formulations within the advanced manufacturing laboratory.

Again, the method described in part 4.2.2.2.1 was conducted.

A total of 25 trial hydrogels were made, 5 casts for each formulation.

The altered formulations of the hydrogel expanders, substituting HEMA for acrylic acid, caused varying amounts of shrinkage. This led to a variation in starting lengths of the expanders. Initial attempt at removal of the hydrogels from their casting involved heating on a hotplate of 50°C and gentle rolling of the cast to break the seal within the tubing. However, the annealing process caused the hydrogels to react with the cast tubing, making them very difficult to remove. Dissection of the hydrogels from their casts using a scalpel was required. This method led to the scoring of lines on some of the hydrogels, creating a weakness that allowed the cylindrical rods to unfold when swelling.

To rectify this, the same formulations were made up again and pipetted into the lids of vials. The vial lids were made of a different, harder plastic and so the hydrogel was less likely to react during the annealing process. However, the direct exposure of the liquid hydrogel to the UV lamp, caused the formulation to react with the heat energy coming from the lamp before the UV rays had completed the annealing process. This was most likely due to the acrylic acid and its affinity to react under heat. Hydrogels numbered 1-5 were pipetted into the original tubular casts, with dimensions of 10mm x ~2.2mm. Hydrogels numbered 6 and 7 are the successful hydrogel that were pipetted into the lids of vials. They had a starting diameter of ~6.7mm and a starting volume of ~100µl.

#### 4.2.2.2.6 Third Trial Formulations Swelling Tests

Following removal from castings, the weight, length and diameter of the hydrogels was measured. The hydrogels were then individually placed in 20ml glass vials with 5ml of phosphate-buffered solution (PBS) and kept at in an incubator at 37°C. The weight, length and diameter were measured daily for the next 10 days.

### 4.2.2.3 Formulation M Printability Tests

#### 4.2.2.3.1 BMF nanoArch S130 Sample Prints

Samples of formulation M were made to test its eligibility for printing the BMF nanoArch S130 3D printer. Ink synthesised for use in this printer generally require the addition of curcumin (the main active ingredient in turmeric) to act as a photoabsorber. Curcumin was initially added at 1% concentration, with subsequent alterations made in attempt to increase the printability of the formula. The following concentrations for sample print 1 were as follows:

| PLA% (w/w) | PEGDA% (w/w) | Acrylic Acid% (w/w) | DMPA% (w/w) | Curcumin% (w/w) |
|---|---|---|---|---|
| 0.5% | 0.5% | 99% | 1% | 1% |
| 0.05g/50µg | 0.05ml/50µl | 9.9ml | 0.1g/100µg | 0.1g/100µg |

**Table 4.4: Concentrations of PLA, PEGDA, Acrylic Acid, DMPA and Curcumin used in the first sample print.**

The following BMF nanoArch S130 printer settings were applied for sample prints 1 – 4.

| Sample Print | Curcumin % | Intensity (%) | Exposure |
|---|---|---|---|
| 1 | 1 | 87 | 0.5 x 4<br>2.7 x 4 |
| 2 | 1 | 147 | 0.5 x 8<br>2.7 x 8 |
| 3 | 0.5 | 147 | 0.5 x 8<br>2.7 x 8 |
| 4 | - | 150 | 0.5 x 4<br>2.7 x 4 |

**Table 4.5: Printer settings applied for BMF nanoArch S130 sample prints 1 - 4.**

#### 4.2.2.3.2 BMF nanoArch S130 Lattice Print Test

The ability for formulation M to be able to form a more complex structure was tested. The formation of a lattice structure was tested. A Curcumin concentration of 0.5% was used.

The following printer settings were used:

- **Intensity – 150%**
- **Expected model height – 1.990mm**

The ink formulation appeared to be very stable before printing. However, after printing the ink became black and unstable, this may have been due to the reaction with the UV light.

The lattice structure did not adhere to the printer platform, but an initial yellow pattern was seen on the printer film. It is thought that the ink formulation contained too much photoabsorber for it to cure successfully.

#### 4.2.2.3.3 Optimising Parameters for Formlabs 1+ Printer

200ml of formulation M was made up for testing its eligibility for printing in the Formlabs desktop stereolithographic 3D printer, Form 1+.

Ink synthesised for use in this printer does not require the addition of curcumin to act as a photoabsorber.

For sample prints 4, 5 and 6 the photoinitiator DMPA was replaced with Irgacure 819.

The following concentrations were used:

| Sample Print | PLA % (w/w) | PEGDA % (w/w) | Acrylic Acid % (w/w) | DMPA % (w/w) |
|---|---|---|---|---|
| 1 | 0.5 | 0.5 | 99 | 1 |
| 2 | 0.5 | 0.5 | 99 | 1 |
| 3 | 0.5 | 0.5 | 99 | 2 |
| 4 | 0.5 | 0.5 | 99 | 1 (Irgacure 819) |
| 5 | 0.5 | 0.5 | 99 | 1 (Irgacure 819) |
| 6 | 0.5 | 0.5 | 99 | 1 (Irgacure 819) |

**Table 4.6: Concentrations of PLA, PEGDA, Acrylic Acid and DMPA used in the first 3D sample print.**

The resin tank of the Form 1+ printer was filled with the 200ml of hydrogel formulation M.

The following Formlabs, Form 1+ printer settings were applied for sample prints 1 – 6.

| Sample Print | Laser Speed (mm/s) | First Layer Passes | Other Layer Passes | Early Layer Passes | Scan Line Spacing (mm) | Z Axis Offset (mm) |
|---|---|---|---|---|---|---|
| 1 | 800 | 20 | 1 | 4 | 0.09 | 0.2 |
| 2 | 800 | 30 | 1 | 8 | 0.09 | 0.2 |
| 3 | 800 | 30 | 1 | 8 | 0.09 | 0.2 |
| 4 | 700 | 30 | 1 | 8 | 0.07 | 0.0 |
| 5 | 700 | 30 | 1 | 8 | 0.07 | 0.2 |
| 6 | 700 | 30 | 3 | 8 | 0.07 | 0.2 |

**Table 4.7: Printer settings applied for Form 1+ sample prints 1 - 6.**

For sample prints 1, 2, 3 and 6 a full-size rod print was attempted, 40mm x 8mm. A reduced size rod, 20x 4mm, was attempted for sample prints 4 and 5.

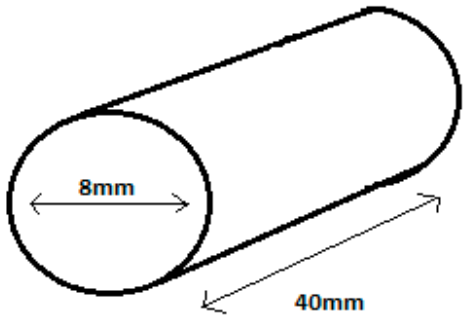


**Figure 4.5: Dimensions of a 'full size' rod.**

The support density and support point size were increased for sample print 6.

| Operating Logic Parameter | Default Value | Sample Print 6 Value |
|---|---|---|
| Support Density | 1.0 | 1.5 |
| Support Point Size | 0.6mm | 1.3mm |

**Table 4.8: Changes made to the support density and point size for the sixth sample 3D print.**

A detailed account of the methodology described above can be found in section 7.3.

#### 4.2.2.4 Reducing Formulation M Reactivity

##### 4.2.2.4.1 Sodium Bicarbonate Neutralisation of Acrylic Acid of Formulation M

It was thought that increasing the pH of hydrogel formulation M would reduce its reactivity with the Form 1+ 3D printer resin tank and platform.

An increase in pH could be achieved by neutralising the acrylic acid component of the hydrogel.

The addition of saturated sodium bicarbonate ($NaCHO_3$) at concentrations of 10%, 5% and 2.5% respectively, were added to 10ml of formulation M in the following concentrations:

| PLA % (w/w) | PEGDA % (w/w) | Acrylic Acid % (w/w) | $NCHO_3$ % (w/w) | Irgacure 819 % (w/w) |
|---|---|---|---|---|
| 0.5% | 0.5% | 99% | 10% | 1% |
| 0.5% | 0.5% | 99% | 5% | 1% |
| 0.5% | 0.5% | 99% | 2.5% | 1% |

**Table 4.9: Concentrations of PLA, PEGDA, acrylic acid, saturated sodium bicarbonate and Irgacure 819 used in the sodium bicarbonate neutralisation formulations.**

Varying amounts of the neutralised hydrogel formulations were pipetted into different volume vessels and its UV curing ability was tested.

First, 150µl of the hydrogel was pipetted into the lid of a small (2ml) vial. The contents were placed under the 380 – 420nm UV lamp for 5 minutes.

Next, 450µl of the hydrogel was pipetted into the lid of a larger (20ml) vial. Again, the contents were placed under the UV lamp for 5 minutes.

Finally, 47µl of the hydrogel was pipetted into Plastic tubing with an inner diameter of ~2mm and 10mm in length. The tubing and hydrogel were placed under the UV lamp for 5 minutes.

It was believed that the concentration of $NaCHO_3$ was too high and was impacting on the hydrogels ability to cure und UV light.

150µl of the hydrogel with 5% $NaCHO_3$ was pipetted into the lid of a small (2ml) vial. The contents was placed under the 380 – 420nm UV lamp for 5 minutes. No curing occurred. Then, 47µl of the hydrogel was pipetted into Plastic tubing with an inner diameter of ~2mm and 10mm in length. The tubing and hydrogel were placed under the UV lamp for 5 minutes.

The formula of 2.5% $NaCHO_3$ hydrogel was pipetted into the lid of a small (2ml) vial, volume of 150µl. This was placed under the 380-420nm UV lamp for 5 minutes.

#### 4.2.2.4.2 Dilution of Acrylic Acid in Formulation M

Another method for reducing the acidity of the acrylic acid component of formulation M was to dilute the acid with another swelling compound. 2-hydroxyethyl acrylate (HEA), an ester of acrylic acid, was added to the hydrogel formula. Equal amounts of acrylic acid and 2-hydroxyethyl acrylate were used in the modified hydrogel formula.

Initially 5ml of hydrogel was synthesised:

| PLA % (w/w) | PEGDA % (w/w) | Acrylic Acid % (w/w) | HEA % (w/w) | Irgacure 819 % (w/w) |
|---|---|---|---|---|
| 0.5% | 0.5% | 49% | 49% | 1% |
| 25µg | 25µl | 2.45ml | 2.45ml | 0.05g |

**Table 4.10: Concentrations of PLA, PEGDA, acrylic acid, 2-hydroxyethyl acrylate and Irgacure 819 used in the dilution of acrylic acid formulation.**

Multiple amounts of 150µl of the hydrogel was pipetted into the lids of small (2ml) vials. The contents were placed under the 380 – 420nm UV lamp. Curing was seen with 2 minutes. The same process was carried out with 450µl of hydrogel into the lids of a larger (20ml) vial.

#### 4.2.2.4.3 Synthesis of Hydrogels with Varying PEGDA Concentrations

The effect of PEGDA concentrations on the swelling of the hydrogels containing equal concentrations of acrylic acid and 2-hydroxyethyl acrylate was investigated. 2ml of each of the following hydrogel formulations was made up:

| Hydrogel Formulation | PLA % (w/w) | PEGDA % (w/w) | Acrylic Acid % (w/w) | HEA % (w/w) | Irgacure 819 % (w/w) |
|---|---|---|---|---|---|
| P | 0.5% | 1% | 48.75% | 48.75% | 1% |
| | 0.1g | 20µl | 975µl | 975µl | 0.02g |
| Q | 0.5% | 1.5% | 48.5% | 48.5% | 1% |
| | 0.01g | 30µl | 970µl | 970µl | 0.02g |

**Table 4.11: Concentrations of PLA, PEGDA, acrylic acid, 2-hydroxyethyl acrylate and Irgacure 819 used in the formulations of the initial PEGDA concentration investigation.**

Multiple amounts of 150µl of the hydrogel formulations were pipetted into the lids of small (2ml) vials. The contents were placed under the 380 – 420nm UV lamp. Curing was seen with 2 minutes. 4 hydrogels of each formula were made at this size. The same process was carried out with 450µl of hydrogel into the lids of larger (20ml) vials. Again, curing was seen within 2 minutes. 2 hydrogels of each formula were made in this size.

Hydrogels numbered 1-4 were pipetted into the lids of small (2ml) vials, with starting dimensions of ~7mm x ~5mm. Hydrogels numbered 5 and 6 are the hydrogels that were pipetted into the lids of larger (20ml) vials. They had a

starting diameter of ~16mm and a height of ~4.5mm. They hydrogels were then individually placed in 20ml glass vials with 5ml of phosphate-buffered solution (PBS) and kept at in an incubator at 37°C.

Most hydrogels synthesised in the above PEGDA concentrations investigation had broken down within 72 hours. It was deemed that a higher concentration of PEGDA would be needed in order for the hydrogels to retain their form.

2ml of each of the following hydrogel formulations was made up:

| Hydrogel Formulation | PLA % (w/w) | PEGDA % (w/w) | Acrylic Acid % (w/w) | HEA % (w/w) | Irgacure 819 % (w/w) |
|---|---|---|---|---|---|
| R | 0.5% | 0.5% | 49% | 49% | 1% |
| | 0.1g | 10µl | 980µl | 980µl | 0.02g |
| S | 0.5% | 2% | 48.25% | 48.25% | 1% |
| | 0.01g | 40µl | 965µl | 965µl | 0.02g |
| T | 0.5% | 2.5% | 48% | 48% | 1% |
| | 0.01g | 50µl | 960µl | 960µl | 0.02g |
| U | 0.5% | 3% | 47.75% | 47.75% | 1% |
| | 0.01g | 60µl | 955µl | 955µl | 0.02g |

**Table 4.12: Concentrations of PLA, PEGDA, acrylic acid, 2-hydroxyethyl acrylate and Irgacure 819 used in the formulations of further PEGDA concentration investigation.**

150µl of the hydrogel formulations were pipetted into the lids of small (2ml) vials. The contents was placed under the 380 – 420nm UV lamp. Curing was seen with 2 minutes. 4 hydrogels of each formula were made, with starting dimensions of ~7mm x ~5mm.

The hydrogels were placed in PBS, at 37°C, for a total of 13 weeks. Recordings of weight and dimension were taken on days 0, 1, 2, 5, 6, 7, 8 and 91.

A detailed account of the methodology described across section 4.2.2.4 can be found in section 7.4.

#### 4.2.2.5 Production of Formulation R Hydrogels via Casting with Moulds.

##### 4.2.2.5.1 Pliable Plastic Moulds

Clear, plastic tubing was used to form a more pliable mould for the curing of formulation R hydrogel. The tubing had an internal diameter of 8mm and was cut to lengths between 40mm and 46mm. The end of the tubing was sealed with 9mm diameter wooden dowel.

**Figure 4.6: Pliable moulds made to produce rods with an 8mm diameter and lengths between 40-46mm.**

8ml of formulation R (0.5% PEGDA) was made up.

The moulds were filled with 2ml of hydrogel resin, or to the top of the mould and then cured under the UV lamp for 5 minutes. The hydrogels were successfully removed from the moulds and the surface of the hydrogel that had been in contact with the wooden dowel was cured for an additional 30 seconds. The weight, height and diameter of the hydrogels was recorded, and they were placed in PBS, at 37°C overnight. The hydrogel removed from the 3D printed mould was also measured and placed in PBS.

#### 4.2.2.6 Production of Formulation U Hydrogels via Casting within Pliable Plastic Moulds.

4ml of formulation U was made up with the following volumes:

| PLA % (w/w) | PEGDA % (w/w) | Acrylic Acid % (w/w) | HEA % (w/w) | Irgacure 819 % (w/w) |
|---|---|---|---|---|
| 0.5% | 3% | 47.75% | 47.75% | 1% |

**Table 4.13: Concentration of PLA, PEGDA, acrylic acid, HEA and Irgacure 819 used in formulation U.**

The resin was pipetted into moulds made from pliable, clear plastic tubing and wooden dowel. The hydrogels were cured under the 380-420nm UV lamp for 5 minutes.

The weight, height and diameter of the hydrogels was measured, and they were placed in PBS, at 37°C overnight.

#### 4.2.2.7 Development of Silicone Moulds for Hydrogels

##### 4.2.2.7.1 Prototype 1, Nusil MED4211 Silicone

A prototype mould for the producing a silicone mould for hydrogels was constructed using a 15ml centrifuge tube, corrugated plastic tubing and duct tape. The centrifuge tube was cut down to the 5ml mark, giving it the following dimensions:

- **Height = 45.24mm**
- **External diameter of open end = 16.01mm**
- **Internal diameter of open end = 13.40mm**

The centrifuge tube was placed inside the corrugated plastic tube and the base of the corrugated tube was sealed with duct tape. Nusil MED4211 silicone was injected around the centrifuge tube, the tube was then held in position with duct tape.

The corrugated tube had the following dimensions:

- **Height = 47.86mm**
- **External diameter = 25.12mm**
- **Internal diameter = 21.19mm**

The silicone was left in the mould for 24 hours at around 40°C.

Removal of the duct tape revealed that the silicone had set solid.

The centrifuge tube was easily removed from the centre of the mould.

The removed the outer corrugated tubing, the top was cut slightly, and the tubing was unravelled.

#### 4.2.2.7.2 Synthesis of Hydrogel U within Prototype 1 Moulds

8ml of formulation U was made up. The hydrogel resin was pipetted into the cone silicone mould, around 4ml in each, and cured under the 380 – 420nm UV lamp. The silicone mould was used twice to produce two solid hydrogels. The first hydrogel took 9 minutes to sure, the second took 3 minutes. The two hydrogels were placed in PBS at 37°for 48 hours.

#### 4.2.2.7.3 Prototype 2, 3D Printing and Nusil MED4211 Silicone

A mould to produce more accurate silicone moulds for hydrogels was designed and printed. Standard Formlabs 1+ resin was used, and the design printed on a Formlabs 1+ 3D printer. The printer selected suitable operating logic parameters for the standard resin.

The moulds were designed to produce a hydrogel rod from a silicone mould. The hydrogel would have the dimension of 40mm x 8mm. The mould for the silicone had the following dimensions:

| Overall Diameter (mm) | Thickness of Outer Wall (mm) | Extruded Cut (mm) | Spool Piece Diameter (mm) | Overall Height (mm) | Height of Base (mm) | Height of Spool Piece (mm) |
|---|---|---|---|---|---|---|
| 14 | 1 | 2 | 8 | 45 | 2 | 40 |

**Table 4.14: The dimensions of the mould, printed with Formlabs 1+, for the silicone**

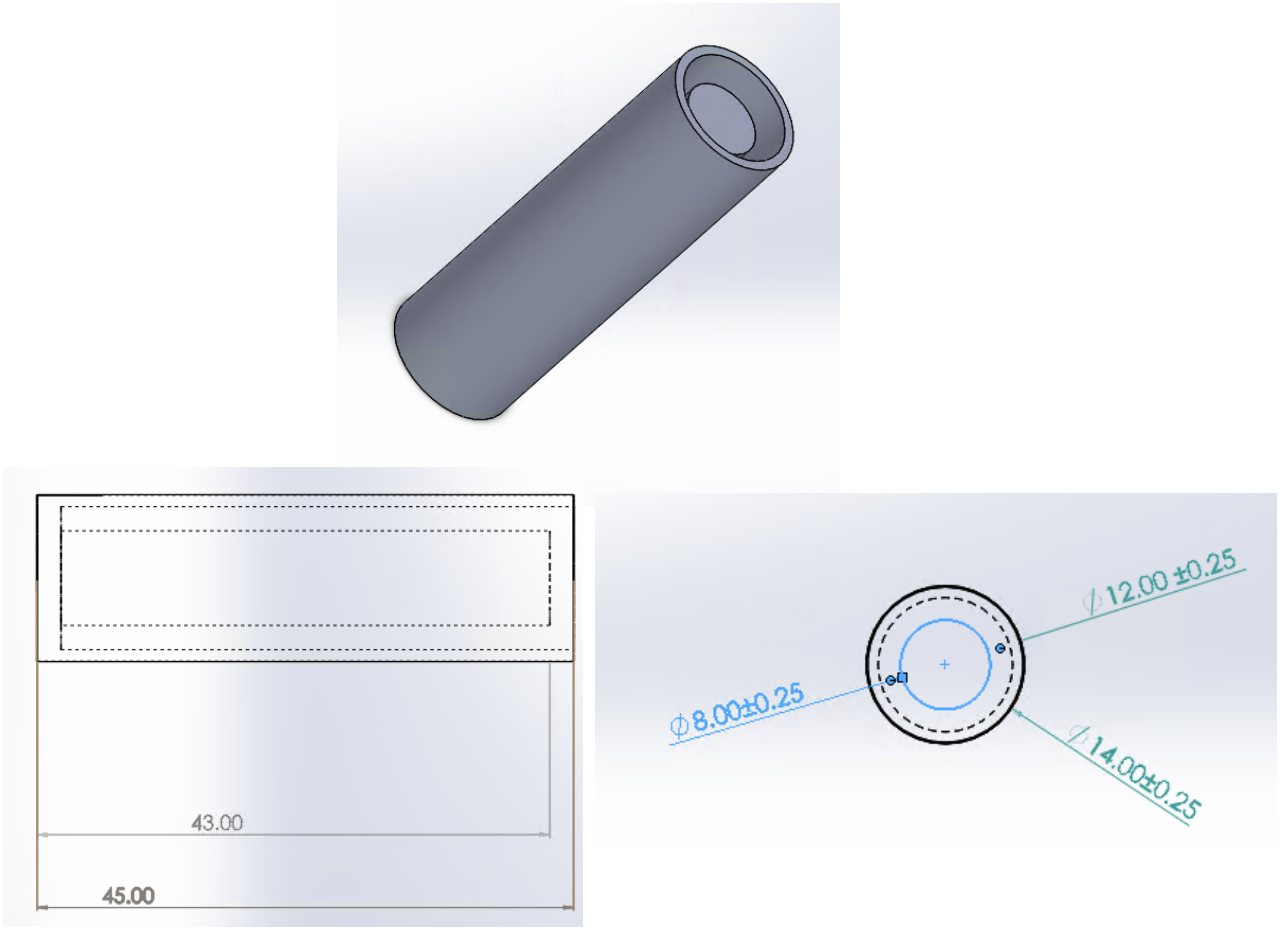


**Figure 4.7: Image and diagram of the 3D printed mould for use with silicone.**

A detailed method of the construction of prototype 2 silicone moulds can be found in section 7.7.1.

Detailed methods of Prototype moulds 3 and 4 can be found in sections 7.7.3 and 7.7.5, respectively

#### 4.2.2.7.4 Prototype 5, Mold Max™ Silicone Moulds

Continued development of silicone moulds for prospective hydrogels (details in appendix) resulted in the following successful method:

Moulds for the Mold Max™ 10T silicone were constructed with corrugated plastic tubing, smooth plastic tubing, plastic caps and cocktail sticks.

Lengths of the smooth tubing were cut. These lengths were made slightly longer to accommodate for the narrowing of the silicone that occurs due to the shape of the base of the mould. A hypodermic needle was used to create pilot holes in the smooth, inner, tubing and the external corrugated tubing. A cocktail stick was threaded through the holes to hold the smooth tubing, suspended, in position.

Two types of moulds were produced. One had the smooth, inner, tubing plugged with wooden dowel at the base end. This was designed to produce a silicone mould for a solid cylinder. In the other, the smooth, inner, tubing was left hollow to allow the silicone to set around and within the tubing. This design was proposed to form a silicone mould with an extruded centre. This would produce a hydrogel in the form of a cylinder with a lumen.

The Mold Max™ 10T silicone was prepared with the following method:

Mix the individual parts, part A and part B, in their containers before measuring out the components. Dispense the required amount of part A into a mixing container, add part B and mix for 3 minutes. For this trial, 200ml of part A and 20ml of part B were used.

After mixing, the silicone was degassed to eliminate trapped air from the mixing. The silicone was placed in a vacuum oven and the pressure was reduced to 0 bar. 220ml of silicone was prepared in a 400ml glass beaker to allow for material expansion. The mixture rose in the container and then fell back to the level of 220ml. Once fallen, the silicone was left in the vacuum oven for 3 minutes. The degassed silicone was poured into the moulds with a steady flow to try to prevent the addition of air. Once poured into the moulds, the silicone was left at room temperature overnight.

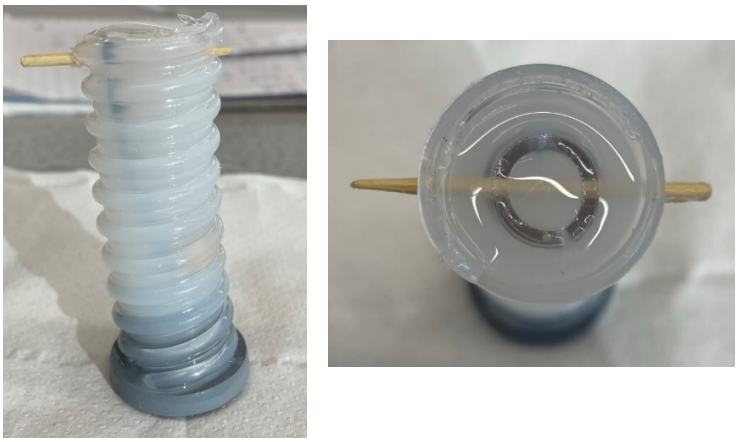

**Figure 4.8: Plastic moulds containing degassed liquid silicone.**

The methodology of Prototype mould 6 can be found in sections 7.7.7.

#### 4.2.2.7.5 Prototype 7, Smaller Hollow Cylindrical Mold Max™ Silicone Moulds

110ml of Mold Max™ 10T silicone was prepared.

Moulds for the silicone were constructed using corrugated plastic tubing, smooth plastic tubing and plastic caps.

They were designed to produce hydrogels with the following dimensions:

- **External diameter = 6mm**
- **Internal diameter = 5mm**

4 moulds were produced in total. Two moulds were designed to produce hollow cylindrical hydrogels with flat, blunt ends. The other two moulds were designed to produce hollow cylindrical hydrogels with a quincke, needle like, end.

The silicone was poured into the moulds and left at room temperature overnight to set.

The silicone was easily removed from the moulds.

A detailed methodology of Prototype 7 mould can be found in section 7.7.9.

#### 4.2.2.7.6 Prototype 8, Solid Tipped, Hollow Cylindrical Mold Max™ Silicone Moulds

110ml of Mold Max™ 10T silicone was prepared.

Four moulds were constructed in total. Two moulds were designed to produce solid cylindrical hydrogels with quincke ends. Two moulds were designed to produce hollow cylindrical hydrogels with solid tapered ends (Fig. 4.9).

The silicone was poured into the moulds. The moulds for solid hydrogels had the non-quincke tip protruding from the silicone. The plastic tubing and eppendorf was completely encased with silicone, with the eppendorf fixed in position at the base of the mould. Whilst filling the moulds, air bubble rose within the silicone, with the majority dissipating once reaching the surface.

**Figure 4.9: Moulds used to produce silicone moulds for hollow cylindrical hydrogels with solid tapered ends.**

The silicone had set overnight.

The exterior and interior tubing that formed the mould for the solid cylindrical hydrogel, with a quincke end, were easily removed.

### 4.2.2.8 Synthesis of Hydrogel U within Silicone Moulds

#### 4.2.2.8.1 Solid Cylinder Hydrogel

5ml of Formulation U was made up. The liquid hydrogel was pipette into the silicone mould designed to produce a solid cylinder hydrogel. The hydrogel was cured under the 380 – 420nm UV lamp and had cured after 3 minutes. The cured, solid hydrogel was easily removed from the silicone mould.

The hydrogel was then placed back under the UV lamp for another minute to ensure completely curing had occurred.

Bubbling of the liquid hydrogel was seen during curing, due to the exothermic properties of the acrylic acid. This led to air bubbles being trapped within the solid hydrogel.

The hydrogel was placed in PBS overnight, kept at 37°C.

#### 4.2.2.8.2 Hollow Cylinder Hydrogel

Formulation U was made up and the resin was pipetted into hollow cylinder producing moulds. 3 hollow cylinder hydrogels were produced. One of the hollow hydrogels was placed in PBS and left at room temperature.

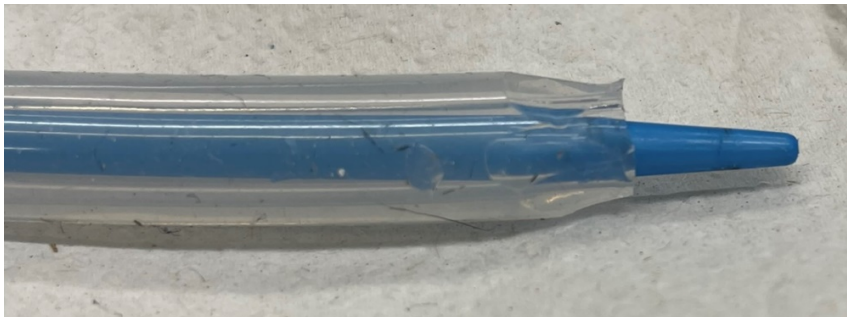

**Figure 4.10: Tapered end design of the hollow cylindrical tubed hydrogels.**

#### 4.2.2.8.3 Smaller Hollow Cylinder Hydrogel

10ml of formulation U hydrogel was prepared.

The hydrogel resin was pipetted into the silicone moulds, each mould held around 1ml of resin.

The hydrogels were cured under the UV lamp for 2 minutes.

In total, 10 hydrogels were cured. 6 hydrogels had quincke ends, 4 had blunt ends.

#### 4.2.2.8.4 Reshaping of Hollow Hydrogels

Once the hydrogels produced had softened sufficiently, due to exposure to air moisture, they could be cut to be reshaped.

Two of the blunt ended hydrogels were cut into the shape of a helix.

These two hydrogels, alongside a quincke ended hydrogel and a complete blunt ended hydrogel, were measured, placed into PBS and left overnight at room temperature.

#### 4.2.2.8.5 Solid Tipped, Hollow Cylindrical Hydrogels

20ml of formulation U hydrogel was prepared.

The hydrogel resin was easily pipetted into the moulds for the solid, quincke ended hydrogels. The hydrogel was placed under the 380 – 420nm UV lamp for 4 minutes.

#### 4.2.2.8.6 Thicker Walled Smaller Hollow Cylindrical Hydrogels

The design for Prototype 6 mould was replicated.

10ml of formulation U was prepared.

To attempt to make the walls of the hydrogel thicker, the silicone extrusion of the mould was stretched out and a needle was placed through the extrusion and rested on the top of the mould (Fig. 4.11). This, in theory, made the extrusion thinner thus resulting in thicker hydrogel walls.

**Figure 4.11: Adjustment made to the silicone moulds to produce hydrogels with thicker walls.** The extrusion of the mould was stretched out and a needle placed through it and rested on the top of the mould.

The hydrogel was pipetted into the moulds and placed under the 380-420nm UV lamp for 3 minutes. Once the hydrogels had cooled, they were removed from the silicone moulds.

## 4.3 Results

### 4.3.1 Oxtex Hydrogel Processing

All three expanders started at very similar dimensions, around 17.8mm x 8.6mm. In the first two days, all devices remained at a similar size. After this time point, device 6 began to increase in size. At day 4, device 4 began to increase in size, device 5 followed on day 5. All the devices underwent a sudden surge in size. After this 'growth spurt' the expander dimensions plateaued. In the case of device 5, the length of the expander appeared to decrease over time.

In general, the width of the devices increased steadily over the course of the measurement period (Table 4.15). Device 5 showed a more sudden increase in width in the initial few days of the experiment (Fig. 4.12).

| Device | Initial length (mm) | Final length (mm) | Length increase (mm) | Initial width (mm) | Final width (mm) | Width increase (mm) |
|---|---|---|---|---|---|---|
| 4 | 17.80 | 19.84 | 2.04 | 8.81 | 10.48 | 1.67 |
| 5 | 17.63 | 19.74 | 2.19 | 8.27 | 10.59 | 2.32 |
| 6 | 17.86 | 20.33 | 2.47 | 8.65 | 11.28 | 2.63 |

**Table 4.15: Table representing the changes in length and width of Oxtex devices 4, 5 and 6.**

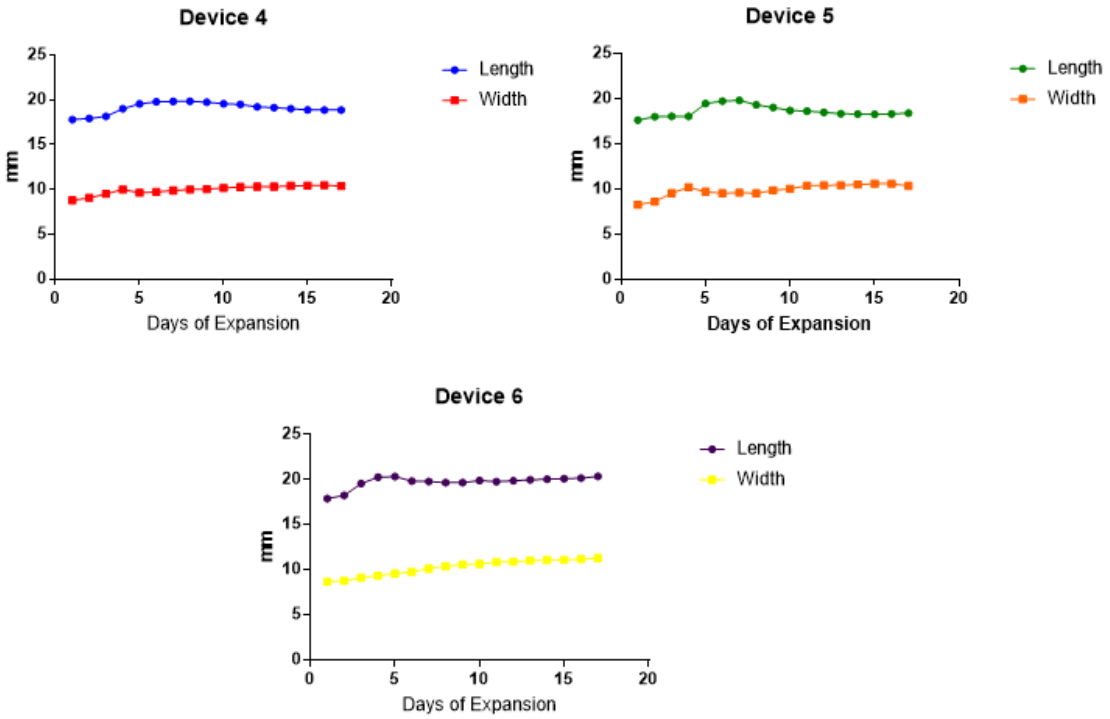


**Figure 4.12: Graphs to represent the changes in hydrogel expander dimensions, whilst kept in a 37°C water bath, throughout the 18-day study.** The devices all started at a similar length and width, after 5 days all the devices commenced expansion.

### 4.3.2 Centre of Additive Manufacturing Hydrogel Development

#### 4.3.2.1 Production of Hydrogel Formulations

##### 4.3.2.1.1 First Trial Hydrogel Formulations Weight

The graphs below show the changes in weight of the various formulations of hydrogels across the 7 days of measurement. The starting weights of the hydrogels ranged from 0.037-0.049g and the trend seen in all formulations was a rapid increase in weight over 24 hours. Some of the hydrogels increased in weight by 50% within the first 24 hours. After this time, the weight changes of the hydrogels plateaued for all the formulations, with the weight of some of the samples decreasing and then increasing over the 7 days (Fig. 4.13).

After 7 days, the hydrogels increased in weight by 31-46%. Overall, the formulation B hydrogels had the highest weight increase, with an average of 44.3% and the formulation C hydrogels had the lowest weight increase, with an average of 35.9%.

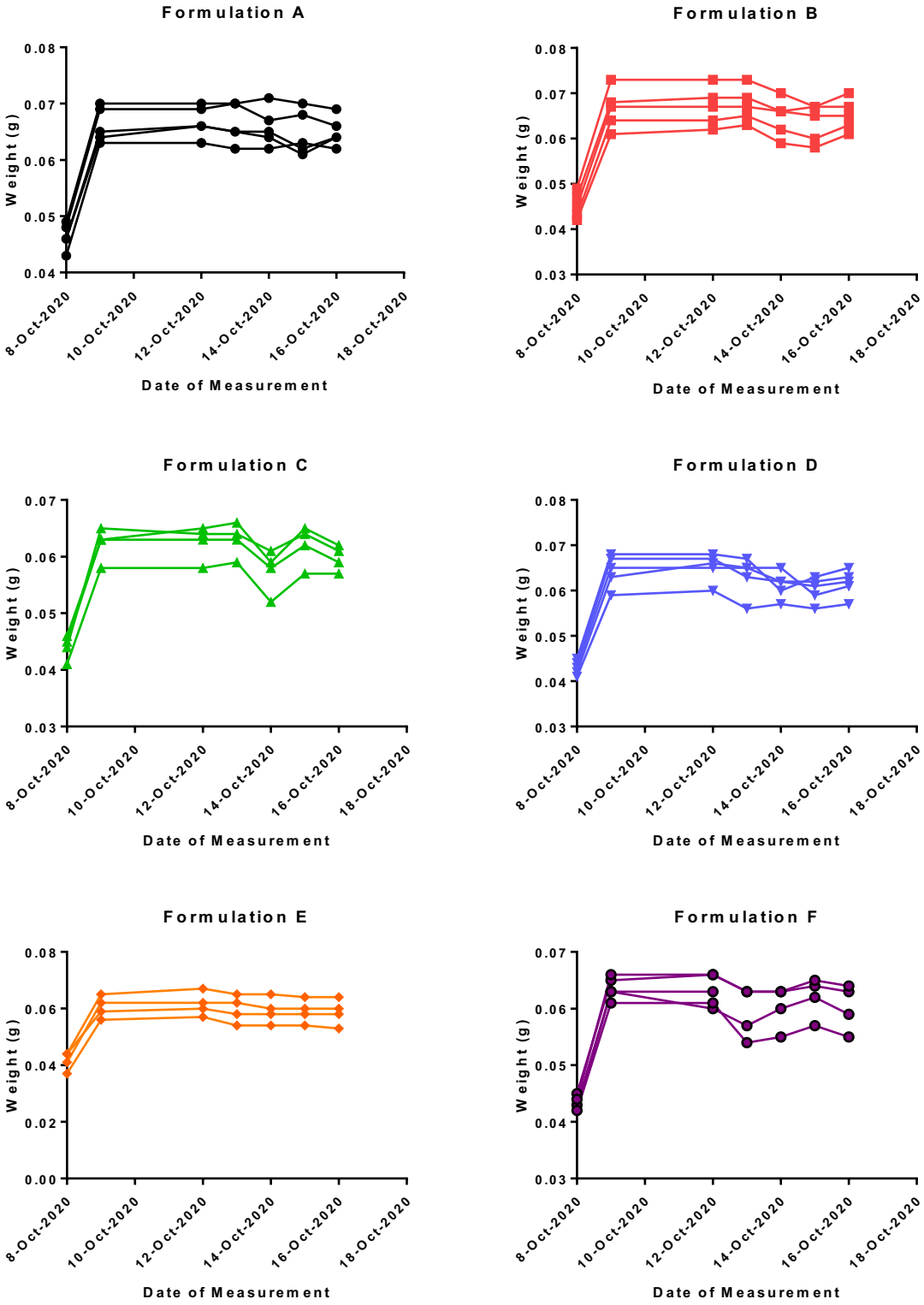


**Figure 4.13: Graphs representing the changes in weight of the various formulations used in the first trial of hydrogels across the 7 days of measurement.**

#### 4.3.2.1.2 First Trial Hydrogel Formulations Height

The graphs below show the changes in length of the various formulations of hydrogels across the 7 days of measurement.

The starting lengths of the hydrogels was between 8.59 – 10.8mm. The variation seen in the lengths could have been due to the varying levels of water tension holding the liquid hydrogel within its cast tubing or to the varying amounts of shrinkage that occurred when curing the hydrogel under the UV lamp.

Again, like the weight measurements, a significant increase in length was seen within the first 24 hours, with the maximum percentage increase being 22.2% (one of the formulation F hydrogels). After the first 24 hours, the lengths of all the various formulations of hydrogels began to plateau, with a slight fluctuation of lengths recorded in the last few days of measurements (Fig 4.14).

After 7 days of recording, the increase in length of hydrogels varied greatly between 6 – 23%, with the measurements on either end of the spectrum coming from formulation F hydrogels. Overall, the formulation A had the highest length increase, with an average of 17.9% and formulation F had the lowest length increase with an average of 15.1%.

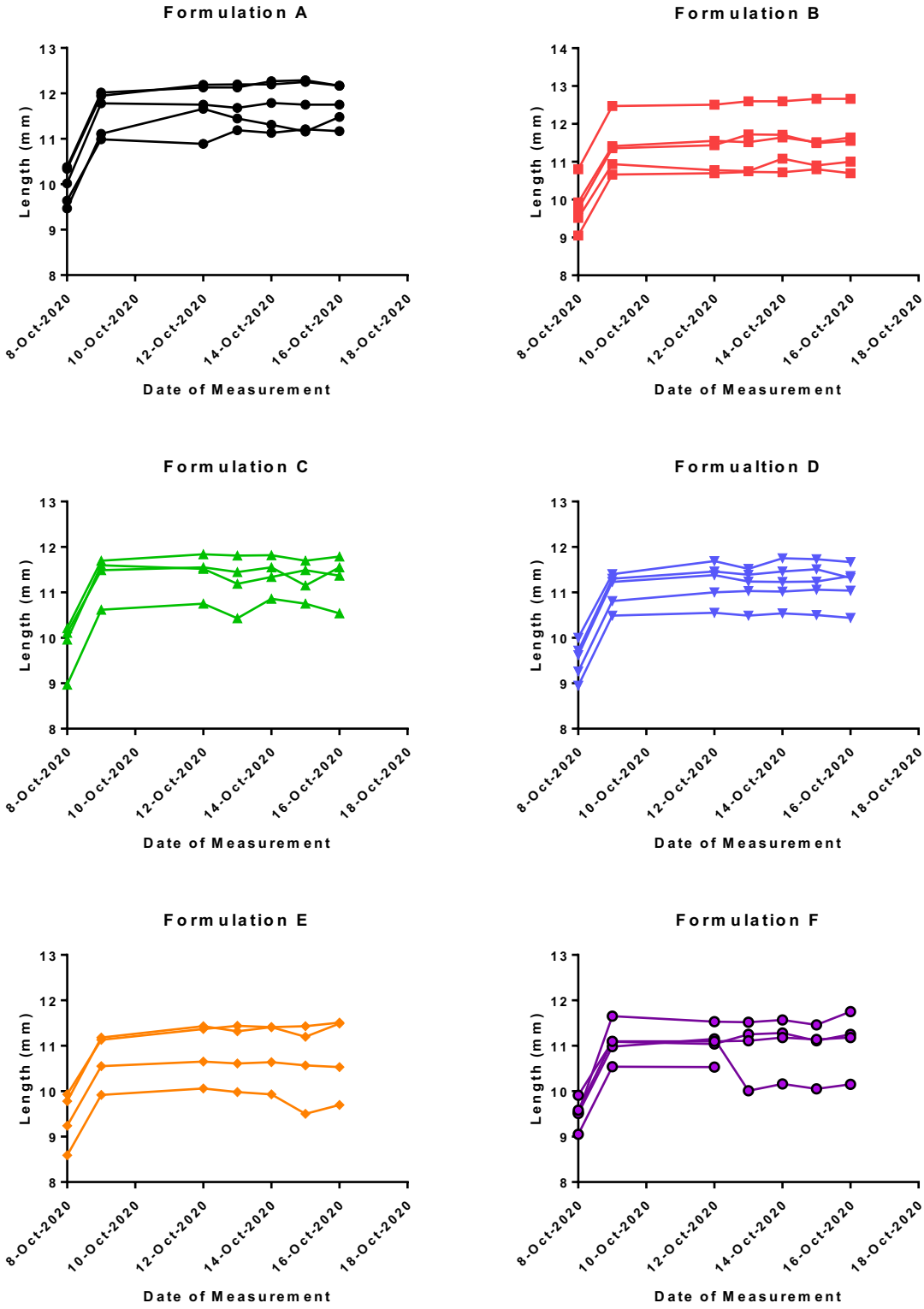


**Figure 4.14: Graphs representing the changes in length of the various formulations used in the first trial of hydrogels across the 7 days of measurement.**

#### 4.3.2.1.3 First Trial Hydrogel Formulations Length

The graphs below show the changes in length of the various formulations of hydrogels across the 7 days of measurement. The starting diameters of the hydrogels was between 2.16 – 2.44mm. The variation seen in the diameters could have been due to the varying levels of water tension holding the liquid hydrogel within its cast tubing or to the varying amounts of shrinkage that occurred when curing the hydrogel under the UV lamp.

Again, like the weight and length measurements, a substantial increase in diameter was seen within the first 24 hours, with the maximum percentage increase being 19.2% (a formulation C hydrogel). After the first 24 hours, the diameters of all the various formulations of hydrogels reached a plateau, with some wavering of diameters recorded in the last few days of measuring (Fig. 4.15).

After 7 days of recording, the increase in diameter of hydrogels varied greatly between 10 – 24%. Overall, the formulation C had the highest diameter increase, with an average of 20.3% and formulation E had the lowest diameter increase with an average of 15.5%.

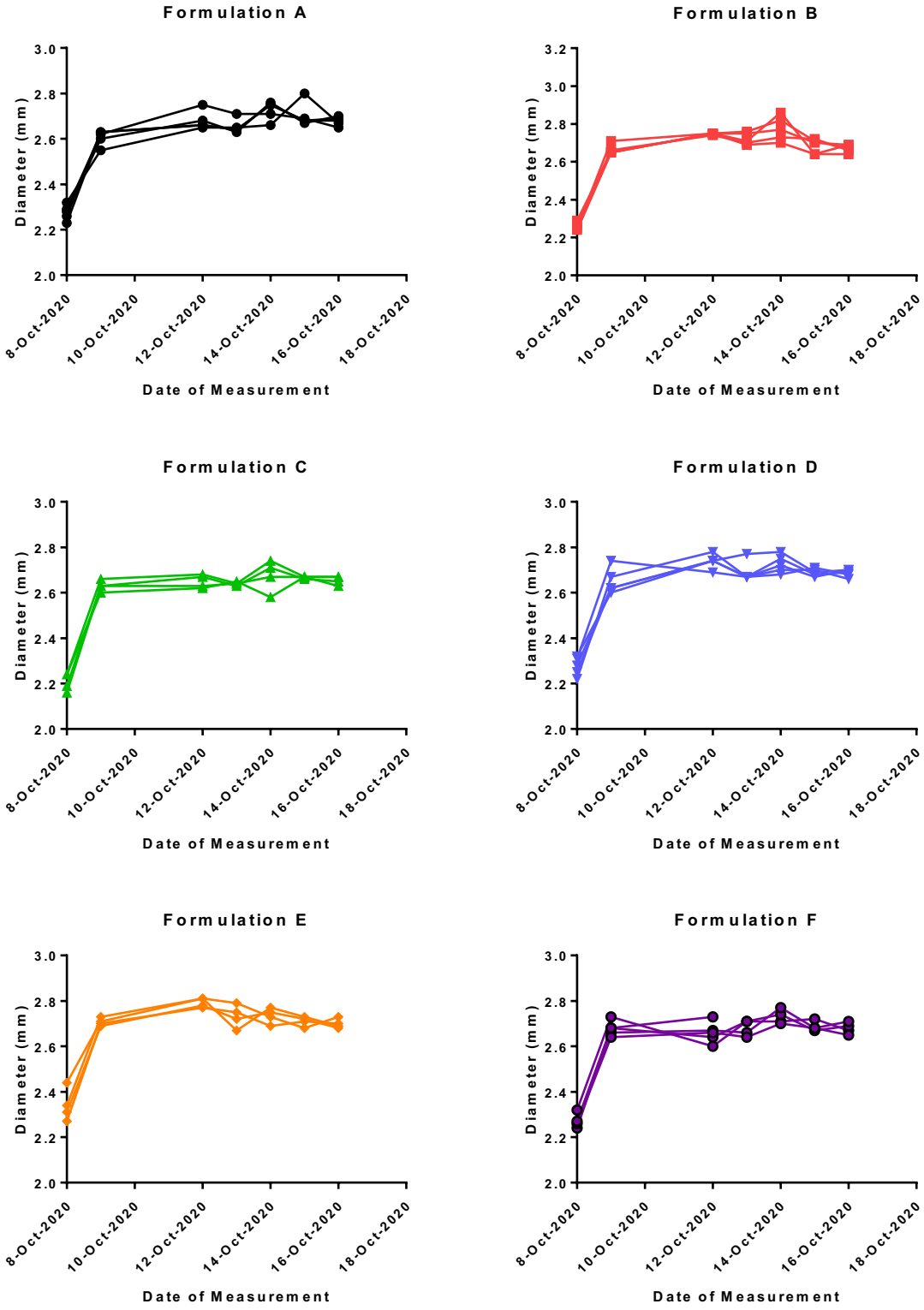


**Figure 4.15: Graphs representing the changes in diameter of the various formulations used in the first trial of hydrogels across the 7 days of measurement.**

#### 4.3.2.1.4 First Trial Hydrogel Formulations Average Hydrogel Measurements

Table 4.16 shows the average total percentage increase of the weight, length and diameter of the hydrogel expanders at various formulations concentrations over the 9 days of measuring.

| Expander | Average % increase of weight | Average % increase of length | Average % increase of diameter |
|---|---|---|---|
| A | 40.15 | 17.86 | 17.68 |
| B | 44.32 | 17.34 | 18.25 |
| C | 35.89 | 15.34 | 20.31 |
| D | 43.22 | 17.42 | 18.05 |
| E | 41.71 | 15.07 | 15.47 |
| F | 40.72 | 15.32 | 18.52 |

**Table 4.16: Average total percentage increase of the weight, length and diameter of the various hydrogel formulations used in the first trial over 9 days of measuring.**

The hydrogel expanders were left in PBS in the 37°C incubator and another set of measurements were recorded 26 days after the first measurements. The average percentage increase calculated from these measurements are represented in the table 4.17, below.

| Expander | Average % increase of weight | Average % increase of length | Average % increase of diameter |
|---|---|---|---|
| A | 45.72 | 17.74 | 5.03 |
| B | 50.09 | 16.75 | 19.49 |
| C | 40.93 | 15.37 | 20.67 |
| D | 46.93 | 17.98 | 18.68 |
| E | 46.06 | 12.92 | 14.39 |
| F | 41.26 | 12.56 | 16.99 |

**Table 4.17: Average total percentage increase of the weight, length and diameter of the various hydrogel formulations used in the first trial, 26 days after first measurement.**

#### 4.3.2.1.5 Second Trial Hydrogel Formulations Weight

The graphs below show the changes in weight of the various formulations of hydrogels across the 9 days of measurements.

The starting weights of the hydrogels ranged from 0.017g to 0.049g and the trend seen in all formulations was a rapid increase in weight over 24 hours. Some of the hydrogels increased in weight by 55.5% within the first 24 hours. After this time, the weight changes of the hydrogels plateaued for all the formulations, with the weight of the majority of the samples remaining consistent over the final 5 days (Fig. 4.16). After 9 days, the hydrogels increased in weight by 41-56%. Overall, the formulation K hydrogels had the highest weight increase, with an average of 53.3% and the formulation G hydrogels had the lowest weight increase, with an average of 44.2%.

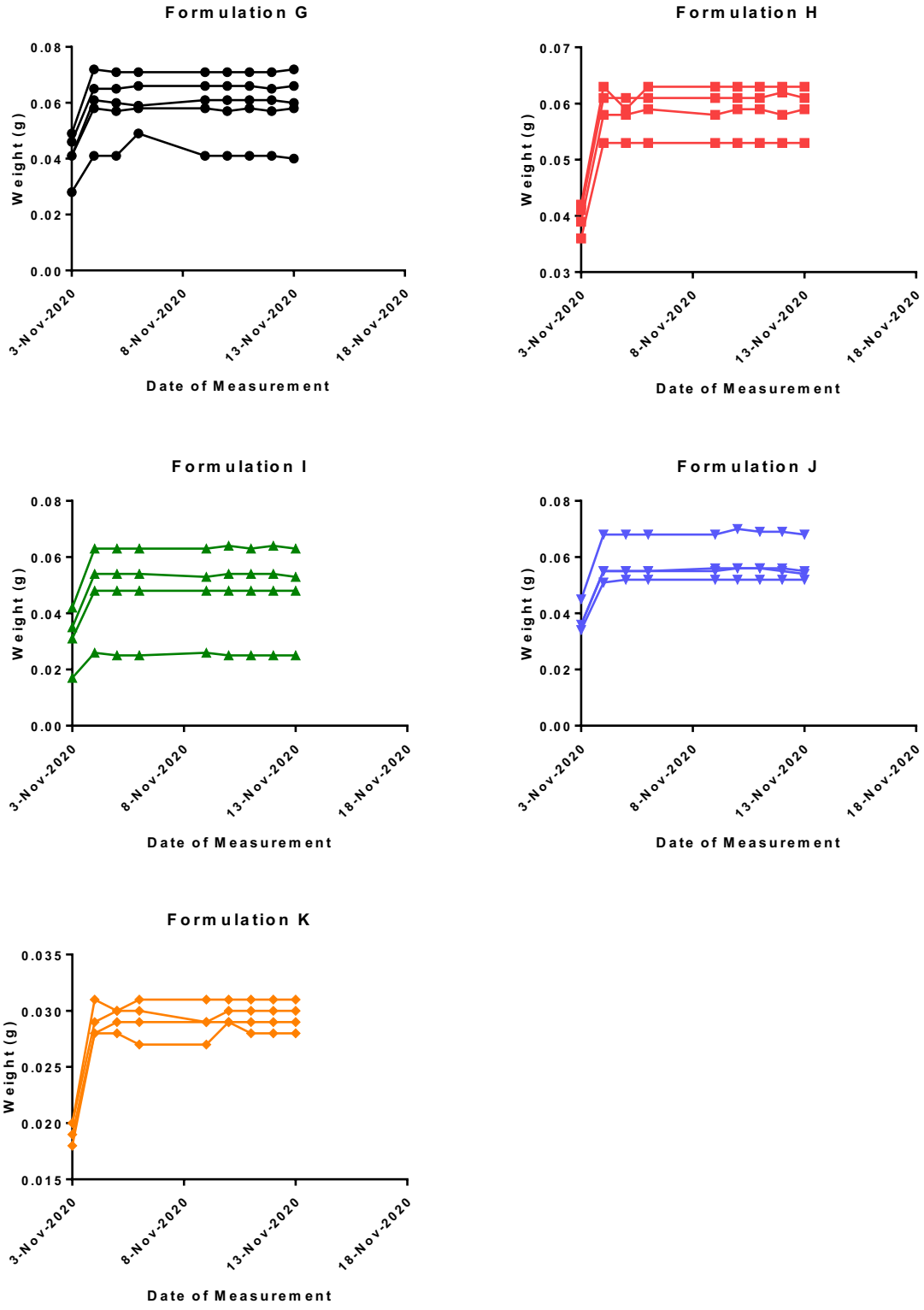


**Figure 4.16: Graphs representing the changes in weight of the various formulations used in the second trial across the 9 days of measurement.**

#### 4.3.2.1.6 Second Trial Hydrogel Formulations Length

The graphs below show the changes in length of the various formulations of hydrogels across the 9 days of measurement.

The starting lengths of the hydrogels was between 5.05 – 10.66mm. The variation seen in the lengths was primarily due to the brittle consistency of the hydrogels and so removal of them from the casts was much more difficult and often resulted in breakages of the expanders. Varying levels of water tension holding the liquid hydrogel within its cast tubing or to the varying amounts of shrinkage that occurred when curing the hydrogel under the UV lamp, could have also been contributing factors to the length variations.

Again, like the weight measurements, a significant increase in length was seen within the first 24 hours, with the maximum percentage increase being 25.3% (one of the formulation I hydrogels). After the first 24 hours, the lengths of all the various formulations of hydrogels began to plateau, with a minimal fluctuation of lengths recorded in the last few days of measurements (Fig. 4.17). After 9 days of recording, the increase in length of hydrogels varied between 13 – 29%. Overall, the formulation I had the highest length increase, with an average of 23.9% and formulation G had the lowest length increase with an average of 15.5%.

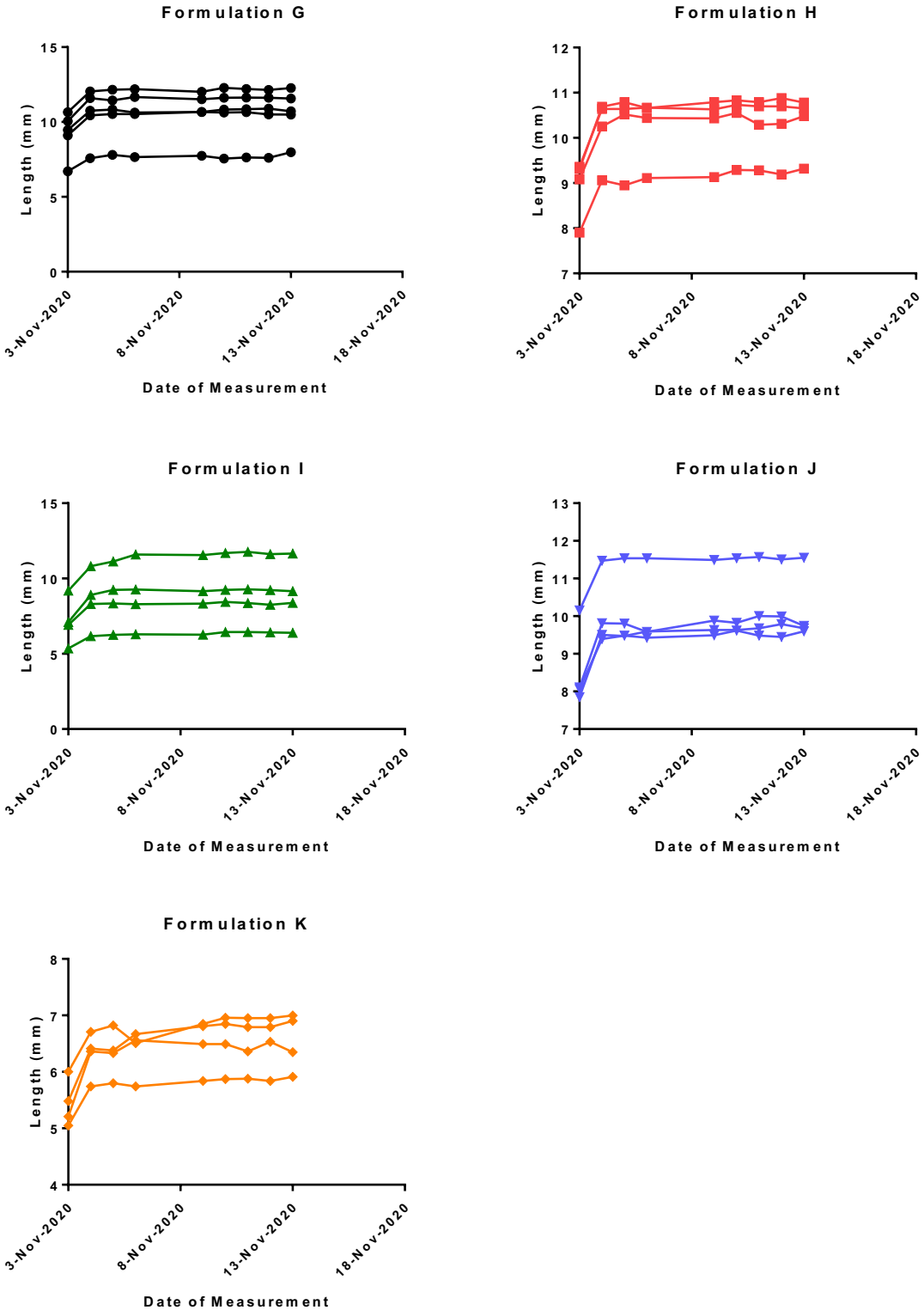


**Figure 4.17: Graphs representing the changes in length of the various formulations used in the second trial of hydrogels across the 9 days of measurement.**

#### 4.3.2.1.7 Second Trial Hydrogel Formulations Diameter

The graphs below show the changes in length of the various formulations of hydrogels across the 9 days of measurement.

The starting diameters of the hydrogels was between 2.04 – 2.35mm. The variation seen in the diameters could have been due to the varying levels of water tension holding the liquid hydrogel within its cast tubing or to the varying amounts of shrinkage that occurred when curing the hydrogel under the UV lamp. Again, like the weight and length measurements, a substantial increase in diameter was recorded within the first 24 hours, with the maximum percentage increase being 33.8% (a formulation I hydrogel).

After the first 24 hours, the diameters of all the various formulations of hydrogels reached a plateau, with some wavering of diameters recorded in the last few days of measuring (Fig. 4.18). After 9 days of recording, the increase in diameter of hydrogels varied greatly between 16 – 36%. Overall, the formulation I had the highest diameter increase, with an average of 28.0% and formulation E had the lowest diameter increase with an average of 18.8%.

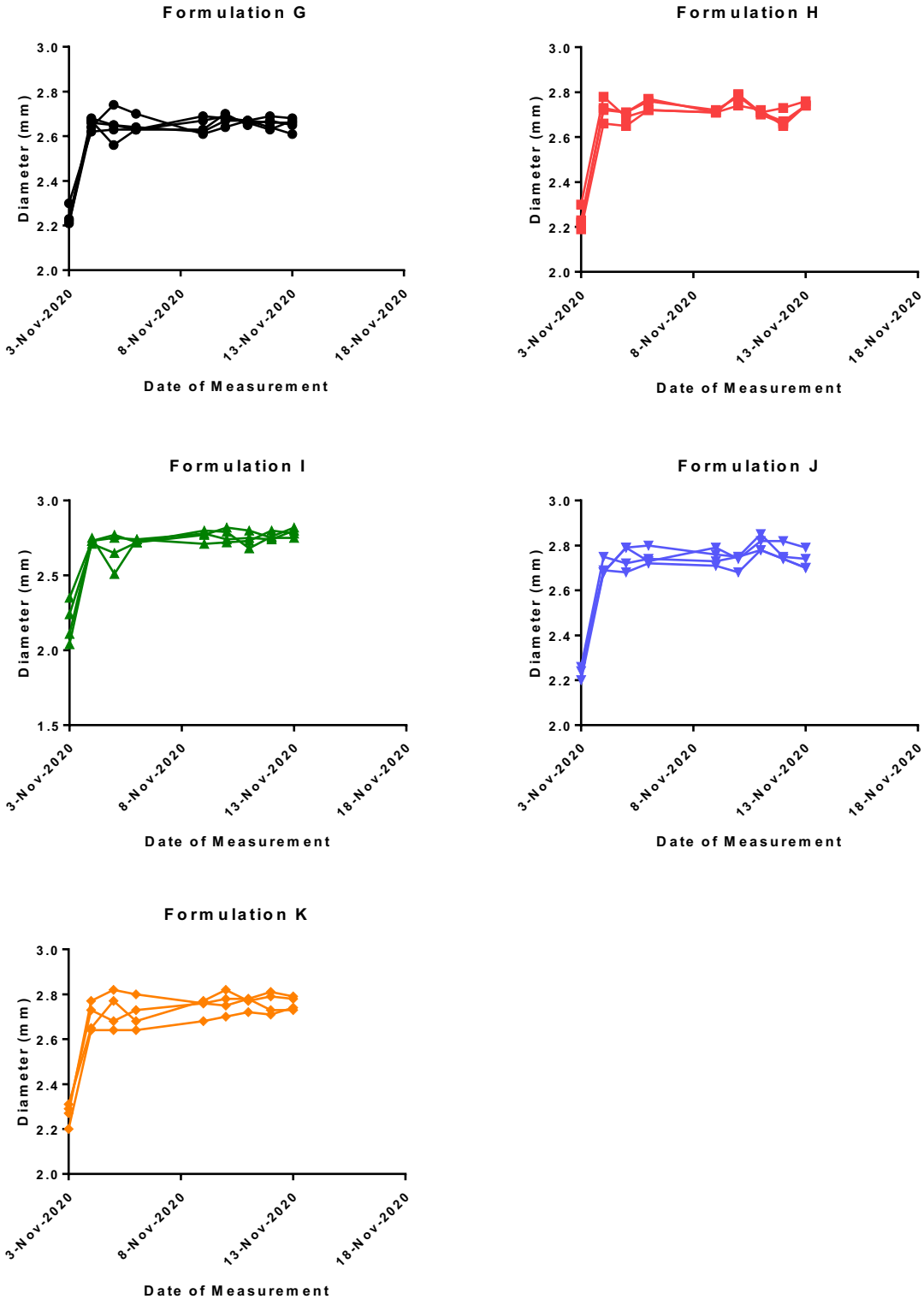


**Figure 4.18: Graphs representing the changes in diameter of the various formulations used in the second trial of hydrogels across the 9 days of measurement.**

#### 4.3.2.1.8 Second Trial Hydrogel Formulations Average Hydrogel Measurements

Table 4.18 shows the average total percentage increase of the weight, length and diameter of the hydrogel expanders at various formulations concentrations over the 11 days of measuring.

| Expander | Average % increase of weight | Average % increase of length | Average % increase of diameter |
|---|---|---|---|
| G | 44.50 | 15.54 | 18.82 |
| H | 49.32 | 15.74 | 22.86 |
| I | 50.83 | 23.94 | 27.97 |
| J | 51.71 | 19.08 | 22.01 |
| K | 53.30 | 20.37 | 21.75 |

**Table 4.18: Average total percentage increase of the weight, length and diameter of the various hydrogel formulations used in the second trial over 11 days of measuring.**

#### 4.3.2.1.9 Third Trial Hydrogel Formulations Weight

The graphs below show the changes in weight of the various formulations of hydrogels across the 8 days of measurements.

The starting weights of the hydrogels ranged from 0.018g to 0.098g and the trend seen was similar to that of previous formulations, a rapid increase in weight over 24 hours. After this time, the weight changes of the hydrogels plateaued for all the formulations, with the weight of the majority of the samples remaining consistent over the final 5 days (Fig. 4.19).

The composition of formulation L resulted in hydrogels that took on a substantial amount of water in 24 hours. After this time, the hydrogels that were cast in the tube no longer resembled their original form but became gelatinous with a similar consistency to egg whites. This result deemed these hydrogels unfit for the project and only the weight was recorded for the remainder of the swelling test.

The formulation with the highest weight increase was M with an average increase of 265.3% and the formulation O hydrogels had the lowest weight increase, with an average of 104.6%.

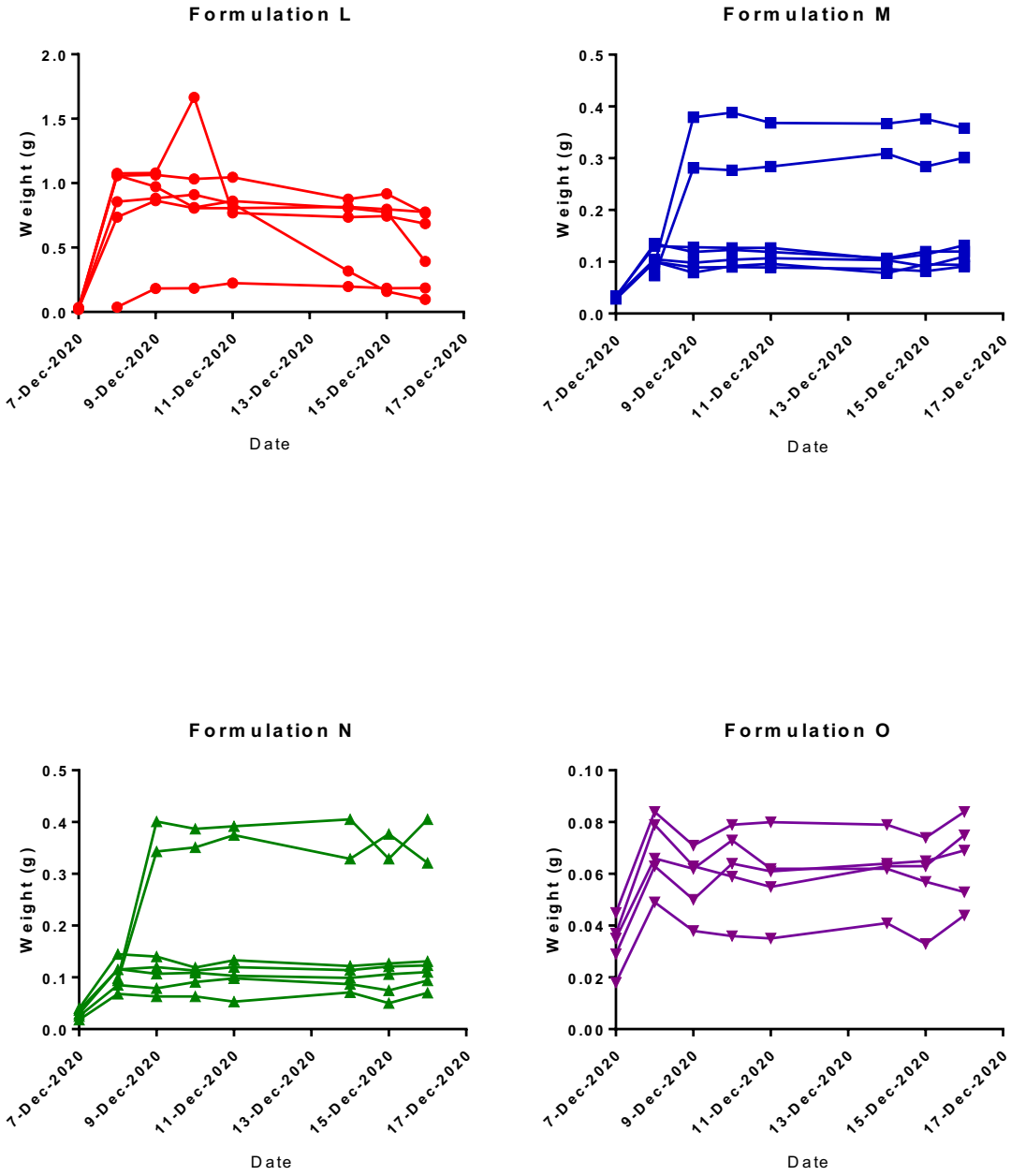


**Figure 4.19: Graphs representing the changes in weight of the various formulations used in the third trial of across the 8 days of measurement.**

#### 4.3.2.1.10 Third Trial Hydrogel Formulations Length

The graphs below show the changes in length of the various formulations of hydrogels across the 9 days of measurement. When measuring the hydrogels that were cast in the lids of vials, the height of the cylinder produced was measured as the length. Hence, these hydrogels seem to have a much smaller starting length than the tubular cast hydrogels.

The starting lengths of the hydrogels was between 1.54 – 9.90mm. Varying levels of water tension holding the liquid hydrogel within its cast tubing or the varying amounts of shrinkage that occurred when curing the hydrogel under the UV lamp were contributing factors to the length variations. Again, like the weight measurements, a significant increase in length was seen within the first 24 hours, with the maximum percentage increase being 84.1% (formulation M, cast in a vial lid).

The length of the formulation L hydrogels was not recorded after this point due to the lack in structure.

After the first 24 hours, the lengths of all the various formulations of hydrogels began to plateau, with a minimal fluctuation of lengths recorded in the last few days of measurements (Fig. 4.20). After 9 days of recording, the increase in length of hydrogels varied between 20.6 – 79.1%. Overall, the formulation N had the highest average length increase of 52.3%, but formulation M produced hydrogels that increased in length by 75.2% and 79.1% when cast in the lid of a vial. Formulation O had the lowest length increase with an average of 24.5%.

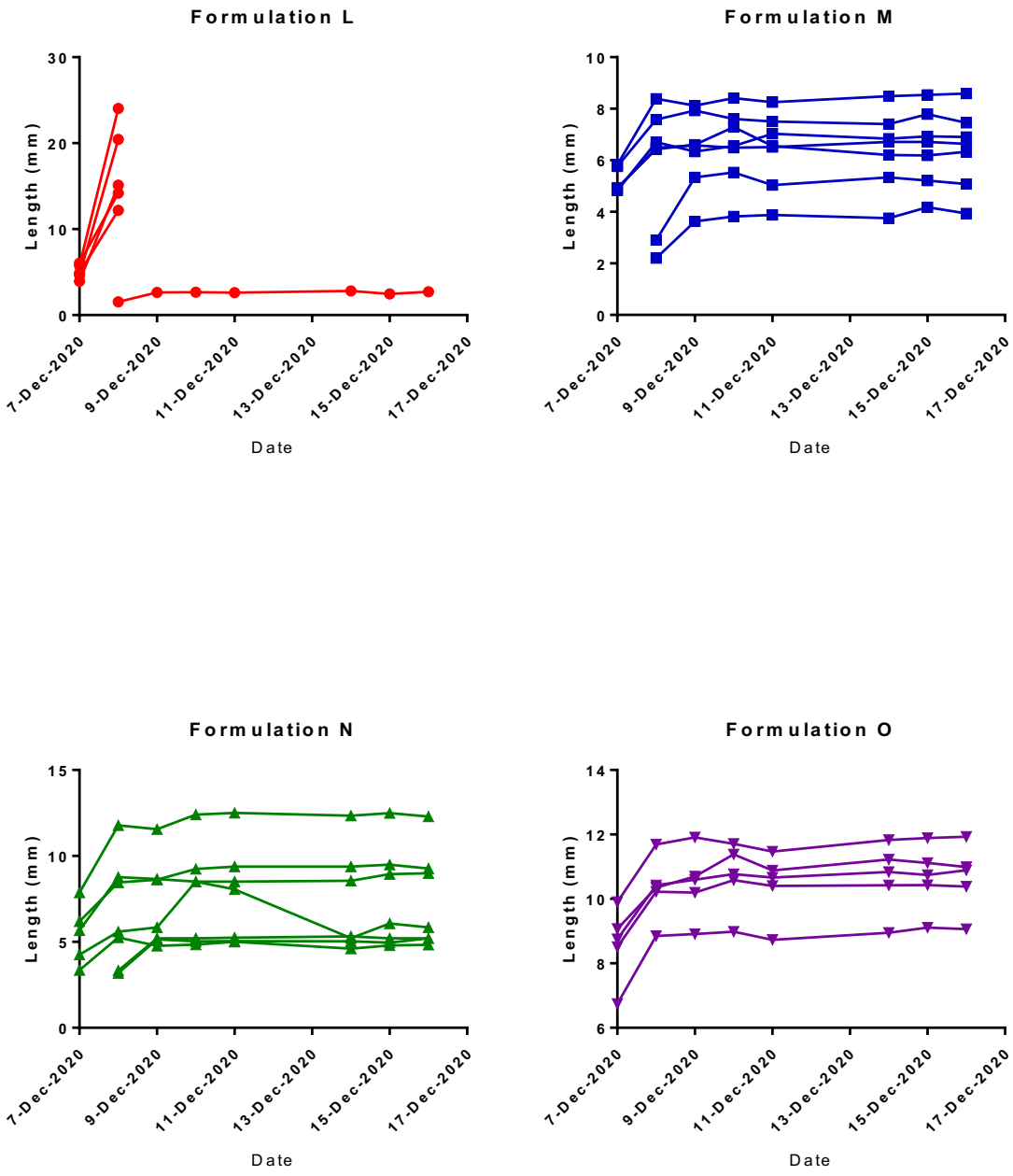


**Figure 4.20: Graphs representing the changes in length of the various formulations used in the third trial of hydrogels across the 8 days of measurement.**

#### 4.3.2.1.11 Third Trial Hydrogel Formulations Diameter

The graphs below show the changes in length of the various formulations of hydrogels across the 9 days of measurement. The starting diameters of the hydrogels was between 1.99 – 6.74mm. The variation in the diameters is due to the tubular casting having to be removed via scalpel and so the hydrogels were not replica of their moulds. The hydrogels with the largest diameter were cast in the lids on vial.

Again, like the weight and length measurements, a substantial increase in diameter was recorded within the first 24 hours, with the maximum percentage increase being 137.3% (a formulation N hydrogel). However, the large increase in diameter is most likely due to the hydrogels splitting at the point of weakness caused by the scalpel scoring the surface during removal from the casts.

The diameter of the formulation L hydrogels was not recorded after this point due to the lack in structure.

After the first 24 hours, the diameters of all the various formulations of hydrogels reached a plateau, with some wavering of diameters recorded in the last few days of measuring (Fig. 4.21). After 9 days of recording, the increase in diameter of hydrogels varied greatly between 30 – 161%. Overall, the formulation M had the highest diameter increase, with an average of 106.1% and formulation O had the lowest diameter increase with an average of 35.7%.

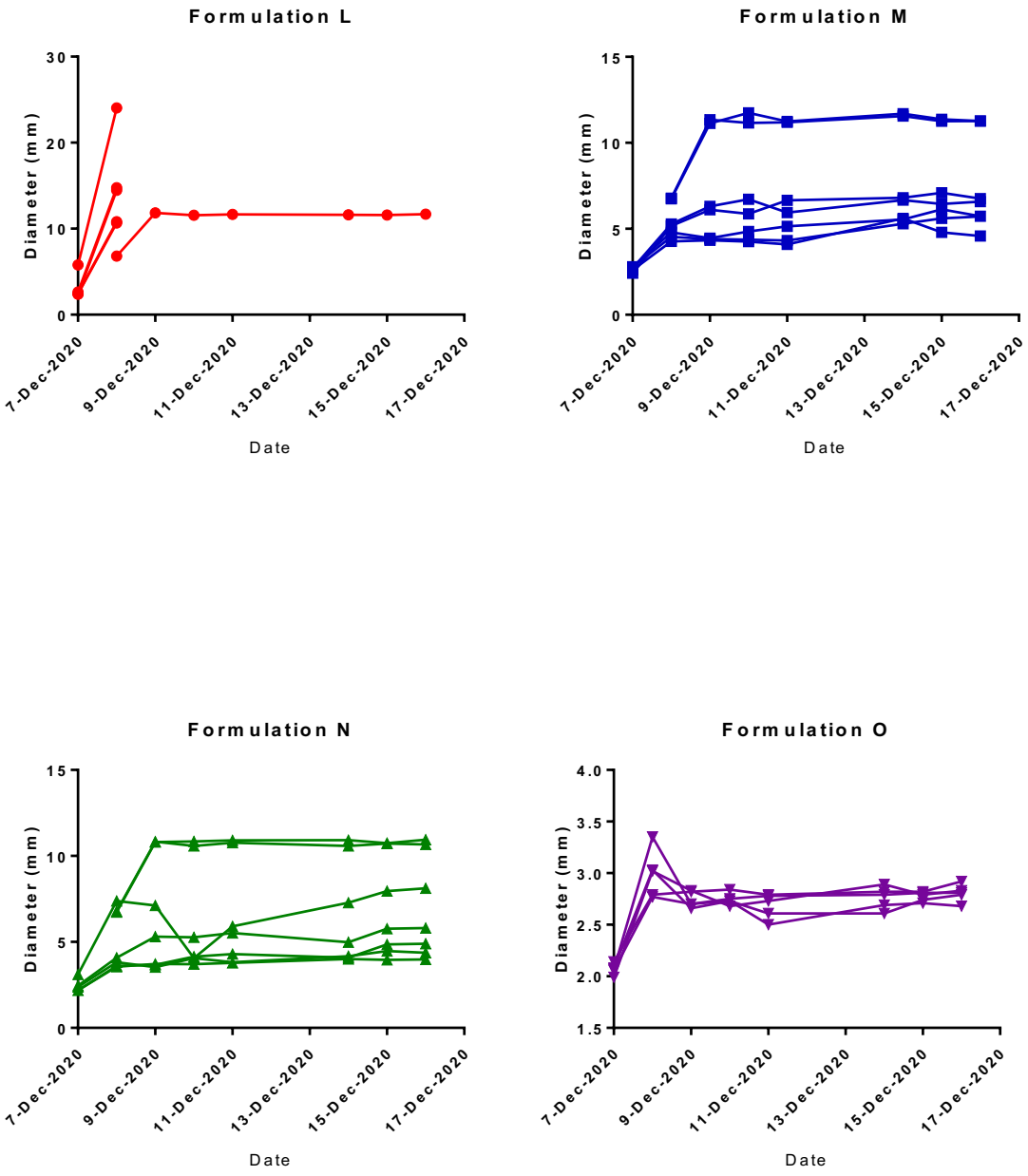


**Figure 4.21: Graphs representing the changes in diameter of the various formulations used in the third trial of hydrogels across the 8 days of measurement.**

#### 4.3.2.2 Third Trial Hydrogel Formulations Average Hydrogel Measurements

Table 4.19 shows the average total percentage increase of the weight, length and diameter of the hydrogel expanders at various formulations concentrations over the 11 days of measuring.

| Expander | Average % increase of weight | Average % increase of length | Average % increase of diameter |
|---|---|---|---|
| L | 1659.52 | - | - |
| M | 265.28 | 48.20 | 106.10 |
| N | 263.75 | 52.29 | 101.12 |
| O | 104.63 | 24.51 | 35.73 |

**Table 4.19: Average total percentage increase of the weight, length and diameter of the various hydrogel formulations used in the third trial over 11 days of measuring.**

#### 4.3.2.3 Formulation M Printability Tests

##### 4.3.2.3.1 BMF nanoArch S130 Sample Prints

Sample prints 1, 2, 3 and 4 of formulation M in the BMF nanoArch S130 printer resulted in no curing of the hydrogel ink.

After sample print 3, the hydrogel ink became black and unstable (Fig. 4.22). This may have been due to its reaction with the ultraviolet light.

**Figure 4.22: Hydrogel ink after use in the BMF nanoArch S130 printer.** It had become black and unstable.

It was noted that the ink was stable before being injected into the nanoArch printer. This attempt at printing formulation M resulted in no curing of the hydrogel ink.

##### 4.3.2.3.2 BMF nanoArch S130 Lattice Print

It was observed that the hydrogel lattice printed did not adhere to the printer platform, but an initial pattern was seen on the printer film.

##### 4.3.2.3.3 Optimising Parameters for Formlabs 1+ Printer

For sample prints 1, 2 and 3 a full-size rod print was attempted.

No resin cured during these attempts at 3D printing formulation M.

For sample print 4 a half size rod print was attempted. It was observed that a partial curing of the hydrogel resin occurred. The initial formation of a base had been built on the platform of the printer (Fig. 4.23). There was also partial formation of the half-sized rod. However, it was observed that the solid resin rod had adhered to the resin tray within the printer and not the platform as expected.

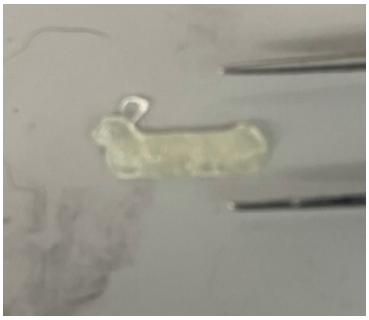

**Figure 4.24: Partial formation of the hydrogel half-sized rod cured during the fourth sample print.**

For sample print 5, a half size rod print was attempted. It was observed that a partial curing of the hydrogel resin had taken place. The altered operating logic parameters had resulted in more of the hydrogel resin curing solid than was observed in sample print 4. Again, a base and supports had begun to form on the printer platform and the partial formation of a solid hydrogel rod was observed (Fig. 4.24). The rod had adhered to the resin tray of the printer and broken away from its supports.

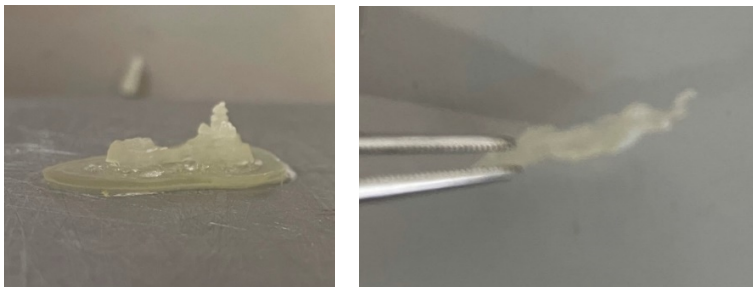

**Figure 4.23: Partial curing of the hydrogel resin that took place during the fifth sample print.**

Again, for sample print 6, a full-size rod print was attempted. Successful curing of the hydrogel resin was observed with these operating logic parameters. However, this sample print resulted in damage being caused to the resin tray of the Formlabs 1+ printer.

The resin had adhered to the polydimethylsiloxane (PDMS) layer of the printer's resin tray. This resulted in the PDMS layer being lifted away from the resin tray as printing continued and the hydrogel resin continued to cure beneath the PDMS layer. Removal of the solid resin print resulted in the entire PDMS layer coming away from the resin tray. The sides of the printer resin tray had begun to come apart from one another. It is believed that the acrylic acid component of the hydrogel resin may have reacted with the glue that affixes the sides of the resin tray together (Fig. 4.25).

The resin had then leaked into the mechanism of the printer, due to the resin tray losing its integrity, with some of the resin landing on the mirror that directs the UV light within the printer. It was possible to remove the resin tray and pour out the remaining uncured hydrogel resin. The internal mechanisms of the printer, including the UV mirror, were able to be cleaned with methanol.

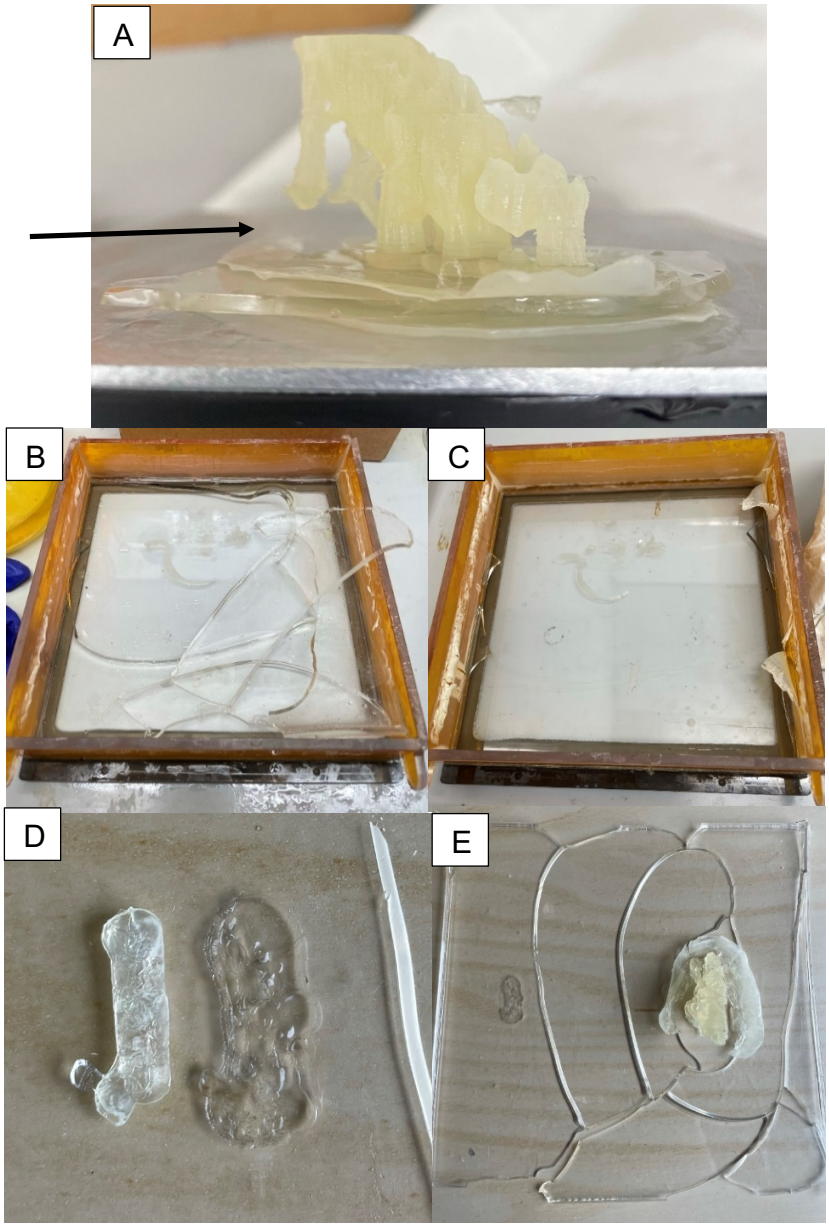


**Figure 4.25: Complications that arose with the sixth sample print. A**. The cured hydrogel resin attached to the printing platform. The form resembles the full-sized rod and the supports it required during printing. The arrow shows the PDMA layer embedded in the resin print. **B**. The polydimethylsiloxane (PDMS) layer within the resin tray was lifted away from the tray. **C**. Removal of the print resulted in the entire PDMS layer coming away from the resin tray. **D**. The area of adhesion of the partially formed hydrogel rod in fourth sample print, to the PDMS layer. **E**. The pieces of the PDMS layer of the 3D printer resin tray placed together, with the solid hydrogel paced in situ.

#### 4.3.2.4 Reducing Formulation M Reactivity

##### 4.3.2.4.1 Sodium Bicarbonate Neutralisation of Acrylic Acid of Formulation M

No curing occurred for the hydrogel formulations containing sodium bicarbonate at concentrations of 10%, 5% and 2.5%.

It appeared that the presence of $NaCHO_3$ in the hydrogel formula was interfering with its ability to cure.

##### 4.3.2.4.2 Dilution of Acrylic Acid in Formulation M

Volumes of 150µl and 450µl of hydrogel successfully cured within 2 minutes under the UV lamp.

#### 4.3.2.4.3 Synthesis of Hydrogels with Varying PEGDA Concentrations

Successful curing of hydrogel formulations, P and Q, was seen with volumes of both 150µl and 450µl. The weight, height and diameter of the hydrogels were recorded as follows:

| Hydrogel | Weight (g) | Height (mm) | Diameter (mm) |
|---|---|---|---|
| P1 | 0.183 | 5.30 | 7.04 |
| P2 | 0.208 | 5.93 | 6.91 |
| P3 | 0.154 | 4.44 | 6.73 |
| P4 | 0.169 | 5.69 | 6.82 |
| P5 | 0.556 | 3.75 | 15.61 |
| P6 | 0.657 | 4.51 | 15.60 |
| Q1 | 0.193 | 5.37 | 6.94 |
| Q2 | 0.170 | 4.87 | 6.72 |
| Q3 | 0.188 | 5.34 | 6.66 |
| Q4 | 0.176 | 5.08 | 7.06 |
| Q5 | 0.616 | 4.63 | 15.88 |
| Q6 | 0.641 | 4.69 | 15.97 |

**Table 4.20: Initial weights, heights and diameters of the cured hydrogel formulations P and Q.**

The hydrogels we placed in PBS, at 37°C, for 3 days to access their swelling ability. After this time, only hydrogels P5 and P6 had retained their shapes, with the following dimensions:

| Hydrogel | Weight (g) | Height (mm) | Diameter (mm) |
|---|---|---|---|
| P5 | 3.134 | 7.48 | 30.78 |
| P6 | 3.327 | 8.29 | 29.50 |

**Table 4.21: Measurements of the hydrogels that had retained their shape after 3 days.**

The remaining hydrogels had broken down into fragments. An increased concentration of PEGDA was believed to improve this result.

#### 4.3.2.4.4 Formulations R, S, T and U Hydrogel Weight

The graphs below show the changes in weight of the various formulations of hydrogels across the 8 days of measurement. The starting weights of the hydrogels ranged from 0.134-0.471g and the trend seen in all formulations was a rapid increase in weight over 24 hours. The average percentage increase in 24 hours was 206.8%, with the weight increase of one hydrogel exceeding 400%. After this time, the weight changes of the hydrogels plateaued for all the formulations (Fig. 4.26).

After 8 days, the hydrogels increase in weight varied greatly from 187.5-460.4%. Overall, the formulation R hydrogels had the highest weight increase, with an average of 395.3% and the formulation S hydrogels had the lowest weight increase, with an average of 210.8%.

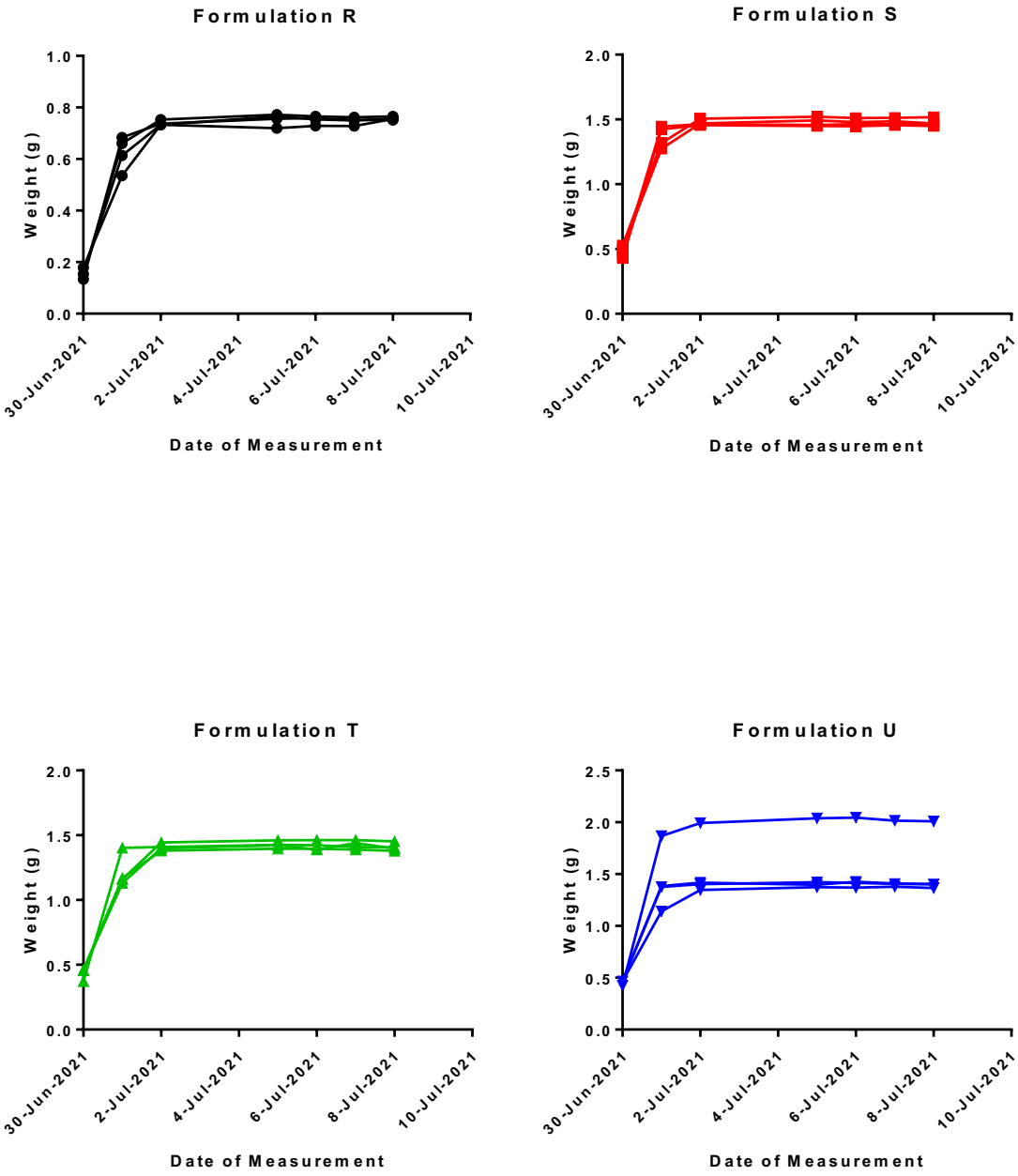


**Figure 4.26: Graphs representing the changes in weight of the various formulations (PEGDA varying formulations) of hydrogels across the 8 days of measurement.**

#### 4.3.2.4.5 Formulations R, S, T and U Hydrogel Height

The graphs below show the changes in height of the various formulations of hydrogels across the 8 days of measurement. The starting heights of the hydrogels was between 3.34 – 5.49mm. The variation seen in the lengths could have been due to the varying amounts of shrinkage that occurred when curing the hydrogel under the UV lamp. A noteworthy increase in height was seen within the first 24 hours, with the average percentage increase being 51.8% and the maximum percentage increase being 74.9% (one of the formulation R hydrogels).

After the first 24 hours, the heights of all the various formulations of hydrogels began to plateau, with a slight fluctuation recorded in the last few days of measurements (Fig. 4.27). After 8 days of recording, the increase in height of hydrogels varied between 44.7 – 86.2%. Overall, the formulation R had the highest length increase, with an average of 79.5% and formulations S and T having the lowest average height increase at 54.2%.

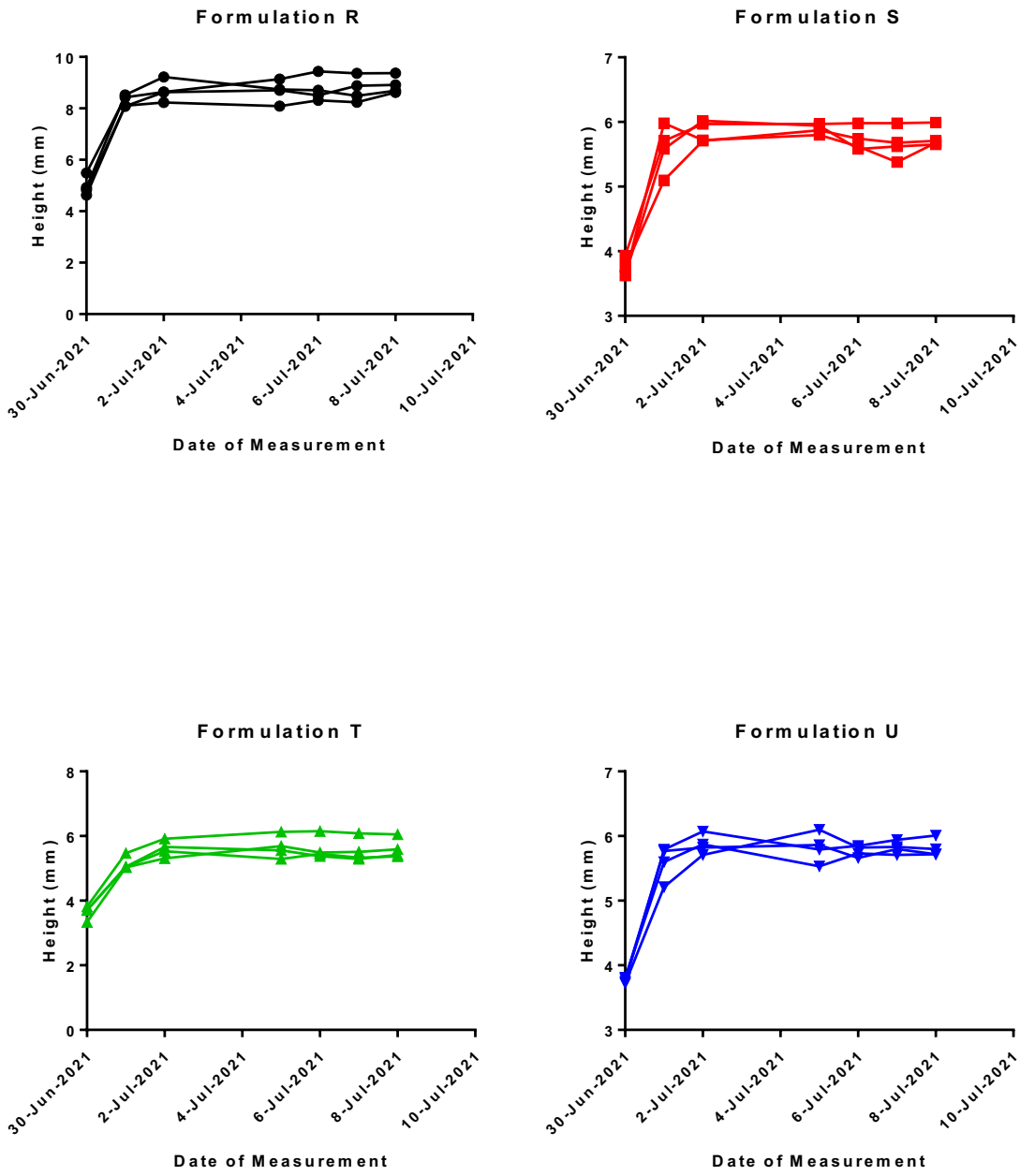


**Figure 4.27: Graphs representing the changes in height of the various formulations (PEGDA varying formulations) of hydrogels across the 8 days of measurement.**

#### 4.3.2.4.6 Formulations R, S, T and U Hydrogel Diameter

The graphs below show the changes in length of the various formulations of hydrogels across the 8 days of measurement. The starting diameters of the hydrogels was between 7.05 – 15.82mm. The variation in the diameters is due to formulation R being cast in vial lids smaller than those used for formulation S, T and U. Again, like the weight and length measurements, a substantial increase in diameter was recorded within the first 24 hours, with the maximum percentage increase being 104.7% (a formulation R hydrogel). An average increase of 62.0% for all hydrogel formulations was recorded.

After the first 24 hours, the diameters of all the various formulations of hydrogels reached a plateau, with some wavering of diameters recorded in the last few days of measuring (Fig. 4.28). After 8 days of recording, the increase in diameter of hydrogels varied between 50.7 – 96.2%. Overall, the formulation R had the highest diameter increase, with an average of 87.6% and formulation S had the lowest diameter increase with an average of 55.2%.

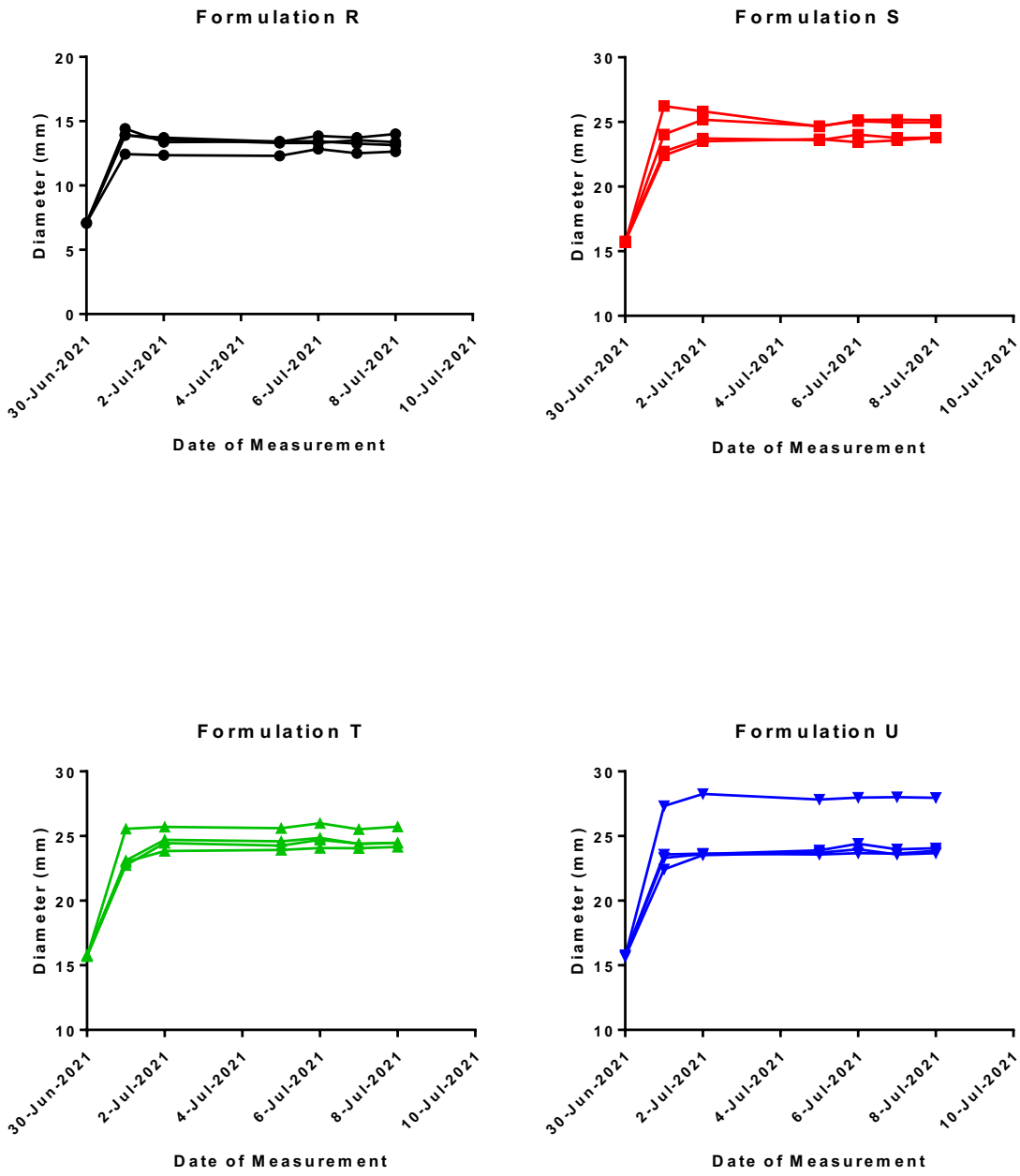


**Figure 4.28: Graphs representing the changes in diameter of the various formulations (PEGDA varying formulations) of hydrogels across the 8 days of measurement.**

#### 4.3.2.4.7 Formulations R, S, T and U Hydrogel Average Measurements at day 8

Table 4.22 shows the average total percentage increase of the weight, length and diameter of the hydrogel expanders at various formulations concentrations over the 8 days of measuring.

| Expander | Average % increase of weight | Average % increase of length | Average % increase of diameter |
|---|---|---|---|
| R | 395.3 | 79.5 | 87.6 |
| S | 210.8 | 54.2 | 55.2 |
| T | 224.1 | 54.2 | 56.8 |
| U | 241.4 | 54.3 | 58.2 |

**Table 4.22: Average total percentage increases of the weight, length and diameter of the hydrogel expanders with varying PEGDA varying concentrations after 8 days of measurement.**

#### 4.3.2.4.8 Formulations R, S, T and U Hydrogel Average Measurements at day 91

Table 4.23 and figure 4.29 shows the average total percentage increase of the weight, length and from day 0 to day 91.

| Expander | Average % increase of weight | Average % increase of length | Average % increase of diameter |
|---|---|---|---|
| R | 394.7 | 71.2 | 83.7 |
| S | 200.9 | 50.8 | 51.9 |
| T | 217.2 | 47.7 | 54.4 |
| U | 211.1 | 44.7 | 56.4 |

**Table 4.23: Average total percentage increases of the weight, length and diameter of the hydrogel expanders with varying PEGDA varying concentrations after 91 days in PBS.**

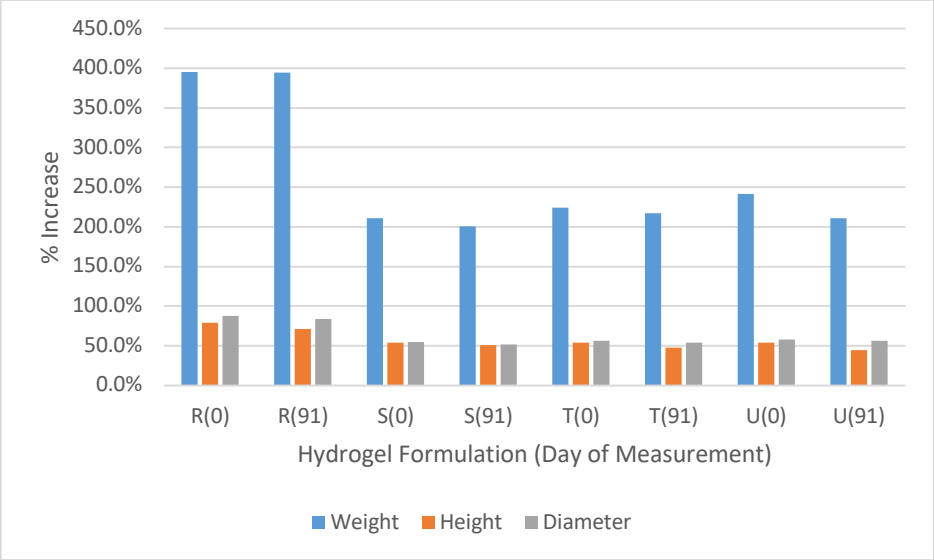


**Figure 4.29: Graph comparing the percentage increases of the weight, length and diameter of the hydrogel expanders with varying PEGDA varying concentrations on days 0 and 91 of measurement.**

#### 4.3.2.5 Production of formulation R Hydrogels via Casting with Moulds.

##### 4.3.2.5.1 Pliable Plastic Moulds

The formulation R hydrogels successfully cured within the pliable plastic moulds and were easily removed.

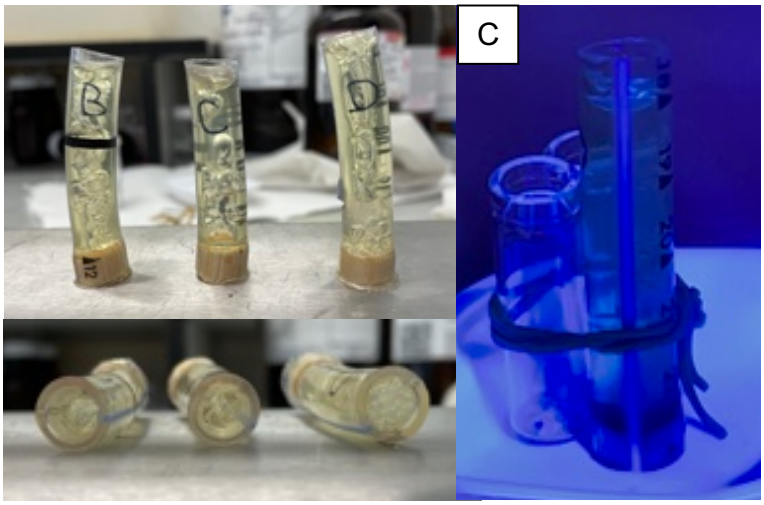


**Figure 4.30: Pliable moulds containing cured formulation R hydrogel**. C shows the mould and resin curing under the UV lamp.

#### 4.3.2.5.2 Swelling Test of Formultion R Hydrogels

The weight, height and diameters of the hydrogels was recorded:

| Hydrogel | Weight (g) | Height (mm) | Diameter (mm) |
|---|---|---|---|
| A* | 2.104 | 40.85 | 8.02 |
| B | 2.164 | 43.33 | 8.02 |
| C | 2.115 | 40.31 | 8.32 |
| D | 2.339 | 46.51 | 7.88 |

**Table 4.24: Initial measurements of the cylinder hydrogel formed in the 3D printed mould and the hydrogels formed in the pliable plastic and wooden dowel moulds.**

*Hydrogel A is the cylindrical hydrogel that was formed in the 3D printed resin mould and removed whole. After 24 hours in PBS at 37°C, the hydrogels were measured again. Only hydrogel A retained its cylindrical form. It had the following measurements:

- **Weight = 4.927g**
- **Height = 58.77mm**
- **Diameter = 12.23mm**

The other hydrogels had broken down (Fig. 4.31).

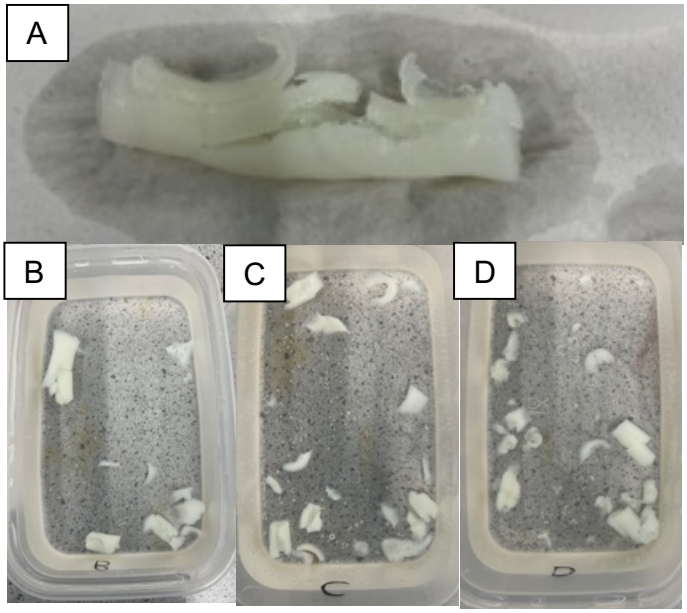


**Figure 4.31: Hydrogels after 24 hours in PBS at 37°C. A**. The hydrogel cured in the 3D printed mould. It had retained its cylindrical form. **B**, **C** and **D** show the breakdown of hydrogels B, C and D after 24 hours. They no longer resemble their original cylindrical form.

Hydrogel A was left in PBS at 37°C for another 4 days and its measurement were taken again. After this time had passed, the hydrogel had broken down, but its cylindrical form could still be seen (Fig. 4.32). The hydrogel had the following measurements:

- **Weight = 5.827g**
- **Height = 61.23mm**
- **Diameter = 13.28mm**

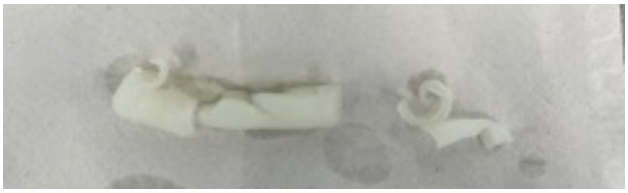

**Figure 4.32: Hydrogel A after 5 days in PBS at 37°C.**

#### 4.3.2.6 Production of Formulation U Hydrogels within Pliable Plastic Moulds

2 hydrogels with a PEGDA concentration of 3% were synthesised and had the following measurements:

| Hydrogel | Weight (g) | Height (mm) | Diameter (mm) |
|---|---|---|---|
| E | 1.976 | 40.79 | 7.65 |
| F | 1.786 | 35.14 | 7.52 |

**Table 4.25: Initial measurements of hydrogels E and F, PEGDA concentration of 3%.**

After 24 hours in PBS at 37°C, both the hydrogels had broken down (Fig. 4.33).

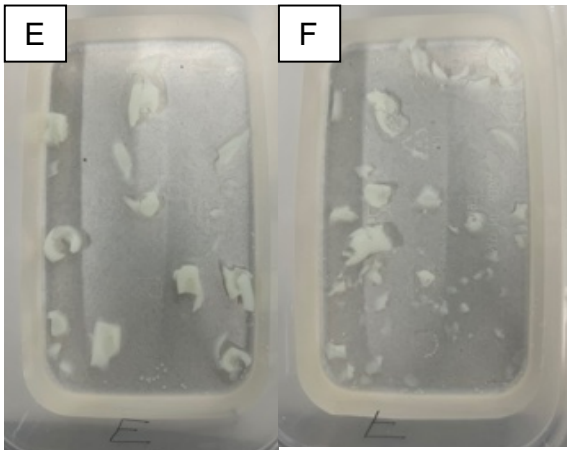


**Figure 4.33: Hydrogels E and F after 24hours in PBS at 37°C.**

### 4.3.2.7 Development of Silicone Moulds for Hydrogels

#### 4.3.2.7.1 Prototype 1, Nusil MED4211 Silicone

A prototype mould for the production of a silicone mould for hydrogels was constructed using a 15ml centrifuge tube, corrugated plastic tubing and duct tape (Fig. 4.34).

**Figure 4.34: Construction of the mould for producing silicone moulds for hydrogels.** The centrifuge tube was placed inside the corrugated plastic tubing and the base of the tubing was sealed with duct tape.

A solid, silicone mould had successfully set (Fig. 4.35).

**Figure 4.35: Solid silicone removed from its mould.**

#### 4.3.2.7.2 Synthesis of Hydrogel U within Prototype 1 Moulds

Two formulation U hydrogels were successfully cured (Fig 4.37). They were measured and then placed in PBS at 37°C for 48 hours.

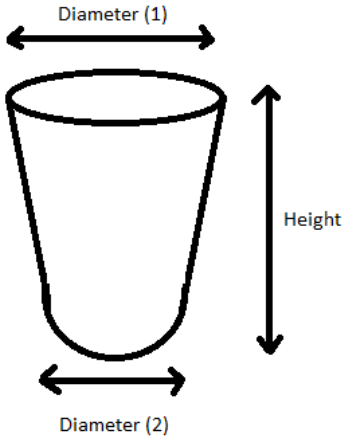


**Figure 4.36: Diagram representing the various measurements taken of the cone shaped hydrogels.**

**Figure 4.37: Successfully cured hydrogel U formulations produced in the silicone mould prototype.**

| Hydrogel | Weight (g) | Height (mm) | $Diameter_1$ (mm) | $Diameter_2$ (mm) |
|---|---|---|---|---|
| A | 4.400 | 32.81 | 15.94 | 5.85 |
| B | 4.111 | 33.50 | 16.21 | 7.38 |

**Table 4.26: Initial measurements of the cone shaped hydrogels.**

After 48 hours in PBS at 37°C, the two hydrogels had broken apart (Fig. 4.38).

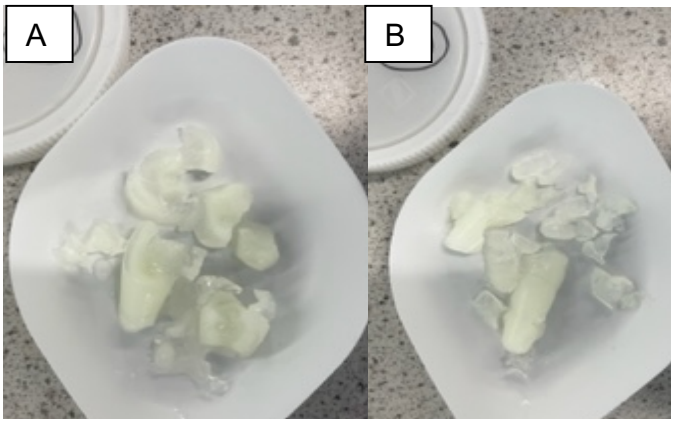


**Figure 4.38: Cone shaped hydrogels A and B after 48 hours in PBS, at 37°C.**

#### 4.3.2.7.3 Prototype 5, Mold Max™ Silicone Moulds

The Mold Max™ 10T silicone had set solid and was removed from the outer corrugated tubing with ease. Both the base of the mould and the inner, smooth tubing were also removed with ease (Fig. 4.39). The silicone was tear resistance and flexible enough to be completely inverted to aid the removal of the inner tubing. This was the case for both mould designs.

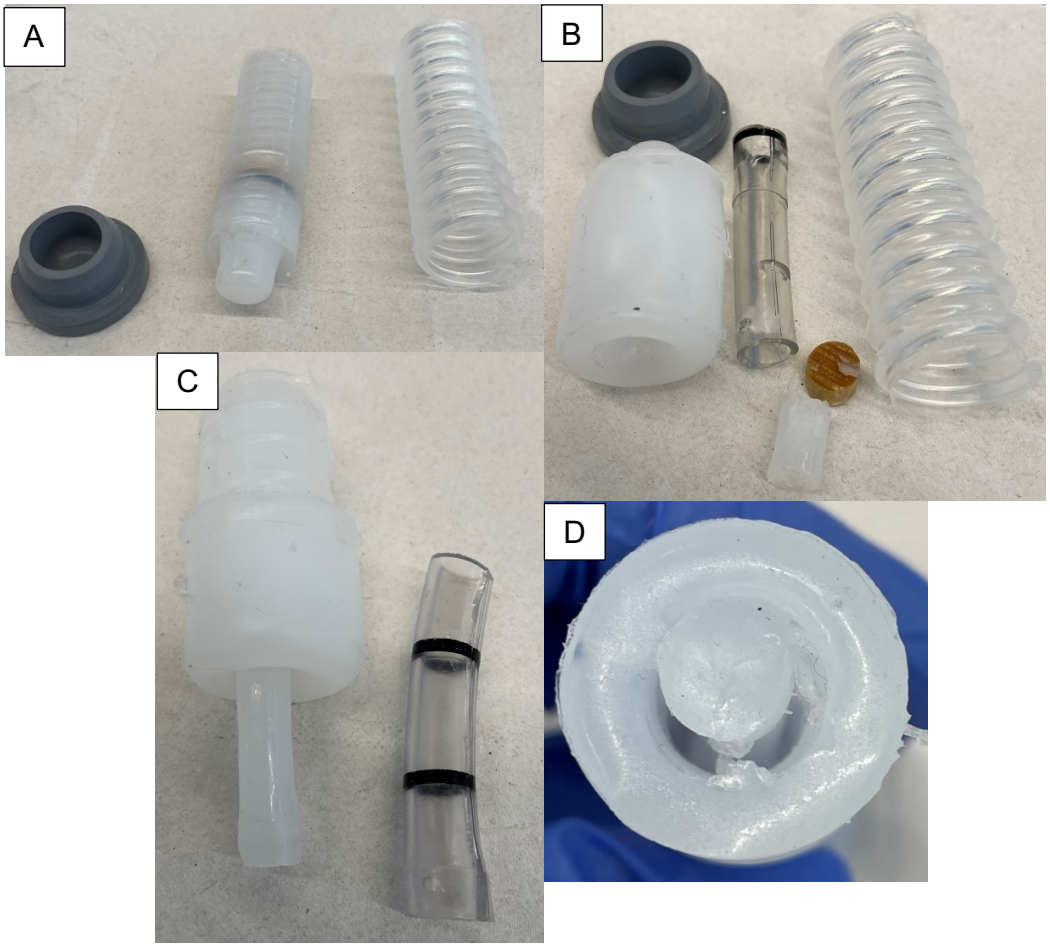


**Figure 4.39: Silicone moulds created with degassed Mold Max™ 10T silicone alongside parts of the plastic moulds they were made in. A** and **B** are the moulds created to produce a solid cylinder hydrogel. **B** shows the flexibility of the silicone when the mould is inverted. **C** and **D** show the moulds created to produce a hydrogel in the form of a cylinder with a hollow lumen. **C** shows the exposure of the silicone exert when the outer walls of the moulds are inverted.

#### 4.3.2.7.4 Prototype 6, Smaller Hollow Cylindrical Mold Max™ Silicone Moulds

The silicone mould had set hard and both the corrugated and smooth plastic tubing were removed with ease (Fig. 4.40).

**Figure 4.40: Silicone mould successfully created to produce a hollow hydrogel with thinner walls.**

#### 4.3.2.8 Synthesis of Hydrogel U within Silicone Moulds

##### 4.3.2.8.1 Solid Cylinder Hydrogel

The hydrogel (formulation U) successfully cured within the silicone mould and was easily removed, undamaged, from the mould. Bubbling of the liquid hydrogel was seen during curing, due to the exothermic properties of the acrylic acid. This led to air bubbles being trapped within the solid hydrogel (Fig. 4.41 (A)). After 24 hours in PBS, at 37°C, the solid hydrogel had broken up into smaller parts (Fig. 4.41 (B)). It was thought that the air bubbles trapped within the hydrogel when it is cured were impacting the integrity of the hydrogel and its ability to retain its solid form.

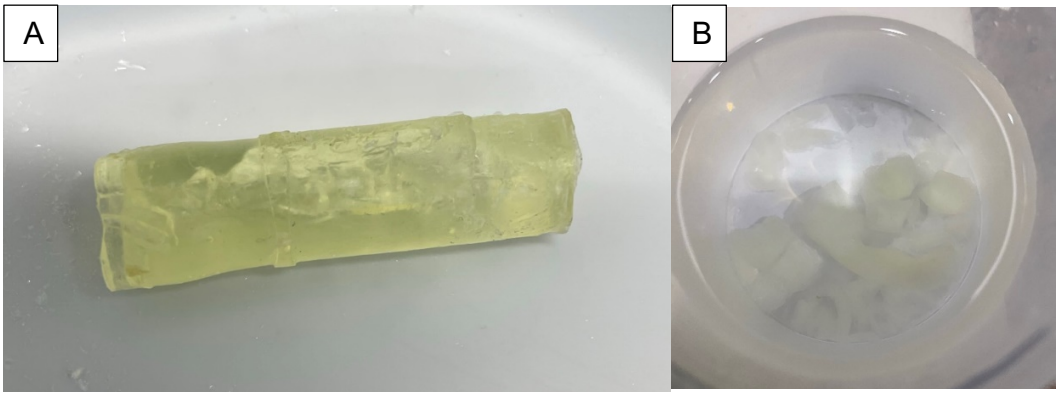


**Figure 4.41: Solid cylinder hydrogel, formulation U, cured in the silicone mould. A** shows the solid hydrogel before being placed in PBS. **B** shows the resultant breakdown of the hydrogel after 24 hours in PBS at 37°C

#### 4.3.2.8.2 Hollow Cylinder Hydrogel

Both the solid and hollow cylindrical hydrogels cured successfully. After 3 days in PBS, at 37°C, the hollow cylindrical hydrogel had retained its shape (Fig. 4.42).

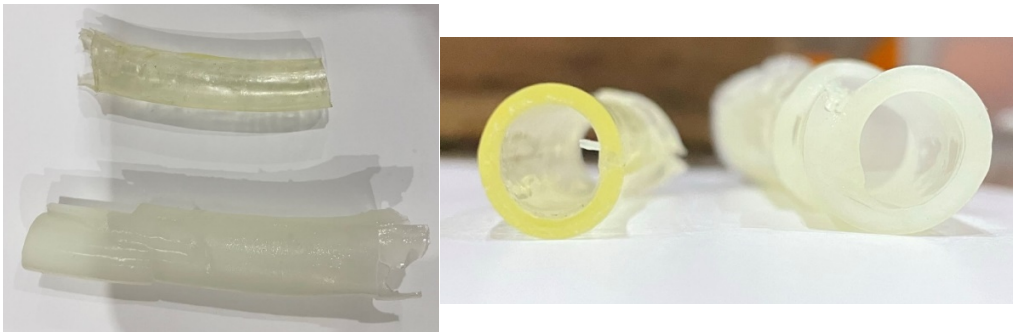

**Figure 4.42: Non-expanded hollow cylindrical hydrogel compared to a hollow hydrogel that had been placed in PBS for 3 days, at 37°C.**

#### 4.3.2.8.3 Thinner Walled Hollow Cylinder Hydrogels

**Figure 4.43: Hollow cylindrical hydrogels that were cured in the silicone moulds. From left to right their lengths are: 57mm, 62mm, 50mm and 38mm.**

The hydrogels cured successfully and had the following lengths:

- **62mm**
- **57mm**
- **50mm**
- **38mm**

All the hydrogels had an external diameter of 9mm and an internal diameter of 5mm.

#### 4.3.2.8.4 Smaller Hollow Cylinder Hydrogels

Hydrogels with quincke ends and blunt ends were successfully cured.

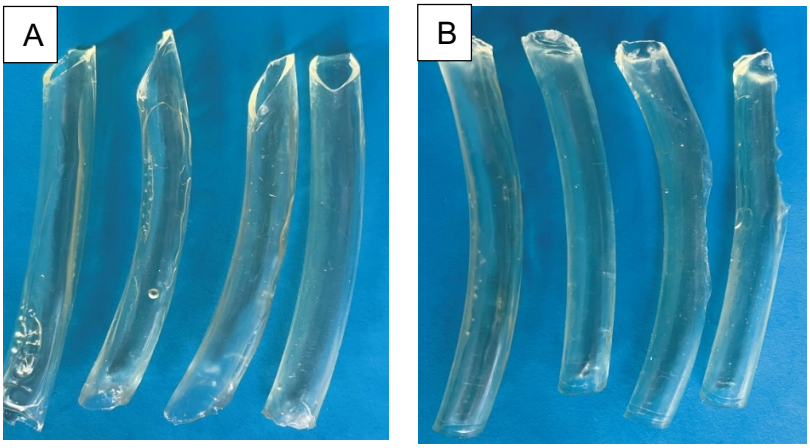


**Figure 4.44: Hollow cylinder formulation U hydrogels produced with quincke (A) and blunt (B) ends.**

#### 4.3.2.8.5 Reshaping of Hollow Hydrogels

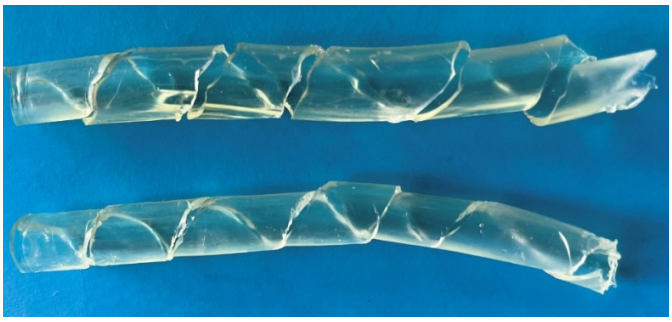

**Figure 4.45: Two blunt ended hydrogels cut into the shape of a helix.**

The two helical hydrogels and two blunt ended hydrogels were measured before and after placement into PBS, at 37°C, for 24 hours:

| Hydrogel | Length (pre-swelling) (mm) | Length (post-swelling) (mm) | Diameter (pre-swelling) (mm) | Diameter (post-swelling) (mm) |
|---|---|---|---|---|
| Quincke end | 55 | 80 | 6 | 10 |
| Blunt end | 55 | 84 | 6 | 10 |
| Helix 1 | 65 | 113 | 5 | 9 |
| Helix 2 | 64 | 89 | 7 | 10 |

**Table 4.27: Lengths and diameters of the various hydrogels pre- and post- swelling.**

**Figure 4.46: Image of the quincke end, blunt end and helical hydrogels post-swelling.**

| Hydrogel | Length % Increase | Diameter % Increase |
|---|---|---|
| Quincke end | 45.46 | 66.67 |
| Blunt end | 52.73 | 66.67 |
| Helix 1 | 73.85 | 80.00 |
| Helix 2 | 39.06 | 42.86 |

**Table 4.28: Percentage increases seen in the lengths and diameters of the hydrogels after 24 hours in PBS.**

#### 4.3.2.8.6 Solid Tipped, Hollow Cylindrical Hydrogels

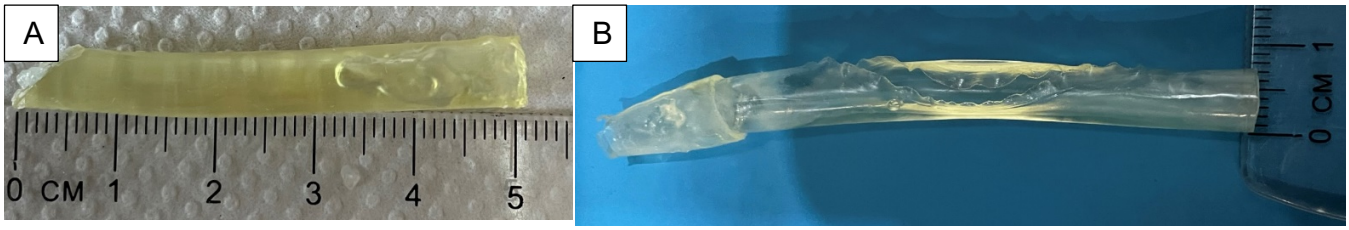


**Figure 4.47: Solid, quincke ended (A), and hollow, tapered solid ended (B), hydrogels.**

Successful curing of hydrogel resin occurred in both the solid moulds and the moulds for hollow cylinders with solid tapered tips. The blunt end of the solid hydrogel had undergone some bubbling when curing. This produced a lumen like appearance at the end of the hydrogel.

The nature of the design of the solid tipped hollow moulds meant that the positioning of the silicone extrusion could not be predicted, and this often resulted in the extrusion touching the walls of the mould, producing an incomplete hydrogel.

As the positioning of the silicone extrusion within the hollow mould could not be anticipated. A trial-and-error approach was required to ensure that hydrogels with complete walls and solid tapered ends were produced.

#### 4.3.2.8.7 Thicker Walled, Smaller, Hollow Cylindrical Hydrogels

The open ended, hollow hydrogels did not form complete walls when curing. The stretching of the silicone extrusion caused it to come in to contact with the sides of the mould, resulting in an incomplete lumen.

## 4.4 Discussions

### 4.4.1 Oxtex Hydrogel Expander Development

This experiment was conducted to access the characteristics of the proposed hydrogel expander design. The results obtained have shown that there is only a small increase in the width of the expanders throughout the experiment. The characteristics of the expanders developed in this chapter would predominantly support longitudinal dilation.

The rise in measured length of the devices was not as high as expected. With an average increase being around 2mm, a similar result to that seen in the width measurements. For the anticipated expander to have an impact on the vagina length of the pig within the proposed expansion time, it will have to increase in length at a faster rate. This issue could be addressed with a couple of alterations in the design of the hydrogel expander. The initial design that was tested in the above experiment involved covering the hydrogel aspect of the device completely with 1mm of silicone. Reducing the thickness of the silicone will increase the rate that the hydrogel component can take up water from its surroundings and thus increase the amount that the device expands by within the set amount of time. There is also the option to introduce small holes into the silicone at the ends of the cylindrical device. Similar to reducing the thickness of the silicone, this method will allow the hydrogel to absorb water faster and increase in size. Unfortunately, the loss of Oxtex as an industrial partner meant that there was no opportunity to discuss these possible alterations.

### 4.4.2 Collaboration with Centre for Additive Manufacturing, University of Nottingham.

This aspect of the project arose from the unsuccessful processing of an anisotropic tissue expander in collaboration with Oxtex. After this industrial partner went into administration and the in-house expander experiments did not obtain positive results, a new collaboration with the Centre of Additive Manufacturing department, part of the Faculty of Engineering at the University of Nottingham, was formed.

Initial meetings included encouraging discussions of the use of 3D printers to produce hydrogel structures. Their expertise in materials development for additive manufacturing as well as inkjet and 3D printing of additive materials has allowed this project to continue. Despite challenges, the staff of the CfAM department prided ongoing support.

### 4.4.3 Synthesis of Hydrogel Resin

The formulation of a hydrogel resin starts with the synthesis of polylactic acid. A synthetic biodegradable poly-lactone commonly used in biomedical devices due to its biocompatibility (Cheng et al., 2009). Polylactic acid was an integral ingredient in all the hydrogel formulations produced and tested during this project.

The initial hydrogel formulations consisted of the following ingredients in varying concentrations: Polylactic acid (PLA), poly(ethylene glycol)diacrylate (Mn 700) PEGDA) and 2-hydroxyethyl methacrylate (HEMA). The swelling tests conducted with these cured resins were performed with hydrogels around

10mm x 2mm in size. This allowed for multiple hydrogels with the same formulation proportions to be tested in one experiment.

The first two hydrogel swelling tests incorporated the usage of hydroxyethyl methacrylate (HEMA) as the main proportion of the formulation. This resulted in some increase in the weight, length and diameter parameters. However, the maximum increase in length for hydrogels containing HEMA was 23.9% and the largest increase in diameter was recorded at 27.97%. If these formulations were scaled up to the size 40mm x 7mm, these percentage increases would result in an implant that would not expand at a rate equal to or faster than the rate of growth of the piglets used in this project. Let alone exert sufficient force to cause tissue to expand. The curing of the HEMA containing formulations resulted in very brittle, solid cylinders that were difficult to remove from their castings. The reliability of these formulations in producing a complete large-scale cylinder for implantation was questionable. With the aim at this stage in the project being to 3D print the implants, a resin that produces a fragile structure when cured may not be able to withstand the mechanisms of the printer was considered undesirable.

The hydroxyethyl methacrylate was replaced with acrylic acid, a component well known for its liquid retention abilities (Pradas et al., 2001). It was believed that this would produce a more stable hydrogel when cured as well as increase the rate and amount of expansion. The resultant HEMA average hydrogel measurements, reported in part 7.3.12, showed a maximum percentage length increase of 52.29% and maximum percentage diameter increase of 106.10%. When discussing these results with advisory consultant paediatric surgeons,

it was decided that an increase in diameter was as desirable as an increase in length.

The next stage in the project was to test the 3D printability of the hydrogel formulation. With the size required for hydrogels suitable for implantation known to be around 40mm x 7mm, almost 4 times the size used in initial experiments, there could be discrepancies between the swelling rates. The main factor to consider was the difference in surface area to volume ratio, with the experimental size of 10mm x 2mm being considerably larger. This could impact the rate of water uptake of the hydrogels and thus their swelling rate. The expectation was that the smaller experimental hydrogel will increase in weight, length and diameter at a faster rate than the implant sized hydrogels. With the rapid increase that was seen in hydrogel swelling experiment 3, a decrease in swelling rate of larger hydrogels would not be a disadvantage to the project. It could be possible that too fast initial swelling could cause trauma to the vagina when implanted. The ideal hydrogel will apply constant pressure to vaginal tissue to initiate cell proliferation without causing ischemia or permanent damage to the tissue.

### 4.4.4 Use of 3D Printers

#### 4.4.4.1 BMF NanoArch S130 3D Printer

It was decided that formulation M hydrogel would be tested as a suitable resin for 3D printing.

The formulation was initially tested in the BMF nanoArch S130 3D printer. This printer uses projection microstereolithography (PμSLA) technology to produce small scale resin builds. This process uses a digital micro display ultraviolet light projector to cure photopolymer resin one layer at a time on a micro scale. PμSLA enables the printing of objects 100 times smaller than a human hair and has the ability for the light intensity of individual pixels to be controlled independently, allowing the material properties of the object to be modified throughout. It also provides the technology for multiple materials to be used in a single print process, including polymer responsive hydrogels and will support the printing of biocompatible materials. The nanoArch S130 can produce a resolution of 2μm, but its main attraction for use in this project was its larger build size, being able to produce items 48 x 27 x 50 mm.

When preparing the hydrogel resin for use in this printer, the addition of curcumin was required. This addition acts as a photoabsorber within the resin, it is the main active component of the spice turmeric, and so give the hydrogel resin a yellow hue (Zhao et al., 2015). The curcumin was added at a 1% w/w concentration initially.

In the first sample print, a lower intensity of 87% was selected. This was to accommodate for the reactivity if the acrylic acid that was observed in earlier formulation testing. However, as no curing of the hydrogel resin had been

observed, it was deemed necessary to increase the intensity to a more standard value of 147%. With still no curing observed, the next alteration to the hydrogel formula was reduction of the concentration of curcumin.

It was possible that too much of the UV light being projected onto the layers of resin was being absorbed by the photoabsorber component and not curing of the resin. The reduction in curcumin concentration (0.5% w/w) did give a positive result. The formulation appeared to have cured to the platform of the printer and so the next stage would be to attempt a larger sized 2mm lattice print.

This sample print resulted with an initial yellow lattice pattern observed on the film of the printer, but no structure had formed on the platform of the printer. The stability of the hydrogel ink appeared to have been compromised during the lattice print test. The ink had changed colour from stable yellow to an unstable black, possibly a result of exposure to UV light. The results from the lattice print were most likely due to the hydrogel ink still containing too high a concentration of photoabsorber.

The final sample print conducted with the BMF nanoArch S130 printer used formulation M hydrogel resin without the addition of curcumin. Unfortunately, this also resulted in no curing of the resin ink. It was decided that a 3D printer with an alternative method for producing structures may be more suitable for the acrylic acid-based hydrogel.

#### 4.4.4.2 Formlabs 1+ 3D Printer

The Formlabs desktop stereolithographic 3D printer, Formlabs 1+, uses the process of microsteroelithography (μSLA) to produce three dimensional structures. This involves exposing photosensitive material (liquid resin) to an ultraviolet laser. The photosensitive resin is poured into a tank, the printers build platform is lowered into the resin and a laser draws a cross-section of the 3D part, causing it to harden layer by layer, whilst the build platform remains lowered in the tank. This procedure is centred on the process of photopolymerization, whereby molecules are fused and solidified when in contact with light to create polymers. The addition of lenses, which can generate very small points of light, as well as the complexity of the galvanometer-directed UV lasers used, allows for the use of more specialised resins within the tank, including custom formulated ones.

The layer resolution of the Formlabs 1+ printer is reported as 25μm. Although this is not as precise as the BMF nanoArch S130, the proposed implant size is larger enough that this difference in resolution is deemed insignificant. The maximum structure build size of the Formlabs 1+ is 125mm x 125mm x 165mm. This is much larger than that of the BMF nanoArch S130 and would mean that the implant design of 40mm x 7mm could be printed at various orientations without risk of reaching the printers limits.

The hydrogel formulation used for this method of printing, formulation M, did not require the addition of curcumin to act as a photoabsorber. The original formula containing PLA, PEGDA, acrylic acid and DMPA was used.

The first three sample prints of formulation M in the Formlabs 1+ printer, made attempts to produce a full-sized implant rod, 40mm x 8mm. After the first sample print has failed to produce any cured resin, the number of first layer passes was increased for the following sample print. This alteration to the operating logic parameters was made to improve the likelihood of the resin adhering to the printers build platform. To ensure adhesion, the Formlabs 1+ printer pushes the build platform firmly against the silicone layer, in the bottom of the resin tray, and 'over-cures' the first layers by tracing the laser path the number of specified times. As a result, less detail is available in the first layers as the UV light bleeds when it traces over the already cured resin. The design of our implant structure incorporated a base, on which build supports could be formed as well as the implant itself. It is in the curing of this base that any detail may be lost. As this base and the supporting structures would be removed once printing had been completed, the loss of detail would not impair the implant design in any way.

After a second unsuccessful sample print the concentration of DMPA was increased (from 1% to 2%). It was thought that this alteration would increase the prospects of the hydrogel resin curing onto the printers build platform. Unfortunately, this was not the case, and no remnants of a cured full-sized rod was seen.

Several changes were made in preparation for the fourth sample print. First the photoinitiator DMPA was replaced by a similar alternative, Irgacure 819 (Bis(2,4,6-trimethylbenzoyl)-phenylphosphineoxide). It was thought that the Irgacure 819 may be more compatible with the UV light laser within the Formlabs 1+ printer. There were also alterations made to the operating logic

parameters. The laser speed was reduced from 800mm/s to 700mm/s. A slower laser speed would expose the resin to UV light for longer and so solid curing would be more likely. The z-axis off set was also reduced from 0.2mm to 0.0mm. This adjustment was made to increase the chances of the resin adhering to the build platform when the first layers of the base of the design are formed. In this sample print, a reduced sized rod of 20mm x 4mm was attempted. This sample print was then re-run with the 0.2mm z axis offset reapplied, forming the fifth sample print.

The half-sized rod (20mm x 4mm) sample prints resulted partial curing of the hydrogel resin. The fourth sample print showed initial formation of a base had been built on the platform of the printer. There was also partial formation of the half-sized rod. However, it was observed that the solid resin rod had adhered to the resin tray within the printer and not the platform as expected. It was for this reason that the fifth sample print was run with the z axis offset reapplied. Increasing the z axis offset should encourage the resin to adhere to the printers build platform as opposed to the silicone coating at the bottom of the resin tank.

Again, the fifth sample print resulted in partial curing of the hydrogel resin, with the print progressing further than the previous half sized rod. It was observed that the base of the structure and supports for the rod had begun to form on the build platform, but the rod itself had adhered to the base of the resin tank and had become detached from its supports.

It was thought that the supports of the smaller print may have been too delicate to detach the rod from the base of the resin tank. The design for the full-size

rod, 40mm x 8mm, contained thicker, more substantial supports to hold the rod in place. These supports may have been able to hold the hydrogel implant in place during printing, and stop it from attaching to the silicone base, and so a full-size rod sample print was run. To increase the integrity of the supports, the support density and support point size parameters were increased from 1.0mm to 1.5mm and 0.6mm to 1.3mm, respectively.

Successful curing of the hydrogel resin was observed with these operating logic parameters. However, this sample print resulted in damage being caused to the resin tray of the Formlabs 1+ printer. The resin had adhered to the polydimethylsiloxane (PDMS) layer of the printer's resin tray. This resulted in the PDMS layer being lifted away from the resin tray as printing continued and the hydrogel resin continued to cure beneath the PDMS layer. Removal of the solid resin print resulted in the entire PDMS layer coming away from the resin tray.

The sides of the printer resin tray had begun to come apart from one another. It is believed that the acrylic acid component of the hydrogel resin may have reacted with the glue that affixes the sides of the resin tray together. The resin had then leaked into the mechanism of the printer, due to the resin tray losing its integrity, with some of the resin landing on the mirror that directs the UV light within the printer. It was possible to remove the resin tray and pour out the remaining uncured hydrogel resin. The internal mechanisms of the printer, including the UV mirror, were able to be cleaned with methanol.

### 4.4.5 Optimisation of Hydrogel Formulation

It appeared that the uncured acrylic acid component of the hydrogel formulation and the glue of the Formlabs 1+ resin tray were not compatible, possibly due to the low pH of the acrylic acid. To rectify this, neutralisation of the acrylic acid within the formula was attempted. The addition of sodium bicarbonate ($NaCHO_3$) to formulation M was tested. At concentrations of 10%, 5% and 2.5% (w/w) no curing of the hydrogel was seen. Although an increase of pH had occurred from this addition, it appeared that the presence of the $NaCHO_3$ was interfering with the resin to cure under UV light.

An alternative to neutralising the acrylic acid component of hydrogel formulation M, was to dilute it with a more neutral element, also with swelling characteristics. 2-hydroxyethyl acrylate (HEA), an ester of acrylic acid, was added to the hydrogel formula. Equal amounts of acrylic acid and 2-hydroxyethyl acrylate were used in the modified hydrogel formula. All initial curing tests with a formulation containing equal parts of acrylic acid and HEA resulted in the successful production of solid, fully cured, hydrogels.

With this result, it was decided that going forward the hydrogel formulation used for the implants would consist of equal parts of acrylic acid and HEA. The final trials for producing the optimal hydrogel formulation were to determine the ideal concentration of PEGDA within the formulation. These investigations compared the swelling capacity of formulations containing 0.5%, 1%, 1.5%, 2%, 2.5% and 3% PEGDA (w/w). The results from this showed that a formulation containing 0.5% PEGDA would give the highest percentage increase in weight, length and diameter of the solid hydrogel, 395.3%, 79.5% and 87.6% respectively. This concentration maintains figures like these even

after 91 days in PBS. However, when this hydrogel formulation was used to produce implant prototypes, rods with dimensions of 40mm x 8mm, the solid hydrogels broke down after 24 hours in PBS. It is possible that the low concentration, 0.5%, of PEGDA was not able to retain the form of the hydrogel when it had been scaled up to its true size. It was decided that despite the earlier PEGDA comparison investigation, a formula with a higher concentration would be better at retaining the shape of the hydrogel implant. Formulation U, with a PEGDA concentration of 3% (w/w) was used for all further hydrogel production.

### 4.4.6 Production of Hydrogel Implants

The complications that arose from using 3D printers, BMF nanoArch S130 and Formlabs 1+, to produce hydrogel implants lead to the remainder of the project focusing on the use of moulds as a method for production.

The first moulds designed for producing hydrogel rods, were generated by the Formlabs 1+ printer, using Formlabs standard resin. This produced clean, precise moulds for a solid cylinder 40mm x 8mm in dimensions. These moulds were used to produce sample implants with hydrogel formulation R (0.5% PEGDA). The hydrogel resin successfully cured within the moulds; however, extraction of intact hydrogel cylinders was unsuccessful. The walls of the mould were too tough and thick to be cut open to reveal the hydrogel cylinder. Attempts to remove the hydrogels from the moulds included trying the snap the mould off of the hydrogel and grinding the mould away from the hydrogel cylinder with course sandpaper. As both the moulds and the hydrogels had be solidified by photopolymerization with UV light, it appeared that the hydrogel resin had annealed to the mould, making it very difficult to distinguish between the two. When trying to sand away the mould, parts of the hydrogel were removed too because of this problem.

Later, moulds with thinner walls (1mm thick as opposed to the 2mm used previously) were designed and the hydrogel formulation U was cured within them. Unfortunately, the same complications arose. It was not possible to remove the hydrogels from their moulds without sanding the moulds or causing damage. Again, the moulds were too brittle and had annealed to the hydrogel too strongly to be removed and the hydrogel still be viable. The notion of integrating 3D printing into this project ceased at this point.

A more pliable plastic tubing was then used to form a mould that could be removed from the cured hydrogels more easily. These moulds produced hydrogels that successfully cured and could be removed easily, by scoring the plastic tubing to reveal the hydrogel. Although solid cylinder hydrogels were successfully made, the integrity of them was compromised once placed in PBS. Both hydrogel formulations R and U broke down after 24 hours in the solution. It is understood to be due to the high proportion of air bubbles produced and trapped within the hydrogels when they are cured under UV light. The reactivity of the acrylic acid component within the hydrogel formulation was the main cause of this, alongside the heat produced by the UV lamp causing the pliable moulds to soften and expand, providing additional volume for air bubbles to form.

It was decided that a mould would have to be constructed by a material with enough elasticity to make the removal of solid hydrogels easy, but also strong enough to resist the expansion of hydrogel resin that may occur from the reactivity of the acrylic acid component and the heat of the UV lamp. The use of Nusil MED4211 silicone, previously used when working with Oxtex and the in-house expander experiments at the University of Nottingham, was trialled as a mould for hydrogel production. For this method, an initial mould for the silicone to be formed around had to be made and the silicone poured in and left to set solid. This process resulted in the production of a solid hydrogel that could be easily removed from its mould. This trial hydrogel visibly had less air bubbles within it, however, it did also break down after 48 hours in PBS. This may have been due to its irregular shape, cone shaped with a larger diameter

at the top of the structure. The breakdown of these trial hydrogels appeared to occur in larger pieces, much less fragmented than previous swelling tests.

With these results, it was decided that the use of a silicone mould would be the best technique for producing hydrogel cylinders for the project. The purchase of a silicone with similar properties to that of Nusil MED4211, minus the medical grade characteristics that are not required for the moulds, was made. Mold Max™ 10T silicone is a water white translucent tin cured silicone rubber compound that has promising tear strength and working properties. This silicone was used to produce two types of moulds. One had the pliable plastic tubing plugged with wooden dowel at the base end. This was designed to produce a silicone mould for a solid cylinder. In the other, pliable plastic tubing was left hollow to allow the silicone to set around and within the tubing. This design was proposed to form a silicone mould with an extruded centre. This would produce a hydrogel in the form of a cylinder with a lumen. The silicone was tear resistance and flexible enough to be completely inverted to aid the removal of the inner tubing. This was the case for both mould designs.

The hydrogel (formulation U) successfully cured within the silicone mould and was easily removed, undamaged, from the mould. Again, air bubbles appeared in the solid cylindrical hydrogel during the curing process and so breakdown was expected once placed in PBS. However, the hollow cylinder hydrogel that have been produced showed no indications of air bubble formation and retained its shape completely after 3 days within PBS. This positive result led to the decision that a hollow cylindrical hydrogel, using formulation U, would be the most suitable for implantation.

### 4.4.7 Modification of Hydrogel Design

In preparation for the second implantation trial, modified hydrogels were designed and produced. In total, 10 hydrogels were cured, 6 with quincke ends and 4 with blunt ends.

Observations from the first implant trial showed that when the hollow hydrogels, unused for implantation, had been exposed to air, over time they had taken up some of the atmospheric moisture. This resulted in softer, pliable hydrogels that could be folded in on themselves and would return to their original shape once released. The dimensions of the hydrogels were unchanged. This new characteristic could be advantageous when developing the implants for the second implantation trial. One way of utilising the pliability of the air exposed hydrogels was to reshape them and then compare the expansion of the reshaped hydrogels with the standard ones. Two of the softened hydrogels were cut into the shape of a helix. When previously discussing the possibilities of 3D printing hydrogel expanders, there was a strong interest in the swelling capabilities of a helical shape. It was thought that this shape would provide additional radial dilatation as well as longitudinal, this was before the results of the acrylic acid and hydroxyethyl acrylate hydrogel swelling tests had been observed. The two reshaped hydrogels were placed in PBS, alongside a standard quincke ended and blunt ended hydrogel, and expansion comparisons were made.

The length and diameter percentage increases recorded showed some discrepancies between the two helical hydrogels, with one increasing in length by 73.85% (helix 1) and the other by 39.06% (helix 2). A similar result was obtained for diameter percentage increase, 80.00% and 42.86% for helix 1

and 2 respectively. These results, compared to the standard quincke and blunt ended hydrogels meant that the impact of the helical structure was questionable. The average length increase of the standard hydrogels was 49.10% and diameter percentage was 66.67% for both. With the inconsistencies seen within the helix hydrogel measurements and the diameter increases from previous swelling test proving that a standard hydrogel will increase in size radially, as well as longitudinally, it was decided that cutting the pliable expanders would not improve the outcome of potential tissue expansion.

Another design alteration looked in to producing a hollow cylindrical hydrogel with a solid tip, like that of a pencil. Silicone mould production for this design required some finesse and the design of the mould meant that the position of the silicone extrusion could not be controlled, sometimes resulting in the extrusion touching the walls of the mould. Successful curing of solid tipped, hollow cylindrical hydrogels did occur. It was thought that the tapered solid tip of these hydrogels would aid their implantation, with the remaining hollow structure providing most of the expansion.

Whilst producing the above hydrogels in preparation for a second in vitro implantation trial, additional solid quincke ended hydrogels were successfully made. Use of the Mold Max™ 10T silicone and reducing the diameter of the implants resulted in the hydrogel resin curing completely solid, with minimal air bubbles occurring at the blunt, open end. This produced a lumen like feature within the implant, which would be advantageous when inserting into the urogenital tract. The dilator used in the previous implantation trail could be

inserted into this lumen structure and aid inserting the implant into the correct position within the tract.

These results meant that self-expanding hydrogels for the use of minimally invasive cloacal repair surgery have been produced. Their expansion rates in PBS are known and when compared to the previous porcine growth experiment it is believed that they will increase in size sufficiently to exert pressure on the vaginal lumen and initiate cellular reproduction and tissue expansion.

# 5 Hydrogel Implantation

## 5.1 Introduction

In this phase, two in vitro trials were performed. These were designed to start addressing the third objective outlined in the introduction of this Thesis. Both trials were undertaken in vitro, with the vaginal tissue being removed from the animals once the hydrogels had been implanted and the expansion of the hydrogels and tissue measured in an organ bath.

The first was conducted to assess the insertion of the hydrogels in the animal model. It included rudimentary organ bath preservation of the tissue, with the main aim being to assess the expansion of the hydrogels in tissue culture media, composition of the solution differs from the PBS used in prior swelling tests, and the ability for the vaginal tissue to withstand the force of implant expansion.

The second implantation trial took place with an altered hydrogel design. The dimensions of the implants were reduced and both a simple quincke ended solid hydrogel and a hollow cylinder with a solid tapered tip were inserted into the vagina of the pig. The insertion ability, vaginal tissue integrity and histological analysis of these two implant designs, as well as a control, were assessed in this experiment.

This chapter does not completely address the objective ‘Implant the developed expander into the vagina lumen of porcine model. Allow for full expansion of the device and then remove the expanded tissue from the animal post-mortem.’ However, the difficulties that arose in the first hydrogel

implantation trial demonstrated that a successful in vitro expansion evaluation was imperative before in vivo techniques could be considered.

## 5.2 Methodology

### 5.2.1 First Implantation Trial of Hollow Cylindrical Hydrogels into Porcine Cadavers

The following experiment was carried out by David Gardner and Alun Williams. Lucy Wilson was isolating due to a positive COVID-19 PCR. Two pigs were euthanised, via schedule 1 euthanasia, for the in vitro implantation of hydrogels. The pigs were 8 weeks old and around 18kg each.

Two hollow cylindrical hydrogels were selected, they had the following diameters:

1. **Length = 50mm**
2. **Length = 38mm**

Both hydrogels had an external diameter of 9mm and an internal diameter of 5mm (Fig. 5.1) . Implantation of the hydrogels into the porcine vagina, whilst the organ was in situ, was endeavoured.

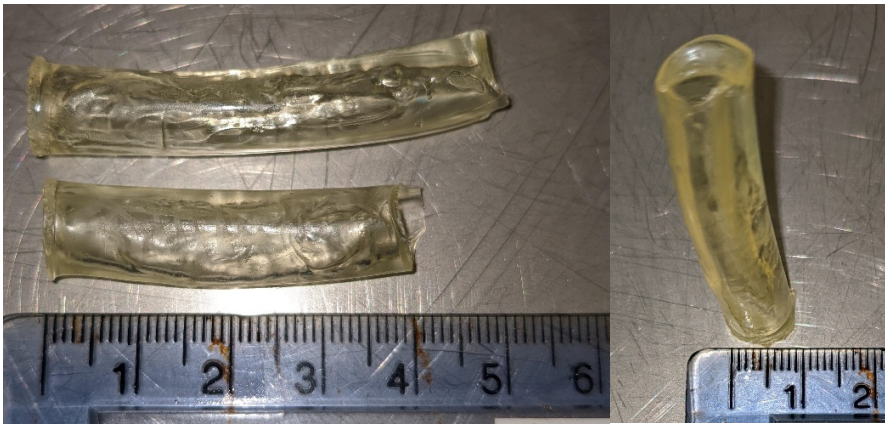


**Figure 5.1: Hollow cylindrical hydrogels used in the first in vivo implantation trial. The images show the length and external diameter of the hydrogels.**

The urogenital tract of the animals had to be removed to aid implantation and to secure the hydrogel in place. On removal it was observed that one of the tracts had a tear, either from pushing the hydrogel blindly into the tract, or from removal of the tract from the cadaver. The tract was stitched up, the hydrogel inserted and held within the tract with a ligature stitch at the opening.

The tracts and hydrogels were placed in an organ bath and kept in the fridge. David Gardner observed and measured the expansion of the tracts on days 1, 2, 4, 7 and 14 after implantation.

### 5.2.2 Second Implantation Trial of Hydrogels into Porcine Cadavers

Eight piglets, aged 8 weeks, were euthanised via schedule 1 procedure. Once euthanised, each pig was implanted with a hydrogel into its vagina. The hydrogels were inserted via the perineal opening of the urogenital sinus of the animal, as would be done in a surgical setting. Three different hydrogels were inserted. Three animals were implanted with a solid, non-expanded, quincke tipped hydrogel. Three were implanted with a non-expanded, hollow hydrogel with a solid tapered tip. Two pigs were implanted with an expanded, solid, quincke tipped hydrogel, these formed the controls of the in vitro expansion experiment. The live weights of the animals were recorded, alongside the type of hydrogel that was inserted into the animal and the dimensions of the hydrogels prior to insertion (Table 5.1).

| Pig Number | Weight (Kg) | Type of Hydrogel | Length of Hydrogel (mm) | Diameter of Hydrogel (mm) |
|---|---|---|---|---|
| 1 | 15.5 | Solid, quincke tip | 35.83 | 6.57 |
| 2 | 14.8 | Solid, quincke tip | 36.05 | 6.89 |
| 3 | 14.8 | Solid, quincke tip | 35.01 | 6.45 |
| 4 | 14.0 | Hollow, solid tapered tip | 41.01 | 6.48 |
| 5 | 11.8 | Hollow, solid tapered tip | 40.82 | 7.25 |
| 6 | 12.4 | Hollow, solid tapered tip | 40.45 | 7.08 |
| 7 | 12.5 | Solid, quincke tip, post-expanded | 39.37 | 9.18 |
| 8 | 11.6 | Solid, quincke tip, post-expanded | 39.46 | 9.32 |

**Table 5.1: Weights of the piglets, the type of hydrogel implanted into each animal and the dimensions of said hydrogels.**

The length of the first hydrogel that was inserted into pig 1 was originally 49.54mm in length. This length was too long for the implant to be secured in place within the vagina, once the urogenital sinus had been removed. A length of 13.71mm was cut off the blunt end of the hydrogel. The remaining hydrogels were trimmed down to similar lengths before being implanted into the remaining pigs.

**Figure 5.3: Hydrogels implanted into the piglets.**

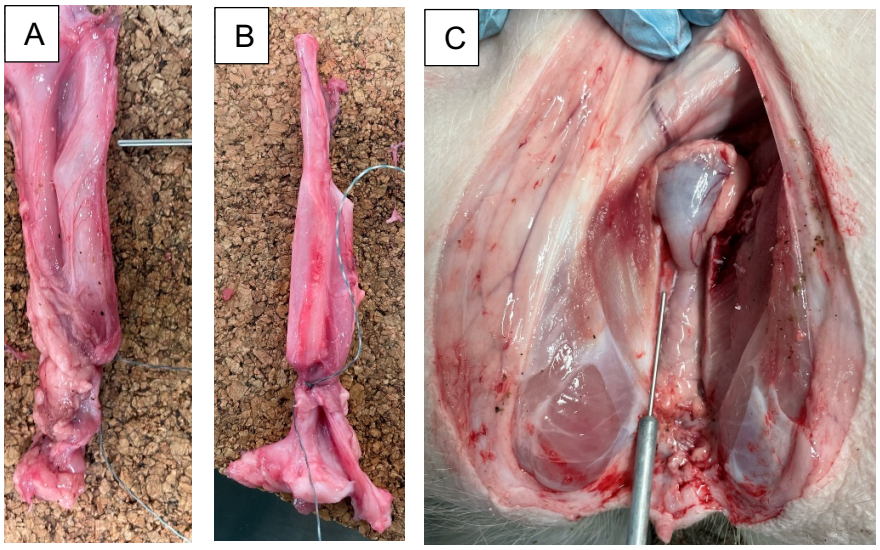


**Figure 5.2: Hydrogels in situ. A** shows a solid, quincke ended hydrogel in the vagina of a piglet. The metal rod points to the quincke end inserted up to the cervix of the animal. **B** shows how the hydrogels were tied into the vaginas of the animals, to ensure that pressure was exerted on the organ whilst expansion took place. **C** shows the implanted hydrogel within the pelvic region of the animal. The finest part of the metal rod runs alongside the hydrogel in situ.

### 5.2.3 Vaginal Tissue Organ Bath

The following combination of tissue culture media (Dulbecco's Modified Eagle Medium), foetal calf serum (FCS), amino acid (L-glutamine) and antibiotic (ampicillin) was used in the organ baths for the expanding vaginal tissues.

| Ingredient | DMEM | FCS | L-Glutamine | Ampicillin |
|---|---|---|---|---|
| % conc. | 89.4 | 8.9 | 1.1 | 0.6 |

**Table 5.2: Concentrations of DMEM, FCS, L-glutamine and ampicillin used in the organ baths for the in vitro expansion of vaginal tissue.**

A total volume of 895ml was made up for the initial organ bath set up and each subsequent media change. The vaginal tissues, with various hydrogels tied in place, were put into Thermo Scientific™ Nunc™ 159910 cell culture treated EasYFlasks™, 175$cm^3$, 800ml. The media solution was divided equally between the 8 tissue samples. The solution was poured into the flasks, with the tissue inside the flask, until the volume came to 125ml. The organ baths were placed in a 37°C incubator, with 5% $CO_2$ overnight. The length and diameter of the hydrogel within the tissue sample was measured every day for 5 days. The media solution within the organ baths was changed each day.

### 5.2.4 Removal of Hydrogels from Vaginal Tissue

After 5 days in the organ baths, the hydrogels within the tissue samples were removed and the tissues were immersed in 10% buffered formaldehyde fixative solution.

The tissues were then placed in PBS for 24 hours and finally into 70% ethanol, once segments for histological analysis had been cut. The tissue samples were embedded in paraffin wax, cut into segments for slides and stained with haematoxylin and eosin stain.

## 5.3 Results

### 5.3.1 First Implantation of Hollow Cylindrical Hydrogels into Porcine Cadavers

After 24 hours of expansion, the hydrogel had considerably increased in both length and diameter. The urogenital tract was observably under strain from the enlargement of the hydrogel within.

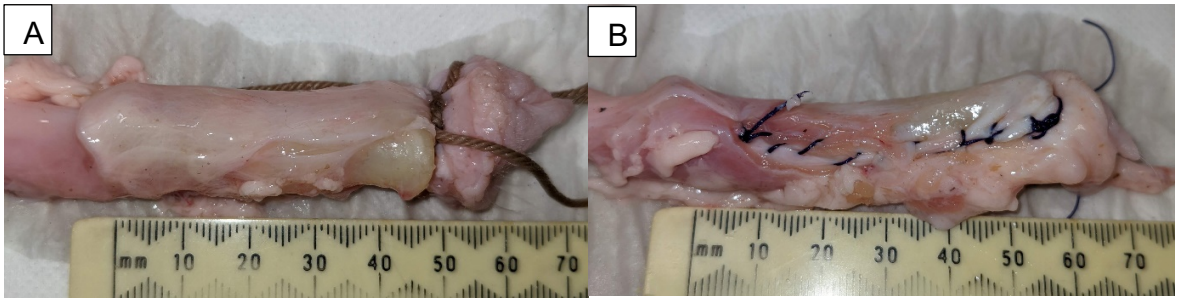


**Figure 5.4: Hollow hydrogels within urogenital tissue after 24 hours of expansion.** A. The hydrogel is beginning to protrude from the tissue where the lumen has been tied off. B. The urogenital tract was repaired after damage caused by insertion or removal of the tract.

Figure 5.4 shows the two hydrogels within their urogenital tracts. The implant in figure 5.4(A) can be seen beginning to protrude from the tissue where the lumen has been tied off. Another observation of note is that the tissue on the right-hand side of the ligature knot appears to be the vulva of the animal. This suggests that insertion of the hydrogel was inaccurate, with the final placement being in the urogenital sinus of the tract and would account for the difficulties that occurred on implantation.

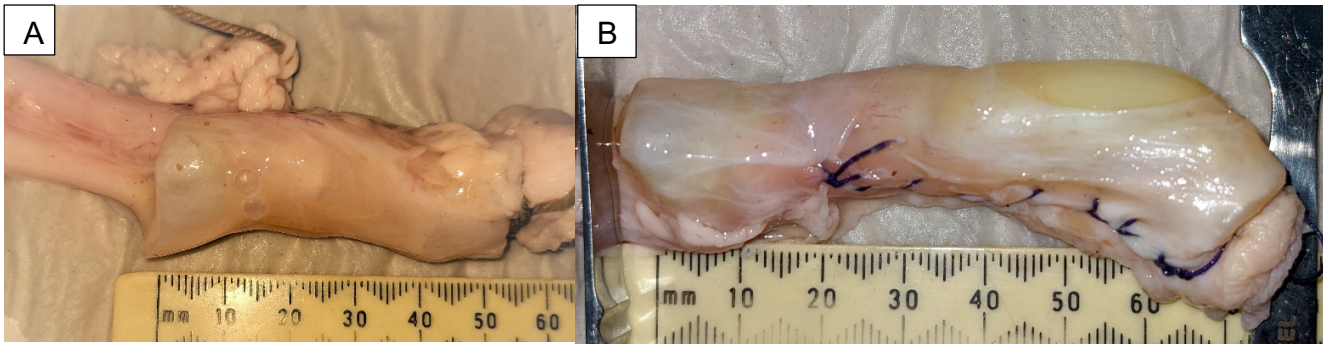


**Figure 5.5: Hydrogels within urogenital tissue after 4 days of expansion.** A clear rupture of the tissue can be seen in image **B**.

After 4 days within tissue culture media, kept in a refrigerator, the hydrogels had clearly ruptured the urogenital tissue, as seen in figure 5.5(B).

### 5.3.2 In Vitro Hydrogel Length Increase of Second Hydrogel Implantation Trial

The graphs below show the changes in length of the various shaped hydrogels within the vaginal tissue across the 6 days of measurement. The starting lengths of the hydrogels was between 35.01mm – 41.01mm. There was a general increase in length and diameter in all three types of hydrogels, including the control hydrogels (Fig. 5.6). These hydrogels had stopped swelling after a week in PBS, but continued expansion was seen once implanted in the vaginal tissue and kept in organ baths.

As with the previous swelling tests conducted on cured hydrogels, there was a rapid increase in length within the first 24 hours in the organ baths. The maximum increase in length within 24 hours was 45.7% (a solid hydrogel).

After the first 24 hours the measurements continued to increase, but at a slower rate. A slight decrease in length was recorded in one of the hollow hydrogels. After 6 days of recording, the increases in length varied between 38.5 – 108.2%. The smallest percentage increase was a control hydrogel and the highest percentage increase in length was seen in a solid hydrogel. Overall, the solid implanted hydrogels had the highest percentage increase in length, with an average of 94.8%, and the controls had the lowest, an average of 41.1%, as expected.

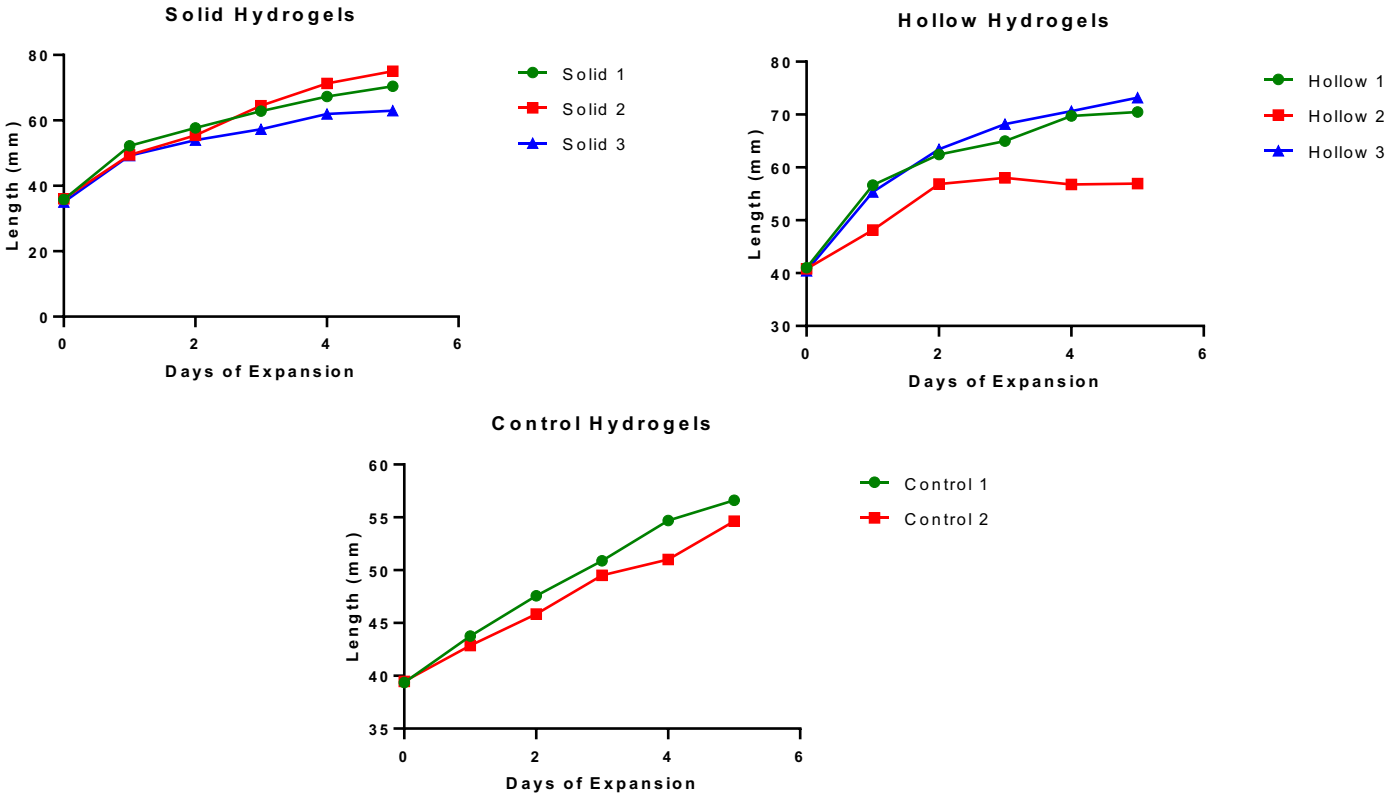


**Figure 5.6: Graphs representing the changes in length of the various shaped hydrogels, via in vitro implantation and organ bath immersion, across the 6 days of measurement.**

### 5.3.3 In Vitro Hydrogel Diameter Increase of Second Hydrogel Implantation Trial

The graphs below show the changes in length of the various shaped hydrogels within the vaginal tissue across the 6 days of measurement.

The starting lengths of the hydrogels was between 6.45mm – 9.32mm, including the post-expanded control hydrogels. As with the changes in the lengths of the hydrogels, there was a rapid increase in diameter within the first 24 hours in the organ baths (Fig. 5.7). The maximum increase in diameter of 61.9% was recorded for a solid hydrogel. After the first 24 hours the measurements continued to increase, but at a slower rate. A slight decrease in diameter was recorded in two of the hollow hydrogels and one solid hydrogel.

After 6 recorded measurements, the increases in diameter varied between 58.5 – 156%. The smallest percentage increase was a control hydrogel and the highest percentage increase in diameter was seen in a solid hydrogel. Overall, the solid implanted hydrogels had the highest percentage increase in diameter, with an average of 138.5%, and the controls had the lowest, an average of 62.9%, as expected.

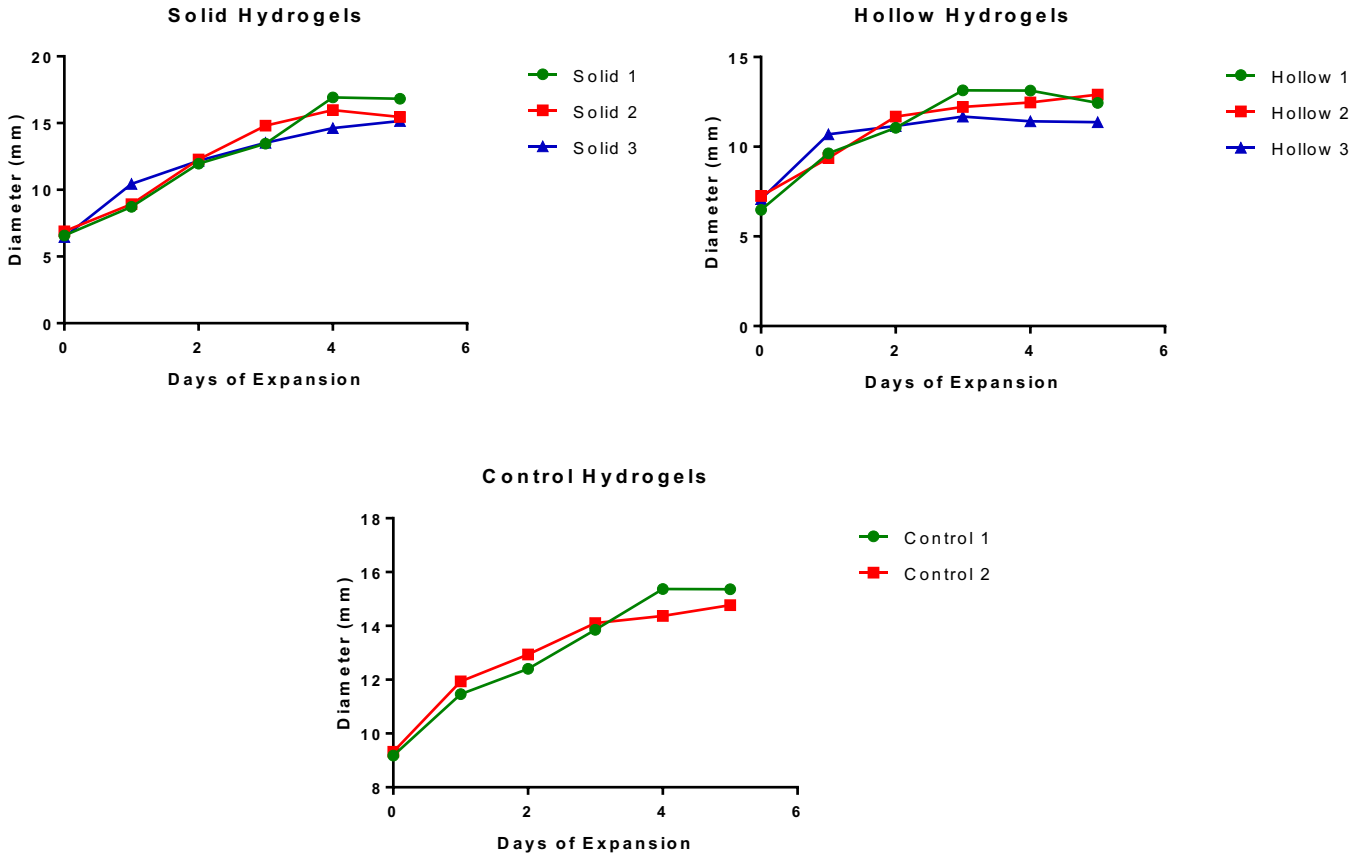


**Figure 5.7: Graphs representing the changes in diameter of the various shaped hydrogels, via in vitro implantation and organ bath immersion, across the 6 days of measurement.**

### 5.3.4 Average in Vitro Hydrogel Measurements at Day 6 of Second Hydrogel Implantation Trial

Table 5.3 shows the average total percentage increase of length and diameter of the various shaped hydrogels within the vaginal tissue after 6 days of recording measurements.

| Expander | Average % increase of length | Average % increase of diameter |
|---|---|---|
| Solid | 94.8 | 138.5 |
| Hollow | 64.1 | 76.9 |
| Control | 41.1 | 62.9 |

**Table 5.3: Average total percentage increases of the length and diameter of the various shaped hydrogels, via in vitro implantation and organ bath immersion, across 6 days of measurement.**

### 5.3.5 Removal of Hydrogels from Vaginal Tissue of Second Hydrogel Implantation Trial

The removal of the expanded and control hydrogels from vaginal tissue took place after 5 days in the organ baths. Care was taken to remove the hydrogels from the urogenital tract and keep the tissue intact. This had varying successes, dependant on the design of the implant and whether tissue rupture had occurred during the in vitro tissue expansion trial.

#### 5.3.5.1 Removal of Solid Hydrogel from Porcine Vaginal Tissue, Number 1.

On observation, the vaginal tissue had ruptured where the surgical knot had been tied (Fig. 5. (B)), to hold the hydrogel implant within the organ. The suture material was removed, and the implant was squeezed out of the lumen of the tissue, starting from the closed cervix. This distal end of the hydrogel broke away on removal (Fig. 5.8 (C)). This was the area of bubble formation that was produced when curing the hydrogel resin under ultraviolet light.

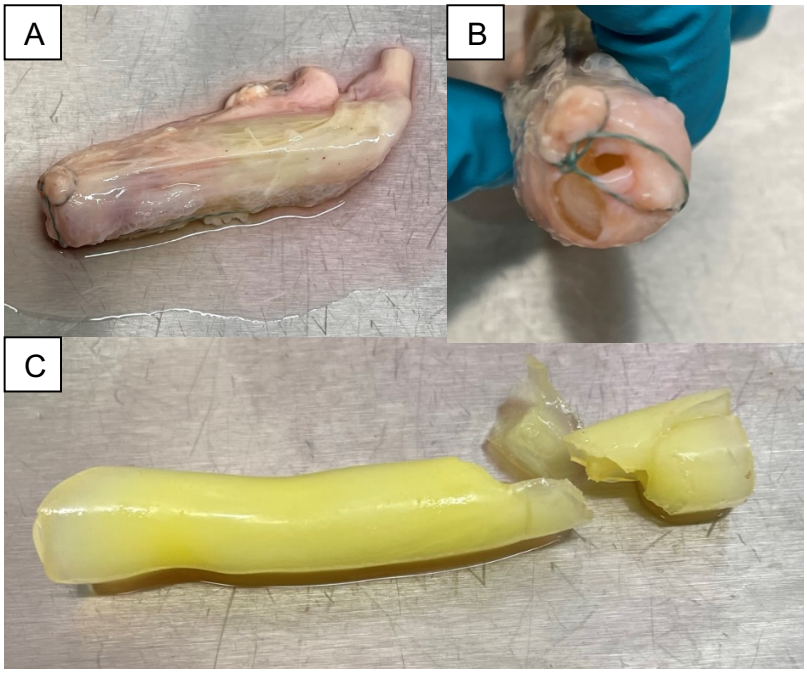


**Figure 5.8: Expanded solid hydrogel implant within porcine vaginal tissue, number 1, and on removal. A** and **B** show the hydrogel within the tissue, with image **B** highlighting the rupture that occurred at the suture material knot at the opening of the vagina lumen. **C** shows the swollen hydrogel once removed from the tissue, the breakage at the distal end can be seen.

#### 5.3.5.2 Removal of Solid Hydrogel from Porcine Vaginal Tissue, Number 2.

The vaginal tissue surrounding the solid hydrogel had remained intact for the entire duration of the in vitro organ bath swelling test. On removal of the suture material, holding the implant in situ, the dimensions of the vaginal opening appeared to be similar to that of pre-expansion (Fig. 5.9 (B)).

The vaginal lumen opening had to be widened to allow for the removal of the hydrogel implant. The solid hydrogel had remained intact during its expansion and its removal from the tissue. There was a minor breakage at the distal end of the hydrogel, however this appeared to have occurred after removal and may have been to over-handling the implant (Fig. 5.9 (C)).

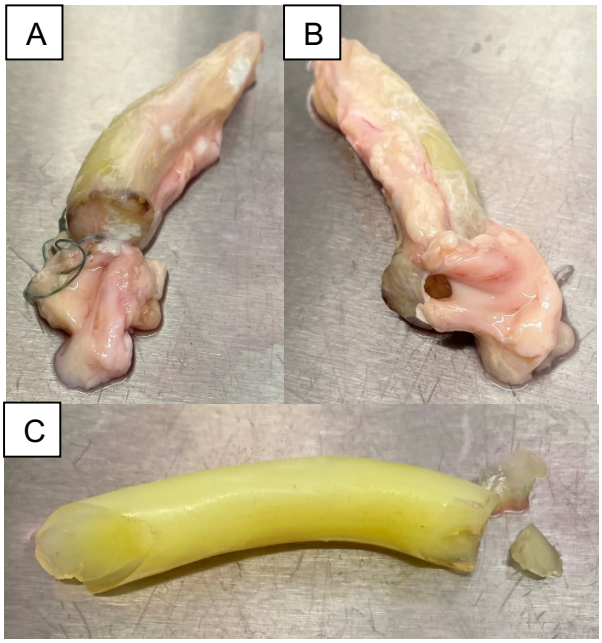


**Figure 5.9: Expanded solid hydrogel implant within porcine vaginal tissue, number 2, and on removal. A** and **B** show the hydrogel within the tissue, with image **B** highlighting the size of the vaginal opening in comparison to the diameter of the expanded implant. **C** shows the hydrogel, post expansion, with the majority of it intact and a minor breakage at the distal end seen.

#### 5.3.5.3 Removal of Solid Hydrogel from Porcine Vaginal Tissue, Number 3.

This solid hydrogel had caused some perforation to the vaginal tissue on expansion. The implant did not retain its straight shape when expanding, meaning it had started to bend within the lumen. The outside of this bend had begun to perforate through the wall of the tissue and could be seen, so that the hydrogel could be seen before its removal from the vagina lumen (Fig. 5.10 (A)).

As with the previous implant, removal of the suture material revealed that the vaginal opening size was similar to that of pre-expansion. A larger opening had to be created to remove the hydrogel. On removal, the implant was observed to be completely intact, including the thinner distal end, where air bubbles had been produced during curing (Fig. 5.10 (C)).

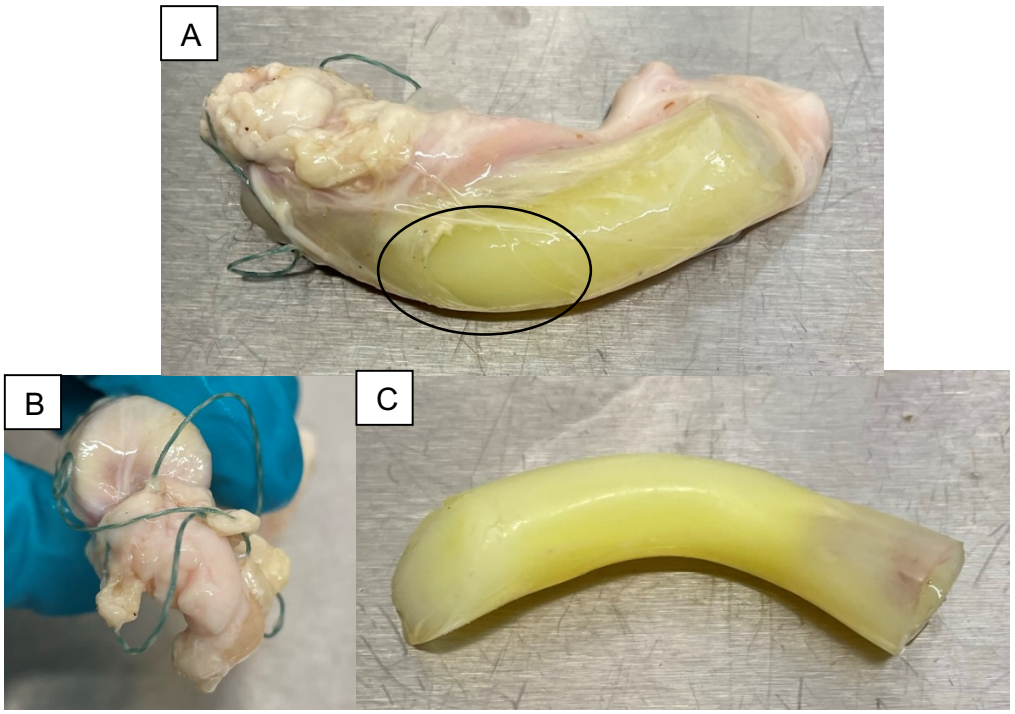


**Figure 5.10: Expanded solid hydrogel implant within porcine vaginal tissue, number 3, and on removal. A** and **B** show the expanded implant within the tissue, with the perforation of the vaginal wall encircled in **A** and **B** showing the suture material knot intact. **C** shows the hydrogel, post expansion, completely intact.

### 5.3.5.4 Removal of Solid Tipped, Hollow Hydrogel from Porcine Vaginal Tissue, Number 4.

The vaginal tissue had remained intact for the duration of the in vitro organ bath swelling test. The implant had remained within the suture material knot during expansion (Fig. 5.11 (A)).

Removal of the suture material revealed that the hollow end of the hydrogel had folded in on itself (Fig. 5.11 (C)). Removal of the implant from the vaginal lumen was difficult. The hollow end of the hydrogel was able to be removed intact, but the solid tip of the implant had expanded to a wider diameter than the hollow cylinder and had broken away from it on removal. Removal of the solid, tapered tip caused damage to the vaginal tissue and broke up into smaller pieces on removal (Fig. 5.11 (D)).

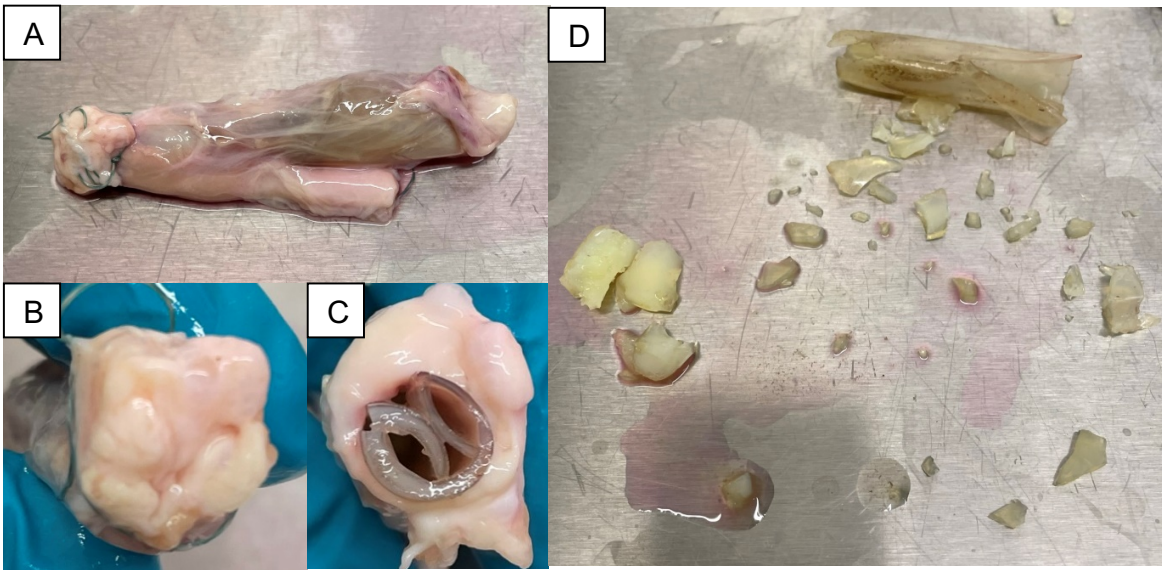


**Figure 5.11: Expanded solid tipped, hollow cylindrical hydrogel implant within porcine vaginal tissue, number 4, and on removal. A**, **B** and **C** show the expanded implant within the tissue, with A showing the entire organ and **B** and **C** focussing on the opening of the tissue. **B** shows the suture material knot having sealed the opening and **C** the hollow end of the hydrogel having folded in on itself. **D** shows the breaking down of the implant that occurred with its removal. The hollow end remains intact, and the solid, tapered tip has come away and broken down into pieces.

### 5.3.5.5 Removal of Solid Tipped, Hollow Hydrogel from Porcine Vaginal Tissue, Number 5.

Before removal of the hydrogel, it was obvious that it had become misshaped during expansion (Fig. 5.12 (A)). The implant was bent and on handling it appeared that the solid, tapered tip of the hydrogel had broken away from the hollow cylinder part. However, the tissue had remained intact during the time in the organ bath.

The vaginal tissue had ruptured at the suture material knot, with the implant protruding from the perforation hole (Figs. 5.12 (B) and (C)). Removal of the hydrogel resulted in the hollow cylinder disintegrating and again, damage was caused to the tissue when removing the solid, tapered tip.

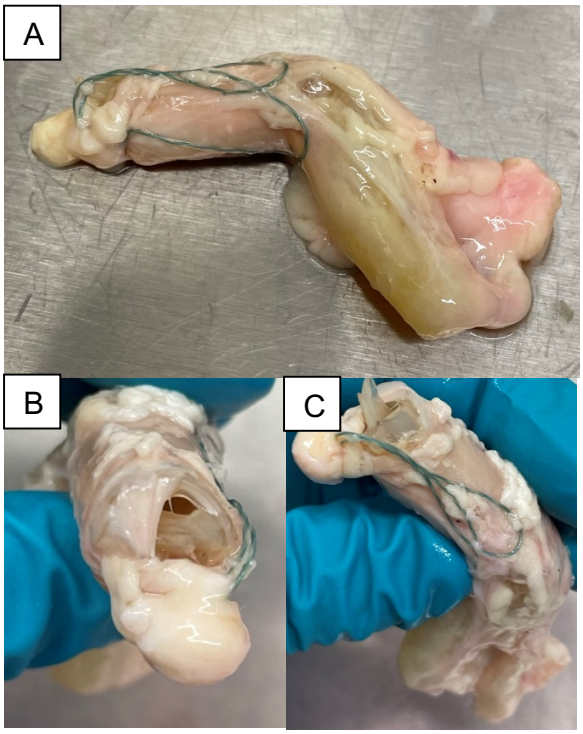


**Figure 5.12: Expanded solid tipped, hollow cylindrical hydrogel implant within porcine vaginal tissue, number 5. A** shows the misshaped hydrogel within the tissue, with an obvious bend in the implant seen. **B** shows the rupturing of tissue around the suture material knot, exposing the implant. **C** shows a side view of the hydrogel protruding from the opening of the vaginal tissue, with the suture knot still in place.

### 5.3.5.6 Removal of Solid Tipped, Hollow Hydrogel from Porcine Vaginal Tissue, Number 6.

The hydrogel had appeared to remain intact or the duration of the in vitro organ bath swelling test (Fig. 5.13 (A)). Perforation had occurred at the suture material knot, holding the implant in place, but otherwise the tissue had also remained intact.

To try to keep the hydrogel intact whilst removing it from the vaginal tissue, the wall of the vagina was cut longitudinally. The hollow cylindrical aspect of the implant broke apart regardless, with the tapered tip coming away from it and a split occurring along the length of the hydrogel (Fig. 5.13 (B)).

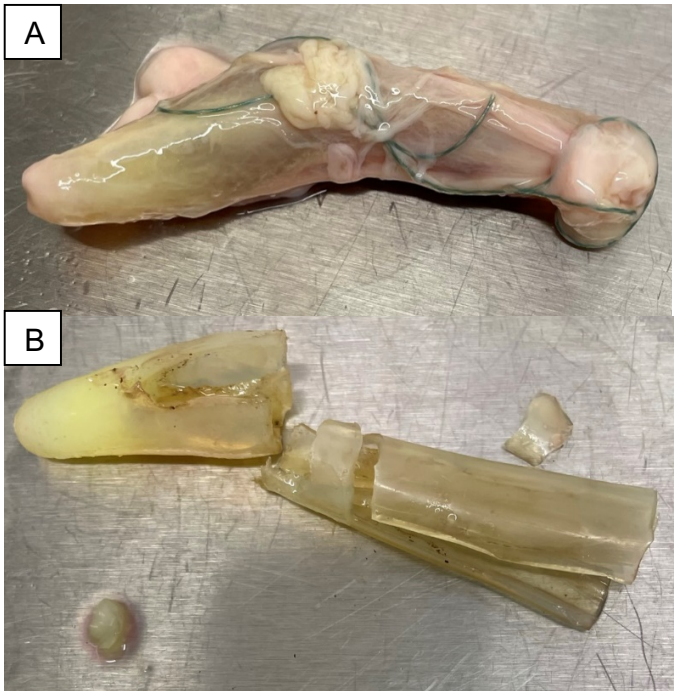


**Figure 5.13: Expanded solid tipped, hollow cylindrical hydrogel implant within porcine vaginal tissue, number 6, and on removal. A** shows the hydrogel within the tissue, intact. **B** shows the implant once removed from the vaginal tissue. Again, the tapered tip came away from the hollow cylinder and the hollow aspect has split.

### 5.3.5.7 Removal of Control Hydrogel from Porcine Vaginal Tissue, Number 7.

The vaginal tissue remained intact for the duration of the swelling test. No perforation was seen at the suture material knot (Fig. 5.14 (C)), and as with some of the solid hydrogels described earlier, a larger opening of the vaginal lumen had to be created to aid removal. On removal, the proximal end of the control hydrogel broke away (Fig. 5.14 (A)). No damage to the tissue was caused removal of the implant.

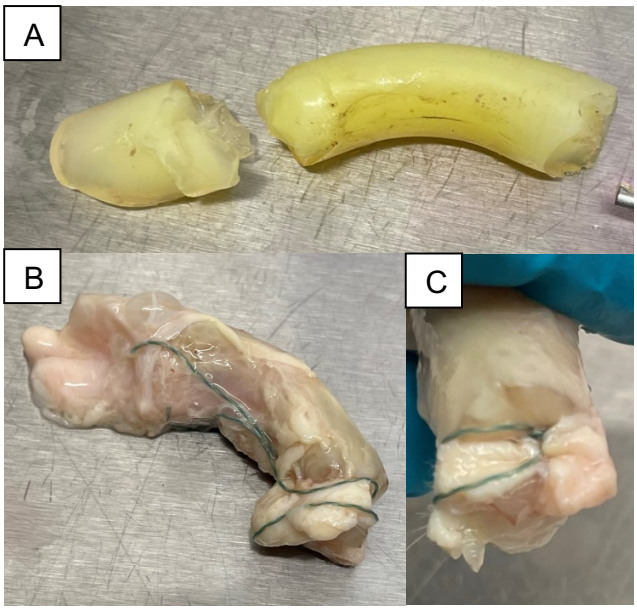


**Figure 5.14: Expanded control hydrogel implant within vaginal tissue, number 7, and on removal. A** shows the hydrogel once removed from the tissue, the proximal end broken away from the remainder of the implant can be seen. **B** and **C** shows the implant within the tissue, with **C** focusing on the suture material knot, showing no perforation.

### 5.3.5.8 Removal of Control Hydrogel from Porcine Vaginal Tissue, Number 8.

As with the previous control hydrogel, the vaginal tissue had remained intact for the duration of the in vitro organ bath swelling test (Fig. 5.15 (A)), and no perforation at the suture material knot was observed (Fig. 5.15 (B)). The entrance to the vaginal lumen had to be widened to aid removal of the implant and the entire hydrogel remained intact during removal. No tissue damage occurred with the removal of the control implant (Fig. 5.15 (C)).

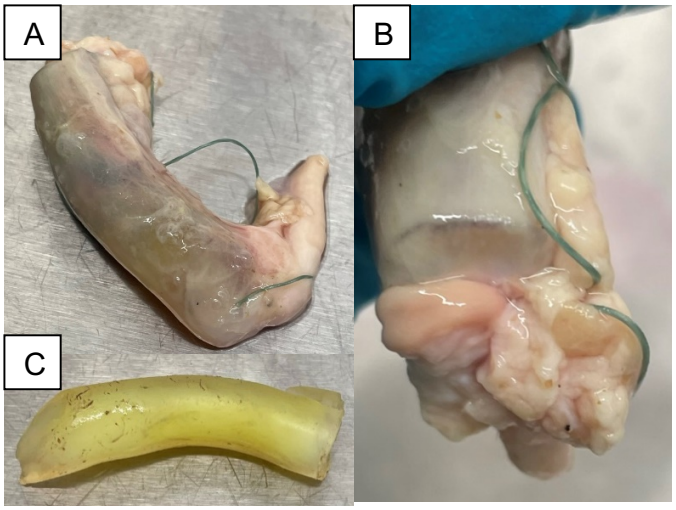


**Figure 5.15: Expanded control hydrogel implant within vaginal tissue, number 8, and on removal. A** and **B** show the expanded implant within the tissue, with **B** focussing on the suture material sealing the opening of the vagina. **C** shows the hydrogel once removed from the tissue, completely intact.

#### 5.3.5.9 Comparison of the Hydrogel Implants, Post Expansion

The image below shows the expanded hydrogels, removed from the porcine vaginal tissue, placed alongside each other. On observation, the solid hydrogels remained, almost, entirely intact. Only one of the solid tipped, hollow cylindrical hydrogel implants retained its form well enough to be positioned for the image (Fig. 5.16).

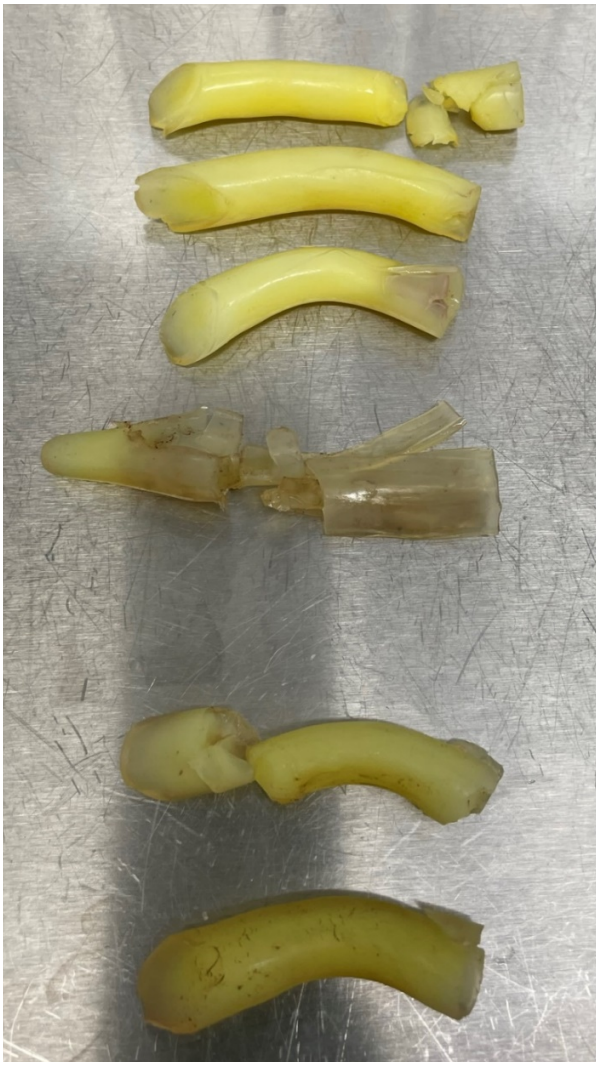

**Figure 5.16: Hydrogel implants removed from porcine vaginal tissue.** The three implants at the top of the image are the solid hydrogels, the middle implant is one of the solid tipped, hollow cylindrical hydrogels and the two implants at the bottom of the image are the control hydrogels.

### 5.3.6 Histology of Second Hydrogel Implantation Trial

Haematoxylin and eosin staining of the tissue, collected from the in vitro organ bath swelling test, was performed. Images of the stained slides were taken and are presented below.

#### 5.3.6.1 H & E-stained expanded tissue, solid hydrogel implant

The swelling of the hydrogel implants within the lumen of vaginal tissue caused visible stretching of the tissue. This was apparent with observations made to the tissue once the implant had been removed and from histological imagery.

Figure 5.17 shows images of the tissue expanded via the solid hydrogel implants. On viewing, several observations can be made. Firstly, the entire tissue appears to have a pink coloured hue to it, eosinophilic. This trait can be observed in all imagery of the tissue collected from the in vitro organ bath swelling tests.

Secondly, at this magnification, evidence of stretching of the tissue can be noted. The entire depth of the tissue can be seen, from epithelium, through to the mesenchyme and outer musculature and blood vessels, all within the frame of the image. The other observation of note is the inability to be able to distinguish between the layer of epithelial cells and the lower mesenchyme. Previous histological studies for this project have shown the epithelium to be darker in colour in comparison to the remainder of the tissue.

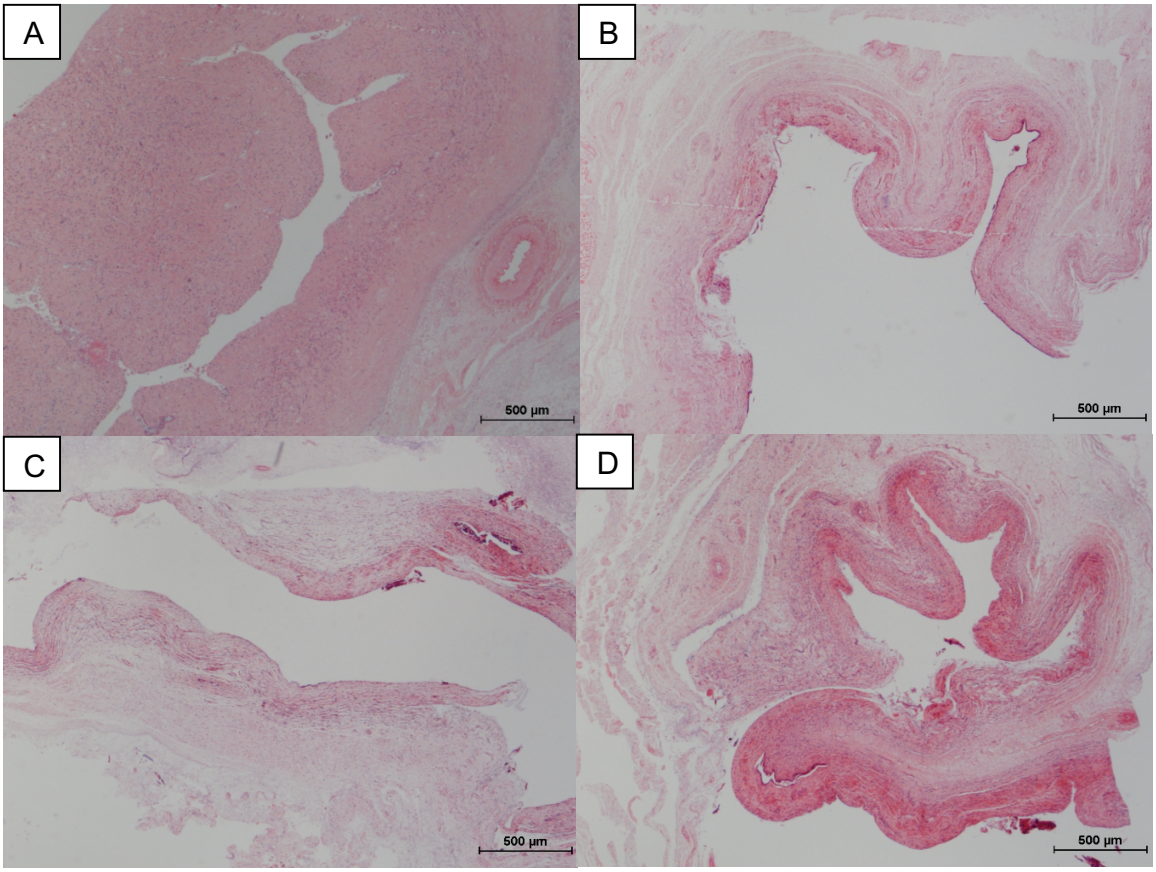


**Figure 5.17: H & E-stained vaginal tissue, expanded by the solid hydrogel implants via in vitro organ bath expansion. 40x magnification. A** is tissue obtained from the proximal end of 'tissue number 1' and **B** is tissue taken from the distal end of that tissue. **C** and **D** are 'tissue number 3', with **C** showing proximal vaginal tissue and **D** showing distal.

Further inspection of the histological images, at a magnification of 200x, revealed that very little epithelium remained attached to the tissue. Figure 5.18 shows images of the 'epithelium' from all three expanded vaginal tissues. The images show clearly that these cells are not present and that only remnants of previously characterised single cell columnar epithelium remain in crevices of the fixed tissue.

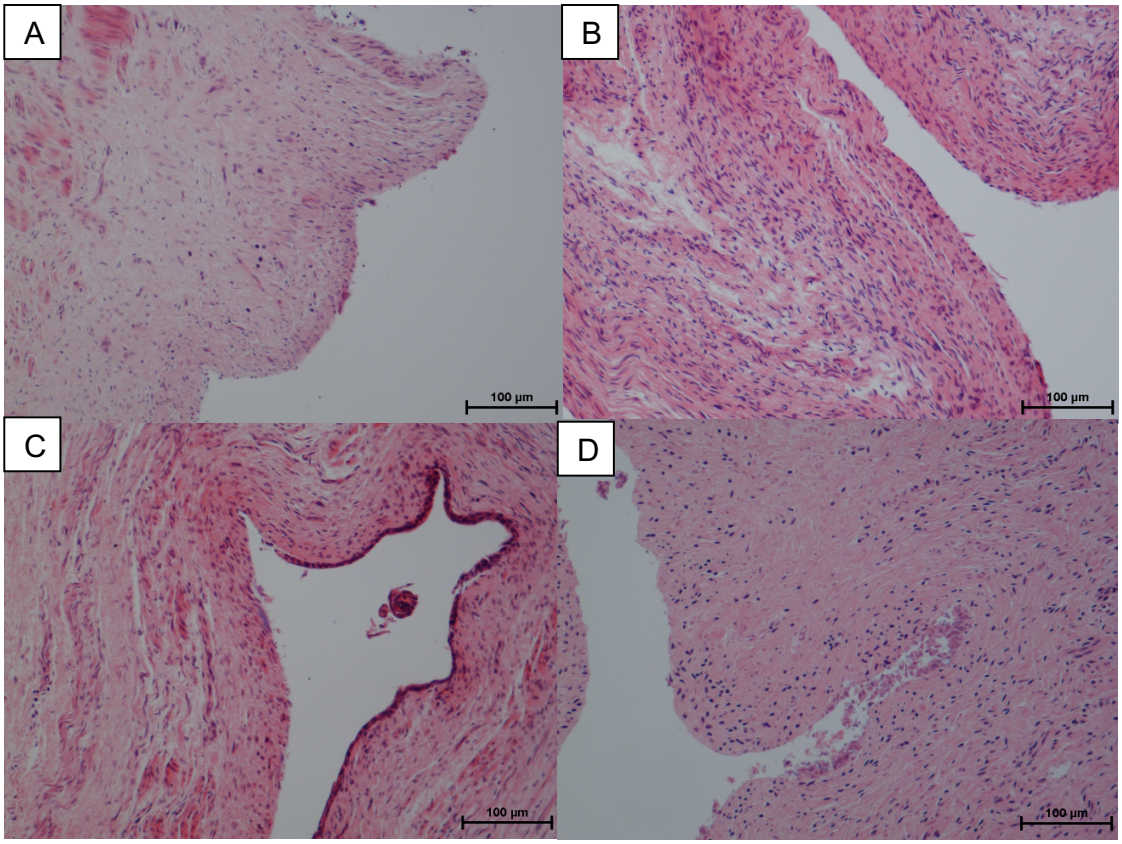


**Figure 5.18: H & E-stained vaginal tissue, expanded by the solid hydrogel implants via in vitro organ bath expansion. 200x magnification. A** is tissue obtained from the proximal end of 'tissue number 2' and **B** is proximal tissue taken from 'tissue number 3'. **C** and **D** are 'tissue number 1', with **C** showing distal vaginal tissue and **D** showing proximal tissue.

### 5.3.6.2 H & E-stained expanded tissue, solid tipped, hollow cylindrical hydrogel

The imaging obtained of the tissue that had been expanded via the solid tipper, hollow cylindrical hydrogel, had a very strong resemblance to that of the solid one.

Again, the tissue has an eosinophilic appearance, the epithelium is difficult to distinguish from the underlying mesenchymal tissue and often the entire depth of the tissue can be seen in one frame of imaging. This can be seen clearly in figure 5.19.

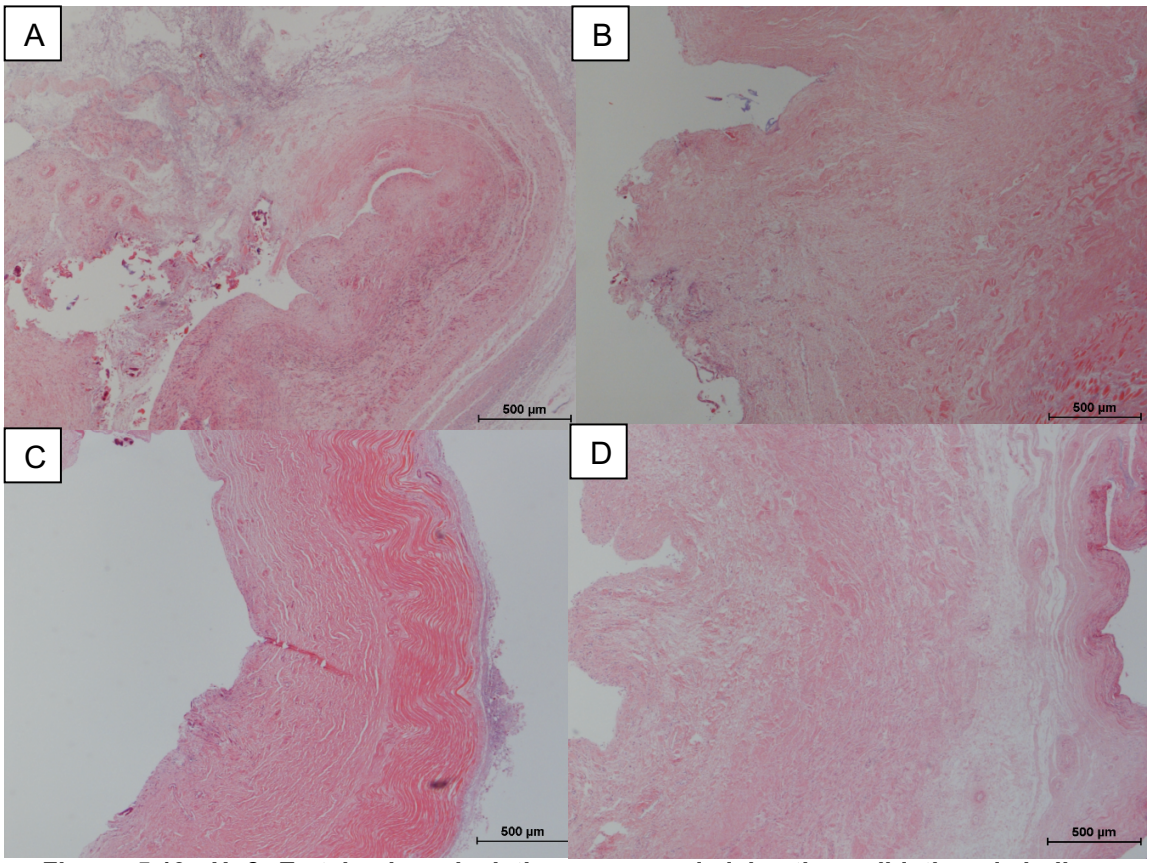


**Figure 5.19: H & E-stained vaginal tissue, expanded by the solid tipped, hollow cylindrical hydrogel implants via in vitro organ bath expansion. 40x magnification. A** is tissue obtained from the proximal end of 'tissue number 4' and **B** is from the distal end of the same tissue. **C** and **D** are of 'tissue number 5', with **C** showing proximal vaginal tissue and **D** showing distal tissue.

Viewing at an increased magnification also showed similar results the solid hydrogel tissue expanders. Figure 5.20 shows the 'epithelium' of all three tissue samples. In images B, C and D the tissue is clearly absent of epithelium cells and only remnants of the cells can be seen in a crevice if tissue in image A.

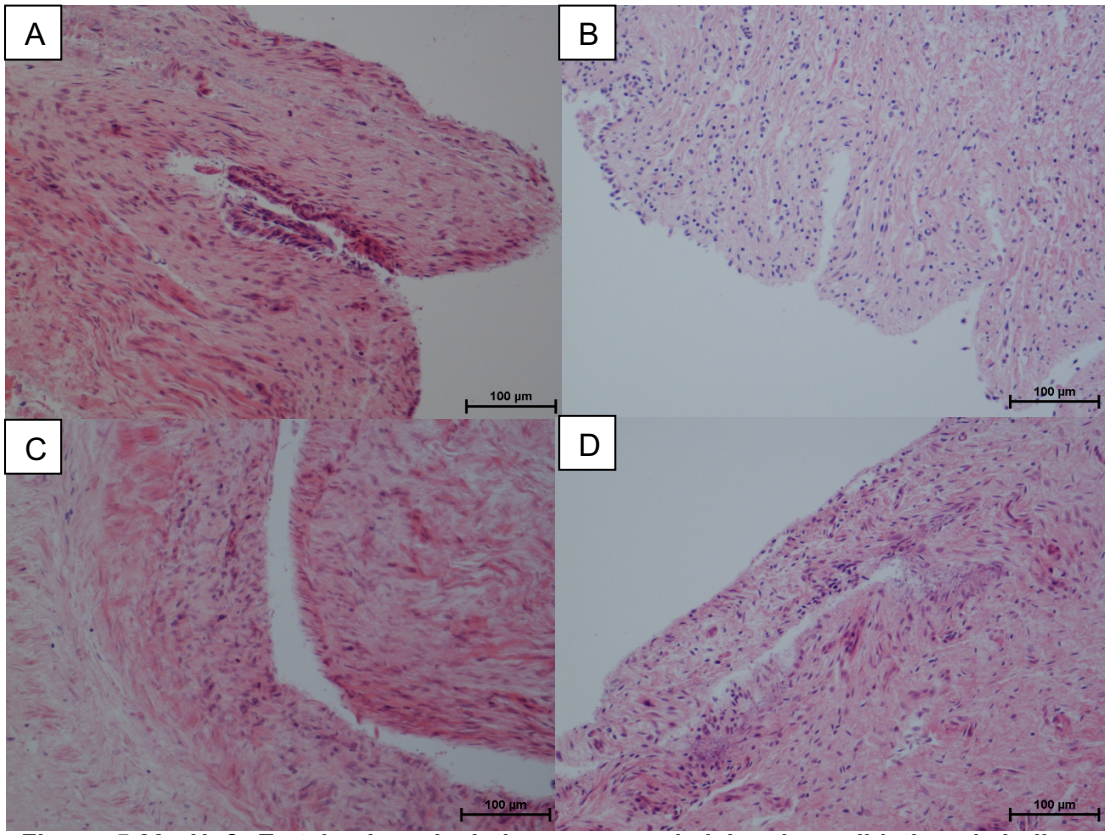


**Figure 5.20: H & E-stained vaginal tissue, expanded by the solid tipped, hollow cylindrical hydrogel implants via in vitro organ bath expansion. 200x magnification. A** is tissue obtained from the proximal end of 'tissue number 4' and **B** is from the distal end of 'tissue number 5'. **C** and **D** are 'tissue number 6', with **C** showing proximal vaginal tissue and **D** showing distal tissue.

### 5.3.6.3 H & E-stained expanded tissue, control hydrogel

Figure 5.21 shows images of the tissue that encased the control hydrogel tissue expanders.

As seen in sections 5.3.6.1 and 5.3.6.2 there is a red eosinophilic appearance, and the characteristic epithelium cannot be readily distinguished. The tissue does appear to be thicker, with the entire depth not always seen in the frame of the 4x image. This is as expected, as the control implant was not designed to increase the dimensions of the tissue.

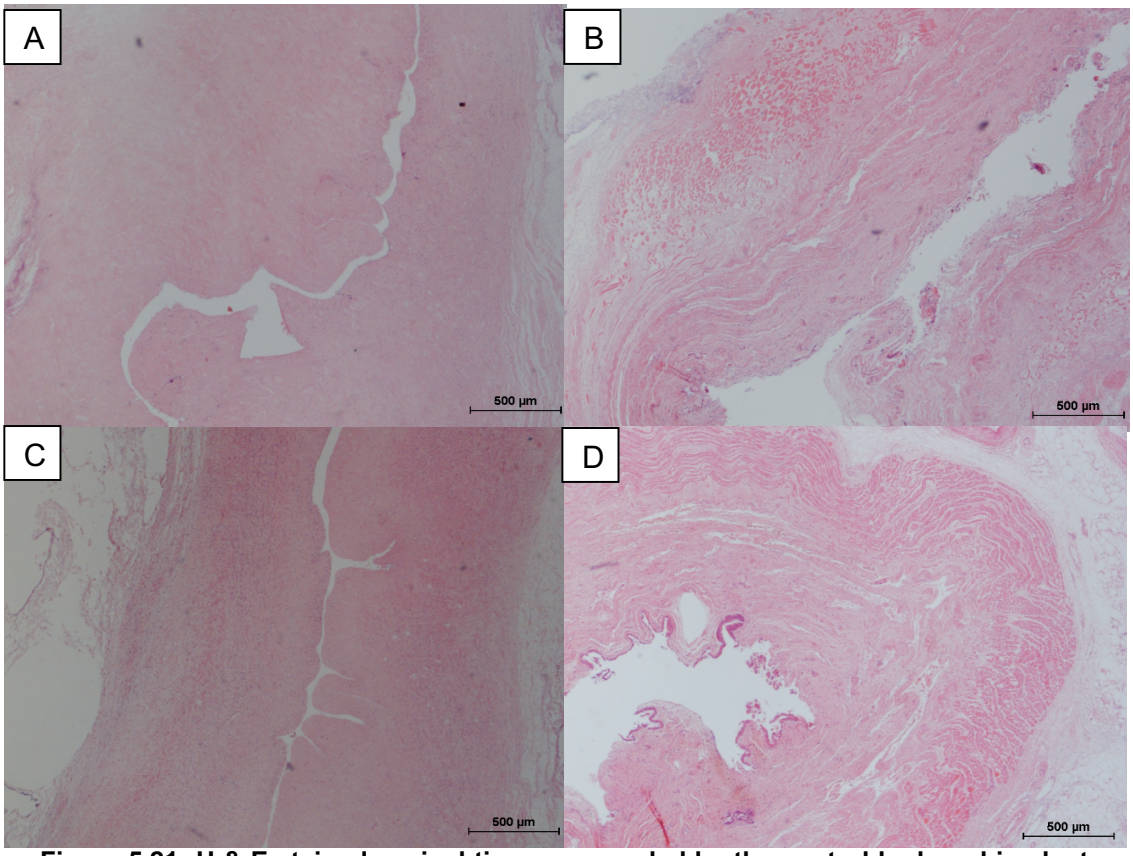


**Figure 5.21: H & E-stained vaginal tissue, expanded by the control hydrogel implants via in vitro organ bath expansion. 40x magnification. A** is tissue obtained from the proximal end of 'tissue number 7' and **B** is the distal end of the same tissue. **C** and **D** are of 'tissue number 8', with **C** showing proximal vaginal tissue and **D** showing distal tissue.

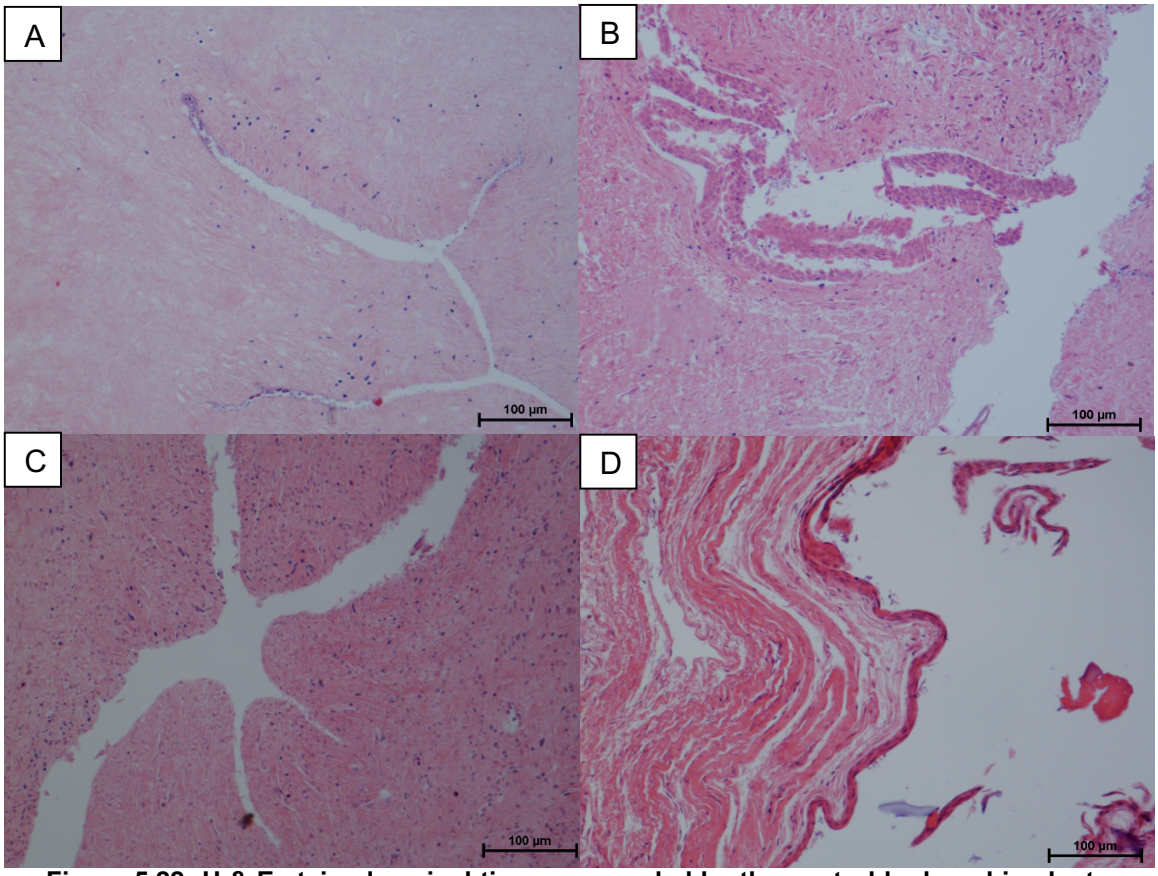


**Figure 5.22: H & E-stained vaginal tissue, expanded by the control hydrogel implants via in vitro organ bath expansion**. **200x magnification. A** is tissue obtained from the proximal end of 'tissue number 7' and **B** is the distal end of the same tissue. **C** and **D** are of 'tissue number 8', with **C** showing proximal vaginal tissue and **D** showing distal tissue.

Figure 5.22 shows the control hydrogel tissue at a higher magnification, 200x. This enhanced imaging shows the presence of some epithelial cells, particularly image B and D, image B shows the reduced adhesion between the epithelium and underlying mesenchymal tissue. Epithelial cells in image B are only present in a crevice of the tissue. The eosinophilic appearance of the tissue can be seen more clearly in image D. The epithelium present in this image is still in contact with the mesenchyme, but detached epithelium can also be seen within the image frame.

## 5.4 Discussions

The in vitro organ bath tissue expansion experiments had multiple objectives.

The first objective of the trials was to assess the ease of implantation of the hydrogel tissue expanders developed in chapter 3. This focused on the ability to implant the expanders into the porcine vagina, without causing damage to the urogenital tract and ensuring correct positioning of the implant i.e., not placing the hydrogel into the urethra of the animal. The use of instruments to aid implantation was also investigated. Earlier stages of the project included the discussions of the use of a paediatric ureteroscope to ensure the correct positioning of the implants and the possible requirement for a small dilator to be used to push the implant further along the tract, ensuring it passed the ureter opening within the urogenital tract.

The next objective of this trial was to investigate the ability of vaginal tissue to withstand the pressure enforced by the expanding hydrogels. Previous trials resulted in perforations of vaginal tissue after 24 hours occurring due to implantation of oversized hydrogels and too rapid expansion, both radially and longitudinally.

The final objective of this in vitro expansion experiment was to access if histological analysis of the tissue, post-expansion, would reveal any unexpected trauma or damage to the tissue that would need to be addressed before adapting the trial for in vivo use.

The most effective hydrogel implant design was also trialled in the second implantation. Both a simple quincke ended solid hydrogel and a hollow cylinder with a solid tapered tip were inserted into the vagina of the pig. The insertion

ability, vaginal tissue integrity and histological analysis of these two implant designs, as well as a control, were assessed in this experiment.

### 5.4.1 First In Vitro Implantation of Hydrogels

In preparation for the first in vitro implantation of hydrogels into porcine vaginal tissue, hydrogels with thicker walls were synthesised. Consultations at the beginning of the project had led to solid implants being more desirable. However, the multiple complications, as discussed previously that arose from attempts to produce a solid hydrogel meant that a modified hollow cylinder was the most suitable alternative. The increase in wall thickness was designed to improve the integrity of the implants as they take on water and expand.

Two of these hydrogels were implanted into the vaginal lumen of porcine cadavers whilst the organ was in situ. This allowed for the assessment of ease of implantation, noting whether the hydrogels needed assisted insertion (dilators of a similar diameter to the hydrogels were available) and if the implants reached the cervix of the animal without having to make an incision. Once the implants were in place, the urogenital tract of the animals were removed, allowing for the impact of implant insertion to be evaluated as well as securing the implant within the vagina lumen. This implantation investigation gave valuable results. The implants were difficult to insert into the vaginal lumen and on observation, once removed from the animal, one of the tracts had torn. The size of the implants was too large to allow for simple implantation. The diameter of the implants had been decided based on an earlier porcine growth experiment, with the aim of the implant to fill the whole

lumen and exert sufficient pressure to cause tissue expansion. It appeared that the hydrogel used in this trial were slightly over sized and not only was insertion difficult, but damage to the tissue may have been caused. The tear observed on one of the urogenital tracts may have arisen from forcing the hydrogel into the tract blindly, or from removal of the tract from the cadaver. The damage caused may have also been due to the design of the implant. The implants inserted has blunt, circular ends, this incorporated with the rigidity of the cured hydrogel may have caught on the tissue during insertion, causing it to tear.

Once removed from the cadaver, the torn urogenital tract was stitched up and the hydrogel repositioned and held within the tract with a ligature stitch at the perineal opening. The second implant had not caused damage to the vaginal organ and again, a ligature stitch was required to hold it within the tract.

The problems that occurred just during the insertion of these hydrogel implants made it clear that adjustments to the design and dimensions was imperative. It was obvious that a smaller diameter design would be required for future trials and the possibility of altering the shape of the end of the hydrogel being inserted first was discussed. The addition of a narrower end, possibly shaped like a pencil tip or a needle quincke was thought to be the simplest way to improve the insertion of the hydrogels.

The urogenital tracts, containing hydrogels, were placed into DMEM tissue culture media and kept refrigerated for 2 weeks, with observations taken throughout this time. After 24 hours, substantial expansion had taken place, with the tissue clearly stretched over the hydrogel. Once 4 days of expansion

had elapsed, both hydrogels had perforated the urogenital tissue containing them. Surprisingly, the sutures that had been placed to repair the torn tissue before implant insertion had successfully held the tissue together and the implant had ruptured on the opposite side of the lumen. This result solidified the fact that smaller implants will be required for future trials.

### 5.4.2 Implantation Method of Second Hydrogel Implantation Trial

Insertion of the hydrogel implants provided very little complications. The designs of the implants, quincke tips and tapered tips, aided their insertion. The implants were able to be placed into the urogenital tracts without the aid of any surgical instruments. Removal of the entire tract after implantation confirmed this.

Each implant could be seen correctly placed in the vagina, with the end of the hydrogel contacting the cervix and the point of confluence between the urethra and urogenital sinus being below the base of the implant. With the implantation of the hydrogels being successful when practised in porcine cadavers, it is possible that this method can be used for future in vivo vaginal tissue expansion trials. The implants were inserted as if conducting an in vivo trial, i.e., no incisions into the animals were made until it was believed that the implants were in the correct position. This resulted in accurate implantation without any damage being caused to the urogenital tract, on each insertion.

### 5.4.3 Expansion of Vaginal Tissue

In general, the vaginal tissue had remained intact for the duration of the in vitro tissue expansion trial. The majority of ruptures caused by the hydrogels occurred at the entrance of the vaginal lumen. It is most likely that damage occurred due to the trauma of tightly tying suture material around the tissue, to hold the implant in place.

The starting dimensions of the implants, ~38mm x ~7mm, were appropriate for the age and size of porcine cadavers used and the rate of expansion appeared to be well tolerated by the tissue when in the organ baths.

### 5.4.4 Histology

The haematoxylin and eosin staining of the tissue samples collected from the in vitro expansion trial resulted in two prominent observations: the hypereosinophilic appearance of the tissue and the lack of single cell epithelia within the lumen of the tissue.

The reddening of the tissue, hypereosinophilia, is a normal observation when tissue is beginning to undergo post-mortem changes. The nutrition provided by the organ baths that the expanding tissues were kept in was evidently insufficient to maintain the integrity of the tissue on a histological level. This explains why the nuclei in some of the images of the tissues cannot be easily differentiated and may have contributed to the sloughing of epithelial cells from their underlying mesenchyme.

The closing of the vaginal lumen, to retain the hydrogel within the organ, may also have contributed to the epithelium beginning to undergo autolysis. Contact between the hydrogel and the epithelium could have impacted the adherence of the epithelium, restricting the organ bath media supply to the lumen of the tissue. Tying off of the vaginal lumen will had hindered the removal of waste media from the organ, limiting its replenishment. A combination of this and the physical removal of the hydrogels from the vaginal lumens will have resulted in only remnants of epithelium cells remaining.

The histological analysis of vaginal tissue from this expansion trial and previous characterisation of vaginal tissue have shown smooth muscle is a major component of the organ. This, alongside the nature of the tissue show that the vagina is adapted to be able to withstand some levels of trauma, as would be expected during copulation. When sufficient sustenance is provided, the tissue, including the epithelium, is more resilient to mechanical trauma. It is believed that the epitheliums adherence to the vaginal lumen will be much more stable with in vivo expansion, and therefore removal of the hydrogel implants will be well tolerated.

One of the most significant disadvantages of histological analysis of in vitro tissue samples is the inability to detect if inflammation of the tissue has occurred. Samples of fresh tissue would show an infiltration of lymphocytes is this was the case. Only an in vivo tissue expansion trial would allow for this.

# 6 Conclusions and Further Work

## 6.1 Conclusions

The research and work conducted throughout this project has ultimately resulted in the development of a self-inflating tissue expander for potential use in minimally invasive cloacal repair operations.

The suitability of a porcine model for cloacal malformations in paediatric patients has been evaluated on a variety of levels. Comparisons of the macroscopic anatomy of female pigs at differing ages has shown that an animal, 8 weeks of age has the most accurate comparative anatomy to that of children at an operative age. Results have even shown that anomalies in normal anatomy can occur in healthy pigs, with one of the urogenital tract samples collected presenting with a duplex vagina, an abnormality well associated with cloacal malformations. Investigations of the histological morphology have correlated positively with human paediatric images. Both species showed an undifferentiated mesenchyme beneath their epithelium and a suitable blood supply to the organ. Though the human histology showed the vaginal epithelium to be more mature than the porcine age equivalent, this feature will be advantageous when human tissue expansion is explored in the future.

Development of a self-inflating hydrogel tissue expander has required diligence and persistence. Multiple setbacks have occurred in this area of the project, including the loss of Oxtex as an industrial partner, due to falling into administration, and the impacts of the COVIC-19 pandemic. Access to both

hydrogel resources and research facilities have been restricted, making maintaining research momentum challenging.

The original design for a hydrogel tissue expander, using Oxtex's patented technologies, revolved around the feature of anisotropic expansion. If successful, this would have resulted in a device that expanded longitudinally, with no radial expansion. Continual discussions with paediatric surgeons, with particular interests in anorectal malformations, has highlighted the potential need for multilateral vaginal tissue expansion, with the general consensus being that the more functional neotissue created, the more likely a surgical procedure is going to have a successful outcome.

The loss of Oxtex as an industrial partner has allowed for this project to be adjusted to cater for the needs of paediatric patients and their surgeons more appropriately. The collaboration that has taken place with the Centre of Additive Materials, University of Nottingham has brought an array of expertise to the project, including knowledge and understanding of the swelling properties of various hydrogel components as well as insight into inkjet and 3D printing of these materials. In vitro implantation of the resultant hydrogel tissue expanders within porcine vaginal tissue and the conduction of in vitro swelling tests within organ baths has provided vital data for future porcine in vivo expansion trials. The method of hydrogel implantation has been studied with the use of surgical instruments to aid insertion also considered. This, alongside confirmation of correct placement of the implants has demonstrated that insertion of the hydrogels can be effortlessly achieved in the porcine model. The ability for porcine vaginal tissue to withstand the pressure of intraluminal expansion in suboptimal conditions (i.e., within an organ bath) has

also been explored. The results of which have shown that the progression of this work into in vivo implantation trials should produce promising results.

## 6.2 Further Work

During the time that work for this Thesis has been conducted there have been multiple obstacles that have required overcoming in order for research to progress. Vital time was lost due to the need to develop and process an original expanding hydrogel and the restrictions put in place to control the COVID-19 pandemic.

The main area of research that I would have wished to have progressed with further during this period is the exploration of in vivo implantation of the developed hydrogels within the porcine model. In vitro trials provided imperative but limited results regarding the success of producing neovaginal tissue via intraluminal expansion. As indicated in the in vitro tissue expansion trial, porcine vaginal tissue can physically withstand the pressure exerted by the hydrogel implants. However, the organ's physiological reaction, particularly the production of lymphocytes or other evidence of inflammation, to the implantation of a foreign object as well as its possible hyperplastic response to an expanding implant can only be gauged histologically, post in vivo expansion. There are multiple elements to be considered when amending in vitro trials methods for use in vivo.

With respect to the implantation of the hydrogel devices, suitable sterilisation will be required. Gamma sterilisation of hydrogels would be convenient, safe and rapid, with the additional advantage of it being neither a heat nor moisture

regenerating process. There is a possibility that this method may result in a reduction of the rate of expansion of the hydrogel implants, due to the creation of additional crosslinks within the hydrogel polymer matrix. This would need to be considered for the in vivo experimental design and should the expansion rate reduce significantly the efficacy of alternative methods of sterilisation (i.e., dry-heat, microwave, infrared or electron beam sterilisation) will need to be explored.

There are two significant aspects of an in vivo implantation trial that will require additional preparation. The first being to devise a method of retaining the hydrogel implants within the vaginal lumen and the second being to ensure that the implants in situ do not disrupt the normal functionality of surrounding organs. In this Thesis, the method of retaining hydrogel implants within the extracted vaginal tissue involved tying a knot at the opening of the lumen with suture material. This is obviously not feasible for an in vivo trial. Insertion of the implants in porcine cadavers led to the hymenal stricture of the animal to loosen and therefore unable to retain the implant, this could also be the case in live animal implantation. There is potential for the smooth muscles of the vagina to contract in an attempt to expel the hydrogel expander and so the method of retention would need to be able to withstand this. It is also possible that the sealing of the vaginal lumen in the in vitro trials enhanced the degradation of the epithelium. It is important to ensure that the vagina is not completely sealed to allow for the flow of normal mucus production and to take into consideration a potential increase in mucus production in response to the insertion of a foreign object. The mucus produced may be absorbed by the hydrogel implants but could also begin to accumulate with the closed vagina

and contribute to the tissue expansion, similar to hydrocolpos complications. This would make it difficult to determine whether the implants alone are able to produce neovaginal tissue via self-inflating expansion.

Another complication that may arise from in vivo hydrogel implantation is the obstruction and disruption of organs surrounding the vagina. One way of overcoming this would be the insertion of a urethral catheter into the bladder of the animal. The use of cystoscope may aid the insertion of the catheter or ultrasonography to confirm its position. The catheter may also provide a mechanical barrier to retain the hydrogel implant in place, without completely sealing the organ. It is not just the insertion of the implants that may cause obstruction, but the increase in its dimensions too, particularly radial expansion of the tissue. However, the orientation of the urogenital tract in the pig means that the vagina, and subsequently its implant, lie within the abdomen in the animal and so are not contained by the solid bone structure of the pelvis. It may also be the case that when the animal urinates, the pressure of the fluid passing through the urethra will relocate the hydrogel in situ and so no obstruction will occur.

To produce thorough results from the in vivo implantation trial, samples of tissues, additional to the expanded vagina, should be collected (i.e., kidney and ureter). Analysis of these tissue can investigate the presence of ascending urinary tract infections and if obstruction has occurred, how that has impacted other urinary tract components.

# 7 Appendices

## 7.1 Project Home Office License



Home Office

PROJECT LICENCE

# Minimally Invasive Cloaca Repair Operation (MICRO): Development of a Novel Anisotropic Tissue Expander for Non-Keratinised Epithelial Tissue

## Project licence holder

David Gardner

This **PROJECT LICENCE** permits the licence holder to carry out a programme of scientific procedures on living animals under the **ANIMALS (SCIENTIFIC PROCEDURES) ACT 1986**.

The project licence holder may carry out the specified programme of work, subject to the restrictions and provisions contained within the Act and any limitations and conditions specified within this licence or by the Secretary of State.

This licence does not authorise the holder or any other person to carry out procedures on any animals unless they hold an appropriate personal licence issued under the Act.

## Granted authority

This licence has been granted based on the information provided during the application process.

This licence authorises, only:

- work to meet the specified project aims
- use of specified animals and procedures
- work at the specified places

## 7.2 In-House Expander Experiments with Oxtex Supplies

### 7.2.1 Methodology

Before investigating the customisation of a hydrogel expander, we measured the rate of the hydrogel rods independently. All the hydrogel rods tested doubled in size within 24 hours. We purchased our own supply of MED4211 silicone, from the same suppliers that Oxtex used, and attempted to create our own self inflating hydrogel devices. We placed the uncrushed hydrogel rods in the silicone casings, both provided by Oxtex, and used the silicone to ‘cap’ the casing. The device was then cured at 40°C for 24 hours. The custom-made expander was placed in a water bath in the same conditions as the experiment described earlier in the chapter.

Another method of utilising the Oxtex products provided was to ‘stitch’ two silicone incased hydrogel rods. A few days into the trial we added holes to the ends of the silicone casings in order to aid water intake and expansion.

### 7.2.2 Results

Development of our own self inflating expanders, via the use of uncrushed hydrogel rods in the silicone casings, both provided by Otex, and MED4211 silicone to ‘cap’ the casing was unproductive. The hydrogel ruptured through the silicone cap within 24 hours of expansion.

The method of ‘stitching’ two silicone incased hydrogel rods together to created a longer starting expander was also unsuccessful. Initially, the

hydrogels were exposed to insufficient water and so expansion did not take place. To overcome this, we added holes to the ends of the silicone casings. This led to a vast increase in hydrogel dimensions and again, the hydrogels ruptured from the silicone casing.

## 7.3 Formulation M Printability Test

### 7.3.1 Sample Print 1

10ml of formulation M were made to test its eligibility for printing the BMF nanoArch S130 3D printer. Ink synthesised for use in this printer generally require the addition of curcumin (the main active ingredient in turmeric) to act as a photoabsorber. Curcumin was initially added at 1% concentration. The following concentrations were used:

| PLA% (w/w) | PEGDA% (w/w) | Acrylic Acid% (w/w) | DMPA% (w/w) | Curcumin% (w/w) |
|---|---|---|---|---|
| 0.5% | 0.5% | 99% | 1% | 1% |
| 0.05g/50µg | 0.05ml/50µl | 9.9ml | 0.1g/100µg | 0.1g/100µg |

**Table 7.1: Concentrations of PLA, PEGDA, Acrylic Acid, DMPA and Curcumin used in the first sample print.**

For the first test print the following printer setting were used:

- **Intensity – 87%**
- **Exposure – 0.5 x 4 and 2.7 x 4**

The intensity was selected as previous formulation testing has shown that the acrylic acid component of the ink can be very reactive under UV light. The ink formulation did not cure when these printer settings were used. It was decided that a higher intensity and exposure may be required.

### 7.3.2 Sample Print 2

For the second sample print 10ml of formulation M was used with the same concentration of curcumin as sample print 1 (1%).

The following printer settings were used:

- **Intensity – 147%**
- **Exposure – 0.5 x 8 and 2.7 x 8**

The ink formulation did not cure when these printer settings were used. It was decided that the concentration of curcumin in the formulation may to too high.

### 7.3.3 Sample Print 3

The third sample print required 10ml of formulation M with curcumin added at 0.5%. The following concentrations were used:

| PLA % (w/w) | PEGDA % (w/w) | Acrylic Acid % (w/w) | DMPA % (w/w) | Curcumin % (w/w) |
|---|---|---|---|---|
| 0.5% | 0.5% | 99% | 1% | 0.5% |
| 0.05g/50µg | 0.05ml/50µl | 9.9ml | 0.1g/100µg | 0.05g/50µg |

**Table 7.2: Concentrations of PLA, PEGDA, Acrylic Acid, DMPA and Curcumin used in the third sample print.**

The following printer setting were used for sample print 3:

- **Intensity – 147%**
- **Exposure – 0.5 x 8 and 2.7 x 8**

The ink formulation appeared to have cured to the printer platform and so the next stage was to try to print a more complex structure.

### 7.3.4 Lattice Print Test

With the initial sample print of formulation M appearing to have been successful. The ability for the ink to be able to form a more complex structure needed to be tested. The formation of a lattice structure was tested. The same concentrations used in sample print 3 were used to test the lattice formation.

The following printer settings were used:

- **Intensity – 150%**
- **Expected model height – 1.990mm**

The ink formulation appeared to be very stable before printing. However, after printing the ink became black and unstable, this may have been due to the reaction with the UV light.

The lattice structure did not adhere to the printer platform, but an initial yellow pattern was seen on the printer film. It is thought that the ink formulation contained too much photoabsorber for it to cure successfully.

### 7.3.5 Sample Print 4

A final sample print of formulation M was tested. This time no curcumin was added to the formulation.

The following concentrations were used:

| PLA % (w/w) | PEGDA % (w/w) | Acrylic Acid % (w/w) | DMPA % (w/w) | Curcumin % (w/w) |
|---|---|---|---|---|
| 0.5% | 0.5% | 99% | 1% | - |
| 0.05g/50µg | 0.05ml/50µl | 9.9ml | 0.1g/100µg | - |

**Table 7.3: Concentrations of PLA, PEGDA, Acrylic Acid, DMPA and Curcumin used in the fourth sample print.**

The following printer settings were used for sample print 4:

- **Intensity – 150%**
- **Exposure – 0.5 x 4 and 2.7 x 4**

No ink cured in the BMF nanoArch S130 3D printer with these settings applied.

## 7.4 Sodium Bicarbonate Neutralisation of Acrylic Acid in Formulation M Hydrogel

### 7.4.110% Sodium Bicarbonate Neutralisation

It was believed that increasing the pH of hydrogel formulation M would reduce its reactivity with the Form 1+ 3D printer resin tank and platform.

An increase in pH could be achieved by neutralising the acrylic acid component of the hydrogel.

The addition of saturated sodium bicarbonate ($NaCHO_3$) was added to 10ml of formulation M in the following concentration:

| PLA % (w/w) | PEGDA % (w/w) | Acrylic Acid % (w/w) | $NCHO_3$ % (w/w) | Irgacure 819 % (w/w) |
|---|---|---|---|---|
| 0.5% | 0.5% | 99% | 10% | 1% |
| 50µg | 50µl | 8.9ml | 1ml | 0.1g |

**Table 7.4: Concentrations of PLA, PEGDA, acrylic acid, saturated sodium bicarbonate and Irgacure 819 used in the 10% sodium bicarbonate neutralisation formulation.**

Varying amounts of the neutralised hydrogel formula were pipetted into different volume vessels and its UV curing ability was tested.

First, 150µl of the hydrogel was pipetted into the lid of a small (2ml) vial. The contents were placed under the 380 – 420nm UV lamp for 5 minutes. No curing occurred.

Next, 450µl of the hydrogel was pipetted into the lid of a larger (20ml) vial. Again, the contents were placed under the UV lamp for 5 minutes. No curing occurred. Finally, 47µl of the hydrogel was pipetted into Plastic tubing with an

inner diameter of ~2mm and 10mm in length. The tubing and hydrogel were placed under the UV lamp for 5 minutes. No curing occurred. It was believed that the concentration of $NaCHO_3$ was too high and was impacting on the hydrogels ability to cure und UV light.

### 7.4.2 5% Sodium Bicarbonate Neutralisation

The addition of sodium bicarbonate to 10ml of formulation M was in the following concentration:

| PLA % (w/w) | PEGDA % (w/w) | Acrylic Acid % (w/w) | $NaCHO_3$ % (w/w) | Irgacure 819 % (w/w) |
|---|---|---|---|---|
| 0.5% | 0.5% | 99% | 5% | 1% |
| 50µg | 50µl | 9.4ml | 0.5ml | 0.1g |

**Table 7.5: Concentrations of PLA, PEGDA, acrylic acid, saturated sodium bicarbonate and Irgacure 819 used in the 5% sodium bicarbonate neutralisation formulation.**

150µl of the hydrogel was pipetted into the lid of a small (2ml) vial. The contents was placed under the 380 – 420nm UV lamp for 5 minutes. No curing occurred. Then, 47µl of the hydrogel was pipetted into Plastic tubing with an inner diameter of ~2mm and 10mm in length. The tubing and hydrogel were placed under the UV lamp for 5 minutes. No curing occurred.

### 7.4.3 2.5% Sodium Bicarbonate Neutralisation

5ml of formulation M was made up, with the addition of $NaCHO_3$in the following concentration:

| PLA % (w/w) | PEGDA % (w/w) | Acrylic Acid % (w/w) | $NaCHO_3$ % (w/w) | Irgacure 819 % (w/w) |
|---|---|---|---|---|
| 0.5% | 0.5% | 99% | 2.5% | 1% |
| 25µg | 25µl | 4.825ml | 0.175ml | 0.05g |

**Table 7.6: Concentrations of PLA, PEGDA, acrylic acid, saturated sodium bicarbonate and Irgacure 819 used in the 2.5% sodium bicarbonate neutralisation formulation.**

The hydrogel was pipetted into the lid of a small (2ml) vial, volume of 150µl. This was placed under the 380-420nm UV lamp for 5 minutes. No curing occurred. It appeared that the presence of $NaCHO_3$ in the hydrogel formula was interfering with its ability to cure.

## 7.5 Production of Formulation R Hydrogels via Casting with Moulds

### 7.5.13D Printing of Moulds Methodology

Moulds for the curing of hydrogel formulation R were designed and printed. The resin used for the moulds was Formlabs 1+ standard resin and the design was printed on a Formlabs 1+ 3D printer. The printer automatically selected suitable operating logic parameters for the standard resin.

The moulds were designed to be able to produce a hydrogel rod with the dimension of 40mm x 8mm. A cylinder, 45mm in length and 12mm overall diameter with an 40mm x 8mm deep, face centred extruded cut was designed. The volume of the moulds was 2.01ml.

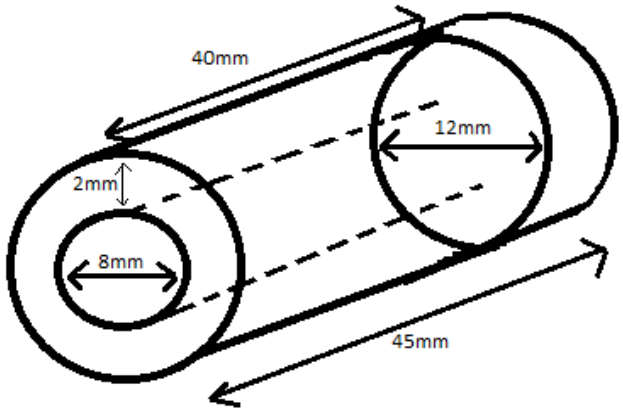


**Figure 7.1: Dimensions of the 3D printed moulds designed to produce a 40mm x 8mm rod.**

The supports created during the printing process were removed and the mould were washed in the formlabs IPA washing machine for 10 minutes. The moulds were them washed in an ultrasonic cleaner, in a beaker of IPA, for a further 5 minutes.

## 7.5.2 3D Printing of Moulds Results

The images below show the moulds that were printed on the Formlabs 1+ 3D

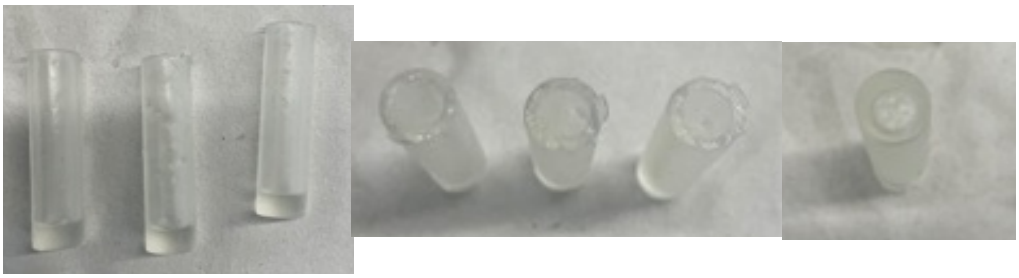

**Figure 7.2: 3D printed moulds for producing hydrogels 40mm x 8mm in dimension.**
printer.

## 7.5.3 Synthesis of Hydrogel R within 3D Printed Moulds

### Methodology

8ml of formulation R was made up using the following volumes:

| PLA % (w/w) | PEGDA % (w/w) | Acrylic Acid % (w/w) | HEA % (w/w) | Irgacure 819 % (w/w) |
|---|---|---|---|---|
| 0.5% | 0.5% | 49% | 49% | 1% |

**Table 7.7: Concentrations of PLA, PEGDA, acrylic acid, HEA and Irgacure 819 used in formulation R.**

The moulds were filled with 2ml of hydrogel R and cured under the 380-420nm

UV lamp.

### 7.5.4 Synthesis of Hydrogel R within 3D Printed Moulds

#### Results

Mould (A) was filled to the brim with hydrogel resin and put in a tabletop UV lamp box, with the UV lamp clamped in position (around 10cm away from the mould and hydrogel). The hydrogel cured in a total of 30 seconds. The resin at the open end of the mould bubbled over the end slightly, making it difficult to distinguish between the mould and the hydrogel.

Mould (B) was filled ‘almost’ to the brim, space to allow for bubbling was left. The mould was put in a larger UV protection box, allowing the UV lamp to be positioned at a further distance from the mould. On curing, the hydrogel shrunk within the mould and took 3 minutes to completely cure.

Mould C appeared to leak when filled with hydrogel resin and so some of the resin pooled before the mould was placed under the UV lamp. The ‘pool’ of resin cured before the contents of the mould did, the solid external hydrogel was removed, and the curing process was continued. Curing took over 5 minutes.

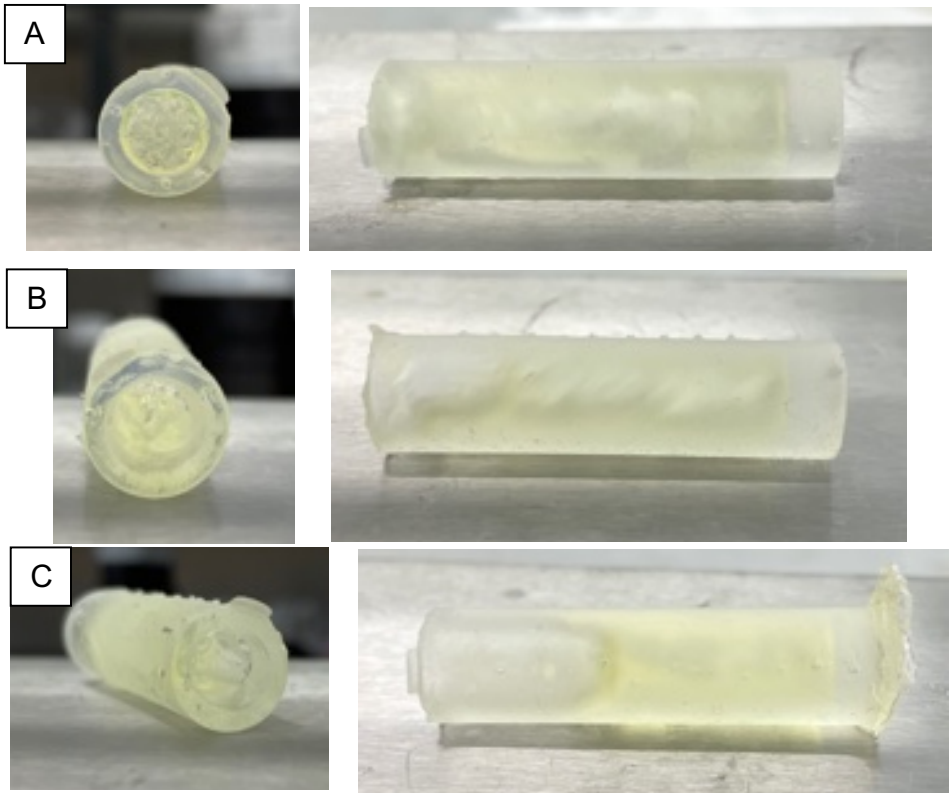


**Figure 7.3: Moulds A, B and C containing cured hydrogel resin.**

### 7.5.5 Removal of Solid Hydrogel R from 3D Printed Moulds Methodology

Removal of hydrogel R from the 3D printed moulds was difficult. The following methods were tried:

A – Mould A was ground away from the hydrogel using course sandpaper. It was difficult to distinguish between the hydrogel and the mould, and therefore to know when to stop sanding.

B – Again, this mould was ground down with sandpaper. However, the hydrogel snapped whilst trying to remove it. It appeared that the hydrogel had not fully cured in the centre.

C – The hydrogel had sunk so far into the mould that neither snapping nor grinding of the mould would release the hydrogel.

### 7.5.6 Removal of Solid Hydrogel R from 3D Printed Moulds Results

Removal of hydrogel R from the 3D printed moulds was difficult. The moulds were too hard and thick to be cut to reveal the hydrogel.

It appeared that the hydrogel and 3D printed mould had annealed to one another during the UV curing of the hydrogel resin.

The images below show the resultant hydrogels removed from 3D printed moulds A and B.

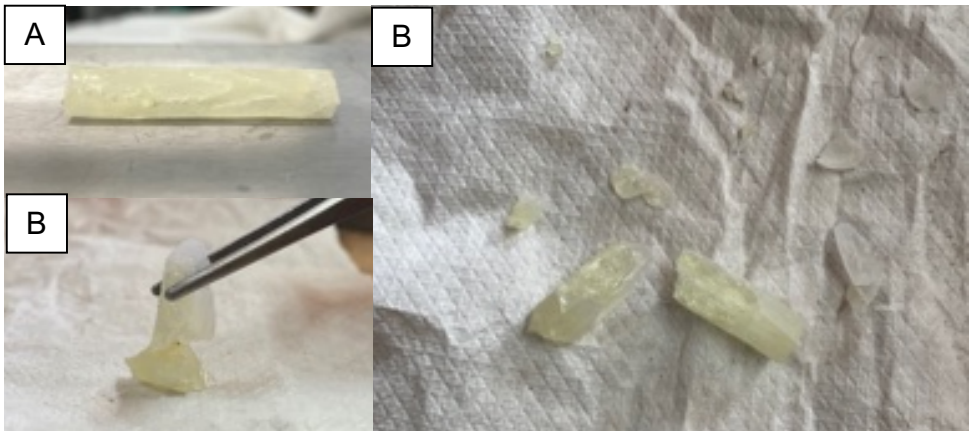


**Figure 7.4: Removal of hydrogels (R formulations) from 3D printed moulds A and B.** Mould A was ground away from the hydrogel and both hydrogel and mould B snapped during attempted removal.

## 7.6 Production of Formulation U Hydrogels via Casting with Moulds

### 7.6.13D Printing of Moulds Methodology

Moulds for the curing of hydrogel formulation U were designed and printed. The resin used for the moulds was Formlabs 2 standard resin and the design was printed on a Formlabs 2 3D printer. The printer automatically selected suitable operating logic parameters for the standard resin.

The moulds were designed to be able to produce a hydrogel rod with the dimension of 40mm x 8mm. A cylinder, 45mm in length and 12mm overall diameter with an 40mm x 8mm deep, face centred extruded cut was designed. The volume of the moulds was 2.01ml.

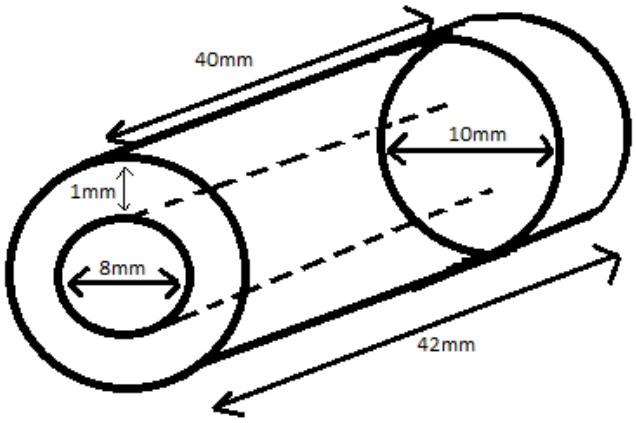


**Figure 7.5: Dimensions of the thinner walled 3D printed moulds designed to produce a 40mm x 8mm rod.**

The supports created during the printing process were removed and the mould were washed in the formlabs IPA washing machine for 10 minutes. The

moulds were them washed in an ultrasonic cleaner, in a beaker of IPA, for a further 5 minutes.

### 7.6.23D Printing of Moulds Results

Moulds for curing hydrogel U formulation were printed. These moulds had walls with a thickness of 1mm.

**Figure 7.6: 3D printed moulds with thinner walls.** The supports and the base of the supports were removed from the mould and IPA washing took place.

### 7.6.3 Synthesis of Hydrogel U within 3D Printed Moulds

5ml of Formulation U was made up. The moulds were filled with 2ml of hydrogel U and cured under the 380-420nm UV lamp, for 5 minutes, with the lamp 15 – 20cm away from the mould.

### 7.6.4 Removal of Solid Hydrogel U from 3D Printed Moulds Methodology

Removal of hydrogel U from the thinner 3D printed moulds was again difficult.

Mould D was ground down with sandpaper.

Removal from mould E, was attempted by trying to cut away the bottom of the mould and then scoring the sides of the mould to try to release the hydrogel. The mould was too brittle and bound to the hydrogel too strongly to be removed and the hydrogel still be useable.

### 7.6.5 Removal of Hydrogel U from 3D Printed Moulds

#### Results

As in part 4.3.3.25.3, the removal of the cured hydrogels from their 3D printed moulds proved to be difficult. Both methods of grinding with sandpaper and

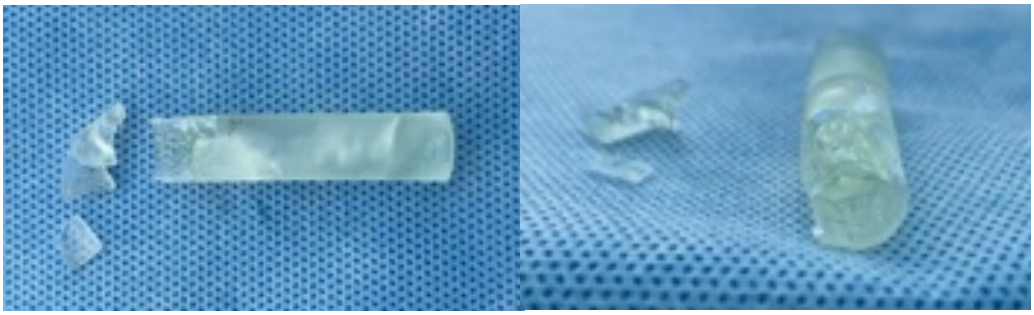

**Figure 7.7: Attempted removal of cured U formulation hydrogel from thinner walled 3D printed moulds.** The images show the attempt to cut away the mould from the hydrogel. The mould was too brittle and bound to the hydrogel too strongly to be removed and the hydrogel still be useable.

cutting and scoring of the moulds were used. The moulds were too brittle and had bound to the hydrogel too strongly when curing to be removed and the hydrogel still be useable.

## 7.7 Production of Silicone Moulds for Hydrogels

### 7.7.1 Prototype 2 Methodology

Initial filling of the 3D printed mould involved injecting Nusil MED4211 silicone into the mould, using the application gun and premixing nozzle. The nozzle of the application gun was too wide to force silicone to fill the whole of the mould, the silicone did not reach the base of the mould. The mould and silicone were left to access the setting time of the silicone. The silicone took over 48 hours to set. For the second attempt of filling the 3D mould with silicone, a pipette tip was added to the mixing nozzle, this allowed the silicone to fil the base of the mould first when being injected. The silicone and the mould were left for 48 hours at 37°C.

### 7.7.2 Prototype 2 Results

Moulds to produce a hydrogel rod from a silicone mould were 3D printed with Formlabs 1+ standard resin.

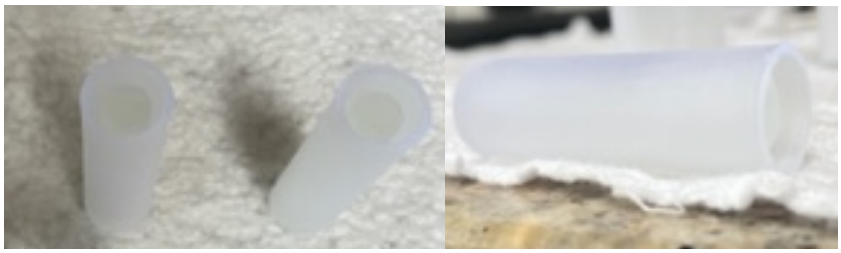

**Figure 7.8: 3D printed moulds that were produced to make the silicone moulds for the hydrogels more accurate.**

The Nusil MED4211 silicone had set solid. Removal of the silicone from its resin mould was difficult. When trying to remove the silicone, the capped end tore away, and the side of the resin mould had to be broken to release the

remaining silicone. The rigidity and brittleness of the resin printed mould was not compatible with the creation of a silicone mould for hydrogel synthesis.

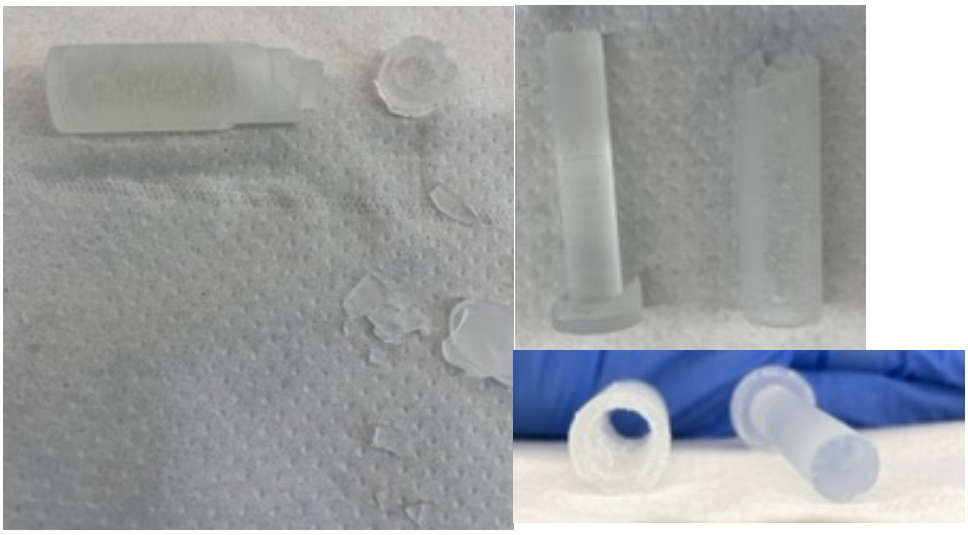

**Figure 7.9: Attempted removal of silicone from the 3D printed moulds.**

### 7.7.3 Prototype 3 Methodology

Another prototype mould for the producing a silicone mould for hydrogels was constructed using a smooth tube, corrugated plastic tubing and duct tape, like the mould assembled previously. An alternative silicone was used. Building sealing silicone sets solid on exposure to air. Unlike the Nusil silicone, it is a single component, with no mixing required. One end of the corrugated tubing was sealed with duct tape and the building sealant silicone was injected into the tube. The smaller, smooth tubing was pushed into the silicone to create an extruded cylinder. Cocktail sticks were pushed through the smooth tubing to prevent it from dropping too far into the silicone, allowing the mould to have a capped end.

### 7.7.4 Prototype 3 Results

After 48 hours the building sealant silicone had not cured. It is believed that this was due to the lack of exposure to oxygen, the air.

**Figure 7.10: Attempt at making silicone moulds for hydrogels from building sealant silicone.**

### 7.7.5 Prototype 4 Methodology

A mould for the silicone was constructed using a similar technique to those previously described. This involved using the corrugated tubing for the external walls of the mould, the smooth plastic tubing to create the lumen of the mould. Duct tape was used to seal one end of the mould and an elastic band was placed around the mould, vertically, to secure the smooth tubing in place once the silicone had been added. The silicone Mold Max™ 10T was prepared with the following method:

Mix the individual parts, part A and part B, in their containers before measuring out the components.

Dispense the required amount of part A and part B into a mixing container and mix for 3 minutes. For this trial, 40g of part A and 40ml of part B were used.

The mixture was then poured into the moulds and left to set. After 1 hour, the silicone had started to leak from the moulds. The silicone has compromised the duct tape, so that the bas of the mould was no longer sealed. An alternative method for sealing the base was required.

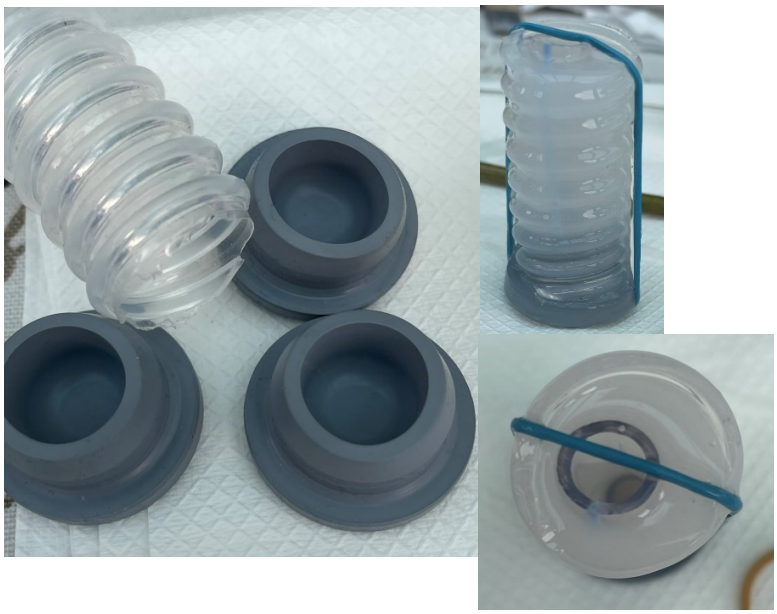

**Figure 7.11: Corrugated tubing and rubber caps used to produce moulds for silicone and the moulds containing liquid silicone that had not been degassed.**

A plug-like plastic bottle cap, with an inner diameter that matched the inner diameter of the corrugated plastic tubing was found. Pushing this cap into the tubing provided an effective seal. New moulds were made using the corrugated tubing, the smooth tubing and the plastic cap. The silicone had yet to set and so was poured into the amended moulds. The elastic bands were position vertically around the mould to hold the smooth tubing in place. After 1 hour, there was no leakage of silicone and so the mould and silicone were left to set overnight at room temperature.

### 7.7.6 Prototype 4 Results

After 24 hours the Mold Max™ 10T silicone had cured solid. The silicone came away from its mould with ease. The components of the mould had been unaffected by the curing of the silicone and were cleaned up for repeated use, if required. The shape of the base of the mould gave the base of the silicone a narrower diameter.

**Figure 7.12: Plastic mould containing silicone and the individual components of the mould alongside the silicone mould.**

### 7.7.7 Prototype 6 Methodology

220ml of Mold Max™ 10T silicone was prepared. A mould for the silicone was constructed using corrugated plastic tubing, smooth silicone tubing and plastic caps. The smooth silicone tubing had the following dimensions:

- **Internal diameter = 4.5mm**
- **External diameter = 9.5mm**

4 moulds were made in total. Two of the moulds were designed to produce hollow cylindrical hydrogels with flat, blunt ends. The remaining two were designed to produce hollow cylindrical hydrogels with tapered ends. The silicone was poured into the moulds and left at room temperature overnight.

This method was repeated, using smooth plastic tubing for the internal component. The smooth plastic tubing had the following dimensions:

- **Internal diameter = 4 mm**
- **External diameter = 9 mm**

4 moulds with this design were produced. The silicone was poured into the moulds and left at room temperature overnight to set. The silicone mould had set hard and both the corrugated and smooth plastic tubing were removed with ease.

### 7.7.8 Prototype 6 Results

The silicone had set hard and was easily removed from the external corrugated plastic tubing. However, the silicone inner tubing had fused with the Mold Max™ 10T silicone during the setting process and two could not be distinguished.

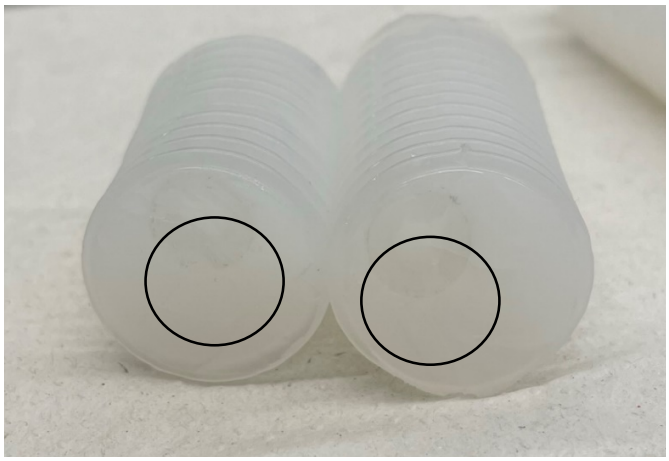

**Figure 7.13: Silicone moulds made to produce hydrogels with thinner walls.** The use of a silicone material as the inner tubing led to the fusing of the liquid silicone with the inner tubing. The circles on the image are surrounding the silicone inner tubing within the set Mold Max™ 10T silicone. It is difficult to distinguish between the two on the image.

### 7.7.9 Prototype 7 Methodology

110ml of Mold Max™ 10T silicone was prepared.

Four moulds were constructed in total. Two moulds were designed to produce solid cylindrical hydrogels with quincke ends. Two moulds were designed to produce hollow cylindrical hydrogels with solid tapered ends.

The moulds designed to produce hollow cylindrical hydrogels with solid tapered end were constructed by attaching small eppendorfs to the small, smooth plastic tubing. The tip of the eppendorf was filled with Blutac to ensure that a solid tip would be produced and the wider cap end of the eppendorf was removed to create a smoother shape to the join between it and the plastic tubing.

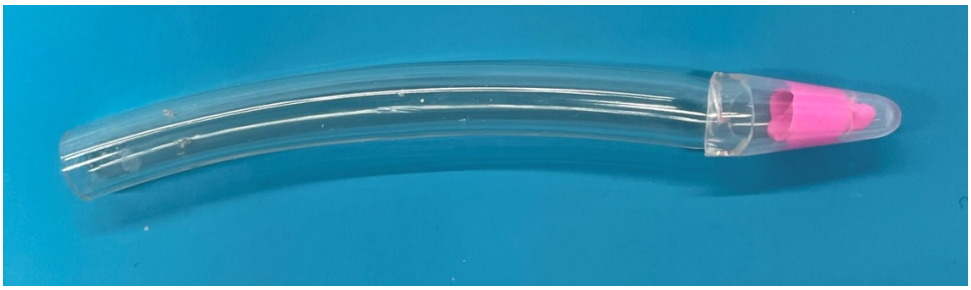

**Figure 7.14: Shape of hollow cylindrical hydrogels with solid tapered ends.**

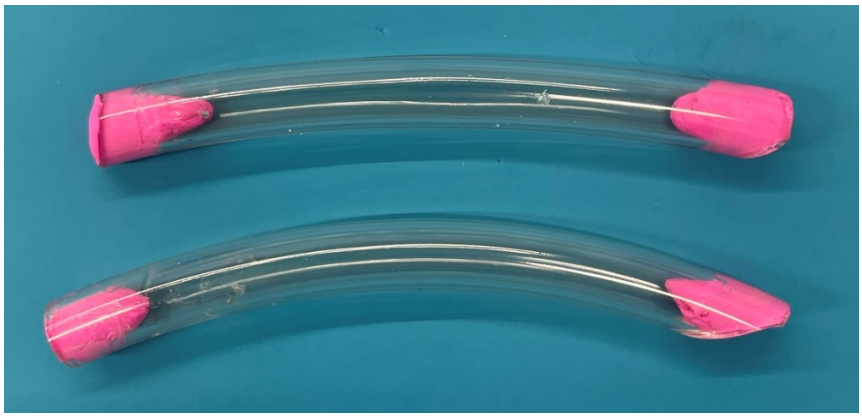

**Figure 7.15: Shape of solid hydrogels with quincke ends.**

The moulds designed to produce solid cylindrical hydrogels with quincke ends were constructed by plugging the ends of the tube with Blutac, ensuring that it was flush with the edges of the tube. Preventing the silicone from filling the tube would create a solid hydrogel.

The silicone was poured into the moulds. The moulds for solid hydrogels had the non-quincke tip protruding from the silicone. The plastic tubing and eppendorf was completely encased with silicone, with the eppendorf fixed in position at the base of the mould. Whilst filling the moulds, air bubbles rose within the silicone, with the majority dissipating once reaching the surface.

**Figure 7.16: Moulds used to produce silicone moulds for hollow cylindrical hydrogels with solid tapered ends.**

The silicone had set overnight.

The exterior and interior tubing that formed the mould for the solid cylindrical hydrogel, with a quincke end, were easily removed.

The exterior plastic tubing of the solid ended hollow mould was easily removed. To remove the inner tubing, the narrower end of the silicone was cut away until the eppendorf could be seen through the silicone. A small hole was made in line with the eppendorf to aid its removal. The eppendorf and plastic

tubing were then pushed through the hole. The eppendorf was easily removed from the silicone, the smooth plastic tubing had to be retrieved from the silicone with tweezers. This often resulted in the extrusion coming out of the hole, the flexibility of the silicone meant that the mould could be easily manipulated to aid the removal of the plastic components.

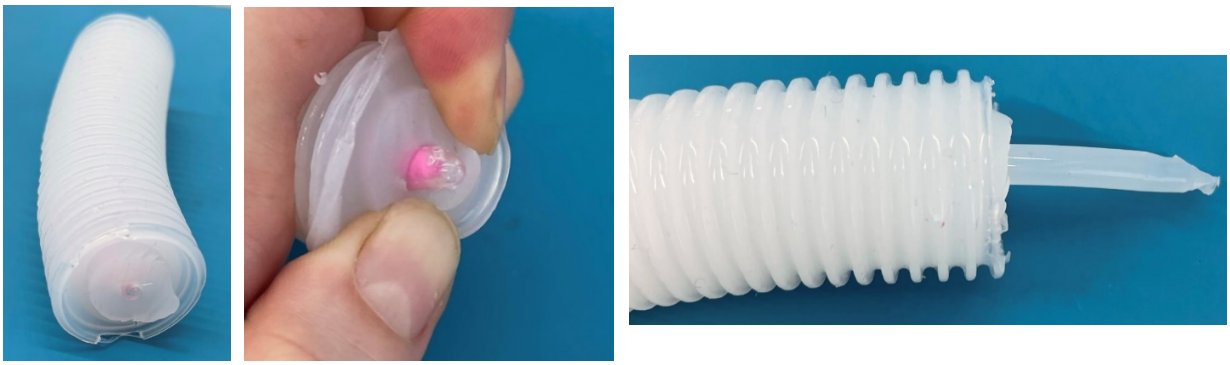

**Figure 7.17: Process of removing the inner plastic tubing from the silicone moulds.**

20ml of formulation U hydrogel was prepared.

The hydrogel resin was easily pipetted into the moulds for the solid, quincke ended hydrogels. The hydrogel was placed under the 380 – 420nm UV lamp for 4 minutes.

To fill the solid tipped hollow moulds, the inner extrusion had to be pulled through the hole and the hydrogel was pipetted into the mould until it appeared to be full. The extrusion was then replaced into the mould and any displaced hydrogel resin was removed from the surface of the mould.

Initially, the hydrogel resin leaked from the hole created by the metal wire holding the inner plastic in place. These were ‘plugged’ with the wire and Blutac to ensure that the hydrogel filled the whole of the mould.

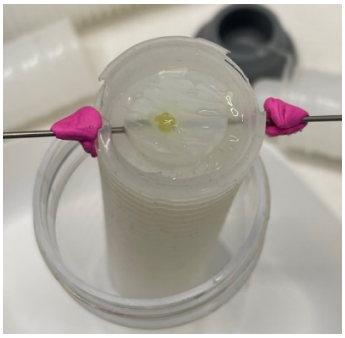

**Figure 7.18: Silicone mould, with 'Blutac' plugs, filled with hydrogel resin.**

The mould and hydrogel were placed under the UV lamp for 3 minutes.

The nature of the design of the mould meant that the positioning of the silicone extrusion could not be predicted, and this often resulted in the extrusion touching the walls of the mould, producing an incomplete hydrogel.

## 7.8 The Impact of the COVID-19 Pandemic on this Research Project

The following statement is an extract from the 'COVID-19 Impact Statement' submitted in support of an application for a funded extension of the research conducted in this Thesis.

### 7.8.1 The Impact on the Research

Prior to this application, my supervisor and I have discussed the possibility of using the money paid by my industrial partner to support my studies as a means to fund the stipend for this research extension. I can confirm that the available funds amount to £13,750, these have been untouched during my research so far. There is also sufficient funding from the BBSRC for the anticipated research expenses that will occur during the extended time period. These currently amount to £7374. This proposal has been discussed with the BBSRC team and the Research Academy Funding team who have given approval in principle for my industrial partner funding to be used in this way. I would like to be considered for a research extension of 6 months, unfunded, with the ability to use some of my industrial partner funding to fund the stipend for this period.

During the second year of my PhD research my industrial partner employed a new CEO of the company. Initially, my industrial partner had agreed to work with me on producing a hydrogel tissue expander using their patented technique. This is an integral aspect of my research and one of the main reasons that my PhD came about was down to the contractual obligation that

my industrial partners had with us to produce a tissue expander that we could use. The new CEO expressed limited interest in my research project or facilitating any possible R and D projects that it may create for them in the future. We received very little contact from my industrial partners throughout that year and it was not until September 2019 that I was informed that the company was no longer 'in a position to further support development of any of its tissue expanders' including the device that we have been working on for my PhD. Though the CEO promised that the company would offer any technical or surgical advice that we might need in order to overcome this obstacle, correspondence ceased completely, and the company entered into Administration on 1st October 2019. This set my PhD back considerably and we were left to develop a hydrogel tissue expander independently, with very little knowledge or support.

We first tried to work with the remaining equipment that was given to me when working with my industrial partner company. However, with the design that we originally wanted to develop coming under the company's patent and our lack of experience of working with hydrogel materials, these attempts were unsuccessful.

We looked into multiple tissue expander companies with the hope of being able to purchase expanders for use during my research. Though conversations were hade and details were exchanged, the majority of companies were not able to produce a custom-made design or the specifications that we required for my project could not be met.

In January 2020, my supervisor and I made enquires with the Centre for Additional Materials, based at the University of Nottingham. They had experience with working with hydrogel materials, including those for in in vivo. We met together in February and proposed a plan to start working on developing a hydrogel tissue expander at the end of March. The national lockdown issued by the government saw the laboratory facilities of the Centre for Additional Materials being closed from the end of March to the end of August. During this time all potential lab work was suspended, and I undertook a voluntary interruption of studies due to the circumstances.

Whilst working from home I tried to work on writing up my thesis and started working on some potential publications. I also tried to continue with any results analysis that could be conducted from home, this mainly included RNA sequencing interpretation. However, with all the setbacks that had occurred due to the lack of support from my industrial partner, developing a tissue expander was the only way for my PhD to progress.

The opportunity for me to start working in the lab did not arise until September 2020. As I would be working in an alternative laboratory than usual, there was health and safety admin to be processed, delaying my access to the lab until October. When working in the lab I would need to be trained and supervised initially and with the lab capacity vastly reduced due to COVID regulations, there were limited times when myself and my trainer could easily work together.

All the work that has been conducted at the Centre for Additional Materials would not have been necessary if my industrial partner had been able to

support the development of a self-inflating tissue expander, as was initially agreed.

### 7.8.2 Actions Taken to Minimise the Impact

As soon as my industrial partner showed a lack of interest in supporting my PhD project my supervisor and I looked into the possibility of using alternative tissue expanders. We first looked at companies that produced self-inflating expanders, similar to that of my industrial partners, but they could not produce anything within the parameters required for my project.

We then investigated using balloon tissue expanders, these require manual inflation with a filling port that has external access. However, the use of these would not be accepted in our home office project license due to the distress that manual filling may cause to the animals and the increased likelihood of infection within the filling port.

The whole premise of my PhD is to investigate a minimally invasive technique of tissue expansion that could eventually be developed for use in paediatric surgery. It is therefore not appropriate to try to use balloon expanders as the results will not be translatable to use in paediatric surgery. The only suitable tissue expander is one that self-inflates in situ. This has now become possible with the work being conducted at the Centre for Additional Materials, but this work has been delayed due to the Coronavirus pandemic. My project would have been completed within the original funded period if my industrial partner had supported my project for its entire duration and if the Coronavirus

pandemic did not cause a delay in access to laboratories due to the lockdown and reduced capacity.

Below is a list of the aspects of my research plan that I have managed to achieve or progress during the period of impact.

- Preliminary development of a self-inflating hydrogel expanded in collaboration with the Centre for Additional Materials, University of Nottingham
- Basic RNA sequencing interpretation and analysis of porcine vaginal and urogenital sinus tissue.
- Writing up of thesis, predominantly updating all materials and methods and results chapters.
- Working on potential publications of research results that were obtained before the period of impact.

### 7.8.3 Next Steps

Below is a list of what I plan to do from now, to both progress my research and in order to continue to lessen the impact on my research, now that you can access research facilities and can resume the specific activities listed above

- Develop and synthesise a hydrogel formulation that will swell at fast enough rate to initiate expansion of the organ it will be implanted in
- Use 3D printing techniques to produce multiple hydrogel implants
- Conduct in vitro implantation and swelling trials to assess the insertion of the hydrogel implants into the porcine model and the ability for vaginal tissue to withstand implantation and expansion.
- Conduct histological analysis of the expanded tissue from the in vitro implantation and swelling trial.
- Conduct in vivo implantation and swelling trials to assess whether the expansion of the hydrogel implants within vaginal tissue leads to an increase in cell number proliferation, as opposed to cell enlargement and tissue stretching.
- Conduct histological analysis of the expanded tissue from the in vivo implantation and swelling trial.

# 8 Bibliography


ABBE, R. 1898. New method of creating a vagina in a case of congenital absence. *Medical Record (1866-1922),* 54**,** 836.

ÁCS, N., BÁNHIDY, F., HORVÁTH-PUHÓ, E. & CZEIZEL, A. E. 2006a. Population-based Case–Control Study of the Common Cold During Pregnancy and Congenital Abnormalities. *European Journal of Epidemiology,* 21**,** 65-75.

ÁCS, N., BÁNHIDY, F., PUHÓ, E. & CZEIZEL, A. E. 2005. Maternal influenza during pregnancy and risk of congenital abnormalities in offspring. *Birth Defects Research Part A: Clinical and Molecular Teratology,* 73**,** 989-996.

ÁCS, N., BÁNHIDY, F., PUHÓ, E. H. & CZEIZEL, A. E. 2006b. Acute respiratory infections during pregnancy and congenital abnormalities: a population-based case-control study. *Congenital Anomalies,* 46**,** 86-96.

ADMINISTRATION, U. S. F. A. D. 2015. *Nonclinical Pharmacology/Toxicology Development of Topical Drugs Intended to Prevent the Transmission of Sexually Transmitted Diseases (STD) and/or for the Development of Drugs Intended to Act as Vaginal Contraceptives* [Online]. Available: https://www.fda.gov/Drugs/GuidanceComplianceRegulatoryInformation/Guidances/ucm125951.htm [Accessed 09/03/2018 2018].

ADRIAENS, E., DHONDT, M. M. M. & REMON, J. P. 2005. Refinement of the Slug Mucosal Irritation test as an alternative screening test for eye irritation. *Toxicology in Vitro,* 19**,** 79-89.

ADRIAENS, E. & REMON, J. P. 2002. Evaluation of an Alternative Mucosal Irritation Test Using Slugs. *Toxicology and Applied Pharmacology,* 182**,** 169-175.

ADSUL, M. G., VARMA, A. J. & GOKHALE, D. V. 2007. Lactic acid production from waste sugarcane bagasse derived cellulose. *Green Chemistry,* 9**,** 58-62.

AHARONI, S. M. 1992. *Synthesis, characterization, and theory of polymeric networks and gels*, Springer.

AHLGREN, S. C. & BRONNER-FRASER, M. 1999. Inhibition of sonic hedgehog signaling in vivo results in craniofacial neural crest cell death. *Curr Biol,* 9**,** 1304-14.

ALESSANDRESCU, D., PELTECU, G. C., BUHIMSCHI, C. S. & BUHIMSCHI, I. A. 1996. Neocolpopoiesis with split-thickness skin graft as a surgical treatment of vaginal agenesis: Retrospective review of 201 cases. *American Journal of Obstetrics and Gynecology,* 175**,** 131-138.

ALWAN , S., REEFHUIS , J., RASMUSSEN , S. A., OLNEY , R. S. & FRIEDMAN , J. M. 2007. Use of Selective Serotonin-Reuptake Inhibitors in Pregnancy and the Risk of Birth Defects. *New England Journal of Medicine,* 356**,** 2684-2692.

ANDERSON, J. E. 1978. *Grant's Atlas of Anatomy*, Williams and Wilkins Co.

ARGENTA, L. C. 1984. Controlled tissue expansion in reconstructive surgery. *British Journal of Plastic Surgery,* 37**,** 520-529.

AURAS, R., HARTE, B. & SELKE, S. 2004. An overview of polylactides as packaging materials. *Macromolecular bioscience,* 4**,** 835-864.

AUSTAD, E. D. 1987. The origin of expanded tissue. *Clin Plast Surg,* 14**,** 431-3.

AUSTAD, E. D. 1988. Contraindications and complications in tissue expansion. *Facial Plast Surg,* 5**,** 379-82.

AUSTAD, E. D. 1991. *Self-Inflating Tissue Expander*. 07/518489.

AUSTAD, E. D., PASYK, K. A., MCCLATCHEY, K. D. & CHERRY, G. W. 1982. Histomorphologic evaluation of guinea pig skin and soft tissue after controlled tissue expansion. *Plastic and reconstructive surgery,* 70**,** 704-710.

AUSTAD, E. D., THOMAS, S. B. & PASYK, K. 1986. Tissue expansion: dividend or loan? *Plastic and reconstructive surgery,* 78**,** 63-67.

AYEHUNIE, S., CANNON, C., LAMORE, S., KUBILUS, J., ANDERSON, D. J., PUDNEY, J. & KLAUSNER, M. 2006. Organotypic human vaginal-ectocervical tissue model for irritation studies of spermicides, microbicides, and feminine-care products. *Toxicology in Vitro,* 20**,** 689-698.

BANHIDY, F., ACS, N., PUHO, E. H. & CZEIZEL, A. E. 2011. Chronic hypertension with related drug treatment of pregnant women and congenital abnormalities in their offspring: a population-based study. *Hypertens Res,* 34**,** 257-63.

BÁNHIDY, F., ÁCS, N., PUHÓ, E. H. & CZEIZEL, A. E. 2010a. Congenital abnormalities in the offspring of pregnant women with type 1, type 2 and gestational diabetes mellitus: A population-based case-control study. *Congenital Anomalies,* 50**,** 115-121.

BÁNHIDY, F., ÁCS, N., PUHÓ, E. H. & CZEIZEL, A. E. 2010b. Teratogenic potential of pholedrine: A sympathomimetic vasoconstrictive drug – A population-based case-control study. *Congenital Anomalies,* 50**,** 122-128.

BÁNHIDY, F., SZILASI, M. & CZEIZEL, A. E. 2012. Association of pre-eclampsia with or without superimposed chronic hypertension in pregnant women with the risk of congenital abnormalities in their offspring: a population-based case–control study. *European Journal of Obstetrics and Gynecology and Reproductive Biology,* 163**,** 17-21.

BARBERINI, F., CORRER, S., SANTIS, F. D. & MOTTA, P. M. 1991. The Epithelium of the Rabbit Vagina: A Microtopographical Study by Light, Transmission and Scanning Electron Microscopy. *Archives of Histology and Cytology,* 54**,** 365-378.

BARBERINI, F., DE SANTIS, F., CORRER, S. & MOTTA, P. M. 1992. The mucosa of the rabbit vagina: a proposed experimental model for correlated morphofunctional studies in humans. *European Journal of Obstetrics & Gynecology and Reproductive Biology,* 44**,** 221-227.

BARHATE, S. 2020. Embryology. *In:* PUNDIR, J., ARORA, M. & MUKHOPADHAYA, N. (eds.) *Part 1 MRCOG Revision Notes and Sample SBAs.* Cambridge: Cambridge University Press.

BAXTER, J. S. 1934. Some Observations on the Development of the Vagina in the Pig. *Journal of Anatomy,* 68**,** 239-250.1.

BERGERON, S., BROWN, C., LORD, M. J., OALA, M., BINIK, Y. M. & KHALIFÉ, S. 2002. Physical therapy for vulvar vestibulitis syndrome: a retrospective study. *J Sex Marital Ther,* 28**,** 183-92.

BIGGAR, W. D., BARKER, C., BOHN, D. & KENT, G. 1985. An experimental model to study blood and inflammatory neutrophils. *Immunological Investigations,* 14**,** 473-477.

BIJL, P. V. D. & VAN EYK, A. D. 2004. Human Vaginal Mucosa as a Model of Buccal Mucosa for In Vitro Permeability Studies: An Overview. *Current Drug Delivery,* 1**,** 129-135.

BISCHOFF, A. 2016. The surgical treatment of cloaca. *Seminars in Pediatric Surgery,* 25**,** 102-107.

BLOMBERG, M. I. & KÄLLÉN, B. 2010. Maternal obesity and morbid obesity: The risk for birth defects in the offspring. *Birth Defects Research Part A: Clinical and Molecular Teratology,* 88**,** 35-40.

BODE, G., CLAUSING, P., GERVAIS, F., LOEGSTED, J., LUFT, J., NOGUES, V. & SIMS, J. 2010. The utility of the minipig as an animal model in regulatory toxicology. *J Pharmacol Toxicol Methods,* 62**,** 196-220.

BONNOT, O., VOLLSET, S. E., GODET, P. F., D'AMATO, T. & ROBERT, E. 2001. Maternal Exposure to Lorazepam and Anal Atresia in Newborns: Results from a Hypothesis-Generating Study of Benzodiazepines and Malformations. *Journal of Clinical Psychopharmacology,* 21**,** 456-458.

BORRUTO, F., CAMOGLIO, F. S., ZAMPIERI, N. & FEDELE, L. 2007. The laparoscopic Vecchietti technique for vaginal agenesis. *International Journal of Gynecology & Obstetrics,* 98**,** 15-19.
BORRUTO, F., CHASEN, S. T., CHERVENAK, F. A. & FEDELE, L. 1999. The Vecchietti procedure for surgical treatment of vaginal agenesis: comparison of laparoscopy and laparotomy. *International Journal of Gynecology & Obstetrics,* 64**,** 153-158.
BOSTWICK, J. 1988. Breast reconstruction after mastectomy. *Seminars in surgical oncology,* 4**,** 274-279.
BOUAPAO, L., TSUJI, H., TASHIRO, K., ZHANG, J. & HANESAKA, M. 2009. Crystallization, spherulite growth, and structure of blends of crystalline and amorphous poly(lactide)s. *Polymer,* 50**,** 4007-4017.
BOYLSTON, J. & BRENNER, C. 2012. Sonic Hedgehog (Shh). *In:* CHOI, S. (ed.) *Encyclopedia of Signaling Molecules.* New York, NY: Springer New York.
BRADY, J., DÜRIG, T., LEE, P. I. & LI, J. X. 2017. Chapter 7 - Polymer Properties and Characterization. *In:* QIU, Y., CHEN, Y., ZHANG, G. G. Z., YU, L. & MANTRI, R. V. (eds.) *Developing Solid Oral Dosage Forms (Second Edition).* Boston: Academic Press.
BRANNON-PEPPAS, L. 1990. Preparation and characterization of crosslinked hydrophilic networks. *Studies in polymer science.* Elsevier.
BROUSSARD, C. S., RASMUSSEN, S. A., REEFHUIS, J., FRIEDMAN, J. M., JANN, M. W., RIEHLE-COLARUSSO, T. & HONEIN, M. A. 2011. Maternal treatment with opioid analgesics and risk for birth defects. *American Journal of Obstetrics & Gynecology,* 204**,** 314.e1-314.e11.
BROWNE, M. L., ZUTPHEN, A. R. V., BOTTO, L. D., LOUIK, C., RICHARDSON, S. & DRUSCHEL, C. M. 2014. Maternal Butalbital Use and Selected Defects in the National Birth Defects Prevention Study. *Headache: The Journal of Head and Face Pain,* 54**,** 54-66.
BRUCKER, S. Y., GEGUSCH, M., ZUBKE, W., RALL, K., GAUWERKY, J. F. & WALLWIENER, D. 2008. Neovagina creation in vaginal agenesis: development of a new laparoscopic Vecchietti-based procedure and optimized instruments in a prospective comparative interventional study in 101 patients. *Fertility and Sterility,* 90**,** 1940-1952.
BRUN, J.-L., BELLEANNÉE, G., GRAFEILLE, N., ASLAN, A.-F. & BRUN, G. H. 2002. Long-term results after neovagina creation in Mayer–Rokitanski–Kuster–Hauser syndrome by Vecchietti's operation. *European Journal of Obstetrics & Gynecology and Reproductive Biology,* 103**,** 168-172.
BUCHHOLZ, F. L. & GRAHAM, A. T. 1998. Modern superabsorbent polymer technology. *John! Wiley & Sons, Inc, 605 Third Ave, New York, NY 10016, USA, 1998. 279*.
CADÉE, J., VAN LUYN, M., BROUWER, L., PLANTINGA, J., VAN WACHEM, P., DE GROOT, C., DEN OTTER, W. & HENNINK, W. 2000. In vivo biocompatibility of dextran-based hydrogels. *Journal of Biomedical Materials Research: An Official Journal of The Society for Biomaterials, The Japanese Society for Biomaterials, and The Australian Society for Biomaterials and the Korean Society for Biomaterials,* 50**,** 397-404.
CAI, B., ZHANG, J., XI, X., YAN, Q. & WAN, X. 2007. Laparoscopically assisted sigmoid colon vaginoplasty in women with Mayer–Rokitansky–Kuster–Hauser syndrome: Feasibility and short-term results. *BJOG: An International Journal of Obstetrics & Gynaecology,* 114**,** 1486-1492.
CALDWELL, B. T. & WILCOX, D. T. 2016. Long-term urological outcomes in cloacal anomalies. *Seminars in Pediatric Surgery,* 25**,** 108-111.
CARMELIET, P. 2000. Mechanisms of angiogenesis and arteriogenesis. *Nature Medicine,* 6**,** 389-395.
CARMELIET, P. & JAIN, R. K. 2000. Angiogenesis in cancer and other diseases. *Nature,* 407**,** 249-57.

CARTER, T. C., DRUSCHEL, C. M., ROMITTI, P. A., BELL, E. M., WERLER, M. M. & MITCHELL, A. A. 2008. Antifungal drugs and the risk of selected birth defects. *American Journal of Obstetrics & Gynecology,* 198**,** 191.e1-191.e7.
CARTER, T. C., KAY, D. M., BROWNE, M. L., LIU, A., ROMITTI, P. A., KUEHN, D., CONLEY, M. R., CAGGANA, M., DRUSCHEL, C. M., BRODY, L. C. & MILLS, J. L. 2013. Anorectal atresia and variants at predicted regulatory sites in candidate genes. *Ann Hum Genet,* 77**,** 31-46.
CASTILLA, E. E., LOPEZ-CAMELO, J. S. & CAMPAÑA, H. 1999. Altitude as a risk factor for congenital anomalies. *American Journal of Medical Genetics,* 86**,** 9-14.
CASTLE, P. E., HOEN, T. E., WHALEY, K. J. & CONE, R. A. 1998. Contraceptive testing of vaginal agents in rabbits. *Contraception,* 58**,** 51-60.
CATALONE, B. J., KISH-CATALONE, T. M., BUDGEON, L. R., NEELY, E. B., FERGUSON, M., KREBS, F. C., HOWETT, M. K., LABIB, M., RANDO, R. & WIGDAHL, B. 2004. Mouse Model of Cervicovaginal Toxicity and Inflammation for Preclinical Evaluation of Topical Vaginal Microbicides. *Antimicrobial Agents and Chemotherapy,* 48**,** 1837-1847.
CATAPANO, D. & LANZINO, G. 2010. Pituitary Carcinoma. *Transsphenoidal Surgery.* Saint Louis: W.B. Saunders.
CHA, Y. & PITT, C. 1990. The biodegradability of polyester blends. *Biomaterials,* 11**,** 108-112.
CHAN, C., VANDI, L.-J., PRATT, S., HALLEY, P., RICHARDSON, D., WERKER, A. & LAYCOCK, B. 2017. Composites of Wood and Biodegradable Thermoplastics: A Review. *Polymer Reviews,* 58**,** 00-00.
CHAVATTE-PALMER, P. & TARRADE, A. 2016. Placentation in different mammalian species. *Annales d'Endocrinologie,* 77**,** 67-74.
CHEN, G., USHIDA, T. & TATEISHI, T. 2002. Scaffold design for tissue engineering. *Macromolecular Bioscience,* 2**,** 67-77.
CHENG, Y., DENG, S., CHEN, P. & RUAN, R. 2009. Polylactic acid (PLA) synthesis and modifications: a review. *Frontiers of chemistry in China,* 4**,** 259-264.
CHERNY, S. S., WONG, E. H. M., CUI, L., NG, C. L., TANG, C. S. M., SO, M. T., YIP, B. H. K., CHENG, G., LUI, V. C. H., SHAM, P. C., TAM, P. K. H. & GARCIA-BARCELO, M. M. 2012. Genome-wide copy number variation in anorectal malformations. *Annual Meeting of the American Society of Human Genetics, ASHG 2012.* United States: American Society of Human Genetics.
CHUDACOFF, R. M., ALEXANDER, J., ALVERO, R. & SEGARS, J. H. 1996. Tissue expansion vaginoplasty for treatment of congenital vaginal agenesis. *Obstet Gynecol,* 87**,** 865-8.
CÍFKOVÁ, I., STOL, M., HOLUSA, R. & ADAM, M. 1987. Calcification of poly(2-hydroxyethyl methacrylate)-collagen composites implanted in rats. *Biomaterials,* 8**,** 30-4.
CORREA, A., BOTTO, L., LIU, Y., MULINARE, J. & ERICKSON, J. D. 2003. Do Multivitamin Supplements Attenuate the Risk for Diabetes-Associated Birth Defects? *Pediatrics,* 111**,** 1146-1151.
CORREA, A., GILBOA, S. M., BESSER, L. M., BOTTO, L. D., MOORE, C. A., HOBBS, C. A., CLEVES, M. A., RIEHLE-COLARUSSO, T. J., WALLER, D. K. & REECE, E. A. 2008. Diabetes mellitus and birth defects. *Am J Obstet Gynecol,* 199**,** 237 e1-9.
CORREA, A., GILBOA, S. M., BOTTO, L. D., MOORE, C. A., HOBBS, C. A., CLEVES, M. A., RIEHLE-COLARUSSO, T. J., WALLER, D. K. & REECE, E. A. 2012. Lack of periconceptional vitamins or supplements that contain folic acid and diabetes mellitus-associated birth defects. *American Journal of Obstetrics & Gynecology,* 206**,** 218.e1-218.e13.

COUTU, D. L., YOUSEFI, A. M. & GALIPEAU, J. 2009. Three-dimensional porous scaffolds at the crossroads of tissue engineering and cell-based gene therapy. *Journal of cellular biochemistry,* 108**,** 537-546.
CRIDER, K. S., CLEVES, M. A., REEFHUIS, J., BERRY, R. J., HOBBS, C. A. & HU, D. J. 2009. Antibacterial medication use during pregnancy and risk of birth defects: National birth defects prevention study. *Archives of Pediatrics & Adolescent Medicine,* 163**,** 978-985.
CUSCHIERI, A. 2002. Anorectal anomalies associated with or as part of other anomalies. *American Journal of Medical Genetics,* 110**,** 122-130.
CZEIZEL, A. E., ERÖS, E., ROCKENBAUER, M., SØRENSEN, H. T. & OLSEN, J. 2003. Short-Term Oral Diazepam Treatment during Pregnancy. *Clinical Drug Investigation,* 23**,** 451-462.
CZEIZEL, A. E. & ROCKENBAUER, M. 1998. A population based case-control teratologic study of oral metronidazole treatment during pregnancy. *BJOG: An International Journal of Obstetrics & Gynaecology,* 105**,** 322-327.
CZEIZEL, A. E., ROCKENBAUER, M. & MOSONYI, A. 2000. A population-based case–control teratologic study of acetylsalicylic acid treatments during pregnancy. *Pharmacoepidemiology and Drug Safety,* 9**,** 193-205.
CZEIZEL, A. E., ROCKENBAUER, M., SIFFEL, C. & VARGA, E. 2001a. Description and mission evaluation of the Hungarian case-control surveillance of congenital abnormalities, 1980–1996. *Teratology,* 63**,** 176-185.
CZEIZEL, A. E., ROCKENBAUER, M., SØRENSEN, H. T. & OLSEN, J. 2001b. Nitrofurantoin and congenital abnormalities. *European Journal of Obstetrics and Gynecology and Reproductive Biology,* 95**,** 119-126.
CZEIZEL, A. E., ROCKENBAUER, M., SØRENSEN, H. T. & OLSEN, J. 2001c. A population-based case-control teratologic study of ampicillin treatment during pregnancy. *American Journal of Obstetrics & Gynecology,* 185**,** 140-147.
CZEIZEL, A. E., ROCKENBAUER, M., SØRENSEN, H. T. & OLSEN, J. 2004. A population-based case–control study of oral chlordiazepoxide use during pregnancy and risk of congenital abnormalities. *Neurotoxicology and Teratology,* 26**,** 593-598.
CZEIZEL, A. E., TÓTH, M. & ROCKENBAUER, M. 1996. Population-based case control study of folic acid supplementation during pregnancy. *Teratology,* 53**,** 345-351.
CZEIZEL, A. E., XF, TH, M., XE, RTA & ROCKENBAUER, M. 1999. No Teratogenic Effect after Clotrimazole Therapy during Pregnancy. *Epidemiology,* 10**,** 437-440.
D'ALBERTON, A. & SANTI, F. 1972. Formation of a Neovagina by Coitus. *Obstetrics & Gynecology,* 40**,** 763-770.
D'CRUZ, O. J., ERBECK, D. & UCKUN, F. M. 2005. A Study of the Potential of the Pig as a Model for the Vaginal Irritancy of Benzalkonium Chloride in Comparison to the Nonirritant Microbicide PHI-443 and the Spermicide Vanadocene Dithiocarbamate. *Toxicologic Pathology,* 33**,** 465-476.
DABBS, D. J. 2018. *Diagnostic Immunohistochemistry: Theranostic and Genimoc Applications*, Elsevier.
DAVIS, B. J., TRAVLOS, G. & MCSHANE, T. 2001. Reproductive Endocrinology and Toxicological Pathology over the Life Span of the Female Rodent. *Toxicologic Pathology,* 29**,** 77-83.
DE CLERCQ, E., KALMAR, I. & VANROMPAY, D. 2013. Animal Models for Studying Female Genital Tract Infection with Chlamydia trachomatis. *Infection and Immunity,* 81**,** 3060-3067.
DEARNALEY, G., ASHER, J., PEACOCK, A., ALLEN, S. & WATKINS, R. 2007. The use of thin layer activation to evaluate ion beam surface treatments of orthopaedic implant materials. *Surface and Coatings Technology,* 201**,** 8070-8075.

DENAYER, T., STÖHR, T. & VAN ROY, M. 2014. Animal models in translational medicine: Validation and prediction. *New Horizons in Translational Medicine,* 2**,** 5-11.
DESROSIERS, T. A., HERRING, A. H., SHAPIRA, S. K., HOOIVELD, M., LUBEN, T. J., HERDT-LOSAVIO, M. L., LIN, S. & OLSHAN, A. F. 2012. Paternal occupation and birth defects: findings from the National Birth Defects Prevention Study. *Occupational and Environmental Medicine*.
DHONDT, M. M. M., ADRIAENS, E., PINCEEL, J., JORDAENS, K., BACKELJAU, T. & REMON, J. P. 2006. Slug species- and population-specific effects on the end points of the Slug Mucosal Irritation test. *Toxicology in Vitro,* 20**,** 448-457.
DHONDT, M. M. M., ADRIAENS, E. & REMON, J.-P. 2004. The Evaluation of the Local Tolerance of Vaginal Formulations, With or Without Nonoxynol-9, Using the Slug Mucosal Irritation Test. *Sexually Transmitted Diseases,* 31**,** 229-235.
DRAVIS, C., YOKOYAMA, N., CHUMLEY, M. J., COWAN, C. A., SILVANY, R. E., SHAY, J., BAKER, L. A. & HENKEMEYER, M. 2004. Bidirectional signaling mediated by ephrin-B2 and EphB2 controls urorectal development. *Dev Biol,* 271**,** 272-90.
DRUMRIGHT, R. E., GRUBER, P. R. & HENTON, D. E. 2000. Polylactic acid technology. *Advanced materials,* 12**,** 1841-1846.
DUONG, H. T., HOYT, A. T., CARMICHAEL, S. L., GILBOA, S. M., CANFIELD, M. A., CASE, A., MCNEESE, M. L. & WALLER, D. K. 2012. Is maternal parity an independent risk factor for birth defects? *Birth Defects Research Part A: Clinical and Molecular Teratology,* 94**,** 230-236.
EEDEN, S. K. V. D., KARAGAS, M. R., DALING, J. R. & VAUGHAN, T. L. 1990. A case-control study of maternal smoking and congenital malformations. *Paediatric and Perinatal Epidemiology,* 4**,** 147-155.
ELKAFRAWI, H. Y. & ABDELAL, A. F. 2013. The Use of Bilateral Pudendal Thigh Flap for Primary and Secondary Vaginal Reconstruction.
ELLENGAARD. *Göttingen Minipigs* [Online]. Available: https://minipigs.dk/ [Accessed 2018].
ELLIOTT, J. E., MACDONALD, M., NIE, J. & BOWMAN, C. N. 2004. Structure and swelling of poly(acrylic acid) hydrogels: effect of pH, ionic strength, and dilution on the crosslinked polymer structure. *Polymer,* 45**,** 1503-1510.
ENDE, M. T. A. & PEPPAS, N. A. 1996. Transport of ionizable drugs and proteins in crosslinked poly (acrylic acid) and poly (acrylic acid-co-2-hydroxyethyl methacrylate) hydrogels. I. Polymer characterization. *Journal of applied polymer science,* 59**,** 673-685.
EROS, E., CZEIZEL, A. E., ROCKENBAUER, M., SORENSEN, H. T. & OLSEN, J. 2002. A population-based case-control teratologic study of nitrazepam, medazepam, tofisopam, alprazolum and clonazepam treatment during pregnancy. *European Journal of Obstetrics and Gynecology and Reproductive Biology,* 101**,** 147-154.
EURELL JA, F. B. 2006. *Dellman's Textbook of Veterinary Histology,* United States of America, Blackwell Publishing.
EXPANIDERM. 2014. *Case Study: Horse Perineal Laceration* [Online]. Available: http://www.expaniderm.com/case-studies/equine-case-studies/perineal-laceration/ [Accessed 2018].
EXPANIDERM. 2015. *Case Study: Horse Benign Melanoma - Lower Eyelid* [Online]. Available: http://www.expaniderm.com/case-studies/equine-case-studies/benign-melanoma-right-eye/ [Accessed 2018].
EXPANIDERM. 2016. *Case Study: Dog- Mast Cell Tumour on Muzzle* [Online]. Available: http://www.expaniderm.com/case-studies/small-animal-case-studies/mast-cell-tumour/ [Accessed 2018].

FALCONE, R. A., JR., LEVITT, M. A., PEÑA, A. & BATES, M. 2007. Increased heritability of certain types of anorectal malformations. *Journal of Pediatric Surgery,* 42**,** 124-128.
FEDELE, L., BUSACCA, M., CANDIANI, M. & VIGNALI, M. 1994. Laparoscopic creation of a neovagina in Mayer-Rokitansky-Küster-Hauser syndrome by modification of Vecchietti's operation. *American Journal of Obstetrics and Gynecology,* 171**,** 268-269.
FEDELE, L., FRONTINO, G., MOTTA, F. & PERUZZI, E. 2011. Davydov's Procedure for the Treatment of Neovaginal Prolapse in Rokitansky Syndrome. *Journal of Minimally Invasive Gynecology,* 18**,** 503-506.
FEDELE, L., FRONTINO, G., RESTELLI, E., CIAPPINA, N., MOTTA, F. & BIANCHI, S. 2010. Creation of a neovagina by Davydov's laparoscopic modified technique in patients with Rokitansky syndrome. *American Journal of Obstetrics and Gynecology,* 202**,** 33.e1-33.e6.
FELDKAMP, M. L., MEYER, R. E., KRIKOV, S. & BOTTO, L. D. 2010. Acetaminophen Use in Pregnancy and Risk of Birth Defects: Findings From the National Birth Defects Prevention Study. *Obstetrics & Gynecology,* 115**,** 109-115.
FICHOROVA, R. N., RHEINWALD, J. G. & ANDERSON, D. J. 1997. Generation of Papillomavirus-Immortalized Cell Lines from Normal Human Ectocervical, Endocervical, and Vaginal Epithelium that Maintain Expression of Tissue-Specific Differentiation Proteins1. *Biology of Reproduction,* 57**,** 847-855.
FICHOROVA, R. N., TUCKER, L. D. & ANDERSON, D. J. 2001. The Molecular Basis of Nonoxynol-9-Induced Vaginal Inflammation and Its Possible Relevance to Human Immunodeficiency Virus Type 1 Transmission. *The Journal of Infectious Diseases,* 184**,** 418-428.
FLORY, P. J. 1953. *Principles of polymer chemistry*, Cornell University Press.
FLORY, P. J. & REHNER JR, J. 1943. Statistical mechanics of cross-linked polymer networks I. Rubberlike elasticity. *The journal of chemical physics,* 11**,** 512-520.
FORRESTER, M. B. & MERZ, R. D. 2002. Descriptive epidemiology of anal atresia in Hawaii, 1986-1999. *Teratology,* 66**,** S12-S16.
FRANK, R. T. 1938. The formation of an artificial vagina without operation. *American Journal of Obstetrics and Gynecology,* 35**,** 1053-1055.
FREGA, A., SCIRPA, P., SOPRACORDEVOLE, F., BIAMONTI, A., BIANCHI, P., DE SANCTIS, L., LORENZON, L., PACCHIAROTTI, A., FRENCH, D. & MOSCARINI, M. 2011. Impact of human papillomavirus infection on the neovaginal and vulval tissues of women who underwent surgical treatment for Mayer-Rokitansky-Kuster-Hauser syndrome. *Fertility and Sterility,* 96**,** 969-973.
FRÍAS, J. L., FRÍAS, J. P., FRÍAS, P. A. & MARTÍNEZ-FRÍAS, M. L. 2007. Infrequently studied congenital anomalies as clues to the diagnosis of maternal diabetes mellitus. *American Journal of Medical Genetics Part A,* 143A**,** 2904-2909.
FUKUSHIMA, K. & KIMURA, Y. 2008. An efficient solid-state polycondensation method for synthesizing stereocomplexed poly (lactic acid) s with high molecular weight. *Journal of Polymer Science Part A: Polymer Chemistry,* 46**,** 3714-3722.
GALLAWAY, M. S., WALLER, D. K., CANFIELD, M. A. & SCHEUERLE, A. 2009. The association between use of spermicides or male condoms and major structural birth defects. *Contraception,* 80**,** 422-429.
GARCIA-BARCELÓ, M. M., LUI, V. C. H., MIAO, X., SO, M. T., LEON, T. Y. Y., YUAN, Z. W., LI, L., LIU, L., WANG, B., SUN, X. B., HUANG, L. M., TOU, J. F., NGAN, E. S. W., CHERNY, S. S., CHAN, K. W., LEE, K. H., WANG, W., WONG, K. K. Y. & TAM, P. K. H. 2008. Mutational analysis of SHH and GLI3 in anorectal malformations. *Birth Defects Research Part A: Clinical and Molecular Teratology,* 82**,** 644-648.

GARNE, E., LOANE, M., DOLK, H., BARISIC, I., ADDOR, M. C., ARRIOLA, L., BAKKER, M., CALZOLARI, E., DIAS, C. M., DORAY, B., GATT, M., MELVE, K. K., NELEN, V., O'MAHONY, M., PIERINI, A., RANDRIANAIVO-RANJATOELINA, H., RANKIN, J., RISSMANN, A., TUCKER, D., VERELLUN-DUMOULIN, C. & WIESEL, A. 2012. Spectrum of congenital anomalies in pregnancies with pregestational diabetes. *Birth Defects Research Part A: Clinical and Molecular Teratology,* 94**,** 134-140.

GERDES, J., LEMKE, H., BAISCH, H., WACKER, H. H., SCHWAB, U. & STEIN, H. 1984. Cell cycle analysis of a cell proliferation-associated human nuclear antigen defined by the monoclonal antibody Ki-67. *The Journal of Immunology,* 133**,** 1710-1715.

GILBERT, S. F. 2010. *Developmental biology*, sinauer associates, Inc.

GILBOA, S. M., STRICKLAND, M. J., OLSHAN, A. F., WERLER, M. M. & CORREA, A. 2009. Use of antihistamine medications during early pregnancy and isolated major malformations. *Birth Defects Research Part A: Clinical and Molecular Teratology,* 85**,** 137-150.

GILL, S. K., BROUSSARD, C., DEVINE, O., GREEN, R. F., RASMUSSEN, S. A. & REEFHUIS, J. 2012. Association between maternal age and birth defects of unknown etiology — United States, 1997–2007. *Birth Defects Research Part A: Clinical and Molecular Teratology,* 94**,** 1010-1018.

GOESSLING, W., NORTH, T. E., LOEWER, S., LORD, A. M., LEE, S., STOICK-COOPER, C. L., WEIDINGER, G., PUDER, M., DALEY, G. Q., MOON, R. T. & ZON, L. I. 2009. Genetic interaction of PGE2 and Wnt signaling regulates developmental specification of stem cells and regeneration. *Cell,* 136**,** 1136-47.

GREEN, P. J., WALSH, F. S. & DOHERTY, P. 1996. Promiscuity of fibroblast growth factor receptors. *Bioessays,* 18**,** 639-646.

GRIFFITH, L. 2000. Polymeric biomaterials. *Acta materialia,* 48**,** 263-277.

GROBE III, G. L., VALINT JR, P. L. & AMMON JR, D. M. 1996. Surface chemical structure for soft contact lenses as a function of polymer processing. *Journal of Biomedical Materials Research: An Official Journal of The Society for Biomaterials and The Japanese Society for Biomaterials,* 32**,** 45-54.

GRUBER, D. D., WARNER, W. B., LOMBARDINI, E. D., ZAHN, C. M. & BULLER, J. L. 2011. Anatomical and Histological Examination of the Porcine Vagina and Supportive Structures: In Search of an Ideal Model for Pelvic Floor Disorder Evaluation and Management. *Female Pelvic Medicine & Reconstructive Surgery,* 17**,** 110-114.

GU, S., YANG, M., YU, T., REN, T. & REN, J. 2008. Synthesis and characterization of biodegradable lactic acid-based polymers by chain extension. *Polymer international,* 57**,** 982-986.

GUDEMAN, L. F. & PEPPAS, N. A. 1995. pH-sensitive membranes from poly(vinyl alcohol)/poly(acrylic acid) interpenetrating networks. *Journal of Membrane Science,* 107**,** 239-248.

GUPTA, B., REVAGADE, N. & HILBORN, J. 2007. Poly (lactic acid) fiber: An overview. *Progress in polymer science,* 32**,** 455-482.

GUPTA, D. 2005. Anorectal Malformations - Wingspread to Krickenbeck. *Journal of Indian Association of Pediatric Surgeons,* 10**,** 75-77.

HARAGUCHI, R., MOTOYAMA, J., SASAKI, H., SATOH, Y., MIYAGAWA, S., NAKAGATA, N., MOON, A. & YAMADA, G. 2007. Molecular analysis of coordinated bladder and urogenital organ formation by Hedgehog signaling. *Development,* 134**,** 525-533.

HARRIS, J., KÄLLÉN, B. & ROBERT, E. 1995. Descriptive epidemiology of alimentary tract atresia. *Teratology,* 52**,** 15-29.

HASSINK, E., RIEU, P., HAMEL, B., SEVERIJNEN, R., STAAK, F. & FESTEN, C. 1996. Additional congenital defects in anorectal malformations. *European journal of pediatrics,* 155**,** 477-82.

HAY, S. & BARBANO, H. 1972. Independent effects of maternal age and birth order on the incidence of selected congenital malformations. *Teratology,* 6**,** 271-279.
HENDREN, W. H. 1980. Urogenital sinus and anorectal malformation: Experience with 22 cases. *Journal of Pediatric Surgery,* 15**,** 628-641.
HENDREN, W. H. 1988. Urological Aspects of Cloacal Malformations. *The Journal of Urology,* 140**,** 1207-1213.
HENSLE, T. W., SHABSIGH, A., SHABSIGH, R., REILEY, E. A. & MEYER-BAHLBURG, H. F. L. 2006. Sexual Function Following Bowel Vaginoplasty. *The Journal of Urology,* 175**,** 2283-2286.
HERDT-LOSAVIO, M. L., LIN, S., CHAPMAN, B. R., HOOIVELD, M., OLSHAN, A., LIU, X., DEPERSIS, R. D., ZHU, J. & DRUSCHEL, C. M. 2010. Maternal occupation and the risk of birth defects: an overview from the National Birth Defects Prevention Study. *Occupational and Environmental Medicine,* 67**,** 58-66.
HERNÁNDEZ, J., BENEDITO, J., ABUELO, A. & CASTILLO, C. 2014. Ruminal Acidosis in Feedlot: From Aetiology to Prevention. *The Scientific World Journal,* 2014.
HICKEY, A. S. & PEPPAS, N. A. 1995. Mesh size and diffusive characteristics of semicrystalline poly (vinyl alcohol) membranes prepared by freezing/thawing techniques. *Journal of membrane science,* 107**,** 229-237.
HIRSHOWITZ, B., KAUFMAN, T. & ULLMAN, J. 1986. Reconstruction of the tip of the nose and ala by load cycling of the nasal skin and harnessing of extra skin. *Plast Reconstr Surg,* 77**,** 316-21.
HOBDAY, A. J., HAURY, L. & DAYTON, P. K. 1997. Function of the human hymen. *Medical Hypotheses,* 49**,** 171-173.
HOFFMAN, A. S. 2012. Hydrogels for biomedical applications. *Advanced drug delivery reviews,* 64**,** 18-23.
HOLSCHNEIDER, A., HUTSON, J., PEÑA, A., BEKET, E., CHATTERJEE, S., CORAN, A., DAVIES, M., GEORGESON, K., GROSFELD, J., GUPTA, D., IWAI, N., KLUTH, D., MARTUCCIELLO, G., MOORE, S., RINTALA, R., SMITH, E. D., SRIPATHI, D. V., STEPHENS, D., SEN, S., URE, B., GRASSHOFF, S., BOEMERS, T., MURPHY, F., SÖYLET, Y., DÜBBERS, M. & KUNST, M. 2005. Preliminary report on the International Conference for the Development of Standards for the Treatment of Anorectal Malformations. *Journal of Pediatric Surgery,* 40**,** 1521-1526.
HOLTZER, H. 1968. Induction of chondrogenesis: A concept in quest of mechanisms. *Epithelial-mesenchymal interactions***,** 152-164.
HONEIN, M. A., PAULOZZI, L. J. & WATKINS, M. L. 2001. Maternal smoking and birth defects: validity of birth certificate data for effect estimation. *Public Health Reports,* 116**,** 327-335.
HOPKINS, M. P. & MORLEY, G. W. 1987. Squamous cell carcinoma of the neovagina. *Obstetrics and gynecology,* 69**,** 525-527.
HUGLIN, M. R. 1989. Hydrogels in medicine and pharmacy Edited by N. A. Peppas, CRC Press Inc., Boca Raton, Florida, 1986 (Vol. l), 1987 (Vols 2 and 3). Vol. 1 Fundamentals, pp. vii + 180, £72.00, ISBN 0-8493-5546-X; Vol. 2 Polymers, pp. vii + 171, £72.00, ISBN 0-8493-5547-8; Vol. 3 Properties and Applications, pp. vii + 195, £8000, ISBN 0-8493-5548-6. *British Polymer Journal,* 21**,** 184-184.
HUNTER, R. H. F. 1975. Physiological Aspects of Sperm Transport in the Domestic Pig, Sus Scrofa. II. Regulation, Survival and Fate of Cells. *British Veterinary Journal,* 131**,** 681-690.
HUNTER, R. H. F. 1977. Physiological Factors Influencing Ovulation, Fertilization, Early Embryonic Development and Establishment of Pregnancy in Pigs. *British Veterinary Journal,* 133**,** 461-470.

INGRAM, J. M. 1981. The bicycle seat stool in the treatment of vaginal agenesis and stenosis: a preliminary report. *Am J Obstet Gynecol,* 140**,** 867-73.
ISMAIL, I., CUTNER, A. & CREIGHTON, S. 2006. Laparoscopic vaginoplasty: alternative techniques in vaginal reconstruction. *BJOG: An International Journal of Obstetrics & Gynaecology,* 113**,** 340-343.
ISOLA, J., HELIN, H. & KALLIONIEMI, O. P. 1990. Immunoelectron-microscopic localization of a proliferation-associated antigen Ki-67 in MCF-7 cells. *Histochem J,* 22**,** 498-506.
JAVERZAT, S., AUGUSTE, P. & BIKFALVI, A. 2002. Javerzat S, Auguste P, Bikfalvi A.. The role of fibroblast growth factors in vascular development. Trends Mol Med 8: 483-489. *Trends in molecular medicine,* 8**,** 483-9.
JOHN, R. P., ANISHA, G., NAMPOOTHIRI, K. M. & PANDEY, A. 2009. Direct lactic acid fermentation: focus on simultaneous saccharification and lactic acid production. *Biotechnology advances,* 27**,** 145-152.
JOHNSON, M. D. & ATKINSON, J. B. 2009. Central Nervous System Tumors A2 - Weidner, Noel. *In:* COTE, R. J., SUSTER, S. & WEISS, L. M. (eds.) *Modern Surgical Pathology (Second Edition).* Philadelphia: W.B. Saunders.
JOHNSON, N., BATCHELOR, A. & LILFORD, R. J. 1991. Experience with tissue expansion vaginoplasty. *Br J Obstet Gynaecol,* 98**,** 564-8.
JOHNSON, P. E., KERNAHAN, D. A. & BAUER, B. S. 1988. Dermal and epidermal response to soft-tissue expansion in the pig. *Plastic and reconstructive surgery,* 81**,** 390-397.
KÄLLÉN, B. 2007. Congenital malformations in infants whose mothers reported the use of folic acid in early pregnancy in Sweden. A prospective population study. *Congenital Anomalies,* 47**,** 119-124.
KÄLLÉN, B. 2014. Congenital Malformations in Twins: A Population Study. *Acta geneticae medicae et gemellologiae: twin research,* 35**,** 167-178.
KÄLLÉN, B., FINNSTRÖM, O., NYGREN, K. G. & OLAUSSON, P. O. 2005. In vitro fertilization (IVF) in Sweden: Risk for congenital malformations after different IVF methods. *Birth Defects Research Part A: Clinical and Molecular Teratology,* 73**,** 162-169.
KÄLLÉN, B. A. J. & OLAUSSON, P. O. 2007. Maternal use of selective serotonin re-uptake inhibitors in early pregnancy and infant congenital malformations. *Birth Defects Research Part A: Clinical and Molecular Teratology,* 79**,** 301-308.
KÄLLÉN, K. 2000. Multiple malformations and maternal smoking. *Paediatric and Perinatal Epidemiology,* 14**,** 227-233.
KALLURI, R. & NEILSON, E. G. 2003. Epithelial-mesenchymal transition and its implications for fibrosis. *The Journal of Clinical Investigation,* 112**,** 1776-1784.
KALLURI, R. & WEINBERG, R. A. 2009. The basics of epithelial-mesenchymal transition. *The Journal of Clinical Investigation,* 119**,** 1420-1428.
KAY, R. & TANK, E. S. 1977. Principles of Management of the Persistent Cloaca in the Female Newborn. *The Journal of Urology,* 117**,** 102-104.
KAZAURA, M., LIE, R. T. & SKJÆRVEN, R. 2004. Paternal age and the risk of birth defects in Norway. *Annals of Epidemiology,* 14**,** 566-570.
KAZY, Z., PUHÓ, E. & CZEIZEL, A. E. 2005. The possible association between the combination of vaginal metronidazole and miconazole treatment and poly-syndactyly: Population-based case–control teratologic study. *Reproductive Toxicology,* 20**,** 89-94.
KHEN-DUNLOP, N., LORTAT-JACOB, S., THIBAUD, E., CLÉMENT-ZIZA, M., LYONNET, S. & NIHOUL-FEKETE, C. 2007. Rokitansky Syndrome: Clinical Experience and Results of Sigmoid Vaginoplasty in 23 Young Girls. *The Journal of Urology,* 177**,** 1107-1111.
KIM, J., KIM, P. & HUI, C. C. 2001. The VACTERL association: lessons from the Sonic hedgehog pathway. *Clin Genet,* 59**,** 306-15.

KJÆR, D., HORVATH-PUHÓ, E., CHRISTENSEN, J., VESTERGAARD, M., CZEIZEL, A. E., SØRENSEN, H. T. & OLSEN, J. 2007. Use of phenytoin, phenobarbital, or diazepam during pregnancy and risk of congenital abnormalities: a case-time-control study. *Pharmacoepidemiology and Drug Safety,* 16**,** 181-188.
KLASING, K. C. 1999. Avian gastrointestinal anatomy and physiology. *Seminars in Avian and Exotic Pet Medicine,* 8**,** 42-50.
KLINGELE, C. J., GEBHART, J. B., CROAK, A. J., DIMARCO, C. S., LESNICK, T. G. & LEE, R. A. 2003. McIndoe procedure for vaginal agenesis: long-term outcome and effect on quality of life. *American journal of obstetrics and gynecology,* 189**,** 1569-1572.
KLUTH, D. 2010. Embryology of anorectal malformations. *Seminars in Pediatric Surgery,* 19**,** 201-208.
KOHLHASE, J., WISCHERMANN, A., REICHENBACH, H., FROSTER, U. & ENGEL, W. 1998. Mutations in the SALL1 putative transcription factor gene cause Townes-Brocks syndrome. *Nature Genetics,* 18**,** 81.
KOKCU, A., TOSUN, M., ALPER, T. & SAKINCI, M. 2011. Primary carcinoma of the neovagina: a case report. *European journal of gynaecological oncology,* 32**,** 588-589.
KÖNIG, H., UNDEN, G. & FRÖHLICH, J. 2009. *Biology of Microorganisms on Grapes, in Must and in Wine*, Springer.
KÖNIG HE, L. H. 2009. *Veterinary Anatomy of Domestic Animals,* Stuttgart, Schattauer.
KÖNIG, H. E., LIEBICH, H. G., HANS-GEORG, H. G. & BRAGULLA, H. 2007. *Veterinary Anatomy of Domestic Mammals: Textbook and Colour Atlas*, Wiley.
KREBS, F. C., MILLER, S. R., CATALONE, B. J., WELSH, P. A., MALAMUD, D., HOWETT, M. K. & WIGDAHL, B. 2000. Sodium Dodecyl Sulfate and C31G as Microbicidal Alternatives to Nonoxynol 9: Comparative Sensitivity of Primary Human Vaginal Keratinocytes. *Antimicrobial Agents and Chemotherapy,* 44**,** 1954-1960.
KRSTIC, Z. D., LUKAC, M., LUKAC, R., SMOLJANIC, Z., VUKADINOVIC, V. & VARINAC, D. 2001. Surgical treatment of cloacal anomalies. *Pediatric Surgery International,* 17**,** 329-333.
KRUEPUNGA, N., HIKSPOORS, J. P. J. M., MEKONEN, H. K., MOMMEN, G. M. C., MEEMON, K., WEERACHATYANUKUL, W., ASUVAPONGPATANA, S., ELEONORE KÖHLER, S. & LAMERS, W. H. 2018. The development of the cloaca in the human embryo. *Journal of Anatomy,* 233**,** 724-739.
KUBOTA, Y. & ITO, K. 2000. Chemotactic migration of mesencephalic neural crest cells in the mouse. *Dev Dyn,* 217**,** 170-9.
KULKARNI, R., PANI, K., NEUMAN, C. & LEONARD, F. 1966. Polylactic acid for surgical implants. *Archives of Surgery,* 93**,** 839-843.
LAITINEN, O., TÖRMÄLÄ, P., TAURIO, R., SKUTNABB, K., SAARELAINEN, K., IIVONEN, T. & VAINIONPÄÄ, S. 1992. Mechanical properties of biodegradable ligament augmentation device of poly (L-lactide) in vitro and in vivo. *Biomaterials,* 13**,** 1012-1016.
LAMPE, K. J., NAMBA, R. M., SILVERMAN, T. R., BJUGSTAD, K. B. & MAHONEY, M. J. 2009. Impact of lactic acid on cell proliferation and free radical-induced cell death in monolayer cultures of neural precursor cells. *Biotechnology and bioengineering,* 103**,** 1214-1223.
LANKFORD, J. A. & HAEFNER, H. K. 2008. Modification of the Ingram bicycle seat stool for the treatment of vaginal agenesis and stenosis. *International Journal of Gynecology & Obstetrics,* 102**,** 301-303.
LANTIER, F. 2014. Animal models of emerging diseases: An essential prerequisite for research and development of control measures. *Animal Frontiers,* 4**,** 7-12.

LAPIN, R., ELLIOTT, M. & JURI, H. 1985. The use of an integral tissue expander® for primary breast reconstruction. *Aesthetic Plastic Surgery,* 9**,** 221-226.
LAPPÖHN, R. E. 1995. Congenital absence of the vagina--results of conservative treatment. *Eur J Obstet Gynecol Reprod Biol,* 59**,** 183-6.
LASKIN, W. B. & MIETTINEN, M. 2002. Epithelial-type and neural-type cadherin expression in malignant noncarcinomatous neoplasms with epithelioid features that involve the soft tissues. *Arch Pathol Lab Med,* 126**,** 425-31.
LASPRILLA, A. J., MARTINEZ, G. A., LUNELLI, B. H., JARDINI, A. L. & MACIEL FILHO, R. 2012. Poly-lactic acid synthesis for application in biomedical devices—A review. *Biotechnology advances,* 30**,** 321-328.
LECHLER, T. & FUCHS, E. 2005. Asymmetric cell divisions promote stratification and differentiation of mammalian skin. *Nature,* 437**,** 275-80.
LEE, C.-L., WANG, C.-J., LIU, Y.-H., YEN, C.-F., LAI, Y.-L. & SOONG, Y.-K. 1999. Case Report: Laparoscopically assisted full thickness skin graft for reconstruction in congenital agenesis of vagina and uterine cervix. *Human Reproduction,* 14**,** 928-930.
LEE, M.-H. 2006. Non-surgical treatment of vaginal agenesis using a simplified version of Ingram's method. *Yonsei medical journal,* 47**,** 892.
LEJOUR, M. 1989. Reconstructive options after cancer surgery of the breast. *European journal of surgical oncology : the journal of the European Society of Surgical Oncology and the British Association of Surgical Oncology,* 15**,** 496-503.
LEVITT, M. A. & PEÑA, A. 2007. Anorectal malformations. *Orphanet Journal of Rare Diseases,* 2**,** 33-33.
LIE, R. T., WILCOX, A. J. & SKJÆRVEN, R. 2001. Survival and reproduction among males with birth defects and risk of recurrence in their children. *JAMA,* 285**,** 755-760.
LILFORD, R. J., JOHNSON, N. & BATCHELOR, A. 1989. A new operation for vaginal agenesis: construction of a neo-vagina from a rectus abdominus musculocutaneous flap. *Br J Obstet Gynaecol,* 96**,** 1089-94.
LIM, L. T., AURAS, R. & RUBINO, M. 2008. Processing technologies for poly(lactic acid). *Progress in Polymer Science,* 33**,** 820-852.
LIN, C., YIN, Y., VEITH, G. M., FISHER, A. V., LONG, F. & MA, L. 2009. Temporal and spatial dissection of Shh signaling in genital tubercle development. *Development,* 136**,** 3959-67.
LIN, S., HERDT-LOSAVIO, M. L., CHAPMAN, B. R., MUNSIE, J.-P., OLSHAN, A. F. & DRUSCHEL, C. M. 2013. Maternal occupation and the risk of major birth defects: A follow-up analysis from the National Birth Defects Prevention Study. *International Journal of Hygiene and Environmental Health,* 216**,** 317-323.
LIN, W. C., CHANG, C. Y. Y., SHEN, Y. Y. & TSAI, H. D. 2003. Use of autologous buccal mucosa for vaginoplasty: a study of eight cases. *Human Reproduction,* 18**,** 604-607.
LINDQVIST, C., SÖDERHOLM, A.-L., HALLIKAINEN, D. & SJÖVALL, L. 1992. Erosion and heterotopic bone formation after alloplastic temporomandibular joint reconstruction. *Journal of oral and maxillofacial surgery,* 50**,** 942-949.
LOCKER, M., AGATHOCLEOUS, M., AMATO, M. A., PARAIN, K., HARRIS, W. A. & PERRON, M. 2006. Hedgehog signaling and the retina: insights into the mechanisms controlling the proliferative properties of neural precursors. *Genes Dev,* 20**,** 3036-48.
LORENZEN, E., FOLLMANN, F., JUNGERSEN, G. & AGERHOLM, J. S. 2015. A review of the human vs. porcine female genital tract and associated immune system in the perspective of using minipigs as a model of human genital Chlamydia infection. *Veterinary Research,* 46**,** 116.

LOVALD, S. T., KHRAISHI, T., WAGNER, J. & BAACK, B. 2009. Mechanical design optimization of bioabsorbable fixation devices for bone fractures. *Journal of Craniofacial Surgery,* 20**,** 389-398.
LU, Y. & MADU, C. 2014. Prostate cancer biomarkers A2 - Gupta, Ramesh C. *Biomarkers in Toxicology.* Boston: Academic Press.
LUNELLI, B. H., ANDRADE, R. R., ATALA, D. I., MACIEL, M. R. W., MAUGERI FILHO, F. & MACIEL FILHO, R. 2010. Production of lactic acid from sucrose: strain selection, fermentation, and kinetic modeling. *Applied biochemistry and biotechnology,* 161**,** 227-237.
LUNT, J. 1998. Large-scale production, properties and commercial applications of polylactic acid polymers. *Polymer degradation and stability,* 59**,** 145-152.
LUNT, J. & SHAFER, A. 2000. Polyactic Acid Polymers from Corn—Applications in the Textiles Industry, for Cargill Dow Polymers LLC. *Minnetonka, MN,* 55345.
MADHAVAN NAMPOOTHIRI, K., NAIR, N. R. & JOHN, R. P. 2010. An overview of the recent developments in polylactide (PLA) research. *Bioresource Technology,* 101**,** 8493-8501.
MALATA, C. M., WILLIAMS, N. W. & SHARPE, D. T. 1995. Tissue expansion: an overview. *J Wound Care,* 4**,** 37-44.
MARCELIS, C., BLAAUW, I. D. & BRUNNER, H. 2011. Chromosomal anomalies in the etiology of anorectal malformations: A review. *American Journal of Medical Genetics Part A,* 155**,** 2692-2704.
MARTÍNEZ-FRÍAS, M. L. 1994. Epidemiological analysis of outcomes of pregnancy in diabetic mothers: Identification of the most characteristic and most frequent congenital anomalies. *American Journal of Medical Genetics,* 51**,** 108-113.
MATERNA-KIRYLUK, A., WIŚNIEWSKA, K., BADURA-STRONKA, M., MEJNARTOWICZ, J., WIĘCKOWSKA, B., BALCAR-BOROŃ, A., CZERWIONKA-SZAFLARSKA, M., GAJEWSKA, E., GODULA-STUGLIK, U., KRAWCZYŃSKI, M., LIMON, J., RUSIN, J., SAWULICKA-OLESZCZUK, H., SZWALKIEWICZ-WAROWICKA, E., WALCZAK, M. & LATOS-BIELEŃSKA, A. 2009. Parental age as a risk factor for isolated congenital malformations in a Polish population. *Paediatric and Perinatal Epidemiology,* 23**,** 29-40.
MCGEADY, T. A., QUINN, P. J., FITZPATRICK, E. S. & RYAN, M. T. 2006a. Differentiation of the Female Duct System in Mammals. *In:* LTD., B. P. (ed.) *Veterinary Embryology.* 1st ed.: Blackwell Publishing Ltd.
MCGEADY, T. A., QUINN, P. J., FITZPATRICK, E. S. & RYAN, M. T. 2006b. Paracrine Signalling During Development. *In:* LTD., B. P. (ed.) *Veterinary Embryology.* 1st ed.: Blackwell Publishing Ltd.
MCGEADY, T. A., QUINN, P. J., FITZPATRICK, E. S., RYAN, M. T. & CAHALAN, S. 2006c. *Veterinary Embryology*, Wiley.
MCINDOE, A. & BANISTER, J. B. 1938. An operation for the cure of congenital absence of the vagina. *BJOG: An International Journal of Obstetrics & Gynaecology,* 45**,** 490-494.
MCQUILLAN, S. K. & GROVER, S. R. 2014. Dilation and surgical management in vaginal agenesis: a systematic review. *International urogynecology journal,* 25**,** 299-311.
MCVEARRY, M. E. & WARNER, W. B. 2011. Use of physical therapy to augment dilator treatment for vaginal agenesis. *Female Pelvic Med Reconstr Surg,* 17**,** 153-6.
MEIER, D. J. 1969. Theory of block copolymers. I. Domain formation in A-B block copolymers. *Journal of Polymer Science Part C: Polymer Symposia,* 26**,** 81-98.
MELNIK, T., HAWTON, K. & MCGUIRE, H. 2012. Interventions for vaginismus. *Cochrane Database of systematic reviews*.

MICHIGAN, M. S. 2018. *Female Reproductive System* [Online]. Available: http://histology.medicine.umich.edu/resources/female-reproductive-system#vagina [Accessed 19.03.18 2018].
MIDRIO, P., DALLE NOGARE, C., DI GIANANTONIO, E. & CLEMENTI, M. 2006. Are congenital anorectal malformations more frequent in newborns conceived with assisted reproductive techniques? *Reproductive Toxicology,* 22**,** 576-577.
MIGLIARESI, C., NICODEMO, L., NICOLAIS, L. & PASSERINI, P. 1981. Physical characterization of microporous poly(2-hydroxyethyl methacrylate) gels. *J Biomed Mater Res,* 15**,** 307-17.
MILI, F., EDMONDS, L. D., KHOURY, M. J. & MCCLEARN, A. B. 1991. Prevalence of birth defects among low-birth-weight infants: A population study. *American Journal of Diseases of Children,* 145**,** 1313-1318.
MILLER, E. A., MANNING, S. E., RASMUSSEN, S. A., REEFHUIS, J. & HONEIN, M. A. 2009. Maternal exposure to tobacco smoke, alcohol and caffeine, and risk of anorectal atresia: National Birth Defects Prevention Study 1997–2003. *Paediatric and Perinatal Epidemiology,* 23**,** 9-17.
MIWA, K., FUKUYAMA, M., MATSUNO, N., MASUDA, S., OYAMA, Y., IKEDA, K. & IKEDA, T. 2006. Superantigen-induced multiple organ dysfunction in a toxin-concentration-controlled and sequential parameter-monitored swine sepsis model. *International Journal of Infectious Diseases,* 10**,** 14-24.
MO, R., KIM, J. H., ZHANG, J., CHIANG, C., HUI, C.-C. & KIM, P. C. W. 2001. Anorectal Malformations Caused by Defects in Sonic Hedgehog Signaling. *The American Journal of Pathology,* 159**,** 765-774.
MONTHEARD, J.-P., CHATZOPOULOS, M. & CHAPPARD, D. 1992. 2-Hydroxyethyl Methacrylate (HEMA): Chemical Properties and Applications in Biomedical Fields. *Journal of Macromolecular Science,* Part C: Polymer Reviews**,** 1-34.
MOORE, K. L. 1982. *The Developing Human - Clinically Orientated Embryology*, W. B. Saunders.
MURPHY, M., DRAGO, J. & BARTLETT, P. F. 1990. Fibroblast growth factor stimulates the proliferation and differentiation of neural precursor cells in vitro. *J Neurosci Res,* 25**,** 463-75.
MYERS, M. F., THE CHINA–, U. S. C. P. F. N. T. D. P., LI, S., THE CHINA–, U. S. C. P. F. N. T. D. P., CORREA-VILLASEÑOR, A., THE CHINA–, U. S. C. P. F. N. T. D. P., LI, Z., THE CHINA–, U. S. C. P. F. N. T. D. P., MOORE, C. A., THE CHINA–, U. S. C. P. F. N. T. D. P., HONG, S. X., THE CHINA–, U. S. C. P. F. N. T. D. P., BERRY, R. J. & THE CHINA–, U. S. C. P. F. N. T. D. P. 2001. Folic Acid Supplementation and Risk for Imperforate Anus in China. *American Journal of Epidemiology,* 154**,** 1051-1056.
NADARAJAH, S., QUEK, J., ROSE, G. L. & EDMONDS, D. K. 2005. Sexual Function in Women Treated with Dilators for Vaginal Agenesis. *Journal of Pediatric and Adolescent Gynecology,* 18**,** 39-42.
NAIR, L. S. & LAURENCIN, C. T. 2007. Biodegradable polymers as biomaterials. *Progress in Polymer Science,* 32**,** 762-798.
NEDKOV, E. & TSVETKOVA, S. 1994. Structure of poly (ethylene oxide) hydrogels obtained by gamma irradiation. *Radiation Physics and Chemistry,* 44**,** 257-261.
NEMOURS, E. D. P. D. 1936. Methacrylate resins. *Industrial & Engineering Chemistry,* 28**,** 1160-1163.
NEUMANN, C. G. 1957. The expansion of an area of skin by progressive distension of a subcutaneous balloon; use of the method for securing skin for subtotal reconstruction of the ear. *Plast Reconstr Surg***,** 124-130.
NIRUTHISARD, S., RODDY, R. E. & CHUTIVONGSE, S. 1991. The effects of frequent nonoxynol-9 use on the vaginal and cervical mucosa. *Sex Transm Dis,* 18**,** 176-9.

NUSSLEIN-VOLHARD, C. & WIESCHAUS, E. 1980. Mutations affecting segment number and polarity in Drosophila. *Nature,* 287**,** 795-801.
O'MEARA, C. P., ANDREW, D. W. & BEAGLEY, K. W. 2014. The mouse model of Chlamydia genital tract infection: a review of infection, disease, immunity and vaccine development. *Curr Mol Med,* 14**,** 396-421.
OXTEX. 2015. *Oxtex Technology* [Online]. Available: http://www.oxtex.com/about/tissue-expansion/technology/ [Accessed 10/05/2018 2018].
ØYEN, N., BOYD, H. A., POULSEN, G., WOHLFAHRT, J. & MELBYE, M. 2009. Familial Recurrence of Midline Birth Defects—A Nationwide Danish Cohort Study. *American Journal of Epidemiology,* 170**,** 46-52.
PARK, H. & PARK, K. 1996. Biocompatibility Issues of Implantable Drug Delivery Systems. *Pharmaceutical Research,* 13**,** 1770-1776.
PARKER, S. E., WERLER, M. M., SHAW, G. M., ANDERKA, M., YAZDY, M. M. & THE NATIONAL BIRTH DEFECTS PREVENTION, S. 2012. Dietary Glycemic Index and the Risk of Birth Defects. *American Journal of Epidemiology,* 176**,** 1110-1120.
PASYK, K. A., ARGENTA, L. C. & HASSETT, C. 1988. Quantitative analysis of the thickness of human skin and subcutaneous tissue following controlled expansion with a silicone implant. *Plastic and reconstructive surgery,* 81**,** 516-523.
PATHAK, C., SAWHNEY, A. & HUBBELL, J. 1992. In situ photopolymerization and gelation of water-soluble monomers: A new approach for local administration of peptide drugs. *Polymer Preprints (American Chemical Society, Division of Polymer Chemistry),* 33**,** 65-6.
PATTON, D. L., THWIN, S. S., MEIER, A., HOOTON, T. M., STAPLETON, A. E. & ESCHENBACH, D. A. 2000. Epithelial cell layer thickness and immune cell populations in the normal human vagina at different stages of the menstrual cycle. *Am J Obstet Gynecol,* 183**,** 967-73.
PEÑA, A. 1989. The surgical management of persistent cloaca: Results in 54 patients treated with a posterior sagittal approach. *Journal of Pediatric Surgery,* 24**,** 590-598.
PEÑA, A. 1990. Persistent Cloaca. *In:* FRANK, J. D. & JOHNSTON, J. H. (eds.) *Operative Paediatric Urology.* 1 ed. Edinburgh: Churchill Livingstone.
PEÑA, A. 1997. Total urogenital mobilization—An easier way to repair cloacas. *Journal of Pediatric Surgery,* 32**,** 263-268.
PEÑA, A. & DEVRIES, P. A. 1982. Posterior sagittal anorectoplasty: Important technical considerations and new applications. *Journal of Pediatric Surgery,* 17**,** 796-811.
PEPPAS, N. 1986. Hydrogels of poly (vinyl alcohol) and its copolymers. *Hydrogels in medicine and pharmacy,* 2**,** 1-48.
PEPPAS, N., BURES, P., LEOBANDUNG, W. & ICHIKAWA, H. 2000. Hydrogels in pharmaceutical formulations. *European journal of pharmaceutics and biopharmaceutics,* 50**,** 27-46.
PEPPAS, N. A. 1991. Physiologically responsive hydrogels. *Journal of bioactive and compatible polymers,* 6**,** 241-246.
PEPPAS, N. A. 1997. Hydrogels and drug delivery. *Current opinion in colloid & interface science,* 2**,** 531-537.
PEPPAS, N. A. 2019. *Hydrogels in medicine and pharmacy: fundamentals*, CRC press.
PEPPAS, N. A. & LANGER, R. 1994. New challenges in biomaterials. *Science,* 263**,** 1715-1720.
PEPPAS, N. A. & MERRILL, E. W. 1976a. Differential scanning calorimetry of crystallized PVA hydrogels. *Journal of Applied Polymer Science,* 20**,** 1457-1465.

PEPPAS, N. A. & MERRILL, E. W. 1976b. Poly (vinyl alcohol) hydrogels: Reinforcement of radiation-crosslinked networks by crystallization. *Journal of Polymer Science: Polymer Chemistry Edition,* 14**,** 441-457.
PEPPAS, N. A. & MIKOS, A. G. 1986. Preparation methods and structure of hydrogels. *Hydrogels in medicine and pharmacy,* 1**,** 1-27.
PEPPAS, N. A. & MONGIA, N. K. 1997. Ultrapure poly (vinyl alcohol) hydrogels with mucoadhesive drug delivery characteristics. *European journal of pharmaceutics and biopharmaceutics,* 43**,** 51-58.
PETER, S., MILLER, M. J., YASKO, A., YASZEMSKI, M. J. & MIKOS, A. 1998. Polymer concepts in tissue engineering. *Journal of biomedical materials research,* 43**,** 422-427.
PETERSON, M. L., AULT, K., KREMER, M. J., KLINGELHUTZ, A. J., DAVIS, C. C., SQUIER, C. A. & SCHLIEVERT, P. M. 2005. The Innate Immune System Is Activated by Stimulation of Vaginal Epithelial Cells with Staphylococcus aureus and Toxic Shock Syndrome Toxin 1. *Infection and Immunity,* 73**,** 2164-2174.
PHILP, A., MACDONALD, A. L. & WATT, P. W. 2005. Lactate–a signal coordinating cell and systemic function. *Journal of Experimental Biology,* 208**,** 4561-4575.
PINCHUK, L., ECKSTEIN, E. C. & VAN DE MARK, M. R. 1984. Effects of low levels of methacrylic acid on the swelling behavior of poly(2-hydroxyethyl methacrylate). *Journal of Applied Polymer Science,* 29**,** 1749-1760.
PRADAS, M. M., RIBELLES, J. L. G., AROCA, A. S., FERRER, G. G., ANTÓN, J. S. & PISSIS, P. 2001. Interaction between water and polymer chains in poly(hydroxyethyl acrylate) hydrogels. *Colloid and Polymer Science,* 279**,** 323-330.
RADOVAN, C. 1982. Breast reconstruction after mastectomy using the temporary expander. *Plastic and reconstructive surgery,* 69**,** 195-208.
RASMUSSEN, S. A., MOORE, C. A., PAULOZZI, L. J. & RHODENHISER, E. P. 2001. Risk for birth defects among premature infants: A population-based study. *The Journal of Pediatrics,* 138**,** 668-673.
REEFHUIS, J., HONEIN, M. A., SCHIEVE, L. A., CORREA, A., HOBBS, C. A. & RASMUSSEN, S. A. 2009. Assisted reproductive technology and major structural birth defects in the United States†. *Human Reproduction,* 24**,** 360-366.
REEFHUIS, J., HONEIN, M. A., SCHIEVE, L. A., RASMUSSEN, S. A. & THE NATIONAL BIRTH DEFECTS PREVENTION, S. 2011. Use of clomiphene citrate and birth defects, National Birth Defects Prevention Study, 1997–2005. *Human Reproduction,* 26**,** 451-457.
REGO, J. M. & HUGLIN, M. B. 1991. Influence of Composition on Properties of Hydrogels of 2-Hydroxyethyl Methacrylate with a Sulphobetaine Comonomer. *Polymer Journal,* 23**,** 1425-1434.
REIS, M. & KÄLLÉN, B. 2010. Delivery outcome after maternal use of antidepressant drugs in pregnancy: an update using Swedish data. *Psychological Medicine,* 40**,** 1723-1733.
ROBERT, E. & FRANCANNET, C. 1996. Subfertility and atresias of the alimentary tract. *Reproductive Toxicology,* 10**,** 125-128.
ROBERTS, C. P., HABER, M. J. & ROCK, J. A. 2001. Vaginal creation for müllerian agenesis. *Am J Obstet Gynecol,* 185**,** 1349-52; discussion 1352-3.
ROEGIERS, F. & JAN, Y. N. 2004. Asymmetric cell division. *Curr Opin Cell Biol,* 16**,** 195-205.
ROSS, A. J., RUIZ-PEREZ, V., WANG, Y., HAGAN, D.-M., SCHERER, S., LYNCH, S. A., LINDSAY, S., CUSTARD, E., BELLONI, E., WILSON, D. I., WADEY, R., GOODMAN, F., ORSTAVIK, K. H., MONCLAIR, T., ROBSON, S., REARDON, W., BURN, J., SCAMBLER, P. & STRACHAN, T. 1998. A homeobox gene, HLXB9, is the major locus for dominantly inherited sacral agenesis. *Nature Genetics,* 20**,** 358.

ROWITCH, D. H., B, S. J., LEE, S. M., FLAX, J. D., SNYDER, E. Y. & MCMAHON, A. P. 1999. Sonic hedgehog regulates proliferation and inhibits differentiation of CNS precursor cells. *J Neurosci,* 19**,** 8954-65.
SAAD, A. G. 2015. Brain Metastasis in Patients with Non-Small Cell Lung Cancer: Immunohistochemical Markers A2 - Hayat, M.A. *Brain Metastases from Primary Tumors.* San Diego: Academic Press.
SASAKI, G. H. 1988. Intraoperative expansion as an immediate reconstructive technique. *Facial plastic surgery : FPS,* 5**,** 362-378.
SASSI, A. B., MCCULLOUGH, K. D., COST, M. R., HILLIER, S. L. & ROHAN, L. C. 2004. Permeability of tritiated water through human cervical and vaginal tissue. *Journal of Pharmaceutical Sciences,* 93**,** 2009-2016.
SATO, H., HASEGAWA, T., ABE, Y., SAKAI, H. & HIROHASHI, S. 1999. Expression of E-cadherin in bone and soft tissue sarcomas: a possible role in epithelial differentiation. *Hum Pathol,* 30**,** 1344-9.
SCHNITZER, P. G., OLSHAN, A. F. & ERICKSON, J. D. 1995. Paternal Occupation and Risk of Birth Defects in Offspring. *Epidemiology,* 6**,** 577-583.
SCOTT, R. A. & PEPPAS, N. A. 1999. Compositional effects on network structure of highly cross-linked copolymers of PEG-containing multiacrylates with acrylic acid. *Macromolecules,* 32**,** 6139-6148.
SECCIA, A., SALGARELLO, M., STURLA, M., LORETI, A., LATORRE, S. & FARALLO, E. 2002. Neovaginal Reconstruction With the Modified McIndoe Technique: A Review of 32 Cases. *Annals of Plastic Surgery,* 49**,** 379-384.
SEELEY, R. R., STEPHENS, T. D. & TATE, P. 1995. *Anatomy and Physiology,* St. Louis, Missouri, USA, Mosby.
SEIFERT, A. W., BOULDIN, C. M., CHOI, K. S., HARFE, B. D. & COHN, M. J. 2009. Multiphasic and tissue-specific roles of sonic hedgehog in cloacal septation and external genitalia development. *Development,* 136**,** 3949-57.
SENGER, P. L. 2012. *Pathways to Pregnancy & Parturition*.
SEO, J. T., CHOE, J. H., LEE, W. S. & KIM, K. H. 2005. Efficacy of functional electrical stimulation-biofeedback with sexual cognitive-behavioral therapy as treatment of vaginismus. *Urology,* 66**,** 77-81.
SERI, M., MARTUCCIELLO, G., PALEARI, L., BOLINO, A., PRIOLO, M., SALEMI, G., FORABOSCO, P., CAROLI, F., CUSANO, R., TOCCO, T., LERONE, M., CAMA, A., TORRE, M., GUYS, J. M., ROMEO, G. & JASONNI, V. 1999. Exclusion of the Sonic Hedgehog gene as responsible for Currarino syndrome and anorectal malformations with sacral hypodevelopment. *Hum Genet,* 104**,** 108-10.
SERRA, J. M., SANZ, J., BALLESTEROS, A., PALOMA, V., BAZÁN, A. & MESA, F. 1993. Surgical treatment for congenital absence of the vagina using tissue expansion. *Surg Gynecol Obstet,* 177**,** 158-62.
SHEFER, A., GRODZINSKY, A. J., PRIME, K. L. & BUSNEL, J. P. 1993. Novel model networks of poly (acrylic acid): synthesis and characterization. *Macromolecules,* 26**,** 5009-5014.
SHIONO, P. H., KLEBANOFF, M. A. & BERENDES, H. W. 1986. Congenital malformations and maternal smoking during pregnancy. *Teratology,* 34**,** 65-71.
SHUTER, M. L., MALATA, C. M., DUFFY, J. S. & SHARPE, D. T. 1994. Determination of relative contributions of 'mechanical' and 'biological' creep in tissue expansion using in vivo pressure monitoring: a preliminary report. *Medical Engineering & Physics,* 16**,** 24-28.
SINGH, B. 2018. *Dyce, Sack and Wensing's Textbook of Veterinary Anatomy*, Saunders.
SINGH, S., SINGH, P. & SINGH, R. J. 2010. Persistent Urogenital Sinus. *Journal of Anatomical Society of India,* 59**,** 242-244.

SMETANA JR, K., VACIK, J., SOUČKOVÁ, D., KRČOVÁ, Z. & ŠULC, J. 1990. The influence of hydrogel functional groups on cell behavior. *Journal of biomedical materials research,* 24**,** 463-470.
SNOJ, N., DINH, P., BEDARD, P. & SOTIRIOU, C. 2009. Molecular Biology of Breast Cancer A2 - Coleman, William B. *In:* TSONGALIS, G. J. (ed.) *Molecular Pathology.* San Diego: Academic Press.
SOBEL, J. D., TCHAO, R., BOZZOLA, J., LEVISON, M. E. & KAYE, D. 1979. Human vaginal epithelial multilayer tissue culture. *In Vitro,* 15**,** 993-1000.
SPERLING, L. & MISHRA, V. 1996. The current status of interpenetrating polymer networks. *Polymers for Advanced Technologies,* 7**,** 197-208.
SQUIER, C. A., MANTZ, M. J., SCHLIEVERT, P. M. & DAVIS, C. C. 2008. Porcine vagina Ex Vivo as a model for studying permeability and pathogenesis in mucosa. *Journal of Pharmaceutical Sciences,* 97**,** 9-21.
STAUFFER, S. R. & PEPPAS, N. A. 1992. Poly (vinyl alcohol) hydrogels prepared by freezing-thawing cyclic processing. *Polymer,* 33**,** 3932-3936.
STEINER, E., WOERNLE, F., KUHN, W., BECKMANN, K., SCHMIDT, M., PILCH, H. & KNAPSTEIN, P. G. 2002. Carcinoma of the neovagina: case report and review of the literature. *Gynecologic oncology,* 84**,** 171-175.
STEPHENS, F. D. & SMITH, E. D. 1986. Classification, identification, and assessment of surgical treatment of anorectal anomalies. *Pediatric Surgery International,* 1**,** 200-205.
STEVENS, M. P. 1990. *Polymer chemistry*, Oxford university press New York.
STOLL, C., ALEMBIK, Y., DOTT, B. & ROTH, M. P. 2007. Associated malformations in patients with anorectal anomalies. *Eur J Med Genet,* 50**,** 281-90.
STOLL, C., ALEMBIK, Y., ROTH, M. P. & DOTT, B. 1997. Risk factors in congenital anal atresias. *Annales de genetique,* 40**,** 197-204.
SWAN, M. C., BUCKNALL, D. G., CZERNUSZKA, J. T., PIGOTT, D. W. & GOODACRE, T. E. 2012. Development of a novel anisotropic self-inflating tissue expander: in vivo submucoperiosteal performance in the porcine hard palate. *Plast Reconstr Surg,* 129**,** 79-88.
SWAN, M. C., BUCKNALL, D. G., GOODACRE, T. E. E. & CZERNUSZKA, J. T. 2011. Synthesis and properties of a novel anisotropic self-inflating hydrogel tissue expander. *Acta Biomaterialia,* 7**,** 1126-1132.
TAI, C. C., SALA, F. G., FORD, H. R., WANG, K. S., LI, C., MINOO, P., GRIKSCHEIT, T. C. & BELLUSCI, S. 2009. Wnt5a knock-out mouse as a new model of anorectal malformation. *J Surg Res,* 156**,** 278-82.
TEMENOFF, J. S. & MIKOS, A. G. 2000. Tissue engineering for regeneration of articular cartilage. *Biomaterials,* 21**,** 431-440.
THIERY, J. P. 2002. Epithelial–mesenchymal transitions in tumour progression. *Nature Reviews Cancer,* 2**,** 442.
THOMAS, J. C. & BROCK, J. W. 2007. Vaginal Substitution: Attempts to Create the Ideal Replacement. *The Journal of Urology,* 178**,** 1855-1859.
THOMPSON, I. O. C., VAN DER BIJL, P., VAN WYK, C. W. & VAN EYK, A. D. 2001. A comparative light-microscopic, electron-microscopic and chemical study of human vaginal and buccal epithelium. *Archives of Oral Biology,* 46**,** 1091-1098.
THOMSON, A. A. & CUNHA, G. R. 1999. Prostatic growth and development are regulated by FGF10. *Development,* 126**,** 3693-3701.
TIPPETT, J. & O'BRIEN, T. 1975. Procedure for purifying 2-hydroxethyl methacrylate and some methods for using it impure in plant histology. *Laboratory practice*.
TSUJI, H. & ISHIDA, T. 2003. Poly(L-lactide). X. Enhanced surface hydrophilicity and chain-scission mechanisms of poly(L-lactide) film in enzymatic, alkaline, and phosphate-buffered solutions. *Journal of Applied Polymer Science,* 87**,** 1628-1633.

TURK, J. R., HENDERSON, K. K., VANVICKLE, G. D., WATKINS, J. & LAUGHLIN, M. H. 2005. Arterial endothelial function in a porcine model of early stage atherosclerotic vascular disease. *Int J Exp Pathol,* 86**,** 335-45.
ULLOA, F. & MARTÍ, E. 2010. Wnt won the war: Antagonistic role of Wnt over Shh controls dorso-ventral patterning of the vertebrate neural tube. *Developmental Dynamics,* 239**,** 69-76.
VAN DER BIJL, P., THOMPSON, I. O. & SQUIER, C. A. 1997. Comparative permeability of human vaginal and buccal mucosa to water. *Eur J Oral Sci,* 105**,** 571-5.
VAN DER BIJL, P., VENTER, A., VAN EYK, A. D. & THOMPSON, I. O. 1998. Effect of temperature on permeability of mucosa to water. *SADJ : journal of the South African Dental Association = tydskrif van die Suid-Afrikaanse Tandheelkundige Vereniging,* 53**,** 504-507.
VAN EYK, A. D. & VAN DER BIJL, P. 1998. The culture of human buccal and vaginal epithelial cells for permeability studies. *Sadj,* 53**,** 497-503.
VAN EYK, A. D. & VAN DER BIJL, P. 2004. Comparative permeability of various chemical markers through human vaginal and buccal mucosa as well as porcine buccal and mouth floor mucosa. *Archives of Oral Biology,* 49**,** 387-392.
VAN GELDER, M. M. H. J., REEFHUIS, J., CATON, A. R., WERLER, M. M., DRUSCHEL, C. M., ROELEVELD, N. & STUDY, T. N. B. D. P. 2009. Maternal Periconceptional Illicit Drug Use and the Risk of Congenital Malformations. *Epidemiology,* 20**,** 60-66.
VAN GELDER, M. M. H. J., ROELEVELD, N. & NORDENG, H. 2011. Exposure to Non-Steroidal Anti-Inflammatory Drugs during Pregnancy and the Risk of Selected Birth Defects: A Prospective Cohort Study. *PLOS ONE,* 6**,** e22174.
VAN RAPPARD, J. H., MOLENAAR, J., VAN DOORN, K., SONNEVELD, G. J. & BORGHOUTS, J. M. 1988. Surface-area increase in tissue expansion. *Plastic and reconstructive surgery,* 82**,** 833-839.
VAN ROOIJ, I., RIEU, P., HENDRIKS, H., BROUWERS, M., DE BLAAUW, I., KNOERS, N. & ROELEVELD, N. 2009. Maternal And Paternal Risk Factors For Anorectal Malformations. *Journal of Pediatric Urology,* 5**,** S78.
VARADARAJAN, S. & MILLER, D. J. 1999. Catalytic upgrading of fermentation-derived organic acids. *Biotechnology progress,* 15**,** 845-854.
VARJOSALO, M. & TAIPALE, J. 2008. Hedgehog: functions and mechanisms. *Genes Dev,* 22**,** 2454-72.
VASUDEV, N. S. & BANKS, R. E. 2011. Biomarkers of Renal Cancer A2 - Edelstein, Charles L. *Biomarkers of Kidney Disease.* San Diego: Academic Press.
VECCHIETTI, G. 1979. Le neo-vagin dans le syndrome de Rokitansky-Küster-Hauser.
VELKEY, J. M., HALL, A. H. & ROBBOY, S. J. 2015. Normal vulva: Embryology, anatomy, and histology. *Vulvar Pathology.* Springer.
VERHEIJEN, R., KUIJPERS, H. J., SCHLINGEMANN, R. O., BOEHMER, A. L., VAN DRIEL, R., BRAKENHOFF, G. J. & RAMAEKERS, F. C. 1989. Ki-67 detects a nuclear matrix-associated proliferation-related antigen. I. Intracellular localization during interphase. *J Cell Sci,* 92 ( Pt 1)**,** 123-30.
VERONIKIS, D. K., MCCLURE, G. B. & NICHOLS, D. H. 1997. The Vecchietti operation for constructing a neovagina: indications, instrumentation, and techniques. *Obstetrics & Gynecology,* 90**,** 301-304.
WAGH, M. S. & DIXIT, V. 2013. Tissue expansion: Concepts, techniques and unfavourable results. *Indian Journal of Plastic Surgery : Official Publication of the Association of Plastic Surgeons of India,* 46**,** 333-348.
WALLER, D., SHAW, G. M., RASMUSSEN, S. A. & ET AL. 2007. Prepregnancy obesity as a risk factor for structural birth defects. *Archives of Pediatrics & Adolescent Medicine,* 161**,** 745-750.

WALLER, D. K., GALLAWAY, M. S., TAYLOR, L. G., RAMADHANI, T. A., CANFIELD, M. A., SCHEUERLE, A., HERNANDEZ-DIAZ, S., LOUIK, C. & CORREA, A. 2010. Use of oral contraceptives in pregnancy and major structural birth defects in offspring. *Epidemiology,* 21**,** 232-9.
WANG, C., GARGOLLO, P., GUO, C., TANG, T., MINGIN, G., SUN, Y. & LI, X. 2011. Six1 and Eya1 are critical regulators of peri-cloacal mesenchymal progenitors during genitourinary tract development. *Developmental Biology,* 360**,** 186-194.
WANG, C., WANG, J., BORER, J. G. & LI, X. 2013. Embryonic Origin and Remodeling of the Urinary and Digestive Outlets. *PLOS ONE,* 8**,** e55587.
WARIS, E., KONTTINEN, Y. T., ASHAMMAKHI, N., SUURONEN, R. & SANTAVIRTA, S. 2004. Bioabsorbable fixation devices in trauma and bone surgery: current clinical standing. *Expert review of medical devices,* 1**,** 229-240.
WARNE, S. A., HIORNS, M. P., CURRY, J. & MUSHTAQ, I. 2011. Understanding cloacal anomalies. *Arch Dis Child,* 96**,** 1072-6.
WEBB, S. E., LEE, K. K., TANG, M. K. & EDE, D. A. 1997. Fibroblast growth factors 2 and 4 stimulate migration of mouse embryonic limb myogenic cells. *Dev Dyn,* 209**,** 206-16.
WEYER, C., GAUTIER, J. F. & DANFORTH JR, E. 1999. Development of beta3-adrenoceptor agonists for the treatment of obesity and diabetes - An update. *Diabetes and Metabolism,* 25**,** 11-21.
WICHTERLE, O. & LIM, D. 1960. Hydrophilic gels for biological use. *Nature,* 185**,** 117-118.
WIDBERG, C. H., NEWELL, F. S., BACHMANN, A. W., RAMNORUTH, S. N., SPELTA, M. C., WHITEHEAD, J. P., HUTLEY, L. J. & PRINS, J. B. 2009. Fibroblast growth factor receptor 1 is a key regulator of early adipogenic events in human preadipocytes. *Am J Physiol Endocrinol Metab,* 296**,** E121-31.
WIESE, G. K., HEINEMANN, D. E. H., OSTERMEIER, D. & PETERS, J. H. 2001. Biomaterial properties and biocompatibility in cell culture of a novel self-inflating hydrogel tissue expander. *Journal of Biomedical Materials Research,* 54**,** 179-188.
WIESE, K. G., VOGEL, M., GUTHOFF, R. & GUNDLACH, K. K. H. 1999. Treatment of congenital anophthalmos with self-inflating polymer expanders: a new method. *Journal of Cranio-Maxillo-Facial Surgery,* 27**,** 72-76.
WIJERS, C., ROOIJ, I., BAKKER, M., MARCELIS, C., ADDOR, M., BARISIC, I., BÉRES, J., BIANCA, S., BIANCHI, F., CALZOLARI, E., GREENLEES, R., LELONG, N., LATOS-BIELENSKA, A., DIAS, C., MCDONNELL, R., MULLANEY, C., NELEN, V., O'MAHONY, M., QUEISSER-LUFT, A., RANKIN, J., ZYMAK-ZAKUTNIA, N., BLAAUW, I., ROELEVELD, N. & WALLE, H. 2013. Anorectal malformations and pregnancy-related disorders: a registry-based case–control study in 17 European regions. *BJOG: An International Journal of Obstetrics & Gynaecology,* 120**,** 1066-1074.
WIJERS, C. H. W. 2016. *Etiology of congenital anorectal malformations: Genetic and non-genetic risk factors.* [S.l. : s.n.].
WIJERS, C. H. W., DE BLAAUW, I., MARCELIS, C. L. M., WIJNEN, R. M. H., BRUNNER, H., MIDRIO, P., GAMBA, P., CLEMENTI, M., JENETZKY, E., ZWINK, N., REUTTER, H., BARTELS, E., GRASSHOFF-DERR, S., HOLLAND-CUNZ, S., HOSIE, S., MÄRZHEUSER, S., SCHMIEDEKE, E., CRÉTOLLE, C., SARNACKI, S., LEVITT, M. A., KNOERS, N. V. A. M., ROELEVELD, N. & VAN ROOIJ, I. A. L. M. 2010. Research perspectives in the etiology of congenital anorectal malformations using data of the International Consortium on Anorectal Malformations: evidence for risk factors across different populations. *Pediatric Surgery International,* 26**,** 1093-1099.

WOOD, D. A. 1980. Biodegradable drug delivery systems. *International Journal of pharmaceutics,* 7**,** 1-18.
WU, X., FERRARA, C., SHAPIRO, E. & GRISHINA, I. 2009. Bmp7 expression and null phenotype in the urogenital system suggest a role in re-organization of the urethral epithelium. *Gene Expr Patterns,* 9**,** 224-30.
YANG, Q., WEN, S. W., LEADER, A., CHEN, X. K., LIPSON, J. & WALKER, M. 2007. Paternal age and birth defects: how strong is the association? *Human Reproduction,* 22**,** 696-701.
YAU, W.-P., MITCHELL, A. A., LIN, K. J., WERLER, M. M. & HERNÁNDEZ-DÍAZ, S. 2013. Use of Decongestants During Pregnancy and the Risk of Birth Defects. *American Journal of Epidemiology,* 178**,** 198-208.
YAZDY, M. M., MITCHELL, A. A., LIU, S. & WERLER, M. M. 2011. Maternal dietary glycaemic intake during pregnancy and the risk of birth defects. *Paediatric and Perinatal Epidemiology,* 25**,** 340-346.
YERKES, E. B. & RINK, R. C. 2010. Surgical Management of Female Genital Anomalies, Disorders of Sexual Development, Urogenital Sinus, and Clocal Anomalies *In:* GEARHART, J. P., RINK, R. C. & MOURIQUAND, P. D. E. (eds.) *Pediatric Urology (Second Edition).* Philadelphia: W.B. Saunders.
YOSHII, E. 1997. Cytotoxic effects of acrylates and methacrylates: relationships of monomer structures and cytotoxicity. *Journal of Biomedical Materials Research: An Official Journal of The Society for Biomaterials and The Japanese Society for Biomaterials,* 37**,** 517-524.
YUAN, P., OKAZAKI, I. & KUROKI, Y. 1995. Anal atresia: Effect of smoking and drinking habits during pregnancy. *Japanese journal of human genetics,* 40**,** 327-332.
YUN, Y.-R., WON, J. E., JEON, E., LEE, S., KANG, W., JO, H., JANG, J.-H., SHIN, U. S. & KIM, H.-W. 2010. Fibroblast growth factors: biology, function, and application for tissue regeneration. *Journal of tissue engineering,* 2010**,** 218142-218142.
ZHANG, J., ZHANG, Z., GAO, H., ZHANG, D. & WANG, W. 2009. Down-Regulation of SHH/BMP4 Signalling in Human Anorectal Malformations. *Journal of International Medical Research,* 37**,** 1842-1850.
ZHANG, X. H., QIU, L. Q. & HUANG, J. P. 2011. Risk of birth defects increased in multiple births. *Birth Defects Research Part A: Clinical and Molecular Teratology,* 91**,** 34-38.
ZHAO, J., LALEVÉE, J., LU, H., MACQUEEN, R., KABLE, S. H., SCHMIDT, T. W., STENZEL, M. H. & XIAO, P. 2015. A new role of curcumin: as a multicolor photoinitiator for polymer fabrication under household UV to red LED bulbs. *Polymer Chemistry,* 6**,** 5053-5061.
ZÖLLNER, A. M., BUGANZA TEPOLE, A., GOSAIN, A. K. & KUHL, E. 2012. Growing skin: tissue expansion in pediatric forehead reconstruction. *Biomechanics and Modeling in Mechanobiology,* 11**,** 855-867.
ZWINK, N., JENETZKY, E., SCHMIEDEKE, E., SCHMIDT, D., MÄRZHEUSER, S., GRASSHOFF-DERR, S., HOLLAND-CUNZ, S., WEIH, S., HOSIE, S., REIFFERSCHEID, P., AMEIS, H., KUJATH, C., RISSMAN, A., OBERMAYR, F., SCHWARZER, N., BARTELS, E., REUTTER, H. & BRENNER, H. 2012. Assisted reproductive techniques and the risk of anorectal malformations: a German case-control study. *Orphanet Journal of Rare Diseases,* 7**,** 65.